Stem cell modelling for the role of *NRXN1* deletion in Autism Spectrum Disorder

Sahar Avazzadeh

A thesis submitted to the National University of Ireland, Galway, for a Degree of Doctor of Philosophy

August 2018

Supervisor: Professor Sanbing Shen
Regenerative Medicine Institute
National University of Ireland, Galway

Table of Contents

List of Figures

List of Tables

Acknowledgement

I would like to first thank my primary supervisor Prof. Sanbing Shen for the great opportunity of working on *NRXN1* project and experiencing a new world of stem cells. Thank you for all your help and support and all the time spent reading my thesis so efficiently, enabling me to submit this thesis before the deadline. Also, I like to thank co-PI of the grant Prof. Louise Gallagher and my co-supervisors, Dr. Leo Quinlan and Prof. Peter Dockery for all their help and support. Special appreciation to Leo for all the help and encouragement in the exciting field of electrophysiology despite all the stress of moving from one building to another and getting the set up ready for me to be able to patch straight away. I would also like to thank Prof. Meng Li for the training of iPSC differentiation and enjoyable time in Cardiff and my GRC members Dr. Dara Cannon, Dr. Una Fitzgerald and Dr. Michelle Roche for all their support throughout my PhD.

I would like to thank Dr. Kerry Thompson and Dr. Peter Owen in Anatomy, and Barbara Coen in Physiology for all their help and support whenever needed. I should thank all members of our group, present and past, for making this PhD more enjoyable. Thanks to my colleague and friend Maojia at REMEDI for all the long chats in cell culture suite, all the experimental discussion and dumpling making night we had together, it's been so much fun!

Special thanks to my colleague Jamie Reilly for all his help and patience with RNA sequencing analyses and to my friend Amir for all the little "R" scripts he wrote for me whenever I asked for, saving me so much time, really thank you! Thanks to all my friends in Galway & Birmingham for all the encouraging words, all the parties, making my PhD life much more interesting. Thanks to my family for all the support and to my little niece who brought so much delight to my life.

Last but not least to my amazing husband which I can't thank him enough, that without him I wouldn't be able to go through this PhD. For all his time listening to my experimental story every single day, all the help in Photoshop and whatever graphic

design or computer problem I encounter, to motivate me in the most stressful times I have passed by and being there for me all the time, thank you and thank you again

Declaration

This thesis describes work that I undertook between 2014 and 2018 at the Regenerative Medicine Institute, National University or Ireland, Galway. This work was supervised and mentored by Professor Sanbing Shen along with co-supervision of Dr. Leo Quinlan and Professor Peter Dockery.

I declare that the results in this thesis are from original experimental work carried out by me for the purpose of this PhD thesis. The results generated for this thesis has but been submitted for degree, diploma or any other qualification at any other institution.

Abbreviations

ADOS	Autism diagnostic observation schedule
ADRB2	Adrenoreceptor Beta 2
aIPs	apical intermediate progenitors
AMPA	α-amino-3-hydroxy-5-methyl-4-isoxazlepropionic acid
AP	Alkaline phosphatase
aRGC	Apical radial glial cell
ASD	Autism spectrum disorder
ATP1A3	ATPase Na+/K+ transporting subunit alpha 3
bFGF	Basic fibroblast growth factor
BMP	Bone morphogenic proteins
bRGCs	Basal radial glial cells
BRN2	Brain-specific homeobox/POU domain protein 2
CACNA	Calcium voltage gated channel
CACNG	Calcium voltage gated channel auxiliary subunit gamma 2
CAMK2B	Calcium/calmodulin dependent protein kinase II beta
CASK	Calcium/calmodulin- dependent serine protein kinase
CDC	Disease Control and Prevention
CDHs	Cadherins
cDNA	Complementary deoxyribonucleic acid
CHRM2	Cholinergic receptor muscarinic 2
CNS	Central nervous system
CNTNAP2	Contactin-associated protein like 2
CNV	Copy number variation
CODD	Childhood-onset disintegrative disorder
CTIP2	COUP-TF-interacting protein 2
DCX	Doublecortin
DIX5	Distal-less homeobox 5
DNA	Deoxyribonucleic acid
DOC2A	Double C2 domain alpha
DTI	Diffusion tensor imaging
E/I	Excitatory/inhibitory
EB	Embryoid body

ER	Endoplasmic reticulum
ESC	Embryonic stem cell
FDR	False discovery rate
FMRP	Fragile X mental retardation proteins
FOXG1	Forkhead Box G1
FPKM	Fragments per kilobase for transcripts per million
GABA	Gamma-aminobutyric acid
GABRA	Gamma-aminobutyric acid type A receptor alpha3 subunit
GABRD	Gamma-aminobutyric acid type receptor delta subunit
GABRE	Gamma-aminobutyric acid type receptor epsilon subunit
GABRP	Gamma-aminobutyric acid type A receptor Pi subunit
GABRR	Gamma-aminobutyric acid type A receptor Rho 1 subunit
GAPDH	Glyceraldehyde 3-phosphate dehydrogenase
GFAP	Glial fibrillary acidic protein
GRIA	Glutamate ionotropic receptor AMPA type subunit
GRIK	Glutamate ionotropic receptor kainate type subunit
GRIN	Glutamate ionotropic receptor NMDA type subunit
GRM	Glutamate metabotropic receptor
GSEA	Gene set enrichment analysis
HCN2	Hyperpolarization activated cyclic nucleotide gated potassium and sodium channel 2
HRH1	Histamine receptor H1
ICM	Inner cell mass
ID	Intellectual disability
IMGSAC	International molecular genetics study of autism consortium
IPCs	Intermediate neural progenitor cells
iPSC	Induced pluripotent stem cell
ISVZ	Inner sub-ventricular zone
KCNA3	Potassium voltage gated channel subfamily A member 3
KCNB2	Potassium voltage gated channel subfamily B member 2
KCNC4	Potassium voltage gated channel subfamily C member 4
KCNF1	Potassium voltage gated channel modifier subfamily F member 1
KCNH3	Potassium voltage gated channel subfamily H member 3
KCNIP1	Potassium voltage gated channel interacting protein 1
KCNJ8	Potassium voltage gated channel subfamily J member 8

KCNK12	Potassium two pore domain channel subfamily K member 12
KEGG	Kyoto encyclopaedia of genes and genomes
KLF4	Krüppel like factor 4
KO	Knockout
LIF	Leukaemia inhibitory factor
LNS	Laminin/neurexin/sex
LRRTM	Leucine-rich repeat transmembrane neuronal protein
MAP2	Microtubule-associated protein 2
MeCP2	Methyl-CpG 2
MEF	Mouse embryonic fibroblast
MOI	Multiplicity of infection
MRI	Magnetic resonance image
NaCl	Sodium chloride
NETBAG	Network-based analysis of genomic variation
NGN2	Neurogenin 2
NLGN	Neuroligin
NMDA	N-methyl-D-aspartate
NPs	Neural progenitors
NRXN	Neurexin
NSC	Neural stem cell
OCT4	Octamer binding transcription factor-4
OSVZ	Outer sub-ventricular zone
PAX6	Paired box 6
PCDHs	Protocadherins
PCLO	Piccolo presynaptic cytomatrix protein
PDGFRA	Platelet derived growth factor receptor alpha
PH3	Phospho-histone H3
PDS-NOS	Pervasive developmental disorders'-not otherwise specified
PSBS	Phosphate buffered saline
PSD-95	Post-synaptic density 95
RAB3C/3B	Ras-related protein Rab-3C/3B
RGCs	Radial glial cells
RNA	Ribonucleic acid
RNA-seq	RNA sequencing

ROI	Region of interest
SATB2	Special AT-rich sequence binding protein 2
SCID	Severe combined immunodeficient
SCN8A	Sodium voltage gated channel alpha subunit 8
SERCA	Sarco/ER calcium ATPase
SHANK	SH3 and multiple ankyrin repeat domains 2
Shh	Sonic hedgehog
SLC12A5	Solute carrier family 12 member 5
SNV	Single nucleotide variation
SOX2	Sex determining region Y box-2
SST	Somatostatin
SVZ	Sub-ventricular zone
SYN1	Synapsin1
SYT	Synaptotagmins
SYTL2	Synaptotagmin like 2
TBR1	T-box brain 1
TEA	Tetraethylammonium
TGF	Transforming growth factor
TPM	Transcripts per million
TTX	Tetrodotoxin
TUJ1	Beta III tubulin
UHG	University Hospital Galway
VGAT	GABAergic vesicular transporter
VGCC	Voltage gated calcium channel
VGKC	Voltage gated potassium channel
vGLUT1	Vesicular glutamate transporter
VGSC	Voltage gated sodium channel
VZ	Ventricular zone

Abstract

Autism spectrum disorder (ASD), a multi-factorial disease, often has co-morbidity with epilepsy, which is associated with excessive neuronal firing. The pre-synaptic protein Neurexin1 (*NRXN1*) signals bi-directionally through both excitation and inhibition, by forming synaptic complexes with post-synaptic Neuroligins, GABAergic or Glutamatergic receptors, and the scaffold proteins SHANKs. Deletions and/or mutations of the *NRXN1* gene have been implicated in a number of neurodevelopmental diseases including ASD. However, patient-derived disease models are lacking. Induced pluripotent stem cells (iPSCs) have the potential to revolutionize human disease modelling *in vitro* and to target unmet clinical needs. We hypothesize that *NRXN1α* gene deletion may dysregulate the balance of synaptic excitation and inhibition. Using skin biopsies from ASD patients with *NRXN1α* deletion and healthy donors, we converted dermal fibroblasts into iPSCs by reprogramming. Their pluripotency was validated by the expression of stem cell markers (OCT4, SOX2, NANOG, SSEA4, TRA-1-60, TRA-1-81). The iPSCs were directionally differentiated into cortical glutamatergic neurons using a dual SMAD inhibition method. Neural stem cells (NSCs) derived from the iPSCs were shown to express the neural progenitor markers of NESTIN, FOXG1 and PAX6. The 100-day-old neurons were shown to express markers of neuronal maturity (MAP2) and synapses (SYN1), as well as ion channels and transporters, at both the RNA and protein levels. They also transcribed pre- and post-synaptic interaction partners of NRXN1, including CASK, MINT, MUNC18-1 PSD-95, NLGNs and Shanks. There was no significant difference between the control and *NRXN1α* deletion groups in the proliferation of iPSCs and NSCs, neuronal differentiation or maturation, suggesting that *NRXN1α* deletion may not affect early neurogenesis. Neuronal function was investigated using single cell patch clamping, and the 100-day neurons with *NRXN1α* deletion displayed higher potassium and sodium currents, with selectively impaired depolarization and repolarization characteristics. The action potential amplitude was significantly increased, whereas the action potential threshold was decreased in *NRXN1α* deletion neurons. The repolarization slope was significantly increased and consequently, the repolarization duration was decreased. Moreover, we have carried out live cell calcium imaging on the 100-day neurons with Fluo4-AM, and neuronal

networks displayed inherent spontaneous firing activity with a significant increase in the frequency and duration of calcium transients in *NRXN1α* deletion neurons. The whole genome transcriptome analyses have demonstrated substantial up-regulation in ion channels and transporter activity, with voltage-gated calcium channels (VGCCs), voltage-gated potassium channels (VGKCs) and voltage-gated sodium channels (VGSCs) being mostly enriched among the differentially expressed genes. In addition, the KEGG pathway analyses have revealed further impairments in calcium signalling, vesicle exocytosis, synaptic transmission and MAPK pathways. Our results show for the first time that heterozygous deletions of *NRXN1α* gene directly impair the non-synaptic function of human neurons, in addition of their calcium transients, illustrating the value of this patient-derived iPSC model with *NRXN1α* deletion for studying ASD disease phenotypes.

Chapter 1. Introduction

1.1 Autism spectrum disorder (ASD)

Based on Manual of Mental Disorders 5th Edition (DSM 5) definition, ASD is a neurobehavioral disorder classified as deficits in verbal and social communication and in developing and maintaining relationships (Kogan et al. 2009). The "autistic disorders" were classified into four categories; Asperger's syndrome, childhood-onset disintegrative disorder (CODD), Rett syndrome and pervasive developmental disorders'-not otherwise specified (PDD-NOS). Later, in 2013 all these conditions were collectively defined as "Autism spectrum disorder".

The prevalence of ASD has been dramatically increased from 4/5 cases per 10,000 in 1966 to almost 1 in 100 in recent years (Tchaconas and Adesman 2013). This occurrence is more prevalent in males than females (Developmental Disabilities Monitoring Network Surveillance Year 2010 Principal Investigators and Centers for Disease Control and Prevention (CDC) 2014). It has been reported that the prevalence of ASD in the UK also has been increased from 0.40 case per 10,000 to 2.98 case per 10,000 (Smeeth et al. 2004). The same kind of increase has been reported and observed in US and Israel (Autism and Developmental Disabilities Monitoring Network Surveillance Year 2008 Principal Investigators and Centers for Disease Control and Prevention 2012; Davidovitch et al. 2013).

Based on DSM-5, the conditions for the diagnosis of ASD must be present from early childhood (Tanguay 2011). Children with ASD have unusual behaviour and certain routines. They may avoid interactions with other children, have brief eye contact and difficulty in initiating conversations. Furthermore, they exhibit repetitive behaviour such as opening and closing of a door or switching on and off the light. They may have excessive attachment to an unusual object, spinning their head or body in a certain way or flapping their hands. Based on DSM-5 there are three levels of severity in ASD: level 1, 2 and 3 (Table 1.1). Therefore, ASD is characterized by deficits in social and repetitive behaviours as well as communication problems. ASD is known to be heterogeneous concerning their clinical phenotypes. Communication deficits include speech and language delay. They often don't understand the body language, and they can't respond accordingly.

Table 1.1. Different levels of ASD severity based on DSM-5.

Level of severity	Social communication	Repetitive behaviours
Level 1	In the absence of support there is evidence of deficits in social interactions and communications. May have difficulties in initiating conversations and lack of social interest. At this level support is required.	There are difficulties in organization and switching among activities.
Level 2	In the presence of support there is an impairment in verbal and non-verbal communications and limited response to social interactions. At this level substantial support is required.	There are difficulties in managing and coping with changes, as well as difficulty in changing focus
Level 3	There is a severe deficit in both verbal and non-verbal communications and very limited response to social interactions. This level required hugely substantial support.	There are extremely difficulties in coping and managing with changes. Repetitive behaviours seen in all aspects of spheres.

Autism Spectrum Disorder is a developmental disorder characterized by impairment in social behaviour, interaction and communication (Gillberg 1993; Wing 1997; Lord and Jones 2012). ASD comprises of great heterogeneity in genetics, anatomical brain structure as well as clinical phenotypes. For example, ASD has comorbidity with epilepsy, intellectual disabilities, developmental and language delay, severe hyperactivity and gastrointestinal disorder (Amaral et al. 2008). Genetically, ASD is associated with hundreds of genetic risk factors (Pinto et al. 2010; Pinto et al. 2014; Vorstman et al. 2017). The heterogeneity in anatomical brain structure and abnormalities in ASD is also huge (Parellada et al. 2014; Varghese et al. 2017).

The neuropathological findings elucidate abnormalities in various brain regions such as hippocampus and cerebellum (Bauman 1991; Fatemi et al. 2002; Schmitz and Rezaie 2008), white and gray matter (Barnea-Goraly et al. 2004; Rojas et al. 2006) and cerebral, prefrontal and cingulate cortex (Zilbovicius et al. 2000; Courchesne and Redcay. 2004; Lewis et al. 2013; Lewis et al. 2014). Abnormality in the cerebellar cortex also involves alterations in brain volume as well as the size and number of Purkinje cells (Courchesne et al. 2011).

1.2 Causes of Autism Spectrum disorder

1.2.1 Epigenetics and environmental factors

Epigenetic mechanisms such as genomic imprinting, DNA methylation and histone modifications regulate gene expression and DNA structure. Genomic imprinting usually happens throughout life when a parental allele becomes inactive and imprinted. There are chromosomal areas termed as "hot spot" for genomic imprinting. These are located on loci 7q and 15q (Luedi et al. 2007), which have also been strongly implicated in ASD (International Molecular Genetic Study of Autism Consortium (IMGSAC) 2001). These evidences clearly indicate the association of epigenetics in the etiology of ASD.

DNA methylation is another epigenetic control affecting gene expression. Mutations in DNA binding protein Methyl-CpG 2 (*MeCP2*) have been implicated in Rett syndrome, seizures and ataxia (Amir et al.1999). MeCP2 have also been shown to regulate the expression of various synapse-related genes such as brain-derived neurotrophic factor (*BDNF*) and distal-less homeobox 5 (*DIX5*) (Chen et al. 2003). All of above suggest that epigenetics can potentially contribute to ASD. However, other researchers suggest that extrinsic factors such as environment can also alter the epigenetics and hence the functionality of the neurons (Jessberger et al. 2007). The extrinsic environmental factors may include parental age, heavy metals, food contaminants and environmental pesticides (Durkin et al. 2008). Organic pollutants can alter calcium signalling and hence deficits in neurotransmitter GABA and acetylcholine (Pessah et al. 2008). Furthermore, pesticides can cause oxidative stress and neuroinflammation and results in neuronal death (Herbert 2010).

1.2.2 Genetics

It is becoming increasingly clear that dysfunctions in synaptic genes are strongly implicated in ASD. These include, cell adhesion molecule, scaffolding proteins, neurotransmitter receptors, ion channels and cytoskeletal proteins. Alteration in synaptic activity and assembly are associated with many neuropsychiatric and neurodevelopmental disorders (Blanpied and Ehlers 2004).

1.2.2.1 Ion channels

Ion channels belong to transmembrane proteins in which ions diffuse down their electrochemical gradient. Ion channels are different in their gating properties. The gating mechanism of voltage-gated ion channels have sensors based on the electrical potential across the membrane. These channels respond to a change in membrane potential by opening and closing, which is essential for action potential propagation. Both voltage-gated and ligand-gated ion channels are essential for regulation of the optimal excitability of the neurons. Mutations in sodium, potassium and calcium channels seem to affect the excitability of cells. Based on SAFARI gene database there is a large number of sodium, potassium and calcium ion channels, which have been impaired in ASD individuals (Table 1.2).

Table 1.2. Sodium, Calcium and potassium channels associates with ASD in SAFARI database.

Gene symbol	Gene name	Genetic category	Autism report/ total report
SCN1A	Sodium channel, voltage-gated, type I, alpha subunit	Rare single gene mutation, syndromic, genetic association	14/46
SCN2A	Sodium channel, voltage gated, type II, alpha subunit	Rare single gene mutation, syndromic	26/49
SCN4A	Sodium channel, voltage gated, type IV, alpha subunit	Rare single gene mutation	3/3
SCN5A	Sodium channel, voltage gated, type V, alpha subunit	Rare single gene mutation	2/2
SCN7A	Sodium channel, voltage gated, type VII, alpha subunit	Rare single gene mutation	3/3
SCN8A	Sodium channel, voltage gated, type VIII, alpha subunit	Rare single gene mutation, syndromic	3/26
SCN9A	Sodium voltage-gated channel alpha subunit 9	Rare single gene mutation	2/5
CACNA1A	Calcium channel, voltage gated, P/Q type, alpha 1A subunit	Rare single gene mutation, genetic association	3/11
CACNA1B	Calcium channel, voltage gated, N type, alpha 1B subunit	Rare single gene mutation, genetic association	4/7
CACNA1C	Calcium channel, voltage gated, L type, alpha 1C subunit	Rare single gene mutation, syndromic, genetic association	10/38
KCNB1	Potassium voltage-gated channel subfamily B member 1	Rare single gene mutation, syndromic	1/4

KCND2	Potassium voltage-gated channel, shall related member 2	Rare single gene mutation, genetic association	2/4
KCND3	Potassium voltage-gated channel subfamily D member 3	Rare single gene mutation, syndromic, genetic association	3/8
KCNJ10	Potassium inwardly-rectifying channel subfamily J, member 10	Rare single gene mutation, syndromic, genetic association	3/10
KCNJ12	Potassium inwardly-rectifying channel subfamily J, member 12	Rare single gene mutation	1/1
KCNJ15	Potassium inwardly-rectifying channel subfamily J, member 15	Rare single gene mutation	2/2
KCNJ2	Potassium inwardly-rectifying channel subfamily J, member 2	Rare single gene mutation	1/1
KCNK7	Potassium two-pore domain channel subfamily K member 7	Rare single gene mutation	1/1
KCNMA1	Potassium large conductance calcium activated channel, subfamily M, alpha member 1	Rare single gene mutation	4/18
KCNQ2	Potassium voltage- gated channel, KQT-like subfamily, member 2	Rare single gene mutation, syndromic, genetic association	2/18
KCNQ3	Potassium voltage- gated channel, KQT-like subfamily, member 3	Rare single gene mutation, genetic association	4/7
KCNT1	Potassium channel, subfamily T, member 1	Rare single gene mutation, syndromic	1/10
KCND13	Potassium channel tetramerization domain containing 13	Rare single gene mutation	2/6

There are nine classes ($Na_V1.1$-1.9) of sodium ion channels which have been functionally characterized (Catterall, Goldin, et al. 2005). They all have 50% similarity in their amino acid sequence (Catterall, Goldin, et al. 2005). They express at either central nervous or peripheral nervous system or both. Nav1.1,1.2 and 1.3 only express in the central nervous system, while Nav1.7, 1.8 and 1.9 are strictly abundant in the peripheral nervous system. Furthermore, Nav1.6 is expressed in both peripheral and nervous system (Catterall, Goldin, et al. 2005). Voltage-gated sodium channels are essential for generating and propagating the action potentials. They are the molecular targets for many neural toxins such as batrachotoxin and tetrodotoxin. They act on the gating properties of sodium channels and block the initiation of action potentials (Cestèle and Catterall 2000).

The alpha subunit of sodium channels have a key role in pore forming of the channels while the kinetics and gating properties of channels are governed by auxiliary β subunit. The α subunit comprises of four homologous domains in which each domain has six segments (S1-S6) (Figure 1.1). S1-S4 of the domain has a role in the opening of the channel upon depolarization, while S5-S6 with extracellular pore loops forming the pore domain of the channel (Figure 1.1).

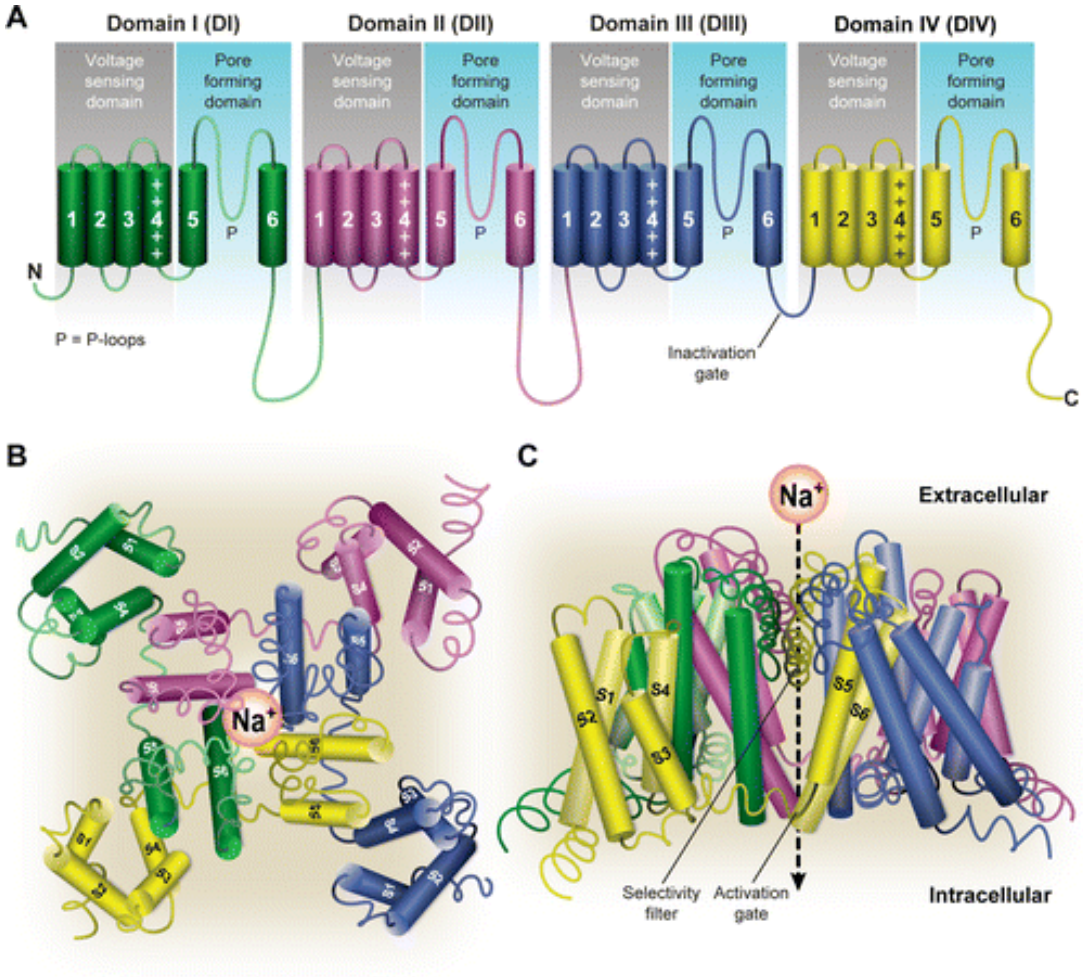

Figure 1.1. Structure of voltage-gated sodium channels. (A) Each channel consists of four homologous domains (in green, purple, blue, yellow) with each domain having six segments (numbered 1-6). Upon membrane depolarization segment six moves and head to the opening of the channel. The pore domain contains segment 5, 6 and the P loops. The intracellular loops have a role in inactivating the channel. (B) The extraocular and (C) the side view of the open channel (Adopted from (de Lera Ruiz and Kraus 2015).

SCN1A (NaV1.1) is a type 1 sodium voltage-gated channel and necessary for action potential propagation and axonal conduction. Mutation in *SCN1A* has been identified in more than 70% of individuals with epileptic encephalopathy (Harkin et al. 2007).

These patients have certain behavioural abnormalities such as impaired social interactions, anxiety, hyperactivity and cognitive impairment (Weiss et al. 2003). These phenotypes are very similar to those observed in ASD, hence a link between *SCN1A*, epilepsy and ASD. Furthermore, a mutation in *SCN1A* also showed autistic-like phenotypes (Li et al. 2011).

Another member of voltage-gated sodium channels is *SCN8A* ($Na_V1.6$) which is highly expressed in the cortex, hippocampus and cerebellum of the central nervous system (Schaller et al. 1995). They are abundantly expressed at the initial segment of axons where they initiate and propagate action potential and hence have a role in neuronal excitability (Schaller et al. 1995).

The proximal end of the axon is where the most sodium channels are highly abundant. In cortical pyramidal neurons, the action potential initiates from the distal part of the axonal initial segment (Van Wart et al. 2007). $Na_V1.6$ is predominantly expressed at the distal part of axons, and patch clamping by step depolarization showed activation threshold of -55 mV, while in axon initial segment the threshold activation was -43 V (Wenqin Hu et al. 2009). This explains the role of $Na_V1.6$ in lowering the threshold activation of action potential initiation. This also means that the membrane that has a higher level of $Na_V1.6$ is more excitable and has higher threshold activation.

Loss of homozygous *Scn8A* in null mice displayed motor deficits and difficulty in learning (Burgess et al. 1995). Heterozygous deletion of *Scn8A* showed the absence of seizures, anxiety and sleep disorder (Papale et al. 2009; Papale et al. 2010). An inherited frameshift mutation was observed in a child with intellectual disability and attention deficit hyperactivity disorder (Trudeau et al. 2006). More than 30 cases of de novo mutations have been identified with early infantile epileptic encephalopathy (Estacion et al. 2014; Vaher et al. 2014; Ohba et al. 2014). There were characterized by the presence of early-onset seizures, intellectual disability and autism (Estacion et al. 2014; Vaher et al. 2014; Ohba et al. 2014).

Potassium channels are heterogenic proteins, essential for setting resting membrane potentials, shaping action potentials and regulating neuronal firing. They contribute towards the neuronal excitability equilibrium. Deletion or mutation of potassium channels in animal models exhibited epilepsy and autistic-like characteristics

(D'Adamo et al. 2013). They were first discovered from a *shaker* mutant of *Drosophila melanogaster* (Tempel et al. 1987). Potassium channels are now classified into twelve members of Kv1 to Kv12 (Chandy and Gutman 1993). They comprise six transmembrane segments with four identical α pore forming subunits (Figure 1.2). Their structure is very similar to VGSCs with having a pore domain responsible for ion selectivity and gating properties (Figure 1.2).

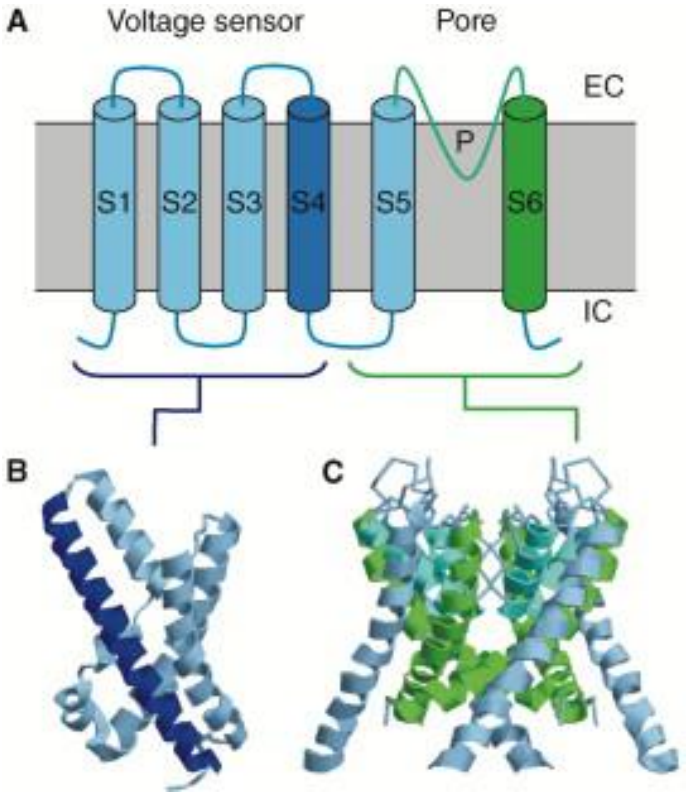

Figure 1.2. Structure of voltage-gated potassium channels. (A) They comprise of four subunits and six segments. S1-S4 act as voltage sensor and S5 and S6 make the pore domain for the passage of ions across the membrane. (B) The structure of the S4 domain in dark blue and S1 to S3 in pale blue. (C) The pore domain structure of the channel with S6 in green.

KCND2 which encodes for Kv4.2 subunit of voltage-gated potassium channels is referred as A-type current generator. They activate at sub-threshold membrane potentials, inactivates quickly and returns to its active states very rapidly (Zhu et al. 1999). They are highly clustered in pyramidal neurons of CA1 region of the hippocampus in which they are responsible for setting action potential threshold and repolarization as well as back-propagating the action potentials (Kim et al. 2007). Given the importance of this particular channel, mutations on this gene have been correlated to many neurological diseases. Mutations, rare variants of *KCND2* in

humans have led to temporal lope epilepsy (Singh et al. 2006) and autism (Okamoto et al. 2011; Mikhailov et al. 2008). Kv4.2 binds to fragile X mental retardation protein (FMRP) and is a contributor to fragile X syndrome, autism and intellectual retardation (Garber et al. 2008). Fragile X syndrome exists in 5% of individuals with ASD. FMRP protein has a key role in the maintenance of long-term depression, long-term potentiation and synaptic plasticity (Weiler et al. 1997; Huber et al. 2000). In the hippocampus, FMRP protein interacts with Kv4.2 and prevents its translation, leading to a reduced expression of Kv4.2 channel (Lee et al. 2011). This means that alterations in expression of Kv4.2 (that are dependent on FMRP abnormalities) can significantly be associated with fragile X syndrome and ASD conditions.

Calcium-activated potassium channels have also been implicated in neuropsychiatric disease (Chandy et al. 1998). For example, missense mutations have been found to alter the *KCNMA1* channel in an individual with ASD (Laumonnier et al. 2006). It is interesting that the family of these channels have been implicated in ASD, via interaction through FMRP protein (Deng et al. 2013).

Voltage-gated calcium channels mediate the influx of calcium into presynaptic terminal upon depolarization. This influx leads to a number of functions including neurotransmitter release and intracellular signalling. They comprise of a α subunit pore domain, determining the channel selectivity. There are ten $\alpha 1$ subunits, clustered into three different subfamilies Cav1, Cav2 and Cav3. They all have different patterns of expression and generate different currents (Catterall, Perez-Reyes, et al. 2005).

A de novo missense mutation in *CACNA1C* results in Timothy syndrome that have features of ASD along with language delay and social impairment (Bader et al. 2011). In addition, a single-nucleotide polymorphism in *CACNA1G* is associated with ASD (Strom et al. 2010), a T-type voltage-gated calcium channels contributing to neuronal firing (Lory et al. 2000). Loss of function mutation in *CACNA1A*, a P/Q type voltage-gated calcium channel has been associated with autism, ADHD, febrile seizures, episodic ataxia and refractory absence epilepsy (Damaj et al. 2015).

1.2.2.2 Cell surface adhesion molecules

Neuroligins are post-synaptic cell adhesion molecules that are expressed in both excitatory and inhibitory synapses (Song et al. 1999; Varoqueaux et al. 2004). They have large and small extracellular and intracellular domains with PDZ binding motif respectively. There are five neuroligin members, with *NLGN3* and *NLGN4X* been implicated in the etiology of ASD (Jamain et al. 2003). Mutant forms of *NLGN3* and *NLGN4X* results in a reduction of binding to cell surface adhesion molecules, neurexins at presynaptic terminals *in vitro* (Chih et al. 2004; Antony A Boucard et al. 2005). *Nlgn3* knockout mice showed deficits in excitatory NMDA receptor signalling (Chubykin et al. 2007). *NLGN2* mutant *Drosophila* showed a reduction in synaptic bouton and transmission (Chen et al. 2012). Many reports have established the Neuroligins are vital for synapse maintenance, function and maturation (Chih et al. 2005; Südhof 2008).

Contactin-associated protein-like 2 (CNTNAP2) belongs to the Neurexin superfamily and have been implicated in ASD (Alarcón et al. 2008). *CNTNAP2* gene encoded a transmembrane domain CASPR2. The main function of CASPR2 is to cluster potassium channels at the juxtaparanodes of myelinated axons (Poliak et al. 2003). It is highly expressed in human fetal brain with a distribution gradient towards the frontal lobe of the cortex, indicating a role for cognition and language and a role in ASD (Abrahams et al. 2007). Individuals with a mutation in *CNTNAP2* exhibit cortical dysplasia-focal epilepsy syndrome, in which they show characteristic features of ASD (Strauss et al. 2006). Rare single base pair mutation in *CNTNAP2* have also been implicated in ASD (Alarcón et al. 2008). *Cntnap2* mutant mice showed impairment in the number of interneurons, deficits in neuronal activity as well as hyperactivity and epileptic seizures (Peñagarikano et al. 2011). Furthermore, treatment of the *Cntnap2* mutants with antipsychotic risperidone was able to reduce repetitive behaviours, confirming the role of *Cntnap2* in neuronal development and ASD in the mouse model (Peñagarikano et al. 2011).

Two other members of cell adhesion molecules are cadherins (CDHs) and protocadherins (PCDHs). They are involved in synaptic function and formation (Arikkath and Reichardt 2008) in which their reduction in brain results in deficits in neuronal functionality and connectivity (Redies et al. 2012). Homozygous deletion of

protocadherins (*PCDH10*) have been reported in children with ASD (Morrow et al. 2008).

Neurexins are another member of cell adhesion proteins which are predominantly expressed in the presynaptic membrane (K Ichtchenko et al. 1995). Neurexins are surface proteins that interact with Neuroligins, glutamate receptor delta 2 and leucine-rich repeat trans-membrane neuronal proteins at the post-synaptic terminus (Dean et al. 2003; Scheiffele et al. 2000). Neurexins are the prime example of adhesion surface proteins at the pre-synaptic terminus, the most extensively studied modulators of synaptic activity (Brose 1999; Ushkaryov *et al.* 2009). Copy number variations are the significant cause of many genetic diseases (Rujescu et al. 2009). *NRXN1* deletions have been associated with many neurodevelopmental and psychiatric disorders (Schaaf et al. 2012; Marshall et al. 2008; Ching et al. 2010; Dabell et al. 2013), presumably causing an imbalance in excitatory and inhibitory synaptic transmission (Chubykin et al. 2007). Such disruptions are involved in ASD (Marshall et al. 2008; Wang et al. 2009; Bucan et al. 2009; Ching et al. 2010; Béna et al. 2013; Viñas-Jornet et al. 2014), schizophrenia (Need et al. 2009; Kirov et al. 2014; Vrijenhoek et al. 2008; Rujescu et al. 2009; Todarello et al. 2014), mental retardation (Zahir et al. 2008), ADHD (Wiśniowiecka-Kowalnik et al. 2010) and epilepsy (Gregor et al. 2011; Møller et al. 2013; Schaaf et al. 2012; Béna et al. 2013; Dabell et al. 2013). A summary of *NRXN1* deletions from the literature was performed in 2015. This includes patient ID number, their coordinate of deletion and indicated phenotypes that they have been diagnosed (ID (intellectual disability), EP (epilepsy), MCD (motor coordination deficit), ASD (autism spectrum disorder), SCZ (schizophrenia), DD (developmental delay), SD (speech delay), MD (motor deficits), ADHD (attention hyperactivity disorder)) (Table 1.3).

Table 1.3. Phenotypic diversity associated with *NRXN1* deletion.

Reference	Patient	Original Coordinates (Hg19)	ID	EP	MCD	ASD	SCZ	DD	LD	SD	MD	ADHD
Schaaf et al	E16	chr2 49885294 50046403		✓		✓						
Schaaf et al	E17	chr2 49885294 50046403		✓		✓						
Wisniowiecka-Kowalnik et al	family 2	chr2 50006408 50200141				✓			✓			
Wisniowiecka-Kowalnik et al	Family 1	chr2 50034351 50413346				✓						
Wisniowiecka-Kowalnik et al	family 3	chr2 50106298 50437268				✓						
Dabell et al	34a	chr2 50118810 50179711				✓		✓				
Bena et al	1	chr2 50194000 51344000	✓			✓						
Gregor *et al*	N2	chr2 50270203 51257206	✓									
Bena F *et al*	13	chr2 50359788 50584706	✓	✓					✓			
Dabell M *et al*	33a	chr2 50271164 50936973						✓				
Bena F *et al*	5	chr2 50376840 50845795	✓	✓					✓			
Dabell M *et al*	29	chr2 50480647 50600362				✓						
Dabell M *et al*	28a	chr2 50503145 50865069				✓						
Schaaf *et al*	E11	chr2 50545885 50922836				✓						
Schaaf *et al*	E12	chr2 50545885 50922836	✓	✓		✓						
Schaaf *et al*	E13	chr2 50545885 50552890		✓	✓							✓
Dabell M *et al*	18	chr2 50664886 51250425	✓			✓						
Bena F *et al*	7	chr2 50642229 51040803	✓			✓		✓	✓			
Dabell M *et al*	30	chr2 50680324 50720466				✓						
Bena F *et al*	17	chr2 50693782 50909965		✓				✓				

Bena F *et al*	12	chr2 50815420 51083778				✓		✓	✓			
Gregor *et al*	N5	chr2 50861527 51090563	✓	✓								
Bena F *et al*	21	chr2 50897002 51006610	✓			✓			✓			
Dabell M *et al*	19	chr2 50900500 51020557				✓		✓				
Schaaf *et al*	E10	chr2 50902643 51036715				✓						✓
Bena F *et al*	22	chr2 50975394 51079873	✓									
Bena F *et al*	2	chr2 50797032 51412595				✓						
Bena F *et al*	6	chr2 50783685 51180001	✓	✓		✓			✓			
Schaaf *et al*	E9	chr2 50753008 51666029	✓									✓
Bena F *et al*	10	chr2 50847740 51170975		✓		✓		✓	✓			
Gregor *et al*	N1	chr2 50860393 51208000	✓	✓								
Dabell M *et al*	12	chr2 50890607 51167934	✓									
Schaaf *et al*	E7	chr2 50892598 51125770				✓						
Bena F *et al*	9	chr2 50894976 51223965	✓			✓			✓			
Dabell M *et al*	13	chr2 50928021 51157870		✓				✓				
Ching *et al*	4	chr2 50936914 51167934				✓						
Bena F *et al*	24	chr2 50941534 51421039				✓			✓			
Bena F *et al*	25	chr2 50941534 51421039				✓			✓			
Dabell M *et al*	11	chr2 50989149 51178152				✓						
Dabell M *et al*	15	chr2 50999149 51130917		✓								
Bena F *et al*	19	chr2 50963194 51144527	✓	✓		✓		✓	✓			
Schaaf *et al*	E5	chr2 51006222 51167932	✓		✓	✓						✓
Schaaf *et al*	E8	chr2 51017041 51307360		✓	✓							✓
Bena F *et al*	18	chr2 51029000 51212526	✓	✓		✓		✓				

Gregor *et al*	N6	chr2 51033865 51496143	✓									
Schaaf *et al*	E4	chr2 51036654 51125770				✓						
Schaaf *et al*	E3	chr2 51056636 51167934	✓		✓				✓			
Ching *et al*	6	chr2 51059410 51316396			✓	✓					✓	
Ching *et al*	7	chr2 51090504 51212385	✓			✓						
Schaaf *et al*	E2	chr2 51096075 51415269										✓
Dabell M *et al*	37	chr2 51124517 51354094		✓				✓				
Dabell M *et al*	4	chr2:50989149-51675291				✓						
Dabell M *et al*	3	chr2 51020497 51178152		✓				✓				
Dabell M *et al*	5a	chr2 50996352 51555511		✓				✓				
Schaaf *et al*	E14	chr2 50160134 50481919				✓						
Bena F *et al*	4	chr2 50638683 51168031						✓				
Ching *et al*	9	chr2 50689280 50853329							✓			
Bena F *et al*	20	chr2 50953916 51105061							✓			
Dabell M *et al*	7	chr2 50788065 51318184						✓				
Ching *et al*	3	chr2 50897002 51212385									✓	
Bena F *et al*	16	chr2 50898579 51114964						✓	✓			
Dabell M *et al*	17	chr2 50900500 51124577						✓				
Dabell M *et al*	9	chr2 50900500 51211695						✓				
Dabell M *et al*	16	chr2 50928021 51124577	✓					✓				
Dabell M *et al*	8	chr2 50989149 51211695							✓		✓	
Dabell M *et al*	6	chr2 50989149 51354094						✓				
Dabell M *et al*	2	chr2 51020497 51178152						✓				
Dabell M *et al*	1	chr2 51079673 51459761						✓				

Todarello G *et al*	family 8 mother	chr2 50270339 50295780					✓					
Todarello G *et al*	family 2 father	chr2 50735657 50800548					✓					
Todarello G *et al*	family 9 mother	chr2 50735657 50800548					✓					
Todarello G *et al*	family 3 mother	chr2 50947040 50979926					✓					
Ching *et al*	10	chr2 50714297				✓						

1.2.3 Copy number variations

Autosomal genes are normally two copies, one copy from father and another from mother. Copy number variation (CNV) refers to genetic alterations as results of microduplication or microdeletion, via either inherited or de novo mutations. CNVs have been implicated on an strong genetic contributor to many complex neurodevelopmental diseases (Sebat et al. 2007; Christian et al. 2008; Marshall et al. 2008; Luo et al. 2012). These CNVs are deletions or duplications of genes in forms of familial or de novo inheritance. The common causes of developmental delays are based on deletions or duplications, in which the structure, expression and function of a gene is disturbed. Deletion and duplication in many loci have been associated with ASD, and even rare cases of CNVs have been detected by genome-wide arrays (Ma et al. 2009), and these include, for example, duplication within 15q13 (Christian et al. 2008), microdeletion within 16p11.2 (Sebat et al. 2007; Marshall et al. 2008; Weiss et al. 2008), Prader-Willi syndrome at 15q11-1 and Williams syndrome within 7q11.23 (Glessner et al. 2009; Sanders and Ercan; Sanders et al. 2011).

Pinto *et al* assessed both de novo and rare CNVs in cohorts of over 2000 ASD individuals to characterize associated ASD genes to identify their biological relationships and pathways (Pinto et al. 2014). This study showed that there were a strong enrichment in post-synaptic density (PSD) and fragile X mental retardation proteins (*FMRP*), underlying the genes which have a susceptibility to ASD (Pinto et al. 2014). *FMRP* belongs to multiple signalling pathways such as P13K-RAS-MAPK and P13K-Akt-TSC-PTEN-mTOR which have been reported before in ASD individuals by both over-expression and under-expression (Ascano et al. 2012). Their results further demonstrated that genes associated with ASD participate in a wide

range of processes and pathways, i.e. MAPK (Pinto et al. 2014) (Figure 1.3). The SAFARI gene analysis also showed that MAPK is one of the top enriched pathways in ASD (Wen et al. 2016).

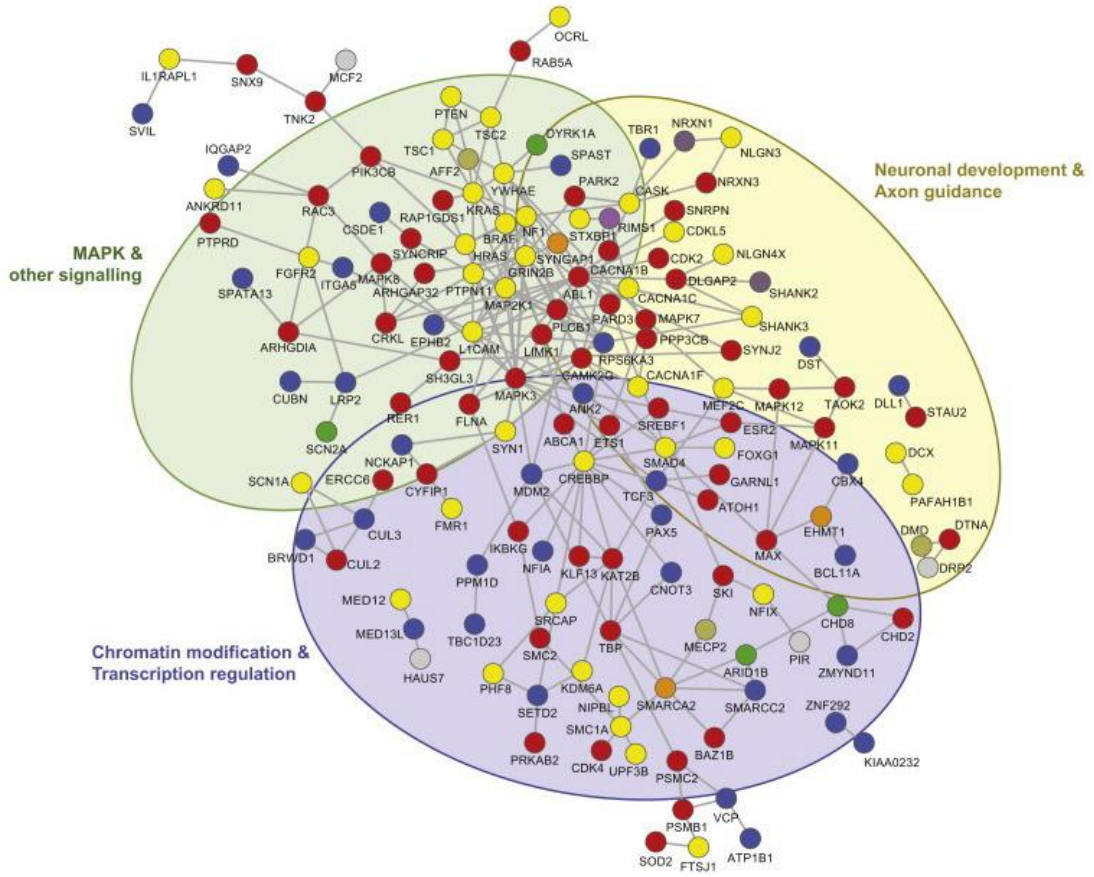

Figure 1.3. Genes affected by CNVs and SNVs in ASD. ASD pathway network are grouped together into three different classes, neuronal development and axon guidance, MAPK & other signalling pathways and chromatin modification and transcription regulation. Genes in red were identified by de novo CNVs, genes in blue were detected by de novo LoF (loss of function). SNVs from published exome sequencing and genes in white were affected by hemizygous LoF. SNVs on the X chromosome of males and genes in yellow were known to be implicated in ASD. Genes in orange, purple, green, dark yellow, or dark purple correspond to those in two or more lists. Shaded ovals represent enriched biological functions with >10% genes in the network involved (Adopted from (Pinto et al. 2014))

Pinto *et al* further evaluated and combined all CNVs with single nucleotide variation (SNVs) from previous exome sequencing (Iossifov et al. 2015; Neale et al. 2012). Among all the genes, 11 were found to be affected on both CNVs and SNVs (*NRXN1*, *SHANK2*, *ARID1B*, *RIMS1*, *TRIP12*, *SMARCC2*, *DLL1*, *TM4SF19*, *MLL3*, *PHF2* and

CSTF2T) (Pinto et al. 2014). Further analysis using network-based analysis of genomic variation (NETBAG), three genes (*NRXN1*, *SHANK2*, *RIMS1*) were found to be enriched and overlapped (Figure 1.4) (Pinto et al. 2014). This strongly suggests the association of *NRXN1* and *SHANK2* in ASD (Figure 1.4).

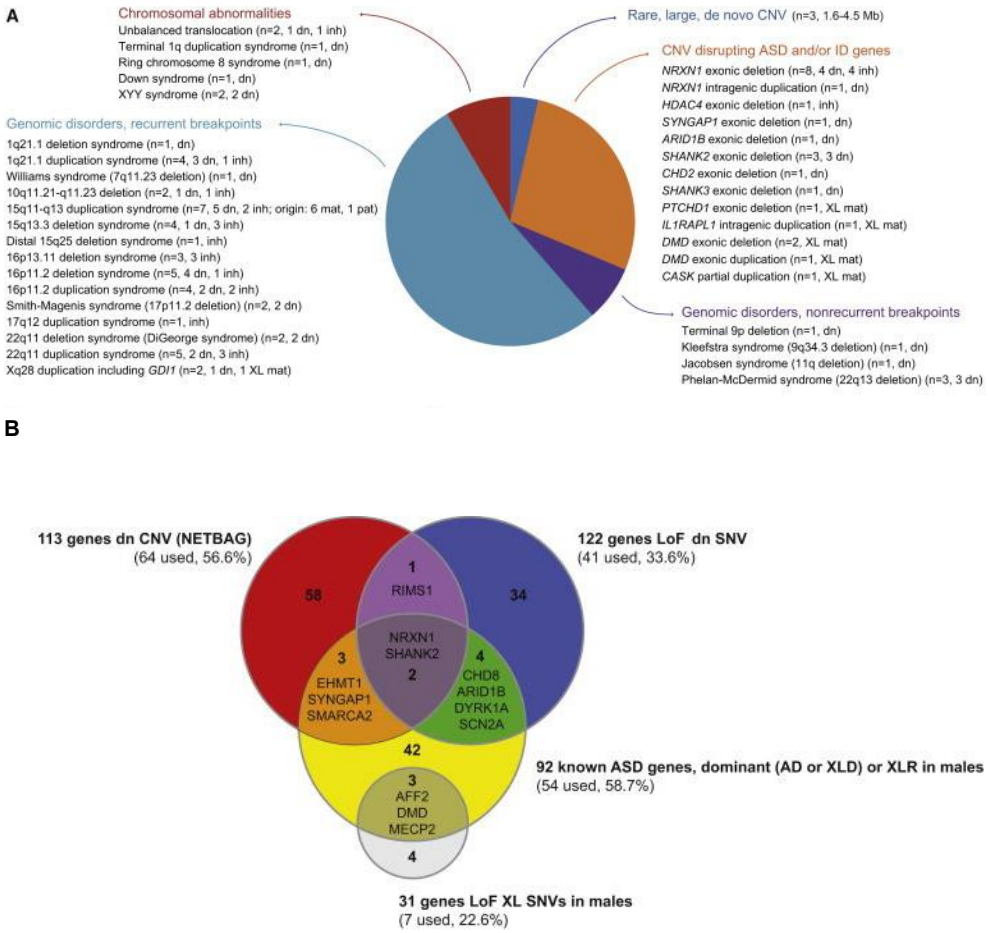

Figure 1.4. NRXN1 is one of the most prominent risk factors in ASD. (A) Pie chart displaying the proportion for each of five categories. The number of events and inheritance are in parentheses. (B) *NRXN1* and *SHANK2* are the common risk factors, from the Venn diagram. This diagram overview 151 genes resulting from a DAPPLE analysis of 336 unique genes, compiled of 113 genes identified from de novo CNVs by NETBAG, 122 genes with de novo LoF SNVs from four published exome sequencing studies, 31 genes with hemizygous LoF SNVs on the X chromosome of male ASD subjects, and 92 ASD-implicated genes previously described as autosomal dominant, X-linked dominant, or X-linked recessive in males (Adopted from (Pinto et al. 2014).

It is interesting that genes which are associated with ASD have a key role in modulating synaptogenesis. For example *NLGN4* (Jamain et al. 2003), *TBX1*, *PCDH10* (Morrow et al. 2008) and S*HANK3* (Gauthier et al. 2009; Durand et al. 2007). In addition, genes such neurexin1 (*NRXN1*) (Marshall *et al.*, 2008; Wang *et al.*,

2009., Bucan *et al.*, 2009; Ching *et al.*, 2012; Bena *et al.*, 2013; Vinas-Jornet M *et al.*, 2014), *CNTNAP2* (Bakkaloglu et al. 2008), *NLGN1* (Glessner et al. 2009) and *DLGAP2* (Pinto et al. 2010) have been implicated as ASD risk factors. A list of all genes implicated in the pathogenesis of ASD are listed in Table 1.4 (Banerjee et al. 2014).

Table 1.4. Conserved genes which are associated and implicated in ASD (Banerjee et al. 2014)**.**

Gene name	Protein description	Nature of abnormality	Reference
NRXN1	Transmembrane	Mutation, CNVs	(Feng et al. 2006)
NRXN2	Transmembrane	Mutation	(Arstikaitis et al. 2011)
NRXN3	Transmembrane	Mutation	(Vaags et al. 2012)
NLGN1	Transmembrane	Genetic association	(Glessner et al. 2009)
NLGN3	Transmembrane	Mutation	(Jamain et al. 2003)
NLGN4	Transmembrane	CNVs	(Jamain et al. 2003)
CNTN3	Ig-CAM	Mutation, CNVs	(Morrow et al. 2008)
CNTN4	Ig-CAM	Mutation	(Roohi et al. 2009)
CNTNAP2	Transmembrane	Mutation, genetic association	(Arking et al. 2008)
NrCAM	Ig-CAM	Genetic association	(Marui et al. 2009)
CDH9/10	Transmembrane	Genetic association	(Bucan et al. 2009)
CDH18	Transmembrane	Chromosomal abnormality	(Marshall et al. 2008)
PCDH9	Transmembrane	Mutation	(Marshall et al. 2008)
PCDH10	Transmembrane	Mutation	(Morrow et al. 2008)
PCDH19	Transmembrane	Mutation	(Bucan et al. 2009)
SHANK1	Scaffolding	Mutation	(Sato et al. 2012)
SHANK2	Scaffolding	Mutation	(Berkel et al. 2010)
SHANK3	Scaffolding	Mutation	(Durand et al. 2007)
DLG4	Scaffolding	SNPs	(Feyder et al. 2010)
HOMER1	Scaffolding	Mutation	(Kelleher et al. 2012)
cAMP-GEF	Cytoskeletal	Mutation	(Bacchelli et al. 2003)
RELN	Secreted	Genetic association	(Persico et al. 2001)
EN2	Transcription factor	Genetic association	(Gharani et al. 2004)

These evidence explain that synaptic plasticity might be an important molecular mechanism in the pathophysiology of autism. For instances, *NRXNs* are presynaptic cell adhesion molecules that interact with Neuroligins at post-synaptic terminals and

have a key role in synaptic formation and maintenance (Missler et al. 2012). Alternative splicing in Neuroligins regulates synaptic diversity by interacting with various receptors at the post-synaptic terminus, i.e. NMDA, AMPA and GABA-ergic receptors (Missler et al. 2012). Furthermore, *SHANKs* are scaffolding proteins that are important for the function of synapses (Böckers et al. 2001) and couples with NRXNs-NLGNs complex.

1.2.4 Brain structure in ASD

Neuroimaging approach has been widely used to detect an abnormality in the brain *in vivo*. Magnetic Resonance Image (MRI) have shed light on the underlying characteristics of many neurodevelopmental diseases (Ecker et al. 2015). For example, by using structural MRI (sMRI) an abnormality in the grey and white matter of ASD individuals have been found (Schumann et al. 2010).

One of the most consistent differences between ASD and typically developing control brain is the total brain volume. Studies showed enlarged total brain volume (frontal and temporal lobes) at early age of 2-4 years in some of ASD individuals (Nordahl et al. 2011). However, this usually follows by a decline or no difference in ASD brain volume at later on in life. (Lange et al. 2015). The pathological mechanism that underlies this enlargement in brain volume is unknown. A recent study showed that the enlarged brain volume before the age of 2 years could be caused by expansion of cortical area rather than its thickness (Hazlett et al. 2011). This explains that the impairment in the white matter of ASD brain affects the acceleration of the cortical gray area.

Different phenotypes observed in ASD such as deficits in social behaviours, language processing and repetitive behaviours are associated with a core region of the brain. For example, the parietal cortex, amygdala and frontal lobe may be associated with social behaviours (Adolphs 2001). Furthermore, the caudate nucleus has been linked to repetitive behaviours (Atmaca et al. 2007).

The thickness of different regions of cortex have been measured in ASD in an age range of 3 to 39 years and showed thinner cortices and a reduction in its surface area in an age-dependent manner (Ecker et al. 2014). The brain overgrowth observed in ASD individuals in childhood might affect the geometry of the brain, i.e. cortical shape

and patterns. The mechanical tension of axonal white matter might be an underlying cause of abnormality in cortical folding (Van Essen 1997). During early adolescence and adulthood in ASD individuals, the cortical folding is accelerated in the bilateral posterior region of cortex with increased gyrification (Wallace et al. 2013). On the other hand, in the right inferior frontal and medial parieto-occipital region of cortex in children with ASD, the level of gyrification is significantly reduced (Schaer et al. 2013). These results show that the level of gyrification in ASD patients alter throughout the lifespan.

1.2.5 Animal models of ASD

There have been many animal studies to model ASD, mostly recapitulating the major phenotypes associated with ASD, including repetitive behaviours and deficits in social and communication interactions. There are many mouse models of ASD available by knockout of specific genes that are thought to contribute to ASD. For example, there are mouse models of Phelan-McDermid syndrome which recapitulate the syndromic forms of ASD achieved by *Shank3* knockout (Peça et al. 2011), *Mecp2* in Rett syndrome (Shahbazian et al. 2002), *Cacna1c* in Timothy syndrome (Bader et al. 2011) and *Fmr1* in fragile X syndrome (Ronesi et al. 2012). There are also knockout mice models which represent a non-syndromic form of ASD, i.e., Neuroligin 3 knockout (Baudouin et al. 2012). Other mouse models of ASD have included a lesion in 16p11.2 model of autism (Horev et al. 2011), 22q11.2 mouse model lacking *Pten* (Zhou et al. 2009), mutant *Shank2* (Won et al. 2012) and *Cntnap2* (Peñagarikano et al. 2011).

There is also a model of autism in rats in which valproic acid is used as an environmentally triggered form of ASD (Rodier et al. 1997). Injection of valproic acid before neuronal tube closure is associated with disrupted inhibitory circuits, reduced Purkinje cells, repetitive behaviour and hyperactivity (Gogolla et al. 2009). Zebrafish also have been used with less popularity to mouse models for modelling the genetic basis of autism (Tropepe and Sive 2003). Zebrafish model has been used to investigate brain development and neuronal connections in ASD, but it is difficult to recapitulate the behavioural phenotypes (Tropepe and Sive 2003).

Studies have shed light on some of the key genes which are associated with ASD, such as Neurexin 1 (Li et al. 2007; Zeng et al. 2007), Neuroligin 1 and 2 (Banovic et al.

2010; Chen et al. 2012) using *Drosophila*. Other invertebrates such as *Aplysia* showed that the interaction between neurexin and neuroligin is essential for storage of long-term memory, a deficit implicated in ASD (Choi et al. 2011). *C. elegans* also been used to study the neuronal synaptic communication and abnormalities which are apparent in ASD (Calahorro and Ruiz-Rubio 2012). All of these ASD models will aid in understanding the complex aetiology of ASD. This will help researchers to find the underlying functional deficits that are implicated in ASD.

1.3 Neurexin and their Significance

Neurexins are a potential risk factor for not only ASD but also other neurodevelopmental and neuropsychiatric diseases, as discussed in previous sections. Neurexins are a particular class of synaptic proteins that are one of the key elements in governing the dynamics of neuronal circuits (Südhof 2008). Currently, they are the most studied regulators of synaptic properties.

1.3.1 Neurexins: Structure & expression

There are three neurexin genes, *NRXN1*, *NRXN*2 and *NRXN*3, and two major isoforms of larger α and shorter β encoded by each neurexin gene (Ushkaryov et al. 1992; Ichtchenko et al. 1996). The long isoform of α-neurexins consists of six laminin/neurexin/sex (LNS) hormone binding globulin domains extracellularly, which are separated by three epidermal growth factor-like domains (Figure 1.5A). They have a short cysteine-loop domain, transmembrane domain followed by a cytoplasmic sequence. The short form of β-neurexins are transcribed from a different promoter and are effectively N-terminally truncated and are a shorter version of α-neurexins with a short and specific N-terminal motif (Figure 1.5A). *NRXN1* and *NRXN3* are much more closely related in comparison to *NRXN2* (Treutlein et al. 2014). All three Neurexins are equally expressed in the brain with subtle neuroanatomical differences, but α-neurexins are much more abundant in comparison to β-neurexins (Aoto et al. 2013; Schreiner et al. 2014). Neurexin expression in the brain occurs early in brain development and is prior to synapse formation, perhaps for synthesizing essential synaptic proteins (Daly and Ziff 1997).

The expression of neurexins varies during development, and over 1000 different isoforms may be produced due to alternative splicing sites and differential promoter usage (Ullrich et al. 1995; Schreiner et al. 2014). The alternative splicing occurs at six different canonical sites (segment 1 -segment 6) (Ullrich et al. 1995; Schreiner et al. 2014). This results in expression of different spliced sequences at a typical neuronal type (Fuccillo et al. 2015). At both single cell level and specified brain region, the expression of all neurexins seems uncorrelated, which creates a significant difference in alternative splicing among neurexins (Figure 1.5B). The *NRXN1* signalling is coupled to both excitatory and inhibitory synapses (Figure 1.5C).

1.3.2 Neurexins: Ligands and receptors

One of the first described Neurexin ligands were Neuroligins (Konstantin Ichtchenko et al. 1995; Ichtchenko et al. 1996). In total, Neurexins binds to at least seven different postsynaptic protein families, i.e. Dystroglycans, Cerebellins, LRRTMs and Latrophilins. There are three well-defined ligands binding site for Neurexins: (1) binding to Neurexophilins and Dystroglycans can be specifically mediated via LNS2 domain of α-Neurexins (Missler et al. 1998; Sugita et al. 1998); (2) LNS6 which is shared between both α and β isoforms and bind to Neuroligins, Cerebellins, Latrophilins, LRRTMs and GABA-A receptors (K Ichtchenko et al. 1995; Ichtchenko et al. 1996; Ko et al. 2009; de Wit et al. 2013; Siddiqui et al. 2013; Uemura et al. 2010; C. Zhang et al. 2010; A A Boucard et al. 2005)**,** and (3) binding to CA10, CA11 and C1qls can be achieved through both α and β isoforms (Sterky et al. 2017; Matsuda et al. 2016) (Figure 1.5D).

All the mentioned ligand-receptor interactions are hugely dependent on alternative splicing (Figure 1.5D). The interactions between Neurexins and Neuroligins are regulated by SS4 splicing sequence, in addition of splicing site called SSB at Neuroligins (Antony A Boucard et al. 2005; Chih et al. 2006). The β -Neurexins with a lack of SS4 insert bind only to Neuroligin1 that contain an insert of SSB (Tanaka et al. 2011). However, all Neuroligins that contain an insert of SSB can bind to all α and β neurexins (Tsetsenis et al. 2014; Chih et al. 2006; Comoletti et al. 2006). Interactions of Neurexins with other postsynaptic ligands are also regulated by alternative splicing at SS4 within the LNS6 domain. For example, Cerebellins only

interact with Neurexins that have an insert of SS4 (Uemura et al. 2010), while Latrophilins only bind to SS4^{-} Neurexins (Boucard et al. 2014).

(A)

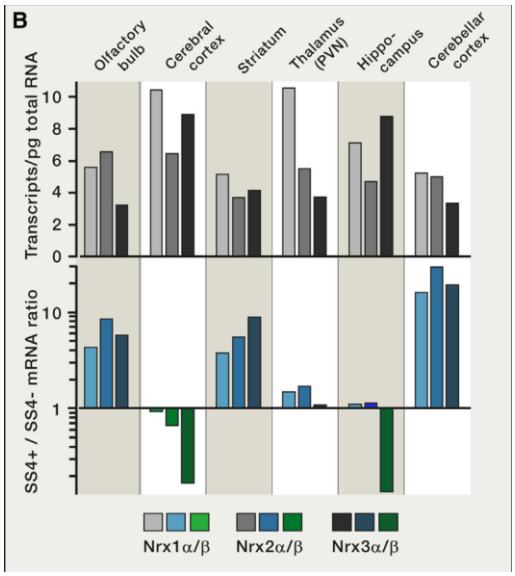

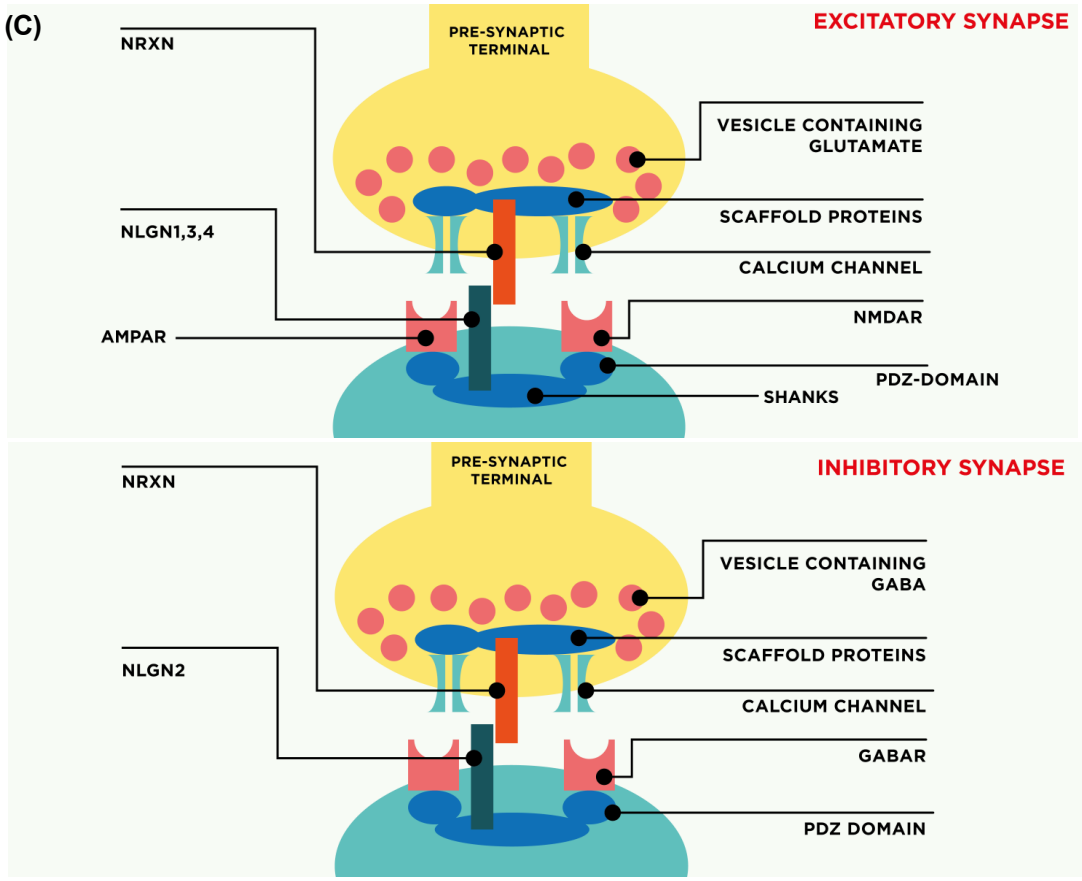
(C)
EXCITATORY SYNAPSE
NRXN
PRE-SYNAPTIC TERMINAL
VESICLE CONTAINING GLUTAMATE
SCAFFOLD PROTEINS
NLGN1,3,4
CALCIUM CHANNEL
NMDAR
AMPAR
PDZ-DOMAIN
SHANKS
INHIBITORY SYNAPSE
NRXN
PRE-SYNAPTIC TERMINAL
VESICLE CONTAINING GABA
SCAFFOLD PROTEINS
NLGN2
CALCIUM CHANNEL
GABAR
PDZ DOMAIN

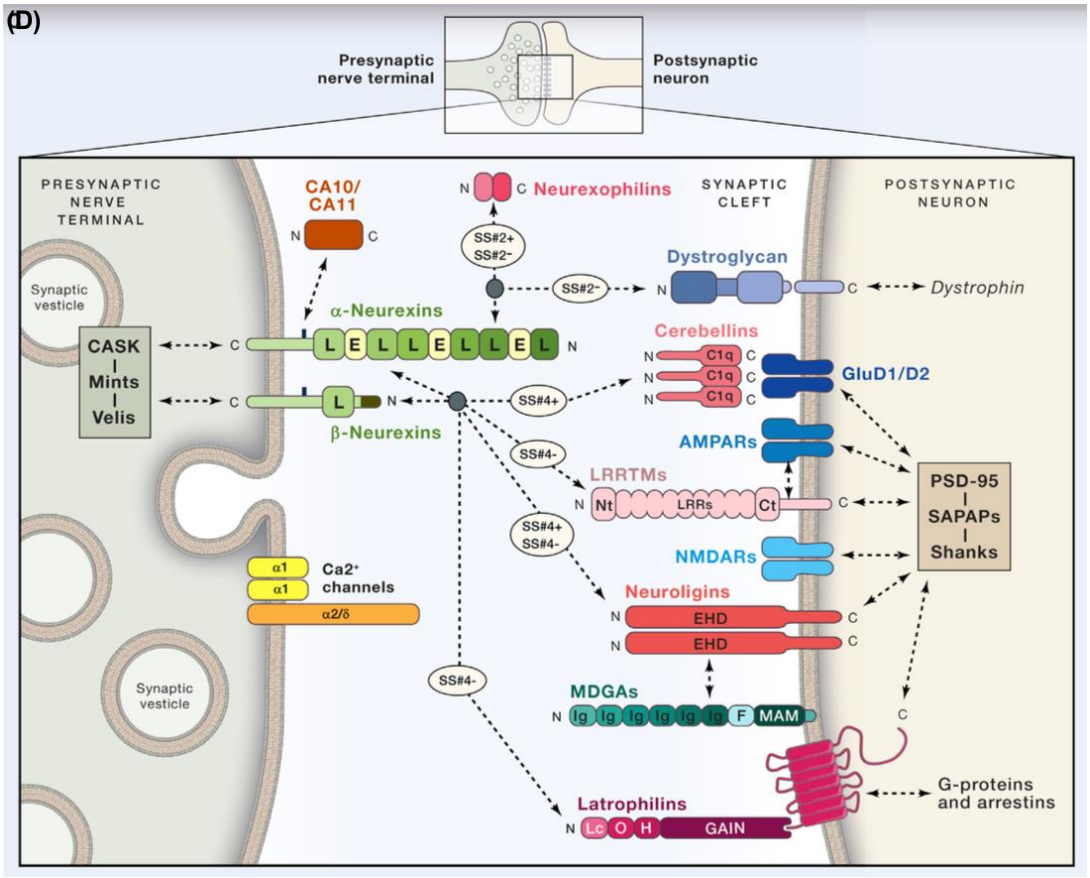
(D)
Presynaptic nerve terminal
Postsynaptic neuron
PRESYNAPTIC NERVE TERMINAL
SYNAPTIC CLEFT
POSTSYNAPTIC NEURON
CA10/ CA11
Neurexophilins
SS#2+ SS#2-
Dystroglycan
Dystrophin
Synaptic vesicle
α-Neurexins
CASK
Mints
Velis
Cerebellins
C1q
GluD1/D2
β-Neurexins
AMPARs
LRRTMs
Nt
LRRs
Ct
PSD-95
SAPAPs
Shanks
NMDARs
α1
α1
α2/δ
Ca2+ channels
Neuroligins
EHD
MDGAs
Ig
F
MAM
Latrophilins
Lc
O
H
GAIN
G-proteins and arrestins

Figure 1.5. Neurexin Domain structure and alternative splicing. (A) The extracellular part of *NRXN1a* consists of six-laminin/neurexin/sex hormone (LNS) binding globulin domains separated by three epidermal growth factor (EGF)-like domains, which are followed by an O-linked sugar attachment domain (O-Glyc). The β-NRXNs are truncated version of α-NRXNs, sharing LNS6, O-linked sugar attachment region, a single transmembrane domain and a short C-terminal tail. (B) total RNA expression of *Nrxn1*,2 and three at different brain region (grey bars at the top) and mRNA expression of the SS4+/SS4- splice isoform ratio (bottom bars blue and green) in mice shows a dramatic difference in Neurexin splice sequencing expression (adapted from review by (Südhof 2017). (C) Neurexin is involved in both excitatory and inhibitory synapses with interaction of α and β Neurexins to different ligands at the postsynaptic membrane (D). Intracellularly Neurexins at presynaptic nerve terminus bind to CASK, Mints and velis. At extracellular region, they bind to various ligands depending on their spliced sequence (B & C are adapted from review by (Südhof 2017).

1.3.3 Neurexins: Function

As mentioned previously, *NRXN1* is significantly associated with ASD (Pinto et al. 2014). Most of the *NRXN1* mutations are heterozygous copy number variations, with truncation or missense mutations being less frequent (Gauthier et al. 2011; Enggaard Hoeffding et al. 2014; Todarello et al. 2014).

Although the exact function of *NRXNs* remains unknown, at this point, there are few key results that may suggest the Neurexin functions. In 2003, the constitutive knockout of all three α Neurexins in mice impaired synaptic transmission through an alteration in calcium influx during an action potential, in addition to early postnatal death caused by a failure in the respiratory system (Missler et al. 2003). Missler *et al.* (2003) showed that deletion of compound α-neurexins in newborn mice caused a reduction in spontaneous neurotransmitter release (Missler et al. 2003). This was performed on cultured slices from neocortex and acute slices from the brainstem (Missler et al. 2003). The results showed a significant reduction in the frequency of both excitatory and inhibitory spontaneous miniature postsynaptic activity (Missler et al. 2003). This reduction was not due to the number of postsynaptic AMPA or GABA-A receptors, but partly due to impairment in calcium channel function (Missler et al. 2003).

Two years later, Zhang *et al.* investigated that Neurexin domain and voltage-gated calcium channel caused this impairment (Zhang et al. 2005). They demonstrated that the transgenic *Nrxn1α* could rescue the alteration in neurotransmitter release and calcium current phenotypes. Furthermore, the N and P/Q type voltage-gated calcium channels are selectively affected by *Nrxn1α* knockouts (Zhang et al. 2005). These

findings suggest that α-Neurexins couple and regulate neurotransmission through N and P/Q type voltage-gated calcium channels (Missler et al. 2003).

Reduction in frequency of miniature excitatory spontaneous synaptic transmission was also observed in hippocampal CA1 pyramidal neurons of homozygous *Nrxn1α* knockout mice (Etherton et al. 2009). The behavioural phenotypes of this model showed impairment in nest building activity and an increase in grooming behaviours and no change in spatial learning, at least in part similar to phenotypes observed in human patients (Etherton et al. 2009). This behavioural phenotype was further studied in heterozygous *Nrxn1α* knockout mice (Laarakker et al. 2012). Their results identified an increase in locomotor activity and habituation when exposed to the new environment, only observed in male mice (Laarakker et al. 2012). This reflects the sex-dependent differences in behavioural phenotypes in a mouse model of heterozygous *Nrxn1α* deletion (Laarakker et al. 2012).

A study by Grayton *et al.* (2013) was designed to investigate the behavioural deficits in the *Nrxn1α* knockout model (Grayton et al. 2013). They showed that the KO male mice had an increased aggressive behaviour, which increases their social approach toward intruders and a reduction in locomotor activity. This aggression was not observed in female *Nrxn1α* (Grayton et al. 2013). The male *Nrxn1α* KO mice showed reduced social approach towards the juvenile conspecific, in social sniffing investigation task. The social behaviour alterations were in contrast with studies reported by Etherton *et al.* (2009) and Laarakker et al. (2012), where no significant alteration was found. However reduction in nest building behaviour, which is an aberrant indication of social behaviour (Lijam et al. 1997), was replicated in both Grayton *et al.* (2013) and Laarakker *et al.* (2012) findings (Grayton et al. 2013).

Conditional knockout of all β-Neurexins also caused a synaptic impairment but no lethality (Anderson et al. 2015). In this study, the presynaptic release probability was suppressed in cultured CA1 hippocampal neurons in the subiculum, and this was caused by disinhibition of postsynaptic endocannabinoid synthesis (Anderson et al. 2015). This results in increased secretion of endocannabinoid, which subsequently activated presynaptic CB1-receptors and hence impairment and inhibition in neurotransmitter release (Anderson et al. 2015). This study strongly suggests that β-

Neurexins have a functional property on post-synaptic endocannabinoid synthesis, independent of α-Neurexins (Anderson et al. 2015).

A recent study has confirmed that Neurexins exert different functions at different types of synapses (Chen et al. 2017). Chen et al. showed that conditional triple knock-out of all Neurexins caused a loss in synapses but no change in action potential-dependent calcium influx in parvalbumin-positive inhibitory neurons in the prefrontal cortex (Chen et al. 2017). In contrast, the same deletion caused no alteration in synapse number, but a significant decrease in action potential triggered calcium influx in somatostatin-positive inhibitory neurons (Chen et al. 2017). These results imply that Neurexins may not have a canonical regulatory function in all types of neurons but have distinct mechanisms in different types of synapses. However, it is still possible that Neurexins have a canonical functional role in presynaptic calcium channel, as the same phenotype observed in both pan-α-Neurexin and pan-αβ-Neurexin knockout mice in the same synapses, but this phenotype were diminished in other synapses with no explained reason (Missler et al. 2003; Chen et al. 2017). It is very difficult to conclude whether each Neurexin in pan-αβ Neurexin knockout shows distinct phenotypes in different synapses. *Nrxn3* is the only well-studied Neurexin member, which can partly answer this question (Aoto et al. 2013; Aoto et al. 2015).

The conditional deletion of *Nrxn3* in mice showed that there was a decrease in AMPA receptor-mediated excitatory response due to a loss in a number of AMPA receptors, when examined in the hippocampal CA1 region (Aoto et al. 2013; Aoto et al. 2015). However, the same deletion also showed a decrease in GABA receptor-mediated inhibitory synapse at olfactory bulb neurons (Aoto et al. 2013; Aoto et al. 2015). These phenotypes were only rescued on the hippocampal neurons with *Nrxn3β* protein (Aoto et al. 2013; Aoto et al. 2015). This clearly shows that the *Nrxn3* performs different functional phenotypes at different types of synapses and neurons, echoing the complex implication of Neurexins in neuronal circuits and synapse assembly.

Although there have been many studies that have been described in a constitutive mouse model of *Nrxn1α* deletion, the functional analyses of cultured neurons were lacking. The only available data were from Etherton *et al.* study in which the homozygous *Nrxn1α* knockout caused an alteration in synaptic transmission, but the

exact association of homozygous or heterozygous deletion remained unknown (Etherton et al. 2009). For this reason at 2015 Pak *et al.* investigated both in heterozygous and homozygous deletion of *Nrxn1α* knockout in cultured cortical neurons (Pak et al. 2015). They found no change in both miniature spontaneous and action potential-evoked excitatory postsynaptic currents (Pak et al. 2015). It is surprisingly interesting that the same deletion showed significantly different phenotypes in two different experimental procedures (Pak et al. 2015).

The complexity of the *Nrxn1* phenotype in animal models has called out loudly a need for human research. *NRXN1* mutations associated with ASD exhibit incomplete penetrance, which means that the genetic background may significantly contribute to the clinical phenotype observed in patients. However, *NRXN1* mutations have widely been associated with many neurodevelopmental and neuropsychiatric diseases (Marshall et al. 2008; Zahir et al. 2008; Bucan et al. 2009; Need et al. 2009; Rujescu et al. 2009; Wang et al. 2009; Ching et al. 2010; Wiśniowiecka-Kowalnik et al. 2010; Gregor et al. 2011; Schaaf et al. 2012; Béna et al. 2013; Dabell et al. 2013; Kirov et al. 2014; Todarello et al. 2014; Viñas-Jornet et al. 2014).

With the advent of induce pluripotent stem cells (iPSCs), it has become increasingly beneficial to study the disease phenotype in human models. Animal models may not always recapitulate the observed phenotypes in humans. This was clearly proven by Pak *et al.* study, in which a significant impairment observed in the induced mutation of ESC derived cortical neurons in contrast to lack of the phenotype in mouse model mentioned above (Pak et al. 2015). They found that the *NRXN1* mutation shows no alteration in differentiation or synaptogenesis, but a severe impairment in neurotransmitter release (Pak et al. 2015). The heterozygous deletion showed a reduction in the frequency of spontaneous miniature excitatory postsynaptic current without changing the synaptic density but due to an impairment in release probability (Pak et al. 2015). This was the first study, investigating the deletion of heterozygous *NRXN1* mutation in humans.

1.4 Pluripotent stem cells

1.4.1 Embryonic stem cells (ESCs)

Stem cells are cells which have the capability of self-renewal and differentiation into all somatic cell types of the human body, or in another word "pluripotent" (Weissman 2000). These are the exact prime characteristics of embryonic stem cells (ESCs). ESCs were first discovered by Evans and Kaufman (1981) from the inner cell mass (ICM) of pre-implementation mouse blastocysts. Since then several ESC lines have become available *in vitro* to generate a variety of cells from different lineages including hepatocytes, neurons and cardiomyocytes (Evans and Kaufman 1981). However, due to ethical and scientific barriers to the use of human ES cells, as well as difficulties associated with immunological incompatibility, other alternative approaches have been explored; i.e. iPSCs.

1.4.2 Induced pluripotent stem cells (iPSCs); history

The iPSCs are similar to ESCs in their self-renewal and differentiation property. This was first generated from mouse embryonic fibroblasts (MEF) and adult mouse tail-tip fibroblasts with retrovirus transfection of four genes (Takahashi and Yamanaka 2006). Initially, three groups of 24 different pluripotency-inducing genes were selected and tested. The first group were a combination of Oct-3/4, Sox2, UTF1, Sall4, Sox15 and Rex1 that were expressed in ESCs (Takahashi, Okita, et al. 2007). The second group related to growth and tumour-specific combined genes of c-Myc, Stat3, β-catenin, Grb2, KLF4, TCL1 and ERas (Yamanaka 2007). The third group were less-defined function genes of ESCs of ECAT1, ESG1, Fbx15, DNMT3L, ECAT8, GDF3, ECAT15-1, ECAT15-2, Fthl17 and Stella (Yamanaka 2007). These genes were injected in MEF using retrovirus transfection. The combination of Oct3/4, Sox2, c-Myc and Klf4 was shown to produce colonies with high resemblance in morphology and proliferation to ESCs (Yamanaka 2007). Mouse iPSCs gave rise to chimeras with the competency for germline transmission, when they were transplanted to blastocysts. These iPSCs were indistinguishable from ESCs in all aspects of pluripotency, proliferation and differentiation.

This was followed by the reprogramming of human somatic cells to iPSCs (Takahashi, Tanabe, et al. 2007). This was achieved by a combination of four reprogramming factors, including Oct4 (Octamer-binding transcription factor-4), Sox2 (Sex-determining region Y)-box 2, Klf4 (Kruppel Like Factor-4) and c-Myc. Human iPSCs have been injected into the severe combined immunodeficient (SCID) mice, where it formed teratomas with cells derived from all three germ layers, representing to their pluripotency (Takahashi and Yamanaka 2006; Takahashi, Okita, et al. 2007; Yu et al. 2007).

1.4.3 Key elements of pluripotency in stem cells

The main and key transcription factors which are associating with pluripotency are Oct4, Sox2, Nanog, Klf4 and c-MYC. Oct4 is also known as Oct3 or Oct3/4 encoded by *Pou5f1***,** first, discovered in mice as a specific ESC transcription factor (Schöler et al. 1990). In humans, it is encoded by *OCF3* gene comprising three isoforms of *OCT4A*, *OCT4B* and *OCT4B1* (Wang and Dai 2010). *OCT4A* is the main isoform which can maintain the stemness of pluripotent stem cells and mostly known as *OCT4*. In mouse embryogenesis, Oct4 is mainly expressed in pluripotent stem cells and decreases upon differentiation. The study shows that the absence of Oct4 results in the death of embryos at the time of implantation in mice (Nichols et al. 1998). Therefore, Oct4 refers to a master regulator of pluripotency during embryonic development.

Sox2 was first discovered as a testis-determining factor (Gubbay et al. 1990). Sox genes are divided into various subgroups in which *Sox2* identified in SoxB1 group along with other members (Sox1, Sox3). However, *Sox2* is the only member which has an indispensable role in embryonic development. The expression of Sox2 was initially detected at morula stage and later in blastocyst and epiblast of the inner cell mass (Avilion et al. 2003). This elucidates that the presence of *Sox2* is a critical factor for the formation of pluripotent stem cell at early stages of embryonic development. Depletion of Sox2 in both mouse and human ESCs causes a loss in their pluripotent state of the cells and morphology (Fong et al. 2008). In an ESC model of the *Sox2*-null mouse, the forced expression of *Oct4* can rescue the pluripotency state of the cells (Masui et al. 2007). This shows that the primary role of *Sox2* is to maintain the appropriate level of *Oct4* (Masui et al. 2007). This means that the level of *Sox2* has to be in equilibrium to maintain the pluripotency of the cells. In addition, *Sox2* corporates

with *Oct4* and Nanog to regulate the pluripotency of the cells (Boyer et al. 2005). Nanog also has an important role in regulating pluripotent epiblast during embryogenesis by preventing the differentiation towards endoderm (Chambers et al. 2003). It has been proved in mouse ESCs that Nanog has the ability to sustain pluripotency (Mitsui et al. 2003).

The ectopic expression of Oct4, Sox2, c-Myc and Klf4 can reverse the differentiated somatic cells. Klf4 belongs to the Krüppel-like factor (Klf) that maintain the proliferation, differentiation and development of cells (McConnell et al. 2007). Furthermore, Klf4 inhibits the differentiation of ESCs in the absence of other pluripotency factors such as leukaemia inhibitory factor (LIF) (P. Zhang et al. 2010). Klf4 suppresses the P53 pathway, a potent inhibitor of Nanog expression in ESC or iPSC differentiation (Lin et al. 2005). This means that Klf4 has a role in maintaining and regulating the expression of Nanog.

Finally, the expression of c-Myc and its role in pluripotency of ESCs have also been investigated (Kim et al. 2008). Disruption of c-Myc at E10.5 caused defects in vascular and hematopoietic cells (Davis et al. 1993). Furthermore, the self-renewal abilities of ESCs are interfered in mouse knockdown model of c-Myc (Varlakhanova et al. 2010). The lack of c-Myc in iPSC generation has been reported to dramatically reduce its efficiency (Nakagawa et al. 2008). C-Myc has a role in suppressing the fibroblast-specific gene expression which is essential in the early stages of the reprogramming process (Sridharan et al. 2009).

1.4.4 Generation of iPSCs

The first step in generating iPSCs is to identify and culture the source cells. Then, the appropriate reprogramming factors to be introduced to the selected source cells. There are two ways of introducing the reprogramming factors; integrating and non-integrating methods. The integrating methods include using retroviral, lentiviral and inducible lentiviral vectors, and non-integrating methods comprise of Sendai virus, episomal vectors and adenovirus (Brambrink et al. 2008; Fusaki et al. 2009). The cells undergo morphological changes and iPSC colonies generated by having round shape, large nucleus and scant cytoplasm (Thomson et al. 1998). The iPSCs were then characterized on the basis of pluripotent transcription factors Oct4, Sox2 and Nanog

and cell surface markers SSEA4 and Tra180 (International Stem Cell Initiative et al. 2007).

Lentiviral and retroviral reprogramming methods have very high efficiency in generating iPSCs, but it poses the risk of insertional mutagenesis. The main advantage of using lentiviral is their ability to transduce both dividing and non-dividing cells. On the other hand, non-integrating models such as episomal reprogramming have the advantage of using only one single transfection to induce reprogramming, as well as removing the potential risk of cancer generation due to the integration of virus. The episomal vectors deliver into the cell using an oriP/EBNA backbone system called "footprint-free" iPSCs. However, their efficiency is lower in comparison to lentiviral (Robinton and Daley 2012).

Sendai virus has grown in popularity in the recent years to eliminate the risk associated with lentiviral reprogramming and the low efficiency implicated using episomal vectors, (Zhou and Zeng 2013). The transgene expression decreased over time in culture and had very high efficiency with high-quality iPSCs and similar morphological characteristics as ESCs (Fusaki et al. 2009).

1.4.5 Potential advantages of iPSCs

The iPSCs are derived from fully differentiated somatic cells such as skin fibroblasts without the requirement of using human oocyte or embryo. This removes the ethical and political issue of using ESCs, in addition to complex methods deriving them. However, the methods used for generating iPSCs are relatively simple and achievable in most laboratories. Direct reprogramming methodology enabled the generation of iPSCs from healthy volunteers, a potential and immediate utility in drug screening and toxicology testing. The potential advantages of iPSCs are the ability to generate iPSCs from patients of various diseases. This is very important in areas of research where *in vitro* human cell models are lacking, i.e. brain, heart.

Human dermal fibroblast has been a robust starting material for inducing iPSCs (Yu et al. 2007). This enables the researchers to use fibroblast from patients to extensively study the disease in vitro. These patient-specific iPSC lines can offer a tremendous opportunity to model a disease, which is not possible through animal research. This can be used for cellular therapy, given that they are derived from the patients,

minimizing the immune rejection.

There are other sources of somatic cells which have been used to generate iPSCs. These are blood cells (Kim et al. 2016), keratinocytes from plucked hair (Lim et al. 2016) and exfoliated renal tubular epithelial cells, and cells from urine (Zhou et al. 2011). Apart from scalp hair, other facial hair sources such as hair from nose, eyebrow and beard can also be used. However, fibroblast is the most commonly used primary cell source. This is obtained from a skin punch biopsy with a common size of 3.5-4mm.

1.4.6 iPSCs as an *in vitro* disease model

There are a large number of disease models which have been developed in the last decade. There are a variety of animal models using species such as mice, rats, dogs and monkeys. However, these models can never recapitulate the human genetic make-up and microenvironment. Hence, iPSCs have been a great alternative in disease modelling, therapeutic interventions and drug discovery (Figure 1.6). iPSCs have the capability to self-renew and differentiate into all different cell types. The first suggestion was based on the neurodegenerative disease for applying iPSCs as a disease model (Park et al. 2008). The proper differentiation to specific subtypes of neurons allows researchers to find potential cures.

One of the most actively studied disease modelling in neurological disorders is Alzheimer's disease (Kondo et al. 2013; Wang and Doering 2012). By using iPSC models, researchers have found that there are various pathophysiology of Alzheimer's disease in Aβ accumulation among different patients (Israel et al. 2012). iPSC models have also been widely studied for amyotrophic lateral sclerosis (ALS) (Kiskinis et al. 2014; Chen et al. 2014), schizophrenia (Brennand et al. 2011), spinal muscular atrophy (Sareen et al. 2012), Rett syndrome (Ananiev et al. 2011), Prader-Willi syndrome (Yang et al. 2010), fragile X syndrome (Urbach et al. 2010), Phelan-McDermid syndrome (Shcheglovitov et al. 2013) and Huntington's disease (N. Zhang et al. 2010).

There have been great advances in using iPSC derived tissues in drug screening. For example, loxapine was identified as a potential drug target for schizophrenia by increasing neurites and connectivity among neurons (Brennand et al. 2011). Using

ALS patient-specific iPSC derived motor neurons, kenpaullone has been proved to be a potential drug candidate for the survival of neurons (Yang et al. 2013). These discoveries show that iPSC technology has taken a significant step to fill the gap between the pathogenesis of diseases. This strongly suggests the possibility of future personalized medicine in therapeutic intervention and application for patients with various neurological and non-neurological diseases.

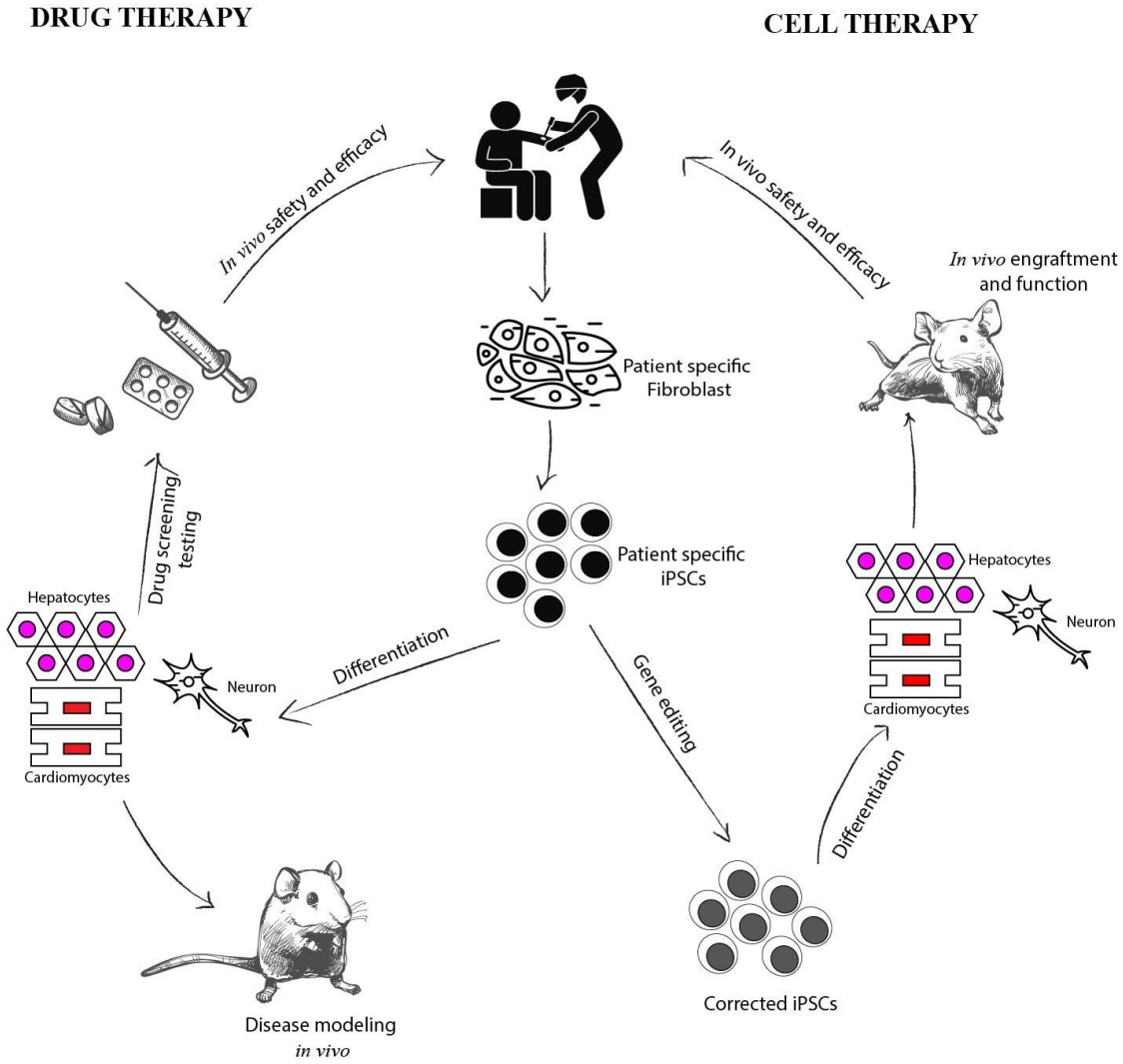

Figure 1.6. Use of induced pluripotent stem cell for drug and cell therapy. This process starts with skin biopsies to generate patient-specific iPSCs. This is followed by directed differentiation to desired cell lines or undergoing gene editing to correct the mutation. For drug discovery, the differentiated cells will be either used for drug screening and testing prior to their application for *in vivo* testing or will be used for animal disease modelling. For cell therapy, the corrected iPSCs will differentiate into desired cell types and will be used first in animals for in vivo engraftment before their application into humans.

1.5 Aims

There have been many studies over the last few decades to identify genes which are associated with ASD and predispose to the clinical phenotypes. However, ASD encapsulates as a very complex neurodevelopmental disorder in which their underlying pathways has yet to be determined. Phenotypes that are associated with ASD are varied from mild to severe and can be attributed to more than one gene mutation, hence it is not possible to model ASD in animals. Moreover, there are many other disorders such as mental retardation, intellectual disabilities, bipolar disorder and epilepsy that have comorbidity with ASD (Volkmar et al. 2004). With the use of iPSCs, many researchers around the world have generated many desired human disease model in a dish. There have been great advances in regenerative medicine to recapitulate patient-specific disease phenotype. This provides a great opportunity for drug discovery and therapeutic interventions.

This study aimed to generate iPSCs from fibroblast obtained from patients with *NRXN1α* deletion who have been diagnosed with ASD and to investigate molecular and functional changes in *NRXN1*-deletion neurons derived from iPSCs.

The derivation of iPSCs was achieved using viral and non-viral reprogramming methods, and iPSCs were extensively characterized using standard methods (Chapter 2). A differentiation protocol was applied to generate mature and functional cortical neurons (Chapter 2). The differentiation capability, synaptogenesis and early and late neuronal development were investigated at the molecular level (Chapter 2).

NRXN1 protein is expressed in both excitatory and inhibitory synapses, and deletion of either heterozygous and homozygous *NRXN1* has been implicated in altering the excitatory and inhibitory postsynaptic transmission as fully discussed in the previous section. Furthermore, Neurexins are essential for coupling voltage-gated calcium channels to the release machinery. This means that *NRXN1* deletion may disturb the electrical firing and calcium signalling of neurons (Chapters 3 and 4). The aim of these chapters was to investigate the impact of *NRXN1* deletion on passive and active properties of neurons (Chapter 3), as well as calcium signalling among neurons (Chapter 4). To further understand the underlying molecular mechanism of any observed phenotype whole genome RNA sequencing were applied (Chapter 5), the

transcriptomes were systematically analysed to uncover the molecular pathways associated with *NRXN1* deletion and altered neuronal functions.

Chapter 2. Differentiation of Induced Pluripotent Stem Cells (iPSCs) into Excitatory Cortical Neurons

2.1 Introduction

2.1.1 Pathology of ASD

Induced pluripotent stem cells are similar to the embryonic stem cells, and both can be differentiated into most cell types in the body. Transformation of adult somatic cells to iPSCs, and then to differentiated disease cell types, has been an innovative technology, which facilitates powerful modelling of various human diseases and overcomes ethical challenges. This allows researchers to underpin the molecular deficits, cellular dysfunction/abnormalities and pathophysiology of human diseases. Indeed, iPSC-derived neurons have been studied in many neurodevelopmental diseases, such as schizophrenia (Brennand et al. 2011), Rett syndrome (Kim et al. 2011; Ananiev et al. 2011; Marchetto et al. 2010; Ricciardi et al. 2012), Fragile X syndrome (Sheridan et al. 2011; Liu et al. 2012) and Timothy syndrome (Paşca et al. 2011; Krey et al. 2013).

The cortical thickness is shown to predict the symptom severity scores of ASD derived from the Autism Diagnostic Observation Schedule (ADOS). Moradi and colleagues were able to correlate the severity of ASD with cortical thickness by analysing 156 ASD individuals and using two main adaptation and learning stage (Moradi et al. 2017). Furthermore, abnormality in the mini-columnar structure of neocortex has also shown to be a common pathological finding in ASD (Amaral et al. 2008). This evidence suggests abnormal corticogenesis during brain development of ASD.

In support of the previous statement, the overgrowth of the brain especially in the first and second year of life was reported as a significant increase in ASD individuals in comparison to healthy controls (Courchesne and Redcay. 2004; Stanfield et al. 2008). This brain enlargement was also observed in neuroimaging studies in the amygdala and cerebellar volume but a reduction in corpus callosum volume (Stanfield et al. 2008; Frazier and Hardan 2009). Cortical thickness and folding have been additionally reported in children with ASD (Ecker et al. 2013).

In a more recent study, Libero and colleagues investigated the neural architecture by comparing a set of 19 high-functioning ASD adults to 18 typically developing peers, using multiple brain imaging modalities of structural MRI, Diffusion Tensor Imaging

(DTI) and Proton Magnetic Resonance Spectroscopy (1H-MRS). Their morphometric analysis also revealed an increase in the thickness of cortex in high-functioning ASD individuals.

An increase in left cingulate and left inferior temporal cortex and a decrease in cuneus and right precentral gyrus have also identified as neuropathology of ASD individuals (Libero et al. 2015). In a subsequent study, they investigated neurochemical balance, and found a significant increase of choline in the cingulate cortex of ASD adults, with a marginal increase in the dorsal anterior cingulate cortex (Libero et al. 2015). An increased number of neurons, decreased volume of neuronal soma and increased neuropil were also observed (Varghese et al. 2017).

On the other hand, diminished cortical width was also reported from a comparative morphometrical study of ASD coronal brain sections and controls. In terms of location and size of the frontal lobes, this reduction was consistent with a diagnosis of focal cortical dysplasia. Spatial statistics identified smaller pyramidal cells and a reduction in a total number of interneurons. During corticogenesis, the cortical malformation resides in heterochronic divisions of periventricular germinal cells, and desynchronising development of the migrating neuroblasts (future pyramidal cells) (Casanova et al. 2013).

Neurons communicate using synapses via excitation and inhibition. GABA is a major inhibitory pathway. The GABAA subunit expression in the postmortem tissues was shown to be decreased in the superior frontal cortex, parietal cortex and cerebellum of subjects with autism (Fatemi et al. 2009). Parvalbumin marks a major subtype of GABAergic interneurons, and Parvalbumin mRNA was significantly lower in Purkinje cells of Crus II of the lateral cerebellar hemispheres in ASD compared to control brains (Soghomonian et al. 2017). However, using induced pluripotent stem cells to model sporadic ASD, ASD-derived organoids were recently found to exhibit overexpression of the *FOXG1*, an accelerated cell cycle and overproduction of GABAergic inhibitory neurons (Mariani et al. 2012).

Evidence also shows that the cortical thickness may indicate the maturation and connectivity of cortex and the development of white matter which largely take place after birth (Shaw et al. 2008; Raznahan et al. 2011). This elucidates that there might

be an impairment in maturation and density of dendritic spines which were also observed in ASD (Varghese et al. 2017). These pathological analyses reveal the heterogeneity, complexity, and even controversy of ASD neuropathology. To a certain degree, we think this reflects the heterogeneity of different genetic factors involved. Meanwhile, little is known about the corticogenesis and excitatory pathways in the pathogenesis of ASD. Understanding normal corticogenesis in mammals and humans will be useful in identifying ASD neuropathology.

2.1.2 Mouse corticogenesis

The cerebral cortex in mammals and humans is a laminar tissue divided into six layers, which are cytoarchitectonically and functionally distinct. Each layer contains a unique subset of neurons, including glutamatergic excitatory projection (pyramidal) neurons and GABAergic inhibitory interneurons. This structure was generated in a cell cycle-dependent manner in which inner layers, i.e. layers 5-6 were generated first during neurogenesis. The ventricular zone in the neural tube comprises of Nestin-positive progenitors. These progenitors undergo an expansion of the neural progenitor pool or later divide into postmitotic doublecortin (DCX) positive cells. The early postmitotic neurons forming preplate will split into superficial layer 1 (Cajal-Retzius) and layer six around E10.5. Later on, at around E12.5, postmitotic neurons migrate along radial glial cells (RGCs) and form layer 5 and 6 of the cortex. Layer 2-4 neurons are produced from the new neurons at E14.5 (Figure 2.1). Thus, six layers are largely completed at E17.5 in mouse embryo before birth.

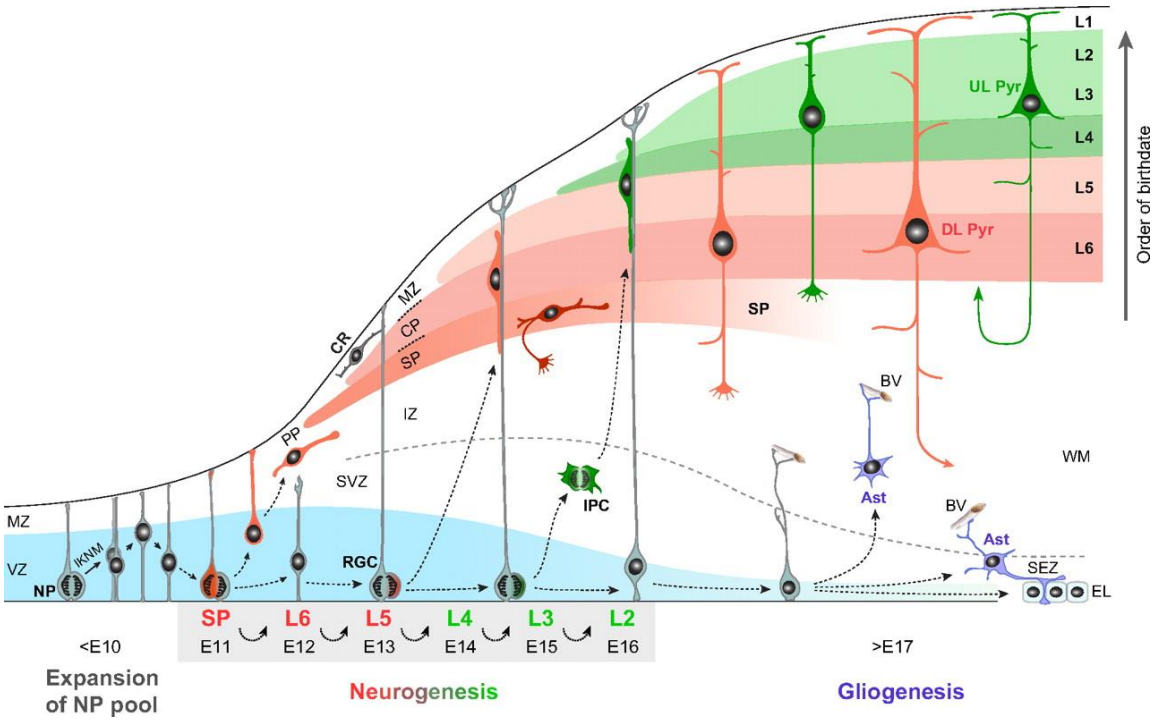

Figure 2.1. Mouse neurogenesis and neuronal migration in the neocortex. At <E10, neural progenitors (NPs) in the ventricular zone (VZ; blue) of the developing neocortex divide symmetrically to expand the NP pool. Corticogenesis occurs in a cell cycle-dependent and inside-out manner. Early-born neurons form the deep layers, whereas later-born neurons migrate past older neurons to form the superficial layers. Diverse subtypes of projection neurons are generated sequentially, first SP neurons, followed by the deep layers (L6 and L5; red), and finally, the upper layers (L4, L3 and L2; green). The significant proportion of upper layer neurons emerge from intermediate progenitor cells (IPCs) which have been migrated to the sub-ventricular zone (SVZ). Finally, NPs undergo gliogenesis, generating astrocytes and ependymal and blood cells at the end of E17.5. CR, Cajal-Retzius neuron; DL Pyr, deep-layer pyramidal neuron; IZ, intermediate zone; UL Pyr, upper-layer pyramidal neuron, WM, white matter (Kwan et al. 2012).

Sox5 and *Tbr1* are the key transcription factors for generation of early-born deep layer neurons. *Sox5* belongs to SOX transcription factors and is expressed in postmitotic SP and L6 neurons. It has a role in migration, axonal projection and differentiation of L6 neurons (Kwan et al. 2008; Lai et al. 2008), and down-regulates L5 transcription factors *Fezf2* and Ctip2 (Kwan et al. 2008; Lai et al. 2008). The expression of *Fezf2* and Ctip2 are essential for the subcortical development of L5 neurons (Arlotta et al. 2005; B. Chen et al. 2005; J.-G. Chen et al. 2005; Molyneaux et al. 2005). *Tbr1* is selectively expressed in L6 corticothalamic projection neurons and L1 Cajal-Retzius neurons (Hevner et al. 2001). *Tbr1* also suppresses and down-regulates the expression of *Fezf2* and Ctip2 in L6 corticothalamic neurons (Han et al. 2011; McKenna et al. 2011). *Tbr1* is also required for differentiation and axonal pathfinding (Hevner et al. 2001; Han et al. 2011; McKenna et al. 2011).

Satb2 is highly expressed in postmitotic L2-L5 projection neurons and is an interacting transcription factor that regulates the upper layer-specific genes *Cux2*, *Cdh10* and *Rorb* (Alcamo et al. 2008), but suppress Ctip2. *Satb2* is involved in many aspects of upper layer neurons such as differentiation, axonal guidance and migration (Alcamo et al. 2008; Britanova et al. 2008). Other transcription factors that are expressed in L2-L5 of projection neurons include Pou3f2 (formerly Brn2) and Pou3f3 (formerly Brn1), and they belong to POU domain transcription factors (McEvilly et al. 2002; Sugitani et al. 2002).

The six layers can be distinguished by layer-specific markers, for example, Calretinin marks layer 1 Cajal–Retzius cells; *Cux1* and *Cux2* are expressed in layer 2 and 3; Brn1 labels layer 2-4; *FoxP2* and *Tbr1* expressed by layer VI, and Ctip2 is positive in layer 5 and 6 neurons (Lizarraga et al. 2010). These markers are important for assessing normal corticogenesis as well as identifying any alteration in both post-mortem tissues and disease model of ASD. Furthermore, the process of corticogenesis can be investigated using proliferating marker Ki67, the S phase marker - BrdU, and M phase marker - phospho-histone H3, the newborn post-mitotic cell marker - *Dcx,* the pan neural/neuronal cell marker - Tuj1, and mature neuronal markers -*Map2* and NeuN.

2.1.3 Human corticogenesis and developmental markers

A prominent feature of the human brain is the fabulous size of the cerebral cortex, and its sophisticated cerebral folding appeared as grooves on its external surface of the cortex. Cortical expansion and folding are essential processes in human brain development, leading to human intellectual and cognition performances. Cortical folding begins from embryonic development to generate a functional brain wiring network and to enable an appropriate fit in a limited cranial volume. An alteration or impairment in cortical folding in humans may correlate to intellectual disability and epilepsy (Walsh 1999; Barkovich et al. 2012). There has been a great advancement in understanding human cortical development in the last 15 years in the field, including the proliferation of NPs, the size of the cortex, novel germinal zones and different types of NPs, and specific genes associated with neocortical expansion (Fernández et al. 2016; Florio et al. 2017).

At the start of corticogenesis in human, neuroepithelial cells possess features of the apical radial glial cell (aRGC) mainly expressing *PAX6* and Vimentin (reviewed by (Taverna et al. 2014)). The neuroepithelial cells (aRGCs) undergo symmetrical divisions of either new postmitotic doublecortin (*DCX*) positive cells or to intermediate neural progenitor cells (IPCs), the same process as at E10 mouse embryogenesis (Englund et al. 2005) (Figure 2.2). More asymmetric divisions will take place in order to generate more IPCs from aRGCs (Noctor et al. 2004). These IPCs generate the majority of excitatory cortical neurons in the cerebral cortex (Kowalczyk et al. 2009). In the ventricular zones, apical intermediate progenitors (aIPs) divide at their apical surface and produce neurons, but the subapical progenitors divide to generate IPCs (Stancik et al. 2010). In SVZ, the basal radial glial cells (bRGCs) express *PAX6*, sharing many similarities to aRGCs (Shitamukai et al. 2011; Wang et al. 2011) (Figure 2.2).

The abundance of aRGCs is much higher in gyrencephalic species than in mouse and rats. This abundance occurs due to the high proportion of neural epithelial cells at early stages of corticogenesis as well as increased self-amplification of aRGCs. The abundance of basal progenitors is further accompanied by separating SVZ into outer and inner SVZ (OSVZ, ISVZ respectively) (Fernández et al. 2016).

The OSVZ comprises two main factors that are crucial for cortical folding and expansion. They are present in various progenitor cell types for high amplification (Lui et al. 2011; Borrell and Götz 2014). In gyrencephalic species, the majority of basal progenitors are bRGCs rather than IPCs, which is abundant in lissencephalic mouse (Borrell and Reillo 2012; Reillo et al. 2011; Betizeau et al. 2013). In gyrencephalic corticogenesis such as in macaque and ferret, the generation and self-amplification of neurons take much longer in comparison to rodents (Kornack and Rakic 1998; Borrell and Reillo 2012) enabling a much greater cell division (Dehay and Kennedy 2007; Florio and Huttner 2014). These statements suggest that OSVZ has an essential role in increasing neurogenesis and cortical folding in mammals (Figure 3.2) (Fietz and Huttner 2011; Borrell and Reillo 2012; Borrell and Götz 2014; Florio and Huttner 2014). This is further examined by forced expression of OSVZ, in which the surface area and folding of cortex dramatically increased, while the suppression and blockade of OSVZ reduced cortical folding (Reillo et al. 2011;

Nonaka-Kinoshita et al. 2013). The OSVZ, therefore, plays a central role in cortical expansion and folding, as they not only prominently contribute to the increased neuron production, but also specifically to its high content of bRGCs.

These discoveries in cortical development, expansion and folding come from many multidisciplinary studies, including investigation of mechanism at the molecular and cellular levels governing neurogenesis, their pattern of folding and growth. These studies also show how genetic evolution steers cortical size, folding during the evolution of human brain development and how genetic alterations may cause human brain diseases.

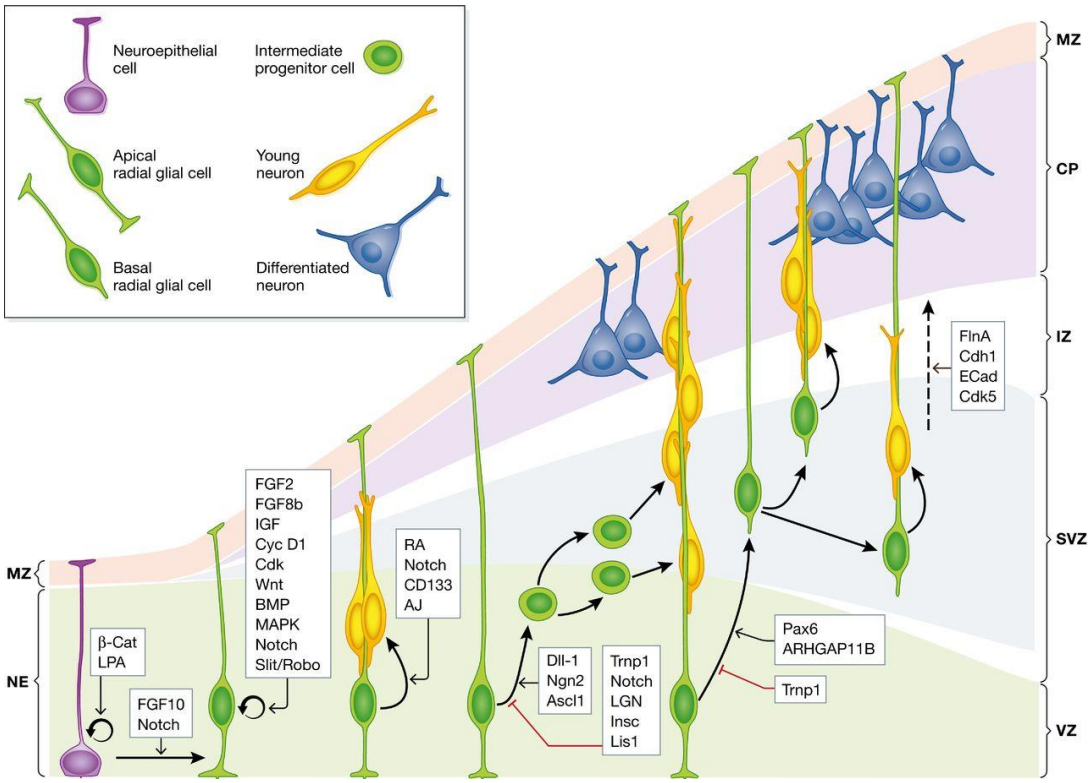

Figure 2.2. Schematic diagram of cerebral cortex development in gyrencephalic brains. This diagram shows the essential types of progenitor cells and their connection and effect on cerebral cortex development. Most neuroepithelial cells undergo amplification to generate apical radial glial cells. Neurons emerge from aRGCs from either basal radial glial or intermediate progenitor cells during the neurogenic phase. This diagram shows the list of molecules playing a role in each phase (adopted from (Fernández et al. 2016).

2.1.4 Neural induction using dual SMAD inhibition and subsequent neuronal cultures

During mammalian cortical development, neurons, radial glial, oligodendrocytes and astrocytes emerge from neural stem cells (NSCs). These are precisely programmed

developmental processes involving cell-cell interactions, environmental signals and intrinsic signalling pathways. Bone morphogenic proteins (BMPs) belong to transforming growth factor β (TGFβ) cytokine superfamily that promotes various cellular events for neuronal fate determination. They also interact with basic fibroblast growth factor (bFGF) and sonic hedgehog (Shh) which play a crucial role in NSC self-renewal and expansion. There are more than 20 different BMPs with distinct functions depending on their interactions with various receptors and the tissues they are accumulating (Mishina 2003). While they have an essential role in stem cell proliferation and self-renewal, they block neuronal differentiation (Ying et al. 2003) and promote non-neuronal (i.e. mesodermal) differentiation (Xu et al. 2002; Ying et al. 2003).

In the last few years, there have been many methods proposed to differentiate ESCs and iPSCs into neural progenitor cells (NPCs) and then to different neuronal lineages (Zhang et al. 2001). A common differentiation protocol was established on the basis of the embryonic body (EB) formation (Clark et al. 2004). This protocol has disadvantages of heterogeneous production of cells and time-consuming procedure. A mono-layer and the serum-free based protocol were established (Ying et al. 2003) based on certain signalling pathways that are required to be inhibited during brain development. BMP signalling pathway inhibitors, such as chordin, Noggin and compound LDN193189, are important in early embryo development through SMAD signalling (Sasai et al. 1994; Smith and Harland 1992). Early studies in *Xenopus* have shown that the BMP signalling prevents neural differentiation (Linker and Stern 2004). In addition, it is shown in chick and *Xenopus* that the antagonist of BMP protects the presumptive neural plate and enhances neuronal differentiation (Vonica and Brivanlou 2006). However, the inhibition of BMP signalling alone is not sufficient for neural induction. In the mouse model lacking all the BMP signalling antagonists, the nervous system is still developed (Mukhopadhyay et al. 2001; Bachiller et al. 2000; McMahon et al. 1998).

Inhibition of another SMAD signalling, TGFβ pathway, is also found to promote neural induction. TGFβ can be inhibited by a small molecule called SB431542 (Patani et al. 2009). Activin and Nodal signalling are members of TGFβ superfamily which are responsible for the maintenance of iPSC pluripotency and self-renewal, as well as

inducing mesodermal differentiation (Vallier et al. 2004; Vallier et al. 2005; Beattie et al. 2005; James et al. 2005). Nodal binds to complexes of Activin receptors (ALK4, ALK7 and ActRII), which eventually affect SMAD signalling (reviewed in (Schier 2003). SB431542 can inhibit TGFβ/ activin/ nodal/ SMAD signalling by acting through the phosphorylation of ALK7, ALK5 and ALK4 (Figure 3.3). This elucidates that nodal signalling not only promotes the differentiation of mesoderm but also provides an inhibition mechanism towards neural fate both *in vivo* and *in vitro* (Smith et al. 2008; Vallier et al. 2004).

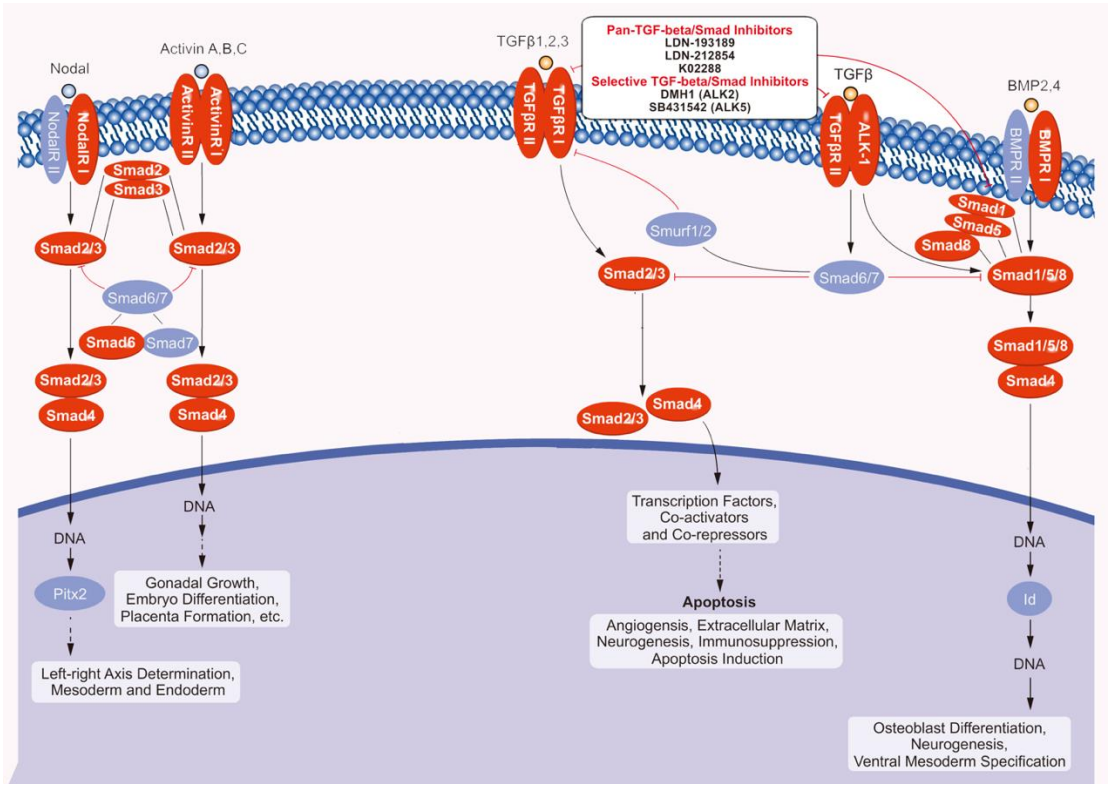

Figure 2.3. TGFβ and BMP signalling pathways. SB431542 molecule inhibits Activin type I receptor and Nodal type I receptor, and both of which are responsible for phosphorylation of SMAD2/SMAD4, which induce mesoderm and ectodermal differentiation. LDN193189 selectively inhibits BMP receptor I, ALK2 and ALK3, which in turn inhibit SMAD1/5/8 activation. Inhibition of TGFβ and BMP pathways drives stem cells toward ectodermal differentiation (www.selleckchem.com/TGF-beta.html).

Their synergic action of both SB431542 and LDN-193189 was shown to drive the iPSCs into NPCs and to specific neuronal subtypes such as pyramidal neurons (Chambers et al. 2009; Shi, Kirwan, Smith, et al. 2012; Espuny-Camacho et al. 2013). Therefore, the dual SMAD inhibition strategy was used to differentiate iPSCs towards the anterior neuroectodermal lineage and telencephalic glutamatergic neurons

(Chambers et al. 2009). This is a key for the generation of cortical neurons. A notable feature of this method is that different classes of neurons can be generated in the temporal order as that *in utero*. Early, deep layer neurons (*TBR1*$^{+}$/CTIP2^{+}) may appear in the first 20/30 days of differentiation, while upper layer cortical neurons (*SATB2*$^{+}$, BRN2^{+}) will be generated as late as 80/90 days (Shi, Kirwan and Livesey 2012). We have used this protocol in this study to generate excitatory cortical neurons from the control and *NRXN1*-deletion ASD iPSCs for phenotypic analyses.

2.1.5 Reprogramming from fibroblast to iPSC

The discovery of iPSCs in 2006 has opened up a new field with many branches of translational and regenerative medicine (Takahashi and Yamanaka 2006; Takahashi, Tanabe, et al. 2007). The iPSCs are derived from adult somatic sources but have the pluripotency resembling ESCs regarding the capability of self-renewal and differentiation to any desired cell lineage. They can, therefore, overcome ethical complication of human ESCs and provide a great opportunity to revolutionize human disease modelling *in vitro* by targeting unmet clinical needs, to study disease in culture dish and to investigate the underlying disease mechanism. Moreover, in terms of cell replacement therapy, the immune rejection upon allogenic transplantation will be less of a concern with cells derived from patient own somatic tissue. Although stem cells can also be derived from umbilical cord blood, blood, bone marrow and adipose tissue (Gnecchi and Melo 2009), the mesenchymal stem cells derived from these sources can only be differentiated to certain cell lineages such as osteocytes, chondrocytes and adipocytes. The human brain is particularly difficult to access, and primary human neurons do not grow well *in vitro*. The iPSC technology has thus provided unique and invaluable opportunity for studying neurological and neuropsychiatric disorders to explore the fundamental molecular and cellular pathways impaired in neurodevelopmental and neurodegenerative diseases, which could be challenging to model in rodents.

The main transcription factors involved in early embryonic development, as well as pluripotency and self-renewal properties, are *SOX2*, *OCT4*, *NANOG* and *KLF4* (Takahashi, Tanabe, et al. 2007). There are various methods which have been developed to convert somatic cells into iPSCs, by the forced expression of essential genes which are critical for the pluripotency identity. The original method of

reprogramming utilized retroviral transduction. This was a simple and efficient model but may cause multiple genomic integrations of transgenes, due to the limited cloning capacity of the retroviral vector. Therefore, multiple vectors are needed to express four transcriptional factors, which made a concern regarding clinical applications of iPSCs and the risk of insertional mutagenesis. This was followed by the development of lentiviral, Sendai virus and episomal vectors (Yu et al. 2007; Takahashi, Tanabe, et al. 2007; Fusaki et al. 2009), with a different "gene cocktail" based on the original discovery (Takahashi, Tanabe, et al. 2007; Yamanaka 2008) to convert somatic cells to iPSCs (Feng et al. 2009; Buganim et al. 2012).

Later, lentivirus with Lox P site was introduced which had a larger capacity to incorporate four reprogramming factors into a single vector, thus minimising the integration sites into the host genomic DNA. In addition, with the aid of Cre recombinase, the floxed reprogramming genes can be removed after the iPSC generation (Chakraborty et al. 2013; Sommer et al. 2010). To further increase the transgene expression, transposons were introduced (Grabundzija et al. 2013). However, none of the genome-integrating vectors is considered safe because the DNA foot-print may remain, and a possible genomic rearrangement or deletion may occur.

This led to the exploration of non-integrating methods for iPSC transgene delivery. These methods involve using plasmid transfections, cell-penetrating proteins and non-integrating viruses, etc. (Stadtfeld et al. 2008; Okita et al. 2008; Kim et al. 2009). Although these methods resolved the issue of possible genetic rearrangement and deletion, the reprogramming efficiency was reduced. Sendai virus is also a non-integrating method with very high efficiency (Fusaki et al. 2009).

A non-integrated and non-viral method is the use of episomal DNA vectors. This is an easy and inexpensive method with limited transfection. This means that there is a very low risk of integration of a transgene into host transfected cells. It is also optimized to be used on feeder-free condition medium. The Epi5 reprogramming is a method which was used by myself for this study for the first time in the laboratory to obtain pluripotent stem cells. The episomal vectors have an oriP/EBNA-1 backbone. The presence of oriP/EBNA-1 backbone ensures the gradual loss of the episomal vectors at a ratio of 5% per cell cycle without any further manipulation. Epi5 reprogramming vectors are a mixture of three episomal vectors, with a replication origin (oriP) element

and *cis*-acting EBV nuclear antigen-1 (EBNA-1) carrying the reprogramming genes Oct4, Sox2, Lin28, L-Myc and Klf4. In addition to the EBNA-1 backbone in the episomal reprogramming, expression of mp53DD improve the reprogramming efficiencies. p53 is a protein which is essential for cell cycle regulation. In the presence of cytotoxic activity, p53 causes cell cycle arrest and cell death. Therefore, the dominant negative mutation of p53 is used in this episomal reprogramming, diluting out gradually after passaging iPSCs.

The source of somatic cells can be fibroblasts, keratinocytes, peripheral blood cells and exfoliated cells from urine (Takahashi, Tanabe, et al. 2007; Aasen and Izpisúa Belmonte 2010; Staerk et al. 2010; Zhou et al. 2012; Takahashi and Yamanaka 2006). The efficiency of reprogramming methods is important to obtain a good yield of iPSC colonies, and iPSC clones shall have less bias to differentiate into any cell type. We therefore have used skin biopsy and derived dermal fibroblasts in this project.

The lines which have been used in this project are derived from lentiviral and episomal vector reprogramming methods. This reflected the history of the project from a single lentiviral vector (integrated) performed by former group member at the initial stage to non-integrated (episomal) method when I joined the project. The expression of the reprogramming genes may vary among iPSC lines. However, all iPSCs have been standardized and efficient expression level of *OCT4*, *SOX2* and *NANOG* have been validated across the lines.

This chapter aims to generate iPSCs and cortical glutamatergic neurons from both control and *NRXN1α*-deletion lines, using dual SMAD inhibition differentiation protocol (Chambers et al. 2009; Shi, Kirwan, Smith, et al. 2012; Shi, Kirwan and Livesey 2012). The molecular and cellular changes of iPSCs to neural progenitors were validated at different early stages of differentiation (i.e. day 10, 20, 30) at both RNA and protein levels. For example, *PAX6* was analysed as it has an important determinant role in the fate of neural progenitors and the density of cortical neurons in the forebrain (Jones et al. 2002). The expression of *FOXG1* transcription factor was also determined at RNA and protein level at early stages of cortical neuron differentiation, as *FOXG1* plays a critical role in proliferation and neurogenesis of pyramidal neurons in the forebrain (Martynoga et al. 2005). We also validated the

protocol with Tuj1, MAP2, SYN1 and excitatory neuronal markers. Expression of Tuj1 is an essential pan-neuronal marker, which is expressed specifically by neural stem cells, developing and mature neurons (Menezes and Luskin 1994). Most of the post-mitotic neurons in forebrain originate from Tuj-1 positive progenitor cells in the anterior part of SVZ (Luskin et al. 1997; Menezes et al. 1995). The iPSC-derived neurons also show expression of mature neuronal marker MAP2, which is a forebrain pyramidal marker, and is mainly present in dendrites of pyramidal cells in the cerebral cortex (Curtetti et al. 2002). Furthermore, the expression of a series of excitatory neuronal markers at pre- and post-synaptic membrane, synaptic marker SYN1 genes and different cortical layer markers were investigated at the RNA and protein levels.

2.2 Material & Methods

2.2.1. Fibroblast culture

Skin biopsies (3mm) were obtained from both control (healthy volunteers) and identified NRXN1α deletion patients at Galway University Hospital. Approval for the study was granted by NUI Galway research ethics committee (reference C.A.750). Skin biopsies were washed in Dulbecco's Phosphate-Buffered Saline (DPBS) (Thermo Fisher Scientific 14190250) containing 5% penicillin/streptomycin (Thermo Fisher Scientific 10,000 U/ml 15140122) and cut in to small pieces using a sterile scalpel blade. Dissected biopsies were cultured in high glucose Dulbecco's Modified Eagle Medium (Thermo Fisher Scientific 11965092) supplemented with 10% fetal bovine serum (Thermo Fisher Scientific HYC-001-354R), 1% penicillin/streptomycin and 1% non-essential amino acids (Thermo Fisher Scientific 11140050).

2.2.2 Derivation of iPSC using lentiviral (By Katya McDonough) and episomal reprogramming method (in conjunction with Katya McDonough)

The iPSCs were generated using lentiviral and episomal reprogramming methods. Table 2.1 provides the details of patient and control lines including their reprogramming method, age where biopsies taken and their deletion regions where applicable (Hg19 builder).

Table 2.1. Source information for iPSC lines.

iPSC line	Reprogramming method	Control or patient	Sex	Age (at biopsy)	Inheritance	Deletion region (Hg19 start-stop)
1CC2	Lentivirus	Ctrl	M	4	N/A	N/A
3VCX1 and 3VC2	Lentivirus	Ctrl	M	21	N/A	N/A
4C3 and 4CX1	Lentivirus	Ctrl	M	19	N/A	N/A
2VC1	Lentivirus	Ctrl	F	20	N/A	N/A
NCRM-1	NIH: episomal	Ctrl	M	Not known	N/A	N/A
ND1 C1	Lentivirus	Patient	M	6	De novo	Exon 6-13 50566968-50897061
ND2 C11 and ND2 CX1	Lentivirus	Patient	M	20	De novo	Exon 1-5: 51122091-51314430
ND4-1 C1 and ND4-1 C2	Episomal	Patient	F	19	De novo	Exon 1-5: 50982113-51446873

2.2.2.1 Lentiviral

Step 1: Day 0 (seeding of fibroblasts): Fibroblasts were seeded at a density of $5.0X10^4$ in a 6-well plate. Cells were maintained at 37º C overnight in 2.5 ml of fibroblast medium, which consisted of DMEM high glucose 4.5g/L (Thermo Fisher Scientific, 11965092), 1% non-essential amino acids (Thermo Fisher Scientific 100X, 11140050), 1% penicillin/streptomycin (Thermo Fisher Scientific, 10,000 U/ml, 15140122) and 10% Hyclone™ fetal bovine serum (Fisher Thermo Scientific, 10309433).

Step 2: Day 1 (1st transduction): Prior to transduction, a control well of fibroblasts were dissociated using Trypsin/EDTA (Thermo Fisher Scientific, 25200056) to count the number of cells, which were used to calculate the multiplicity of infection (MOI) for reprogramming of other un-dissociated fibroblasts which were seeded with same cell numbers at the same time. The MOI of 5 were used in this protocol to achieve high and efficient reprogramming of the cells. One vial of Human STEMCCA Constitutive Polycistronic (OKSM) virus (Merck-Millipore Cork, Ireland, SCR510) was thawed in ice after its removal from -80°C. For a batch with the titre value of $3.2X10^9$ infectious units (IFU), the viruses were diluted in 1:100 in DMEM high glucose medium. The cultural medium in the reprogramming 6-well plates was

replaced with 1 ml of fresh fibroblast medium. Polybrene (Merch Millipore, TR-1003) was diluted in 1:10 with culture grade water (Sigma Aldrich 59900C) and 5µl of this was added to each well for obtaining 5µg/ml final concentration. The virus volume was calculated using the formula: number of cells/virus titre x MOI /1 ml x1000 and required amount of virus was added directly to the fibroblast well. The plate was rocked gently to distribute the virus across the well and cells were incubated at 37º C overnight.

Step 3: Day 2 (2nd transduction of fibroblasts): On the following day, the second transduction was applied to the fibroblasts using the same approach as the previous day. To calculate the correct virus volume on the second day, using an additional well of control fibroblasts seeded at day 0.

Step 4: Day 3 (change of medium with bFGF): On day 3 of reprogramming, the medium was aspirated, and cells washed three times in DPBS (Thermo Fisher Scientific, 14190250). The medium was replaced with Knockout DMEM medium, which was made of 195 ml Knockout DMEM (Thermo Fisher Scientific, 10829108), 50 ml Knockout serum supplement (Thermo Fisher Scientific, 10828010), 2.5 ml non-essential amino acids, 2.5 ml L-glutamine (Thermo Fisher Scientific, 200 mM, 25030081), 182 µl β-mercaptoethanol (Thermo Fisher Scientific, 50mM, 31350-010), and 10 ng/ml bFGF (Peprotech UK, 154 a.a). The medium was changed every day with the fresh addition of bFGF, and the morphology of cells was monitored with light microscopy.

Step 5: Day 5 (MEF layer preparation): The inactivated mouse embryonic fibroblasts (MEF) (Thermo Fisher Scientific, A24903) were seeded on 6-well plates pre-coated with 0.1% gelatin for 1 hour at 37º C. Then, the gelatin was aspirated, and $1.5X10^5$ inactivated MEF were seeded on each well of 6-well plate and incubated at 37º C overnight.

Step 6: Day 6 (1st passage of fibroblast): At this stage, transduced fibroblast cells are 80-90% confluent and are ready to be passaged onto MEF-coated plates. The MEF medium was aspirated, and the well was washed once with DPBS. Transduced fibroblasts were trypsinised and seeded at a density of $4.0X10^4$ cells per MEF-coated

well. The medium was changed every other day and inactivated MEF were added every seven days.

2.2.2.2 Episomal

Step 1: Day 0 (seeding fibroblast): The density of $1.0X10^5$ cells were used as a starting point for transfection. $1.0X10^5$ cells were resuspended in 100 µl of nucleofection buffer (Nucleofector kits for Human Dermal Fibroblast (NHDH), Lonza, CC-2509) in addition to 1 µl of Epi5™ reprogramming vectors (Table 2.2) and 1 µl of the Epi5™ p53 & EBNA vectors (Table 2.2). The mixture pCE-hOCT3/4, pCE-hSK and pCE-hUL vectors delivers 5 essential factors for iPSC generation. The mixture of pCE-mP53DD and pCXB-EBNA1 improves the reprogramming efficiency by delivering mp53DD and EBNA1. The solution was placed in a transfection cuvette and electroporated using Nucleofector 2b device (Lonza) under programme U0023. The cells were immediately transferred into geltrex-coated 6-well plate with the addition of 3 ml fibroblast medium. The cells were incubated at 37º C overnight.

Step 2: Day 1 (medium change and maintenance): The medium was aspirated and replaced with N2B27 medium, which was made of DMEM/F12 with HEPES (Thermos Fisher Scientific 11330032), 1% N2 supplement 100X (Thermo Fisher Scientific 17502048), 2% B27 supplement 50X (Thermo Fisher Scientific 12587010), 1% non-essential amino acids, 0.5% glutamax 100X (Thermo Fisher Scientific 35-050-061), β-mercaptoethanol 1000x, and 10 ng/ml bFGF. The medium was changed every other day until day 15 of reprogramming.

Step3: Day 15 (medium change): The medium was then aspirated and replaced with essential E8 medium (E8™, Thermo Fisher Scientific, A1517001). The E8 medium was changed every other day, and iPSC colonies were picked using 10 µl pipette tip from day 20-30 of reprogramming period. Each colony were isolated and placed into an individual pre-coated geltrex well.

Table 2.2. Epi5 episomal reprogramming vectors.

Vectors	Genes
pCE-hOCT3/4, pCE-hSK, pCE-hUL	Oct4, Sox2, Klf4, L-Myc, Lin28
pCE-mP53DD, pCXB-EBNA1	mp53DD, EBNA1

2.2.3 Monolayer neuronal differentiation of iPSCs derived from control and *NRXN1α*-deletion patients

The differentiation protocol starts as following (Figure 2.4):

1) iPSC propagation (Day -2/-3): iPSCs were washed once in 1ml of DPSB and incubated with 1ml of gentle cell dissociation reagent (Stem Cell Technologies 070174) at room temperature for approx. 5 minutes. Once signs of detachment visible, the reagent were removed, and the cells washed gently with 1 ml of DPBS and replaced with 1 ml of E8 medium containing ten µM rock inhibitor (Stem Cell Technologies, Y27632). Cells were detached and scratched using 5 ml pipette to evenly dissociate cells, which were plated at a very high density of 45,000 – 50,000 cells/cm^2 on a 6-well plate pre-coated with geltrex (Thermo Fisher Scientific, A1413302). Geltrex-coated 6-well plates were prepared by adding ~1.5 ml geltrex into a 6-well plate which was kept at 37º C for at least one hour. Cells were fed with E8 medium every day and grown for the maximum of 3 days until they reached approximately 80-85% confluency.

2) Neuronal induction (Day 0): The E8 medium was removed from the well, washed with 1ml of DPBS and replaced with neural induction medium. The Neural induction (N2B27) medium comprised of 2/3 (v/v) of DMEM F/12 (Thermo Fisher Scientific, BE12-719F), 1/3 (v/v) of Neurobasal (Thermo Fisher Scientific, 21103-049), 1/150 (v/v) of N2 supplement (Thermo Fisher Scientific, 17502048), 1/150 (v/v) of B27 w/o Vitamin A (Thermo Fisher Scientific, 12587010) and 0.1 mM of β-mercaptoethanol (Thermo Fisher Scientific, 31350-010), supplemented with 100 nM LDN193189 (BMP signalling inhibitor, Stem Cell technologies, 72102) and 10 nM SB431542 (TGF-β signalling inhibitor, Sigma, S4317).

3) Neural progenitor generation (Day 1-12): Half of the medium was changed every day for up to day 10-12 with the fresh addition of SB431542 and LDN193189 to N2B27 medium. This is dependent on the formation of the thickened neuroepithelial sheet and the appearance of neuronal rosettes, elongation of cells which are variable between lines.

4) First passage of neural progenitors (Day 10-12): N2B27 medium was removed, cells were washed once with 1ml of DPBS and replaced with 1ml of conditioned medium (N2B27 + fresh 10 µM rock inhibitor) and incubated for 1 hour at 37º C. Following the incubation, the conditioned medium was collected and placed in a 15 ml falcon tube. Cells were washed once in 1ml of DPBS and replaced with 1 ml of 0.02% EDTA for 1-2 minutes at 37º C. The EDTA was aspirated, and the conditioned medium was added to the cells. Cells were gently and evenly scratched with 5 ml pipette tip to generate a big cluster of cells. Cells were collected into a 15 ml falcon tube. The remaining cells in the well of 6-well plate were washed with 3ml of N2B27 containing ten µM of rock inhibitor and transferred to the falcon tube. Cells from each 6-well plate were passaged into four wells of a 12-well plate and then incubated at 37º C until the next day.

5) Neural progenitor maintenance (Day 10/12 - 20): Half of the medium was changed every two days with N2B27 medium until day 20-22. This might be slightly variable between lines as this was determined by the confluency of the cells and when multi-layered of cells become visible.

6) Second passage for terminal differentiation **(Day 20-22):** At this stage cells were passaged for terminal differentiation without any further passaging. Cells were plated on Poly-D-Lysine-coated 12-well plates or 15 mm coverslips (Fisher Scientific 12362138) or ibidi 8-well chambers (ibidi, 80826) for different analyses at the end of experiments. Cultural plates, coverslips or ibidi chambers were prepared by adding required amount of Poly-D-lysine (10µg/ml in DPBS) for 1 hour at 37º C. Then cultural wares were washed three times with DPBS and incubated with 10µg/ml of laminin at 37º C for overnight. On the following day, plates were washed once with DPBS prior to use. Cells were passaged on Poly-D-Lysine/Laminin-coated culture-wares as described on step 4, with the following passaging ratios: 1:2 from 12-well to12-well plates, 1:3 from 12-well to 15mm coverslips and 1:8 from 12-well to 8-well ibidi chamber slides.

7) Maintenance for mature neuronal differentiation (Day 20/22-100): Cells were fed every 2-3 days with half of the new N2B27 (w/o vitamin A) medium until day 26,

and then switch to N2B27 plus (with vitamin A, Thermo Fisher Scientific, 17504044) from day 27 to 100 for neuronal differentiation and maturation.

At day 100, cells were processed for immunocytochemistry, western blotting, RNA sequencing, electrophysiology and calcium imaging experiments.

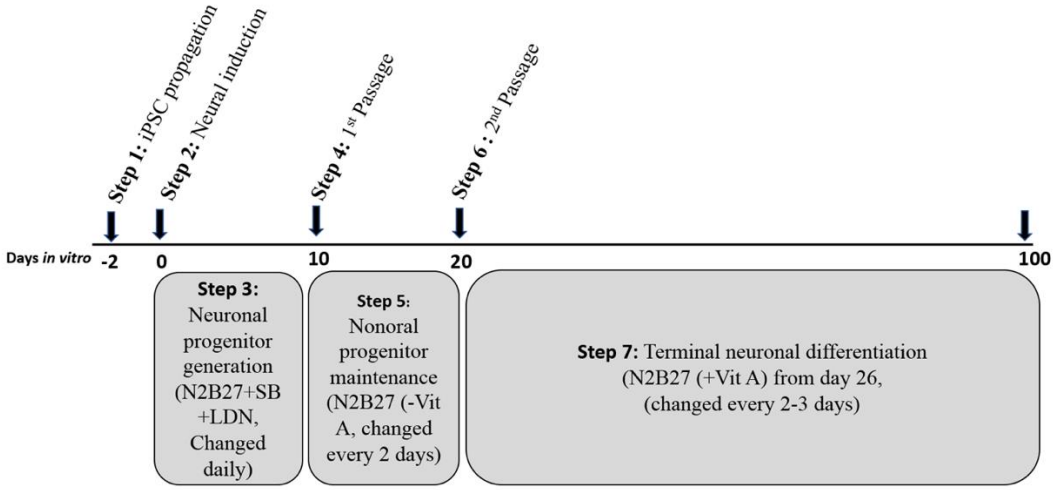

Figure 2.4. Flow diagram of cortical neuronal differentiation.

2.2.4 Immunocytochemistry

Cells were washed with PBS and fixed in 4% paraformaldehyde (Santa Cruz 30525-89-4) for 20 minutes at room temperature (RT). The cells were then washed 3 times in PSB for 5 minutes before the blocking solution with 0.2% bovine serum albumin (Sigma Aldrich A2153) in 0.1% trition-X100 in PBS for 1 hour at RT. Following blocking, cells were incubated with primary antibodies at desired dilution (Table 2.3) prepared in blocking solution at 4º C overnight. The following day the primary antibodies were aspirated and cells were washed 3 times in PBS before incubating in secondary antibody. Cells were incubated with appropriate fluorophore conjugated secondary antibody in blocking solution for 1 hour at RT (Table 2.4). Cells were washed 3 times in PBS and then imaged using Andor confocal microscope. Image J were used for quantification and normalized to the number of DAPI- positive nuclei in that images.

Table 2.3. list of primary antibodies used.

Target	Manufacture	Dilution	Species	Lot No.
Oct4	Cell Signalling	1:200	Rabbit	2840S
Sox2	Cell Signalling	1:200	Rabbit	3579S
SSEA4	Cell Signalling	1:200	Mouse	4755P2
Tra-180	Cell Signalling	1:200	Mouse	4745P2
Ki67	Abcam	1:500	Rabbit	Ab15580
P-Histone H3	Cell Signalling	1:500	Mouse	9706S
Nestin	Abcam	1:400	Mouse	Ab18102
Pax6	Abcam	1:400	Rabbit	Ab5790
Map2	Abcam	1:200	Rabbit	Ab32454
Tuj1	Abcam	1:1000	Mouse	Ab78078
Synapsin1	Abcam	1:1000	Rabbit	Ab8
Doublecortin	Abcam	1:1000	Rabbit	Ab18723
GFAP	Dako	1:200	Rabbit	20028619

Table 2.4. list of secondary antibodies used.

Target	Label	Manufacture	Dilution	Species	Lot No.
Rabbit	Alexa Fluor 488	Cell Signalling	1:1000	Goat	4412S
Mouse	Alexa Fluor 555	Cell Signalling	1:1000	Goat	4409S

2.2.5 Western blotting

Medium were aspirated and cells were washed with PBS and centrifuged at 100g for 2 minutes to get a pellet. The pellet of cells were lysed in RIPA buffer (Sigma Aldrich R0278) containing 1x phosphatase inhibitor (Roche 906845001), 1x protease inhibitor (Roche 05892970001) and 1ml Phenylmethylsulfonyl fluoride (Sigma Aldrich 000000010837091001). The concentration of proteins determined using BCA assay (Thermo Fisher Scientific 23227). The lysates prepared in 1x sample buffer (62.5 mM Tris-HCl (pH 6.7), 0.5 M sodium pyrophosphate, 1.25 mM EDTA, 1.25% (w/v) sodium dodecyl sulphate, 0.06% (w/v) bromophenol blue, 12.5% (v/v) glycerol and 50 mM dithiothreitol; all from Sigma Aldrich). Five or ten µg of protein sample was run on a 10% acrylamide/bisacrylamide gel for around 70 minutes at 120V. Proteins were transferred to a Polyvinylidene difluoride membrane (Amersham 0600023) for

60 minutes at 100V. The membrane blocked in 5% BSA Tris buffered saline-Tween20 (TBS-T) for 1 hour at RT, following an incubation with desired primary antibody, diluted in blocking solution at 4° C overnight. On the following day, the membrane washed 3 times in TBST and incubated with appropriate HRP-conjugated secondary antibody. Bands were visualized using chemiluminescence (Thermo Fisher Scientific 32106) and developed using X-ray film (Medical Supply Company 34088).

2.2.6 Quantitative real time polymerase chain reaction (qRT-PCR)

Medium were aspirated and cells washed with PBS and RNA extracted using RNeasy Mini kit (Qiagen 74104) following the manufacture's instructions. RNA concentration and purity measured using Nanodrop. 1µg RNA transcribed in to complementary DNA (Qiagen QuantiTect Reverse Transcription kit 205311) and run at final concentration of 10 ng cDNA per well (in triplicate) on a Step One or Roche LightCycler 480 (Table 2.5). The resulted cycle threshold (ct) value were normalized to their GAPDH. The relative quantities of mRNA expression were calculated as being 2^{-ddCt} using the average dCt of a fibroblast or an iPSC line.

Table 2.5. List of qRT PCR primers.

Primer Name	Forward	Reverse
GAPDH	AGGGCTGCTTTTAACTCTGGT	CCCCACTTGATTTTGGAGGGA
OCT4	ACTTCACTGCACTGTACTCCTC	CACCCTTTGTGTTCCCAATTCC
SOX2	AGACTTCACATGTCCCAGCACT	CGGGTTTTCTCCATGCTGTTTC
NANONG	ATAACCTTGGCTGCCGTCTC	ATAACCTTGGCTGCCGTCTC
FOXG1	CCTGCCCTGTGAGTCTTTAAG	GTTCACTTACAGTCTGGTCCC
SYN1	CCCCAATCACAAAGAAATGCTC	ATGTCCTGGAAGTCATGCTG
TUBB3	GCTCAGGGGCCTTTGGACATCTCT	TTTTCACACTCCTTCCGCACCACAT
PAX6	CGGTGAATGGGCGGAGTTAT	CCCTCCCATAAGACCAGGAGA
NESTIN	GCACTTCAAGATGTCCCTC	GGGAAGTTGGGCTCAGGACTG
PSD-95	AGTCAGAAATACCGCTACCAAG	CCG TTCACCTGCAACTCATATC
VGLUT1	TCAATAACAGCACGACCCAC	TCCTGG AATCTGAGTGACAAT
SHANK2	GAGCAGCAGCCTCTATGCTT	GGGAGAGCTTGAGGGTGAAC
SHANK3	ACTCATCCTTCCGCCAACAG	CCCACAGGTGAGTGTGAGAC
GRIN1	AGGCCGTGAGAGACAACAAG	GCCATTCTCGTGGGACTTGA
GRIK1	TCCCGATGGCAAATATGGGG	CCATTGGGCTTCCGGTAGAG
GRIK3	CAATGCCGTCCAGTCCATCT	GGATGAGCCCTGTACTGTCG
GRIA1	GCCATCAGTTTTTGTGCGGA	CTGCTCGTTCAGTTTCTCAGG
GRIA4	CGGTTGAGCGAATGGTCTCT	ACTGATGGCTCTGCTGATCG
CASK	CGACGCAAAGGAACTAAAG	AATAGGGAGAGGTGGGAG
MINT1	CTCCACAATCACCACACCTA	GACCTGATCCACTTCTCCAAG
MUNC18-1	TTCTTATGCCAGTGCCCATAG	CAAACTTGACACCAAACACTACC
NRLG1	GCTGAGTGCAGTTGTAATGAC	CGGTTGGGTTTGGTATGAATG
MAP2	CAGTTTCTGCGCCCAGATTTTA	TCCCAATCAATGCTTCCTCG
NRXN1	TGGACATGGGGTCAGGTACT	TCTCACTCTCACCAGGAGCA
NRXN1	CCGGAGCCAGGAACTTAGAC	GAGCATCGGAGATGAGGTCC
NRXN1	GTCCGCCTCGCAAGGAT	ATTTCCATGGCAGCAGCAAG
CACNA1A	CAGACACCAGCCCCATGAAG	GGTCATGCTCAGGTCTGTCC

2.3 Results

2.3.1 Fibroblast isolation and culture

Human fibroblasts were used as an ideal source of somatic cells for the derivation of iPSCs. Skin biopsies can be obtained from patients/healthy volunteers with ethically approved procedures, and fibroblasts are relatively easy to culture. The skin biopsies have high viability after the biopsy collection and transport, and a high rate of subsequent attachment of cells upon seeding and growing. Human dermal fibroblasts can reach high confluency on 6-well plates around 14 days after seeding with high success rate, making them an ultimate starting material to study disease-related cellular phenotypes.

The skin biopsies were 3mm in diameter obtained with round Visipunch instrument. The biopsy procedures were carried out by a trained clinician at University Hospital Galway (UHG). They were placed in DEME with high P/S and 10% glucose favouring the growth of fibroblasts. The 6-well plates were scrapped with tips at the culture surface to increase roughness. Biopsies were mechanically cut into few pieces and dragged along the scraped surface of 6-well plate to enhance attachment. This method has advantages over enzymatic dissociation of biopsy, which requires lengthy enzymatic treatment, which can reduce cell viability, and over-digestion and difficulty of handling cells can also occur.

An outgrowth of cells from the biopsies could start 3-5 days after the initial plating (Figure 2.5), which became very confluent after 8-14 days, where they were passaged into 6-wells or T25 flask. The success rate of this method is very high, and only one newborn biopsy failed to produce fibroblasts out of over 60 biopsies collected in our laboratory.

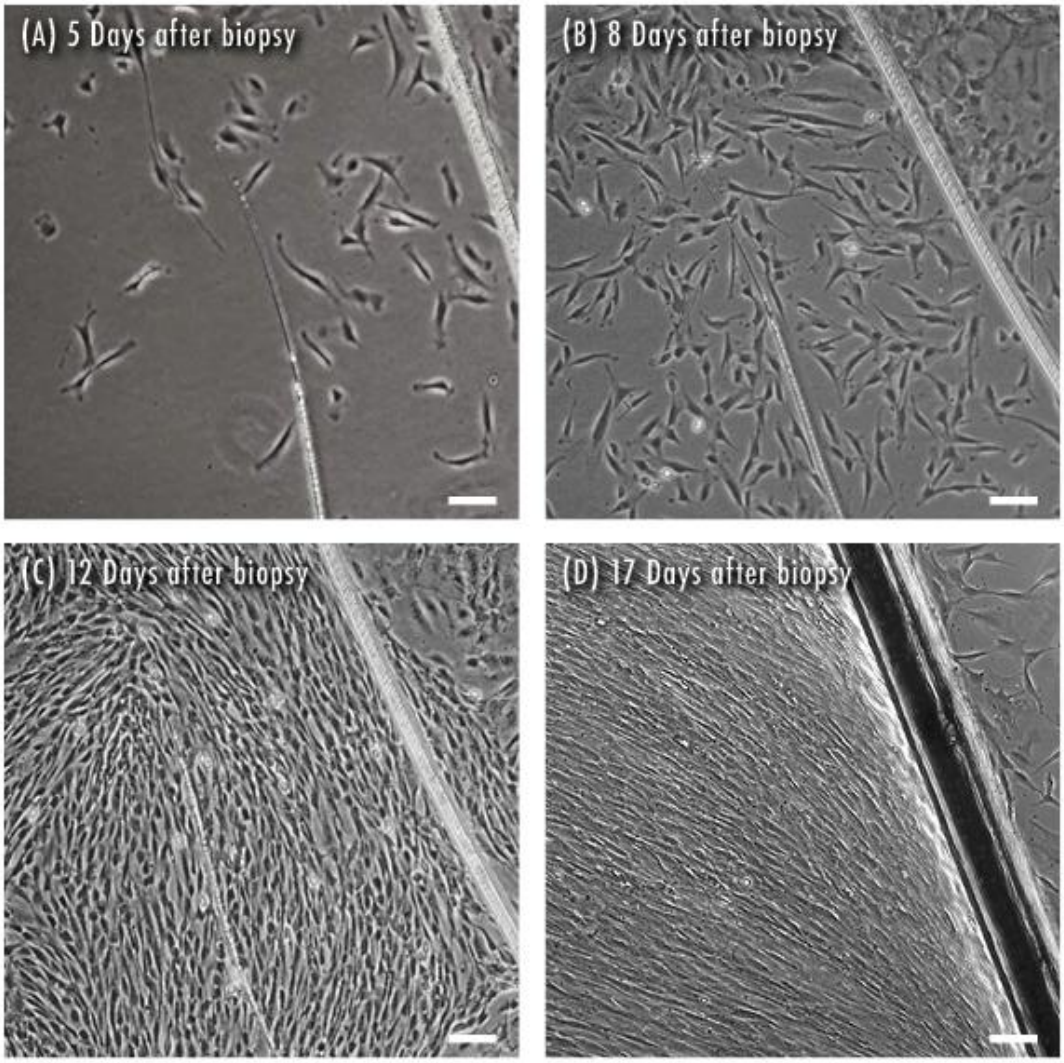

Figure 2.5 Fibroblast outgrowth from skin biopsy. A piece of biopsy was plated in 6-well plate at day 1 and left untouched for 48 hours. Cells started to migrate out of the biopsy after 3-5 days (A) of culture and became progressively confluent after 8-17 days of culture (B-D). Representative images were from the ND4-1 biopsy. Scale bar is 15um. (representative images are from patient line ND4-1). Scale bar is 50μm is at A, B, C, D.

2.3.2 Episomal reprogramming

While most of the cell lines mentioned in Table 2.1 were generated by Katya McDonough, the lines on Table 2.2 were generated by myself, including an ND4-1 line on Table 2.1. In Professor Shen's lab, episomal reprogramming was first trailed by myself in the group (Table 2.6). The reprogramming efficiencies varied a lot between fibroblast lines. It seemed that there was no direct correlation between

age/passage number to the number of colonies collected from this small cohort of experiments.

Table 2.6. Summary of Epi5 episomal reprogramming.

Fibroblast Line	Passage number	Age of the donor	Number of colonies	Number of starting cells
ASD-CB	4	4	14	$1x10^5$
ASD-CD2	4	6	2	$1x10^5$
4C3	12	30	2	$1x10^5$
NRXND4-2*	?	53	3	$1x10^5$
NRXND4-1*	3	30	11	$1x10^5$

*** In conjunction of work with other members of the group for transfection, maintenance and picking up colonies.**

The Epi5 episomal reprogramming contains five vectors. The mixture of three vectors deliver five reprogramming factor Oct4, Sox2, Klf4, L-Myc, and Lin28, and the mixture of two vectors express mp53DD and EBNA1. The vectors were delivered by single transfection using electroporation (programme U-023), following by immediate transfer into feeder-free conditions. The starting number of fibroblast cells was $1x10^5$, with a considerable amount of cell death after electroporation at day 0. The morphology of cells was noticed to change from an elongated shape of fibroblast to smaller cytoplasm and bigger nucleus: cytoplasm ratio of ESC-like cells. This happens at approx. Day 3-7 of post-transfection. The iPSC colonies started to appear after approx. Day 14 (Figure 3.6D). iPSC colonies generated by forming a very clear edge and boundary around them, making them distinguishable from surrounding fibroblasts (Figure 2.6F).

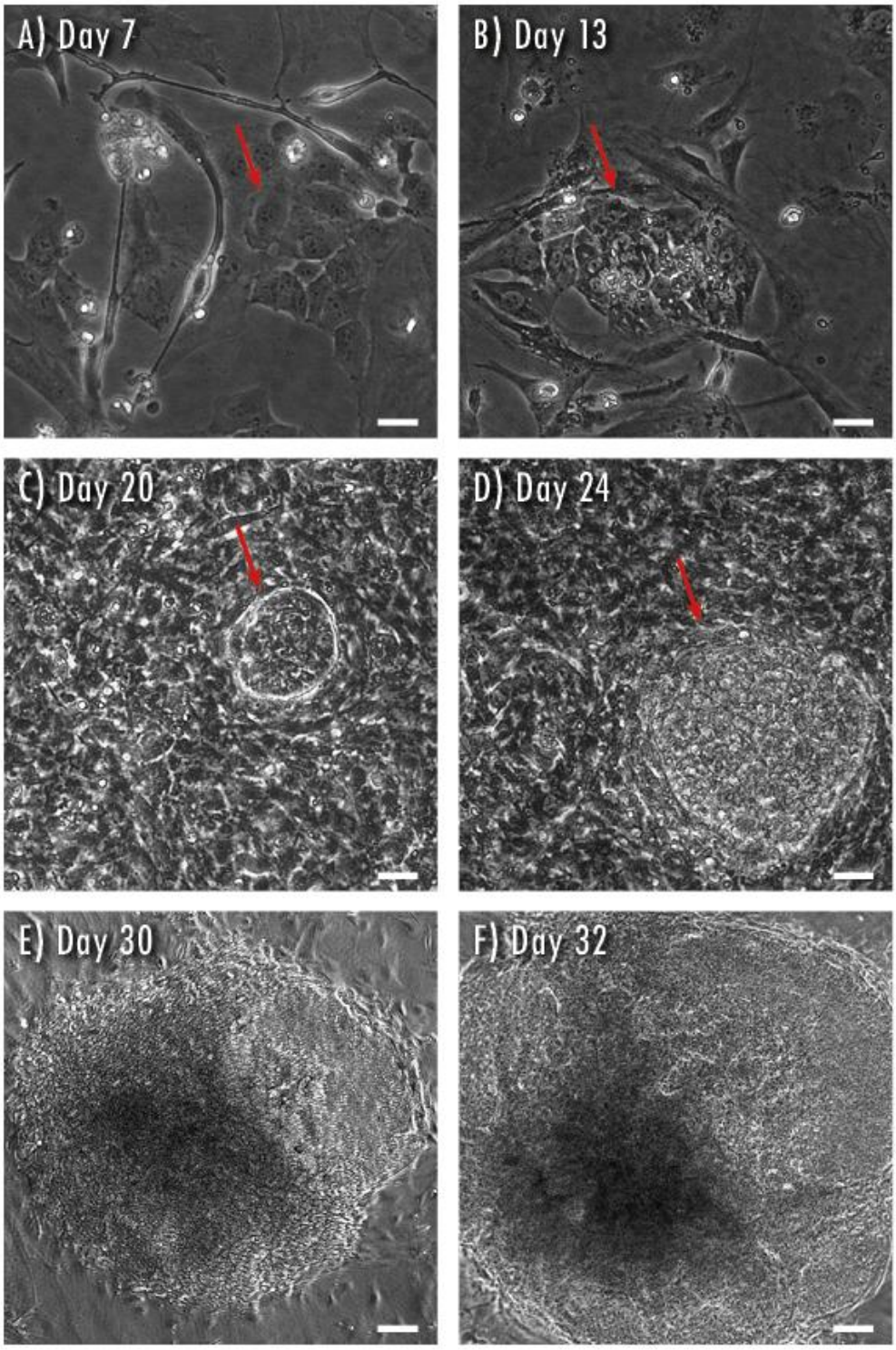

Figure 2.6. Representative images of different stages of episomal reprogramming. Patched reprogramming cells appeared from day 3-7 following electroporation (A). At this stage, the morphology of cells starts to change. Cells are getting clump together and small clear-edge iPSC colonies begin to appear from day 13 above (B). The colonies start getting bigger in size, and they are visible with the naked eye (E-F). Representative images are from ASD-CB and 4C lines. Scale bar is 25 μM for day 7, 13, 20, 24 and 50 μM for day 30 and 32.

The iPSC colonies were mechanically picked and grown on geltrex-coated plates. They were passaged after 5-6 days mechanically using cut-paste, or chemically using gentle cell dissociation reagent (Figure 2.7).

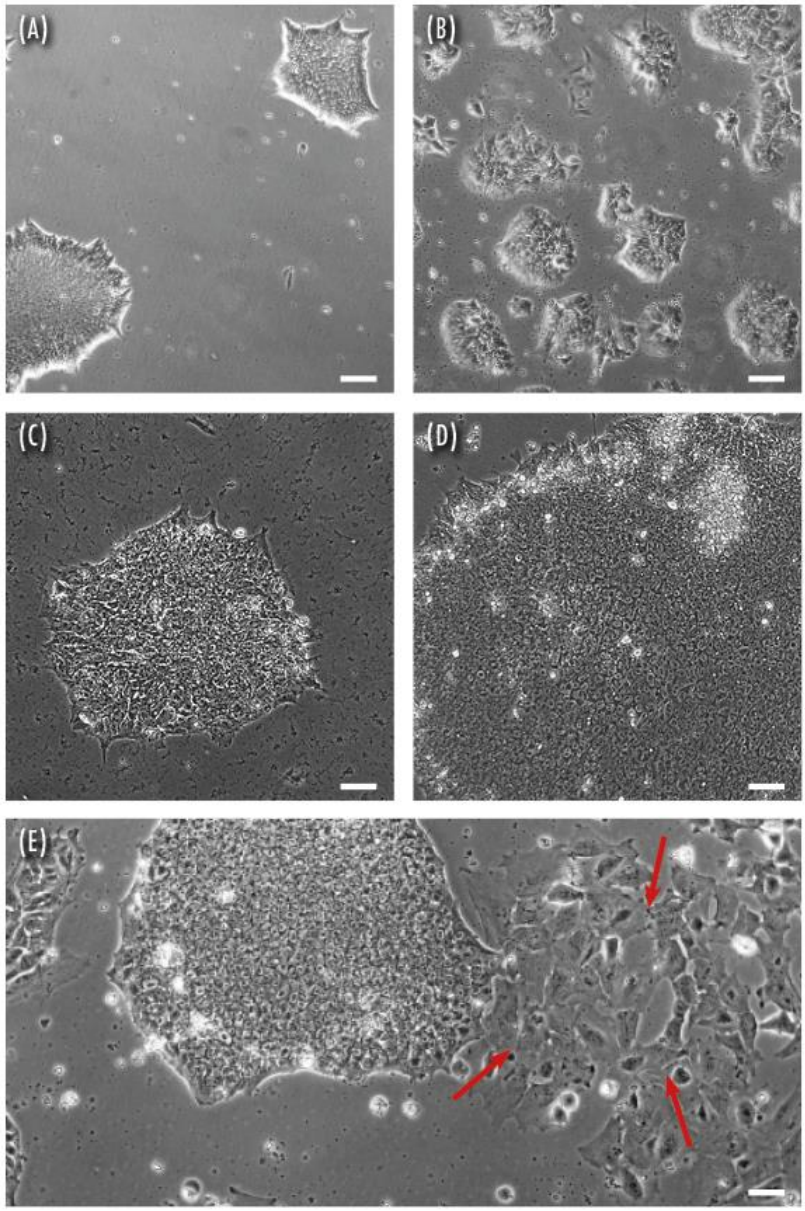

Figure 2.7. iPSCs passaged with mechanical and chemical manipulation. iPSCs were passaged with cut-paste method (A) or gentle cell dissociation reagent (B) every 5-6 days and maintain their pluripotency by keeping their ESC-like morphology (round and small cytoplasm and big nucleus) (C). With the cut-paste method, only 40-50% of cells will attach to the geltrex-coated plates (A). At later passages, iPSC can be passaged using gentle cell dissociation reagent with the much higher attachment of over 80% (b). At early stages of iPSC generation, iPSC may go through spontaneous differentiation, which needs to be mechanically removed (c, red arrows). (A, B 03VC2, C, D ASD-CD2, E 04C iPSC lines). Scale bar is 25 μM for A, B, C, D and 50 μM for E.

When iPSC colonies become stable, they have the morphology resemblance to ESCs (Figure 2.8).

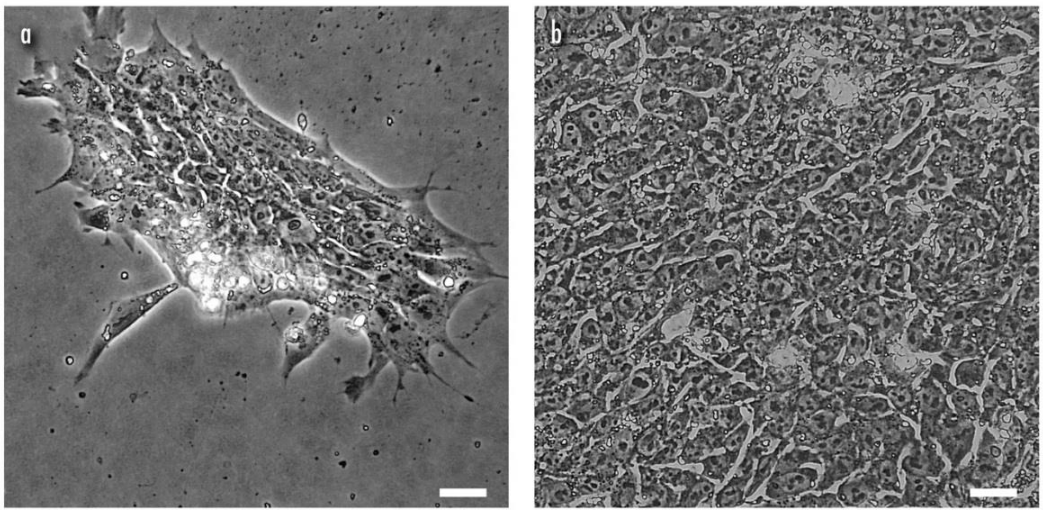

Figure 2.8. iPSC colonies resembling ESC-like morphology. iPSCs can be easily identified under a bright field microscope (a, b). They have round and very small cytoplasm to nucleus ratio (b). This morphology provides an early indication for healthy iPSC colonies to be picked for expansion, maintenance and further application, i.e. differentiation. Scale bar is 25 μM.

After iPSC generation, the first step is to characterize the cells and confirm their pluripotency and their capability for differentiation. The characterization of almost all iPSC lines was carried out by Katya McDonough. There are standard arrays of molecular characterization techniques to verify the pluripotency of iPSCs.

Alkaline phosphatase (AP) staining is a simple method for confirming the pluripotency of iPSCs. AP is a hydrolysing enzyme which dephosphorylates proteins and nucleotides. Pluripotent iPSCs turn to a purple/dark pink colour after staining with high levels of the enzyme (Figure 2.9), while differentiated cells remain colourless.

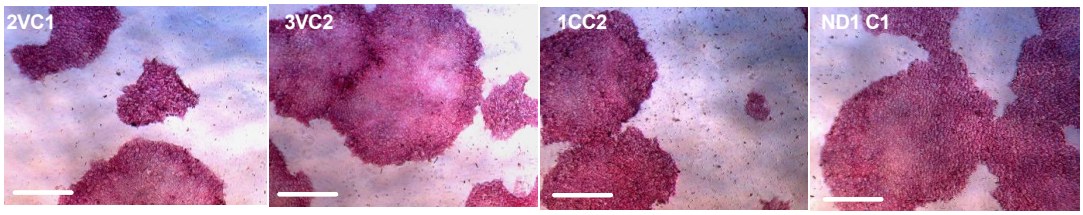

Figure 2.9. iPSCs are positive for alkaline phosphatase staining. Representative images of control and patient lines. Both patient and control lines demonstrate positive staining for alkaline phosphatase. Scale bar in 100 μM.

While AP staining is a reliable method and indicator for pluripotency, more robust assays were required for validation of iPSCs pluripotency. Next, it was necessary to validate and quantify the level of endogenous expression of pluripotent genes expressed in iPSCs. For this reason, RNA was harvested from 3 different iPSC clones from each line to reduce the heterogeneity among iPSCs. Quantitative qRT-PCR was performed to measure the expression of *OCT4* and *SOX2* (Figure 2.10).

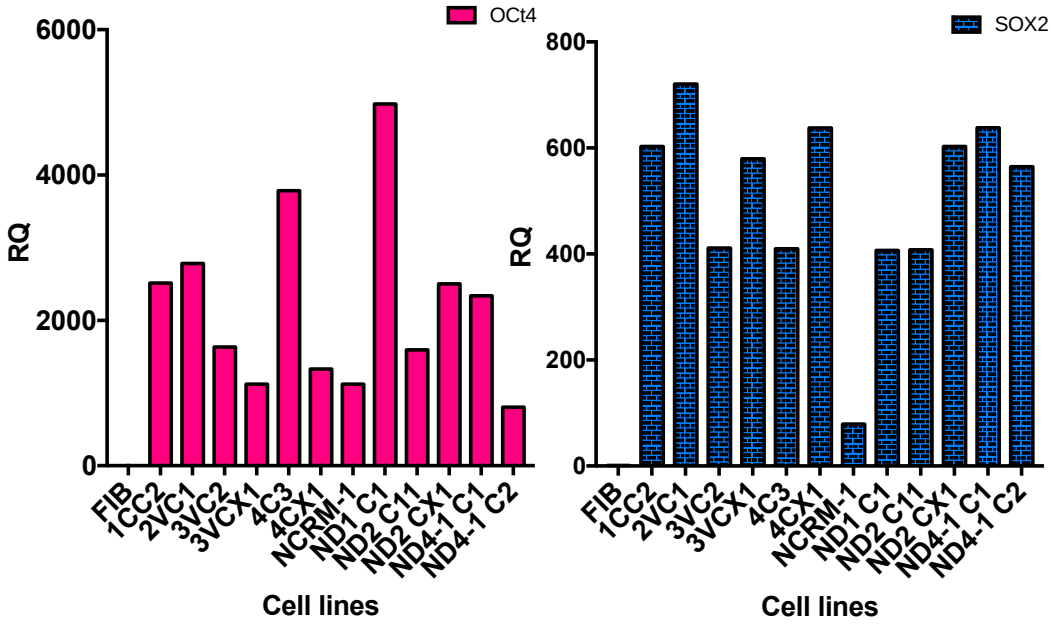

Figure 2.10. iPSCs express pluripotency markers verified by qRT-PCR. iPSCs from all control and *NRXN1α* deletion lines used in this study showed positive expression of *OCT4* and *SOX2*. GAPDH used as a housekeeping genes and fibroblast (FIB) as a negative control.

Next, immunocytochemistry staining was used to validate the expression of endogenous associated pluripotency markers OCT4, SOX2 at the protein level (Figure

2.11, 2.12), as well as surface markers SSEA4, TRA-1-60 and TRA-1-81 (data not shown). All cell lines demonstrated for this study showed very high levels of expression for all the pluripotency markers.

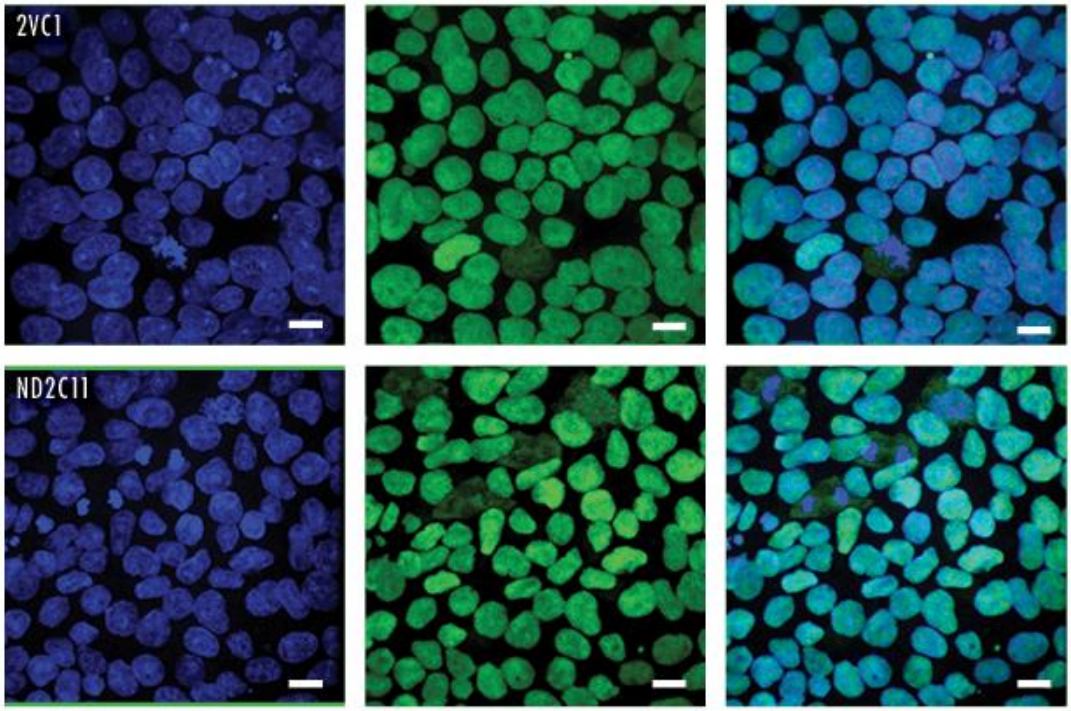

Figure 2.11. iPSCs positively express pluripotency markers. Representative images of Control and a patient line showing positive expression of OCT4 (green) with DAPI (blue) (Adopted from Katya McDonough PhD thesis). Scale bar 10 μM.

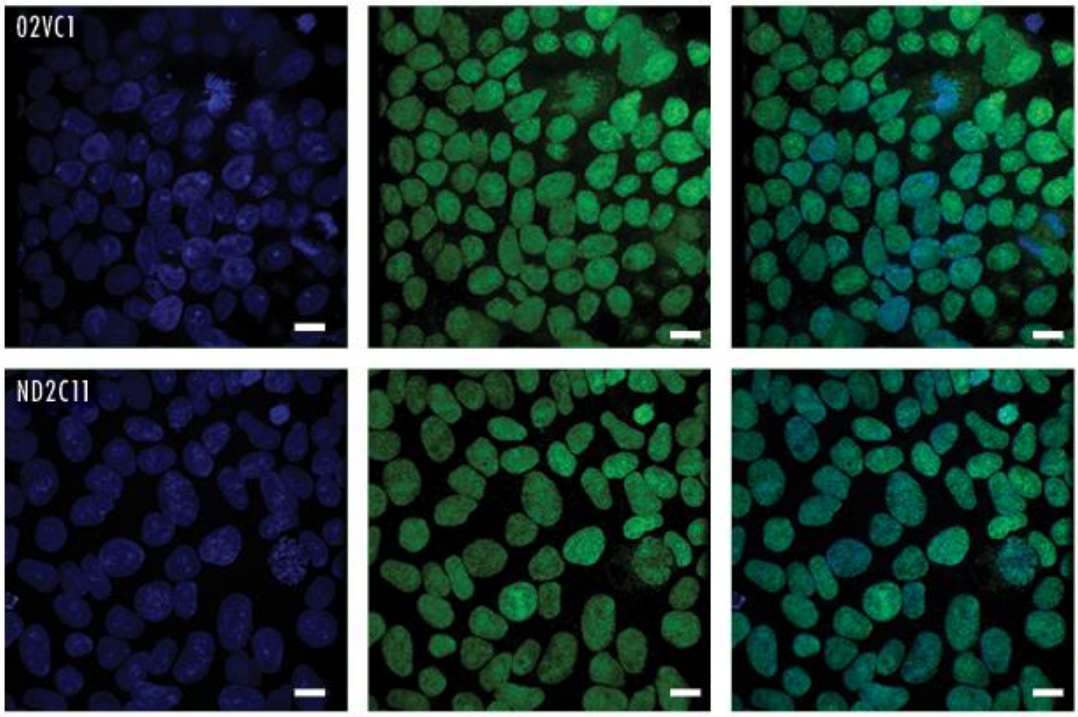

Figure 2.12. iPSCs positively express pluripotency markers. Representative images of Control and a patient line showing positive expression of SOX2 (green) with DAPI (blue) (Adopted from Katya McDonough PhD thesis). Scale bar 10 μM.

For iPSCs to be able to differentiate to any germ layers, embryoid bodies (EBs) were generated. This was to confirm the capability of iPSCs into the tri-lineage differentiation, giving rise to three germ layers. $2.0X10^5$ iPSCs were dissociated with accutase and transferred into Aggrewell plates. EBs were transferred in suspension culture into a flask after only 24 hours of culture. This resulted in generating 800-1100 EBs per line. To validate the pluripotency of the cells, the EBs were picked and seeded into Geltrex-coated 8-well chamber slides. Different types of spontaneously differentiated cells emerged from the EBs after subsequent six days of culture. Cells were stained for makers for all three germ layers (alpha-fetoprotein for endoderm, alpha-smooth muscle actin for mesoderm and beta III tubulin for ectoderm (Figure 2.13).

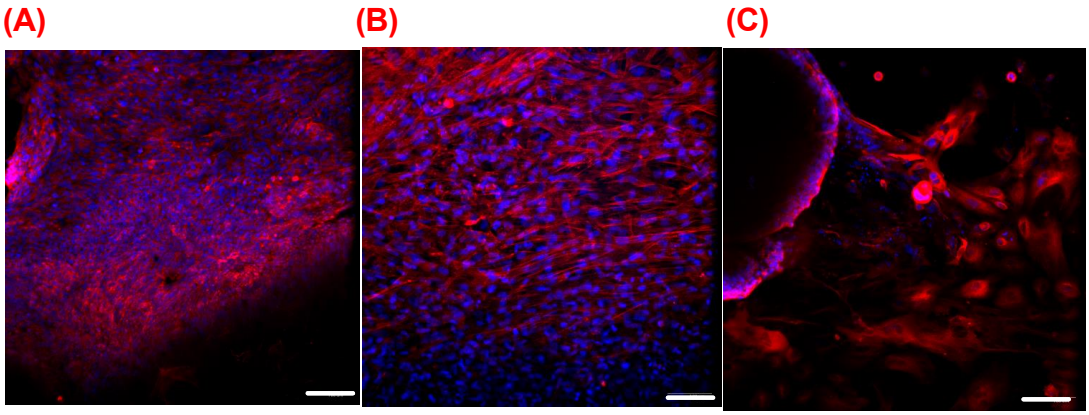

Figure 2.13. EBs shows tri-lineage differentiation into endoderm, ectoderm and mesoderm. Representative images of control line 02VC1 of EBs spontaneously differentiate to (A) AFP+ (endoderm), (B) TUJ+ (ectoderm) and (C) ASM+ (mesoderm). Scale bar 100 μM. (Adopted from Katya McDonough PhD thesis).

Finally, the isolated RNA from iPSCs were further validated with pluritest. This was a widely used method to replace the teratoma formation assay. The RNA samples were shipped to Cedars Sinai, Los Angeles for pluritest test to be performed. Pluritest did not carry test of all the iPSC lines, but at least one clone for each patient and control line were tested (Table 3.4).

Table 2.7. Summary of all pluripotency tests performed on iPSC line from the lines which were used in this study.

Cell line	AP stain	qRT-PCR (OCT4, SOX2, NANOG)	Immunostaining (OCT4, SOX2, NANOG, SSEA4, TRA-1-60, TRA-1-81)	EB formation	Pluritest
01C	✓	✓	✓	✓	✓
02V	✓	✓	✓	✓	✓
03V	✓	✓	✓	✓	✓
04C	✓	✓	✓	✓	✓
ND1	✓	✓	✓	✓	✓
ND2	✓	✓	✓	✓	✓
ND4*	✓	✓	✓	✓	✓

*All tests were performed by Dr Katya McDonough (I partly involved in generating, maintaining, picking up colonies and qRT-PCR for ND4).

To validate the deletion of *NRXN1α* gene, whole genomic sequencing was performed at University College Dublin (UCD) Academic Centre on Rare Disease by Professor Sean Ennis. The CNV data confirmed *NRXN1α* deletion in all patient iPSC lines (Table 2.5) with no *NRXN1α* deletion in control lines.

Table 2.8. Whole genomic DNA sequencing of *NRXN1α* iPSC lines.

Cell line name	**ND1 C1**	**ND4-1 C1**	**ND4-1 C2**	**ND2 C11**
Chromosome position (Hg19)	chr2:50711687-51044633	chr2:50983186-51471321	chr2:50983186-51471321	chr2:51120335-51360666
No. SNP	116	131	131	71
Length (bp)	332,947	488,136	488,136	240,332
Deletion/Duplication	Deletion	Deletion	Deletion	Deletion
Copy number	1	1	1	1
Start SNP	rs10221724	rs17041014	rs17041014	rs17041090
End SNP	rs10185764	rs2193392	rs2193392	rs11125335

2.3.3 The iPSC proliferation remained unchanged in *NRXN1α* deletion lines

To assess the proliferation rate of iPSCs, immunostaining was performed in control and patient lines. Proliferating cells were presented by the percentage of Ki67 positive cells and cells at the mitotic phase (M) using PH3 antibody. The statistical analyses showed that there was no significant difference between control and patient iPSCs in relation to proliferating cells and mitotic cells (Figure 2.14).

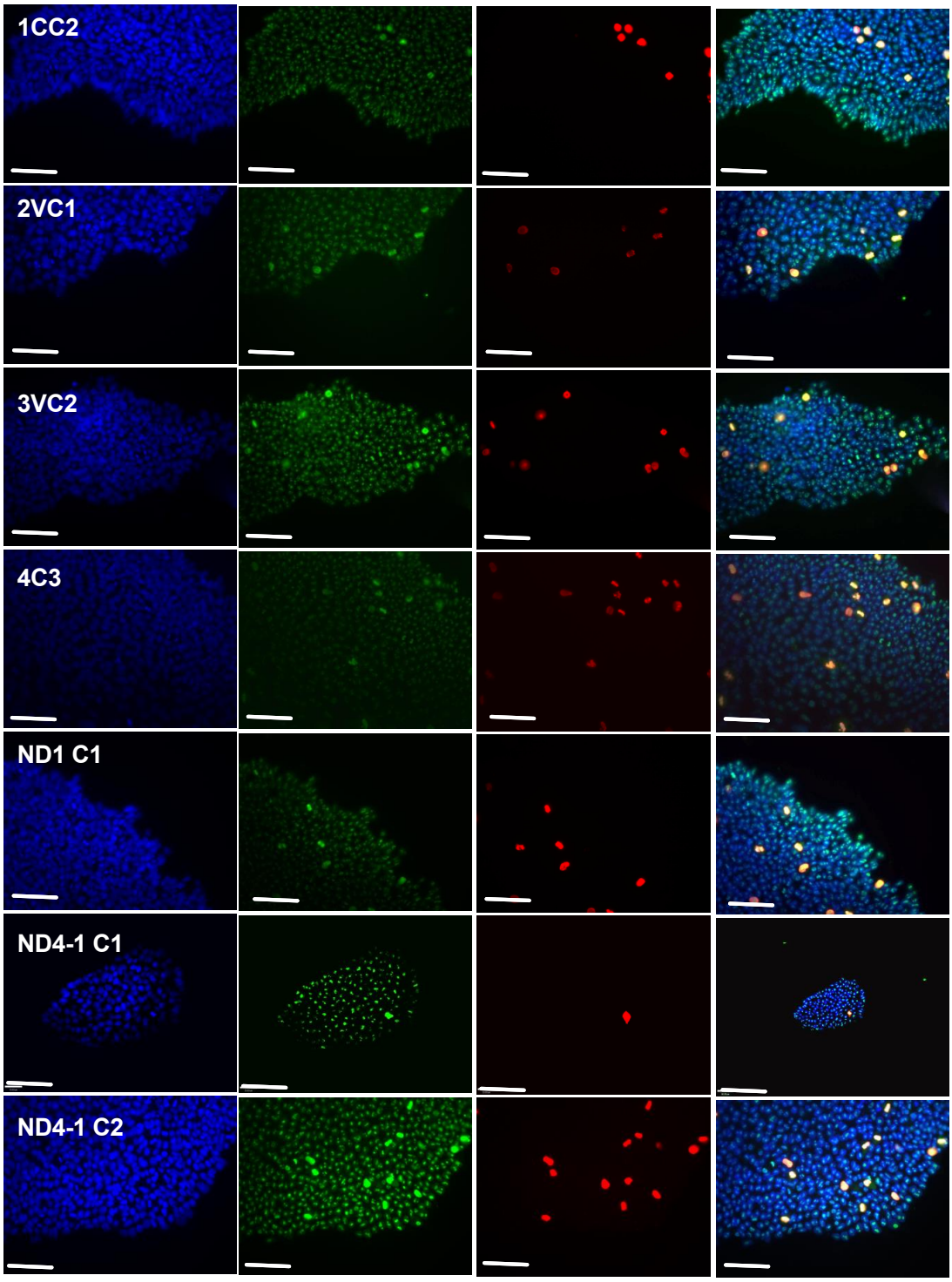
1CC2
2VC1
3VC2
4C3
ND1 C1
ND4-1 C1
ND4-1 C2

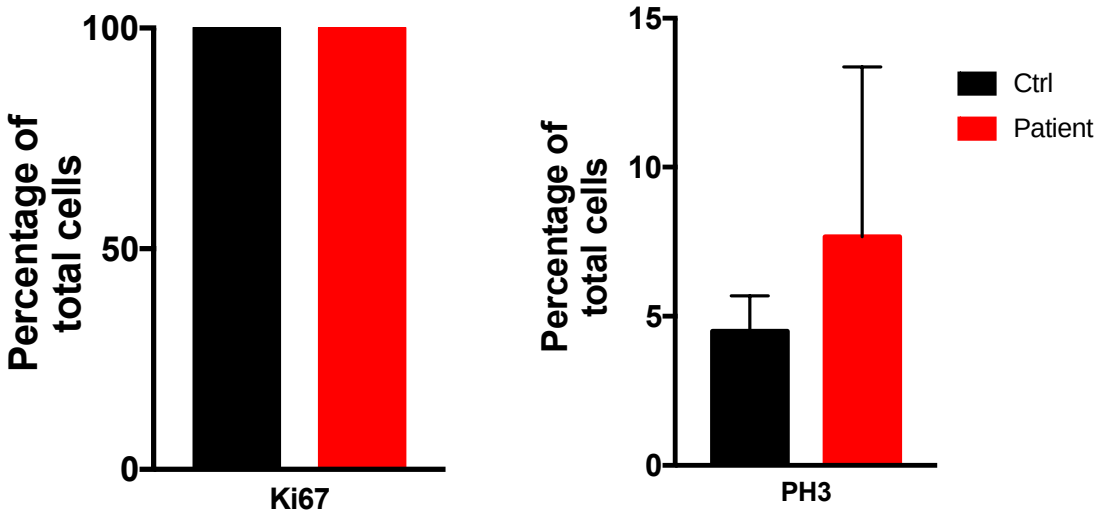

Figure 2.14. There is no significant difference in proliferation rate between control and patient iPSCs. Representative images of double immunostaining of Ki67 (red) and PH3 (green) of undifferentiated iPSCs from control individuals and *NRXN1α* deletion patients. The diagram shows the percentage of cells positive for Ki67 and PH3. (Ctrl n=4, Patient n=3). All data summary were means ± SEM. Scale bar 60 μM for all except for ND4-1 C1 which is 100 μM.

2.3.4 Neural induction using dual SMAD inhibition

IPSCs were plated in 3.7 cm^2 dish (12-well plate) at very high confluency (90%) for the maximum of three days. The SMAD inhibitors LDN193189 and SB431542 were added daily for neural induction period for 10-12 days, leading to a thick and very dense layer of neuroepithelium formed. During this period, the large nuclei of iPSCs gradually replaced with small and elongated nuclei of neuroepithelial cells. The high number of cell death was also aberrant after around day 5-6, depending on the cell line (Figure 2.15A).

Cells at day 10-12 were then passaged in 1:2 ratio of aggregates of 300-500 cells by pipetting up and down 3~4 times to gently suspend cells in neural induction medium. The neuronal rosettes were observed under an inverted microscope after the split. These were a developmental signature and a good indication of NPCs (Figure 2.15A). The cells during this stage lost their pluripotency by lacking the expression of pluripotent markers such as *OCT4* and gradually increased the expression of neural progenitor cell (NPC) marker such as *PAX6* (Figure 2.15B).

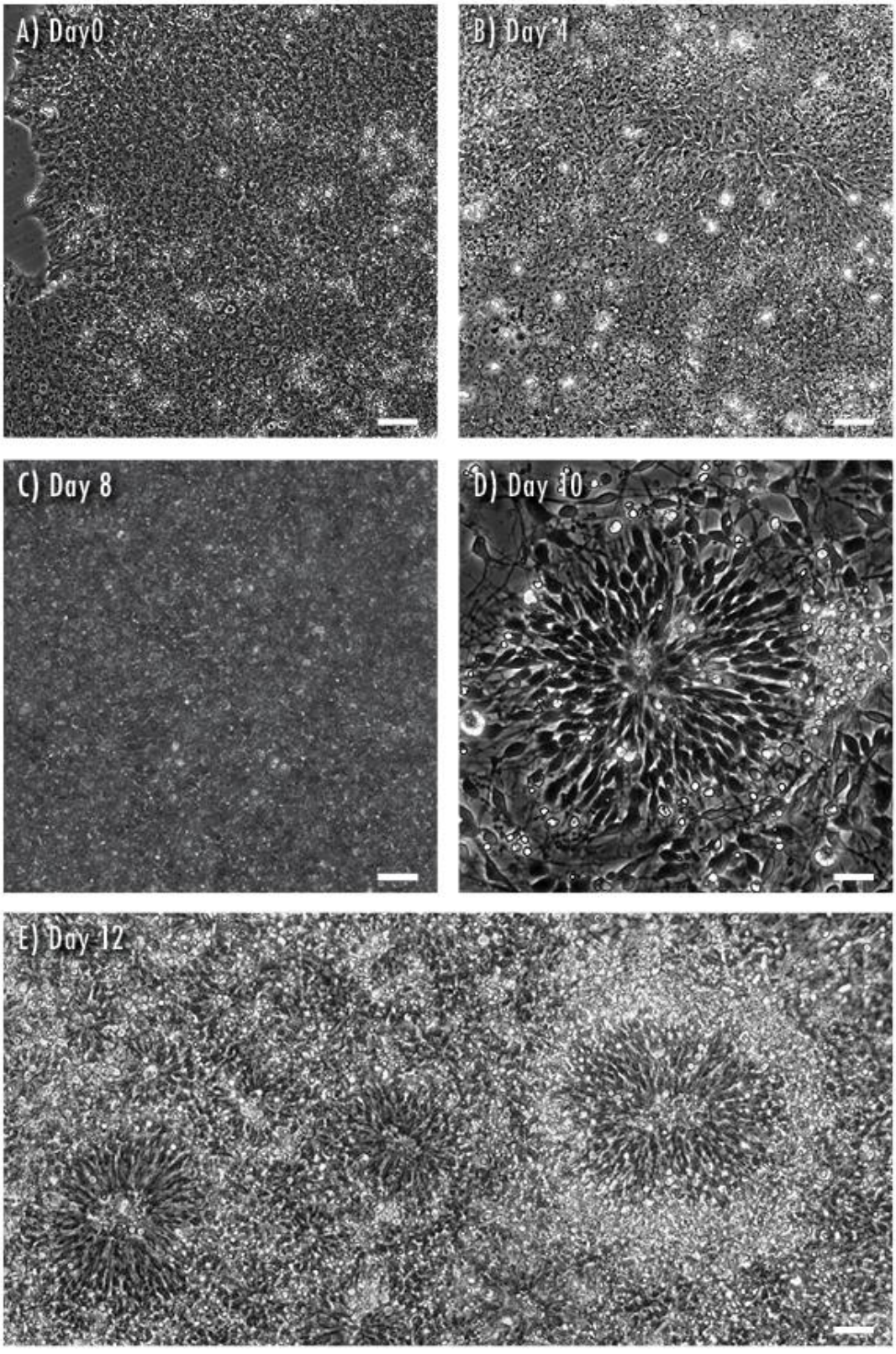
A) Day0
B) Day 4
C) Day 8
D) Day 10
E) Day 12

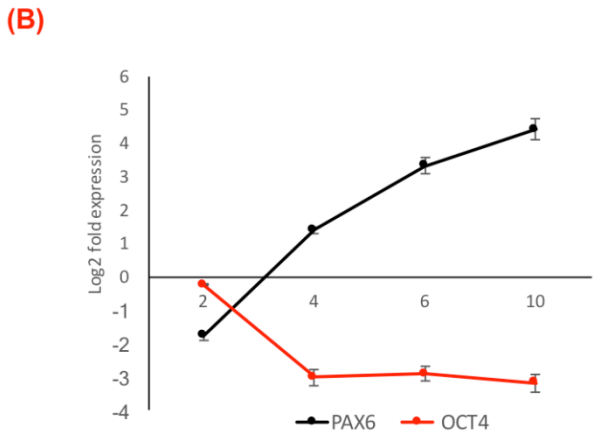

Figure 2.15. Successful neuronal induction generating neuronal rosettes, a signature indicator of neural progenitors. (A) Time-dependent generation of neuronal rosettes through the course of neural induction from day 0 to 12 (top to bottom). Cell morphology changes from small, round, big nucleus of iPSCs into columnar shape, bigger and elongated cytoplasm of NPCs (red arrow). Scale bar 40 µM in day 0, 4, 8, 10, and 100 µM in day 12 (B) successful confirmation of neural induction by down-regulation of pluripotent marker *Oct4* and expression of cortical progenitor marker *PAX6* by qRT-PCR (control n=2).

2.3.5 Validation of iPSC derived neurons at an early stage of differentiation

NPCs undergo proliferation, and the culture dish becomes very dense. At the stage of day 20, NPCs were validated and quantified by the positive expression of *PAX6*, *NESTIN*, *FOXG1* and *NGN2* at RNA level using qRT-PCR (Figure 2.15A). The expression of *PAX6* ($p<0.60$), *NESTIN* ($p<0.29$), *FOXG1* ($p<0.10$) and *NGN2* ($p<0.74$) showed no significant difference between the control and *NRXN1α* deletion neural progenitors.

To further verify the NPCs, cells stained with NESTIN (Figure 2.16C) and PAX6 (Figure 3.2D) which were found in 87% and 82% of cells, respectively (Figure 2.16B). This further indicate that the majority of the cells were of the dorsal identity of the progenitors. Moreover, the expression of PAX6 at day 20 was also quantified using western blot along with its negative expression in iPSCs (Figure 3.16E), and abundant PAX6 proteins were also detected in NPCs differentiated from all lines of iPSCs.

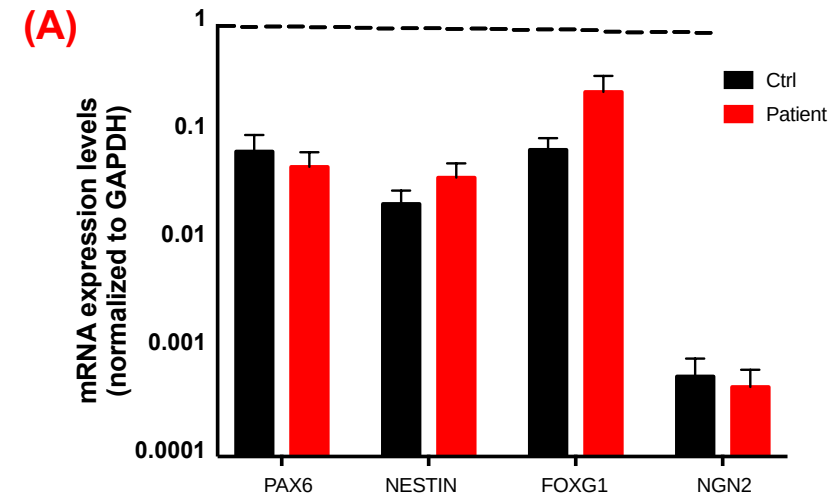
(A)
mRNA expression levels (normalized to GAPDH)
1
0.1
0.01
0.001
0.0001
Ctrl
Patient
PAX6
NESTIN
FOXG1
NGN2

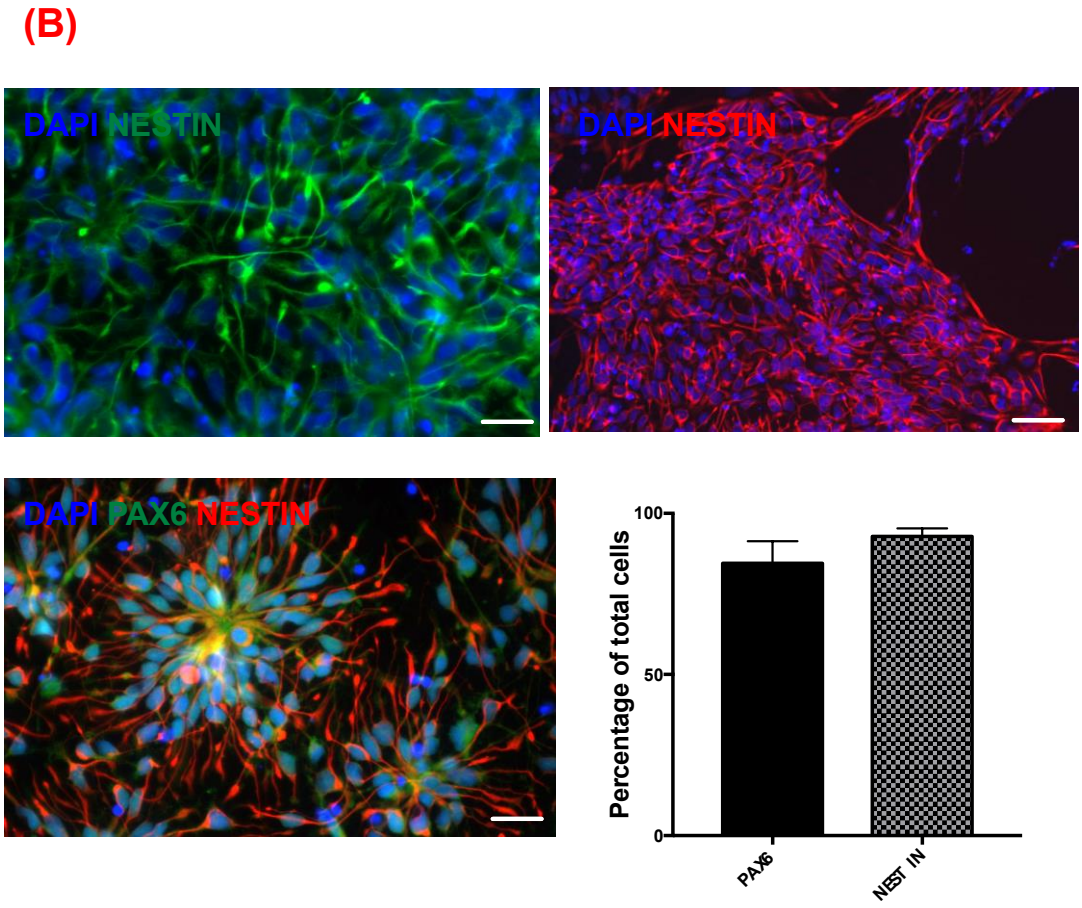
(B)
DAPI NESTIN
DAPI NESTIN
DAPI PAX6 NESTIN
Percentage of total cells
100
50
0
PAX6
NEST IN

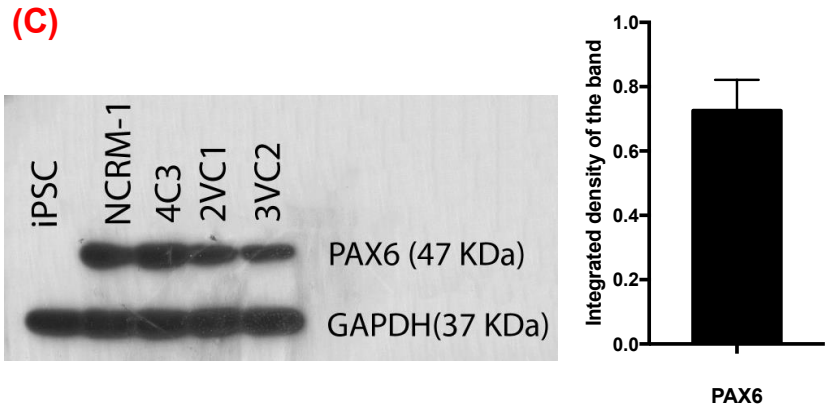

Figure 2.16. Dual SMAD inhibition allows highly efficient generation of neural progenitors in feeder-free monolayer differentiation. (A) Real-time PCR shows the relative positive expression *PAX6, NGN2, FOXG1* and *NESTIN* in Control [n=4 (1CC2, 3VC2, 4CX1, NCRM-1] and patients [n=4 (ND4-1C1, ND2C11, ND1C1, ND2CX1)], iPSCs shown as dashed bars as negative control. (B) Representative images of NESTIN and PAX6 with quantitative analysis (Control n=2 (3VC2, 4CX1)). (Scale bar 50 μM for DAPI/NESTIN images and 25 μM for DAPI/NESTIN/PAX6 image). (C) Quantitative positive measurement of PAX6 in western blotting in neuro progenitor cells and negative expression in iPSC line [Control (3VC2, 4CX1, NCRM-1, 4C3)] (normalized to GAPDH). All data summary are means ± SEM.

The proliferation rate of NPCs was evaluated by the positive expression of Ki67 at day 20 of differentiation. This was compared between a group of control and patient lines, and no significant change was observed ($p<0.21$) (Figure 2.17).

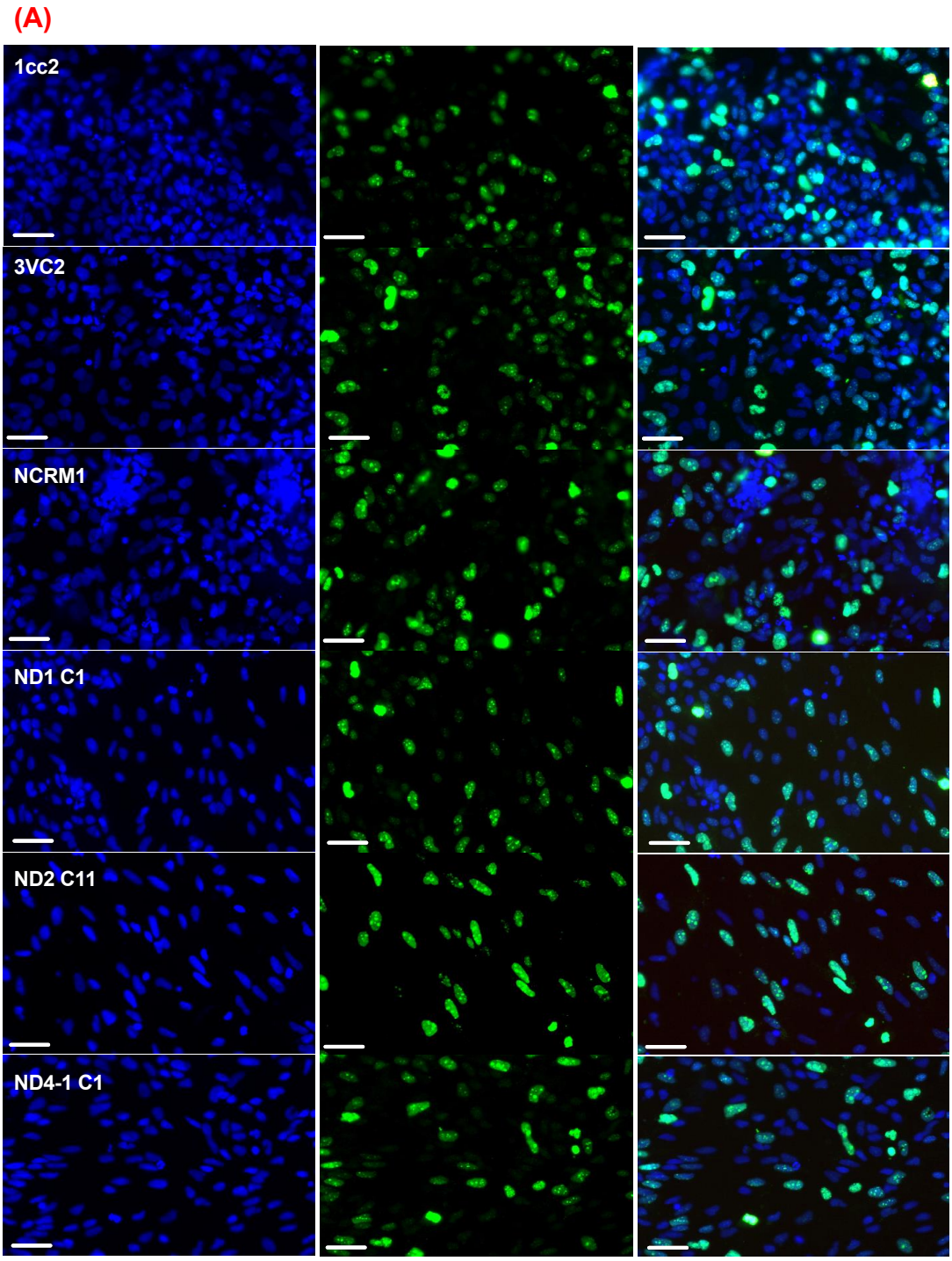
(A)
1cc2
3VC2
NCRM1
ND1 C1
ND2 C11
ND4-1 C1

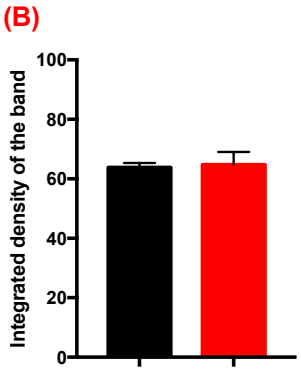

Figure 2.17. NPC proliferation remains unchanged in NRXN1α deletion neurons. (A) Representative images of Ki67 marker (green) in control [1CC2, 3VC2, NCRM-1] and patients (B) [ND4-1C1, ND2C11, ND1C1]. (C) The proportion of Ki67+ neuronal progenitors in control and patients shows no significant difference. Scale bar 30 μm. All data summary are means ± SEM.

Cells were further passaged at day 20 of differentiation in 1:2 ratio into poly-D laminin 12-well plates with aggregates of 300-500 cells using 5 ml pipette. Cells at day 30 of differentiation were validated and assessed using qRT-PCR and immunofluorescence staining.

The expression of PAX6 was significantly reduced on the next consecutive 10 days by day 30 of differentiation at the cellular level using immunofluorescent staining, and $PAX6^{+}$ cells were reduced from 87% at day 20 to 47% at day 30 ($p<0.0009$, Figure 2.18A), indicating more cells come out of cell cycles during the period. Post-mitotic newborn neurons express doublecortin (DCX), essential for developing and migration of cortical neurons. The expression of DCX was shown to significantly increase at early stages of differentiation at the RNA level ($p<0.0001$) between day 20 and 30 of differentiation (Figure 2.18B). Consistent with the birth of neurons, the relative expression of pan-neuronal marker TUJ1 was significantly increased in day 30 cultures ($p<0.007$).

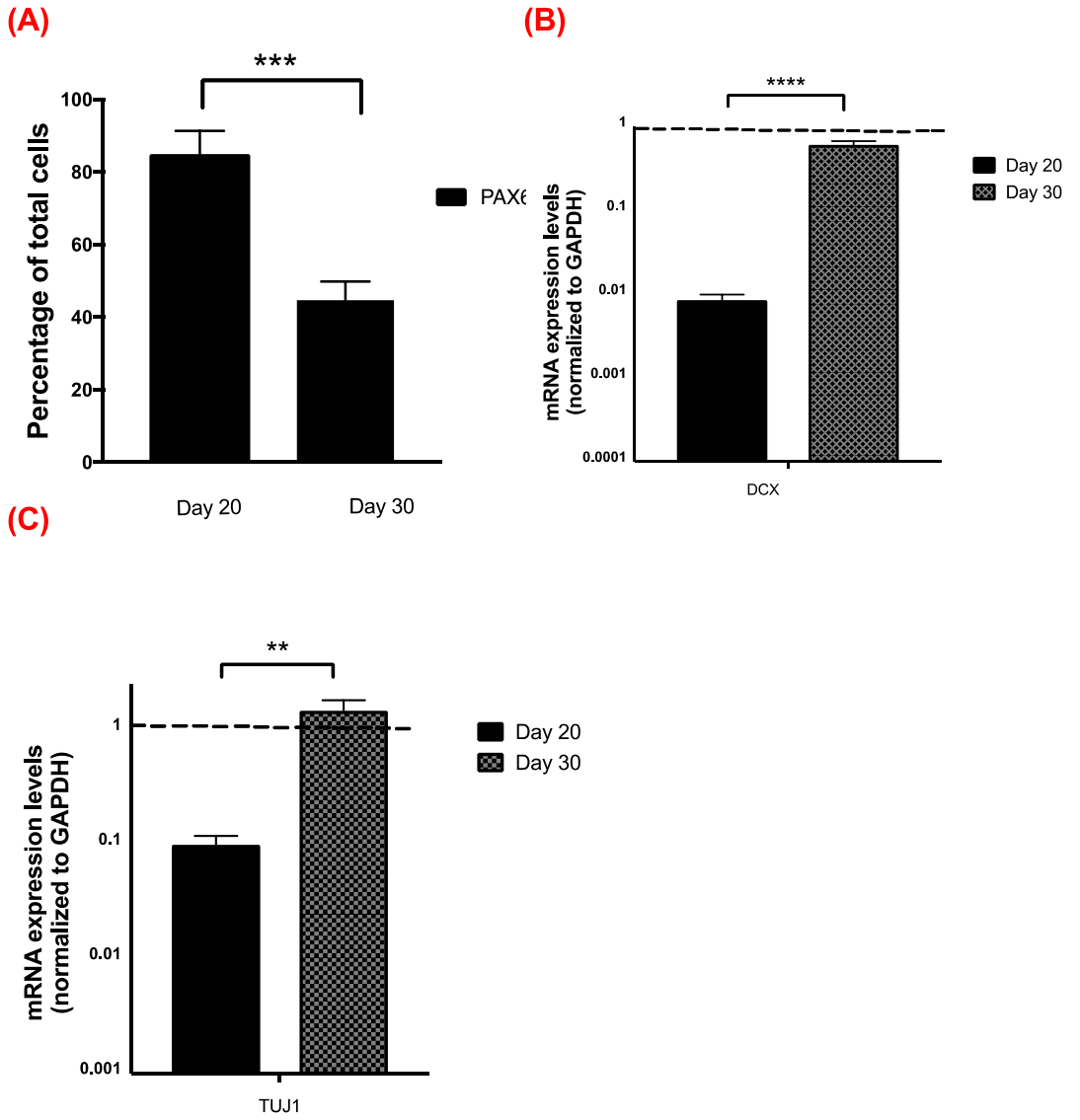

Figure 2.18. Expression level of PAX6, DCX and Tuj1 at early stages of differentiation. (A) The PAX6+ cells were reduced by 40% from day 20 (87%) to day 30 (47%) ($p < 0.0009$) using immunofluorescence staining (control n=2). (B) Comparative analysis reveals a marked increase of post-mitotic marker *DCX* mRNA expression between day 20 and 30, suggesting a significant birth of new-born neurons during the period. [Control n=4 (1CC2, 3VC2, 4CX1, NCRM-1)]. (C) Comparative analysis of pan-neuronal marker *TUJ1* using qRT-PCR also showed a significant increase from day 20 to 30 of differentiation [Control n=4 (1CC2, 3VC2, 4CX1, NCRM-1)]. Statistical analysis evaluated using ttest (*$p<0.05$), **$p<0.01$, *** $p<0.001$). All data were presented as means ± SEM.

To examine the effect of *NRXN1α* on early neuronal development and differentiation, the expression of various proteins were investigated at day 30 of differentiation. Quantitative expression, *DCX* (double cortin), *TUJ1* (pan neuronal marker) and *GFAP* (astrocyte marker) measured at the RNA level using qRT-PCR (Figure 2.19A). There

was no significant difference between control and *NRXN1α* deletion cultures [(*DCX* p<0.22), (*TUJ1* p<0.19), (*GFAP* p<0.37)].

To quantitatively measure the appearance of early post-mitotic neurons and proliferating cells, DCX and Ki67 examined at day 30 of differentiation. This confirmed that the proliferation of neurons at early stages of differentiation was similar between control and patient samples (Figure 2.19B).

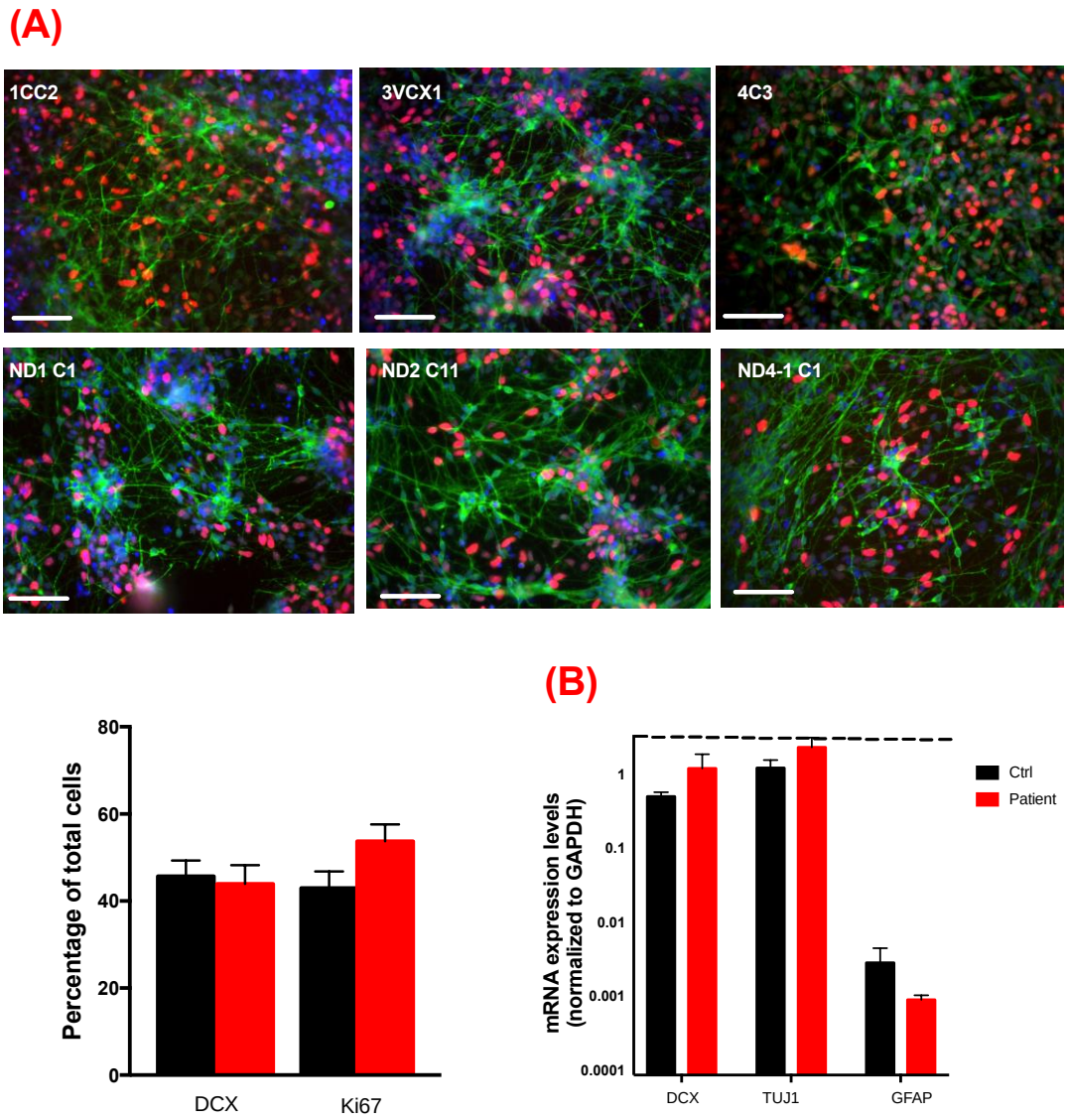

Figure 2.19. Expression of early post-mitotic and proliferating marker at 30 days of differentiation. (A) Representative immunofluorescence imaging of DCX (green) Ki67 (red) with nuclear staining DAPI (blue), with quantification graph at the bottom left. Scale bar 50 µm. (B) Comparative analysis of *DCX, TUJ1* and *GFAP* at day 30 of differentiation using qRT-PCR [Control n=6 (1CC2, 3VCX1, 4C3, 3VC2, 2VC1, 4CX1), Patient n=4 (ND4-1C1, ND2C11, ND1C1, ND2CX1)]. All data summary are means ± SEM.

To examine the morphology of the neurons at early days of differentiation, the cell body size and the diameter of the cells were measured in TUJ1 positive cells at day 30 of differentiation (Figure 2.20A). There was no significant difference between control and patients (Figure 2.19B).

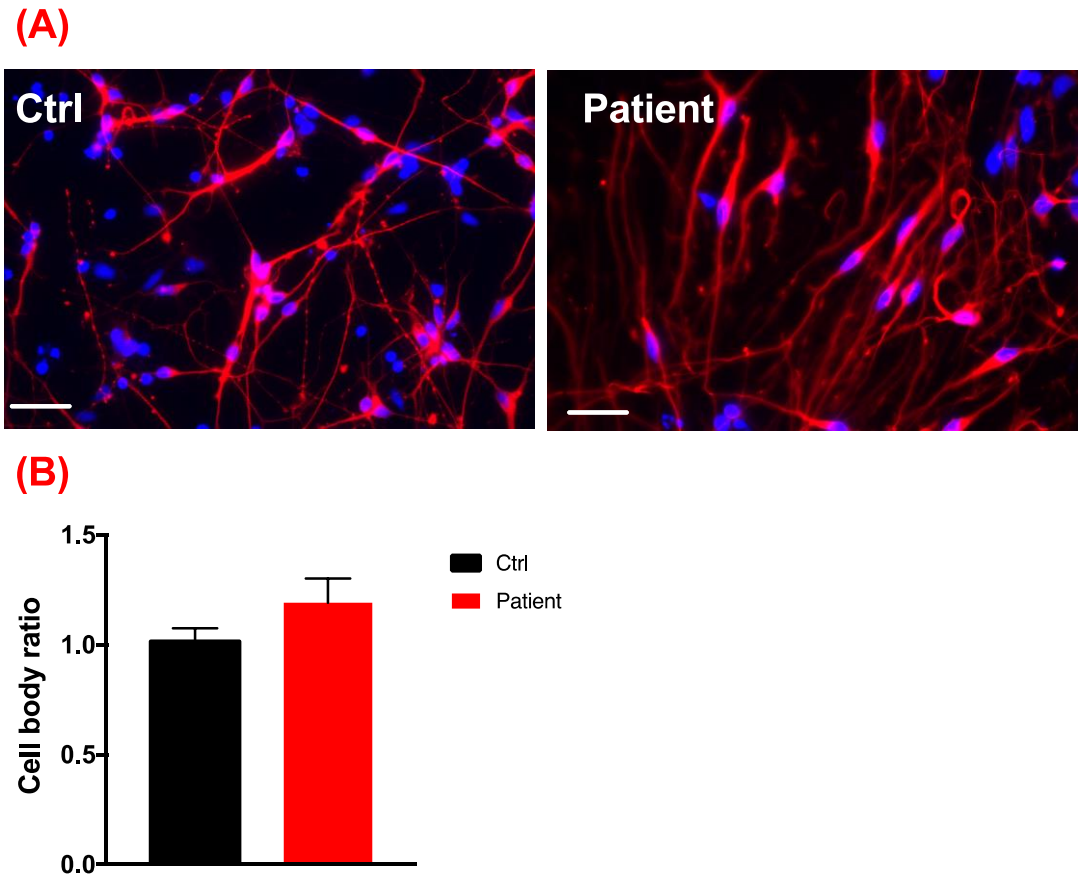

Figure 2.20. The morphology of cell remains unchanged in NRXN1α deletion neurons. (A) Representative images of TUJ1^{+} cell staining. (B) The cell body size and diameter of TUJ1 positive cells showed no significant difference ($P<0.48$, $P<0.52$ respectively) (Control n=3 (1CC2, 3VCX1, 4C3; Patient (ND4-1C1, ND2C11, ND1C1, ND2CX1). Scale bar 25µm. All data summary are means ± SEM.

2.3.6 100 days neurons express different classes of excitatory cortical neurons

NPCs were cultured for up to 100 days to become mature neurons and to generate different classes of excitatory cortical neurons. The post-mitotic population of neurons emerged from neuronal rosettes and created a very dense neuronal network throughout the course of differentiation (Figure 2.21).

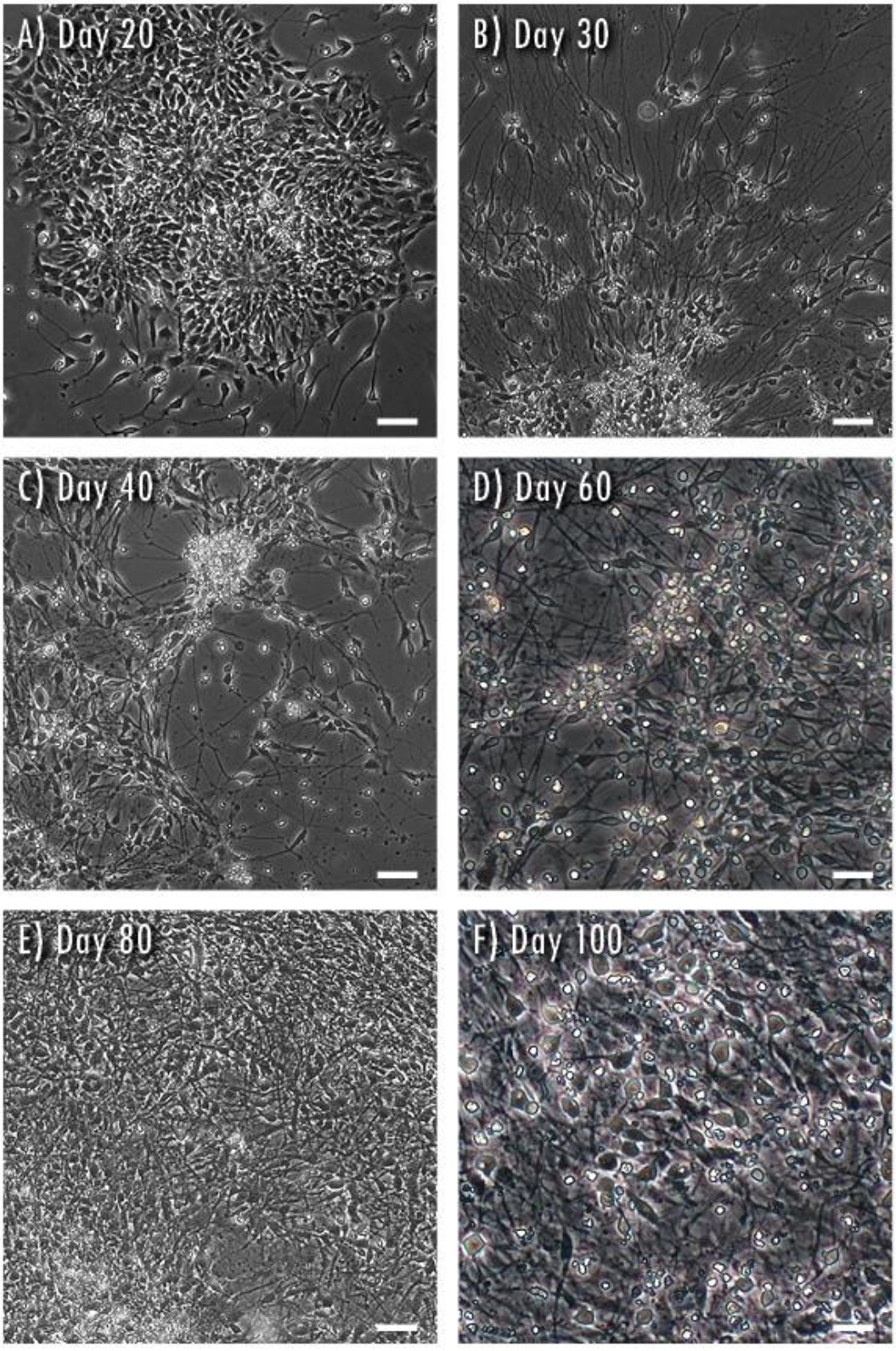

Figure 2.21. Morphological changes in iPSC-derived cultures during neuronal differentiation. (A) Neurons emerged from neuronal rosettes (a) and differentiated into a very dense network of cells by day 100 of differentiation. Scale bar 30 μM at day 20, 40, 60, 80 and 100, and 60 μM at day 30.

To characterize the subsets of excitatory neurons, total RNA was harvested, and the expression of lower layer cortical markers (*TBR1*, *CTIP2*) and upper layer markers (*BRN2*, *SATB2*) was quantitatively measured at day 100 of differentiated neurons using qRT-PCR (Figure 2.22A). It appeared there was no significant difference in *NRXN1α* deletion neurons in their differentiation capability to different subsets of cortical neurons (*TBR1* p<0.63, *CTIP2* p<0.41, *BRN2* p<0.23, *SATB2* p<0.06)].

The expression of these markers was further evaluated at the RNA level using highly sensitive whole genome RNA sequencing method. The transcript per million (TPM) of *TBR1*, *CTIP2*, *BRN2* and *SATB2* shows the same trend of expression as in qRT-PCR, confirming our previous results and differentiation protocol (Figure 2.22B) with no statistical difference. This suggests that *NRXN1α* deletion may not alter the architecture of excitatory cortical cell types if migration is not taken into count. To further confirm the expression of the selected markers, CTIP2 and TBR1 also measured at the cellular level using immunofluorescent staining, which showed 36.18% of $CTIP2^{+}$ cells and 23.35% of $TBR1^{+}$ lower layer cortical neurons among the total population (Figure 2.23B). However, the expression of major inhibitory markers, such as Parvalbumin and SST, showed very little expression in comparison to excitatory markers (Figure 2.23B). This further confirmed that the majority of the iPSC-derived cells were the excitatory cortical neurons.

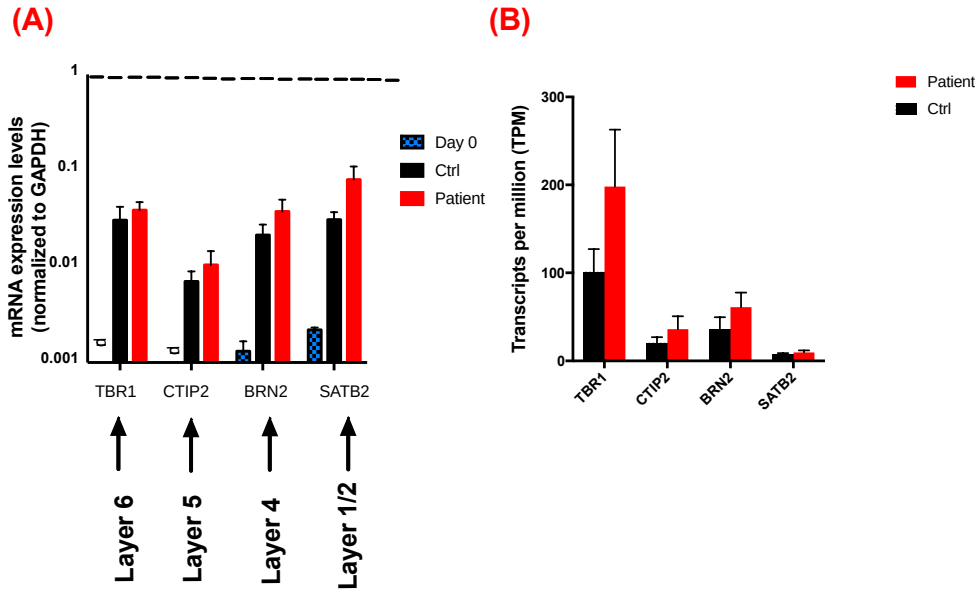

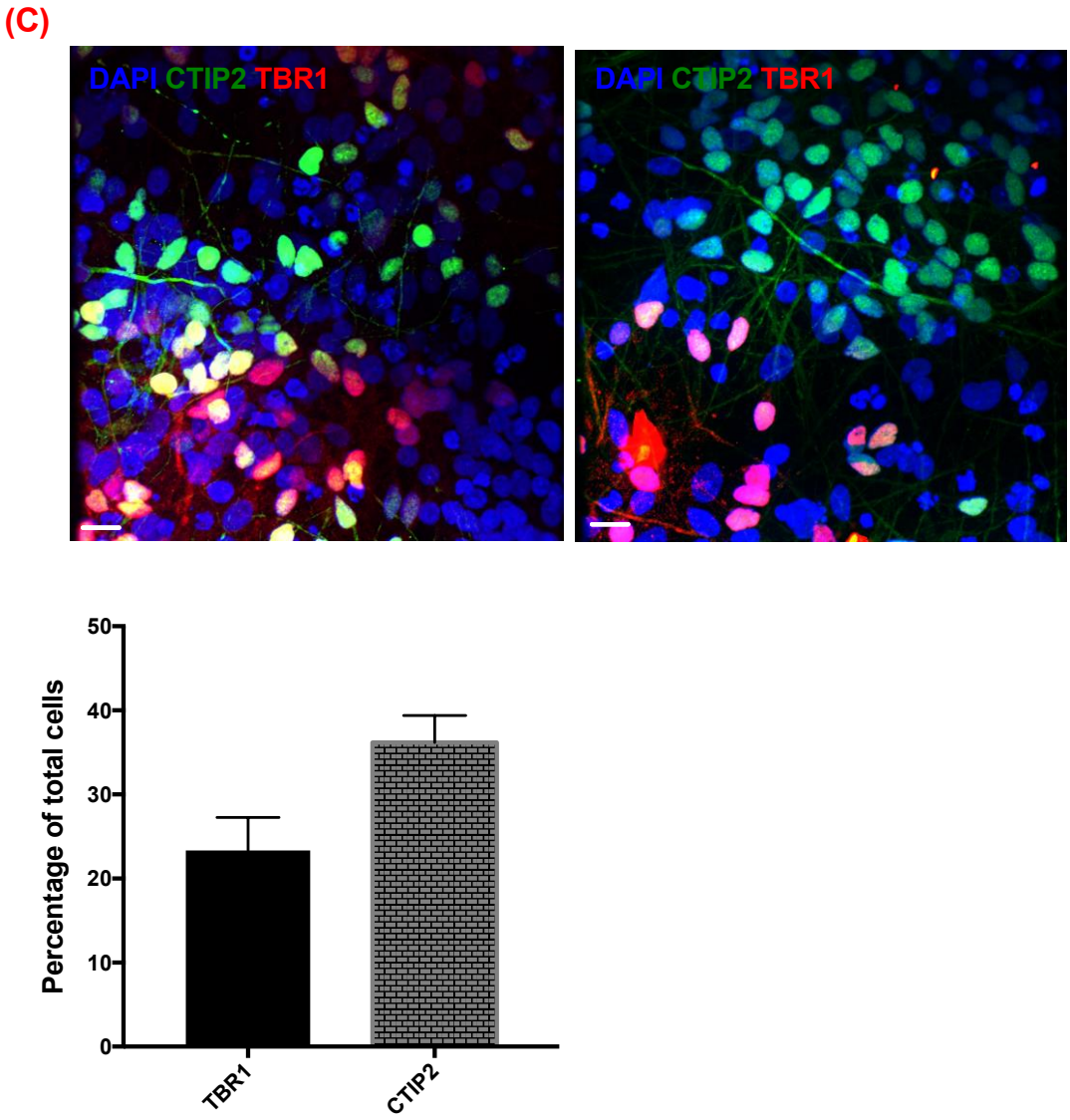

Figure 2.22. Successful generation of cortical neurons from control and NRXN1α deletion iPSCs. (A) Comparative analysis of mRNA expression of excitatory cortical neurons *TBR1, CTIP2, BRN2* and *SATB2* using qRT-PCR and RNA sequencing. (B). Day 0 indicate an iPSC line as a negative control and n.d stands for not detected as the value was too small to be seen on the graph. [qRT-PCR samples: 1CC2, 3VCX1, 4C3, 3VC2, 2VC1, 4CX1, ND4-1C1, ND2C11, ND1C1, ND2CX1)]; [RNA-Seq samples: 3VCX1, 4C3, 3VC2, 2VC1, 4CX1, NCRM-1, ND2C11, ND1C1, ND2CX1, ND4-1C2]. RNA was harvested from independent duplication of the differentiation. (C) Quantitative expression of TBR1 and CTIP2 at selected control lines (n=2; 4C3, 3VC2) showed ratios of lower layer cortical neurons. All data were summarized as means ± SEM. Scale bar is 25 μM.

2.3.7 100 days of neurons express excitatory pre- and post-synaptic neuronal markers

To further assess the differentiation of iPSC-derived excitatory cortical neurons, quantitative RT-PCR was carried out to examine the expression of excitatory post-synaptic markers (*SHANK1, SHANK2, SHANK3, PSD-95*), vesicular glutamate transporter (*VGLUT1*) and series of inotropic NMDA receptors (*GRIN1, GRIN2A*), AMPA receptors (*GRIA1, GRIA4*) and Kainate (*GRIK1, GRIK3*) receptors. The statistical analyses showed that there were no significant effects of *NRXN1α* deletion on expression of *PSD-95* ($p<0.23$), *VGLUT*1 ($p<0.97$), *SHANK1* ($p<0.09$), *GRIN2A* ($p<0.22$), *GRIK1* ($p<0.23$) or *GRIA4* ($p<0.41$) (Figure 2.23A). However, *SHANK2* ($P<0.03$), *SHANK3* ($p<0.009$), *GRIK3* ($p<0.03$) and *GRIN1* ($p<0.04$) were significantly elevated in *NRXN1α* deletion neurons (Figure 2.23A).

The nature of the 100-day differentiated cultures was evaluated by transcriptome analyses for the excitatory/inhibitory neuronal types. The whole panel of inhibitory markers, including vesicular GABA transporter (*VGAT1*) and ionotropic GABAergic receptors (*GABRA1, GABRA4, GABRA6, GABRB1, GABRD, GABRE, GABRG1, GABRP, GABRR1, GABRR2, GABRR3*), were showed to have very low levels of expression in the 100-day cultures (Figure 2.23B). On the other hand, substantially higher levels of excitatory transcripts, i.e., *PSD-95, VGLUT1, SHANK1, SHANK2, SHANK3, GRIN2A, GRIK1, GRIK3, GRIA4 and GRIN1*, were detected (Figure 2.23B). These data cross confirmed that the majority of the 100-day cultures were excitatory neurons.

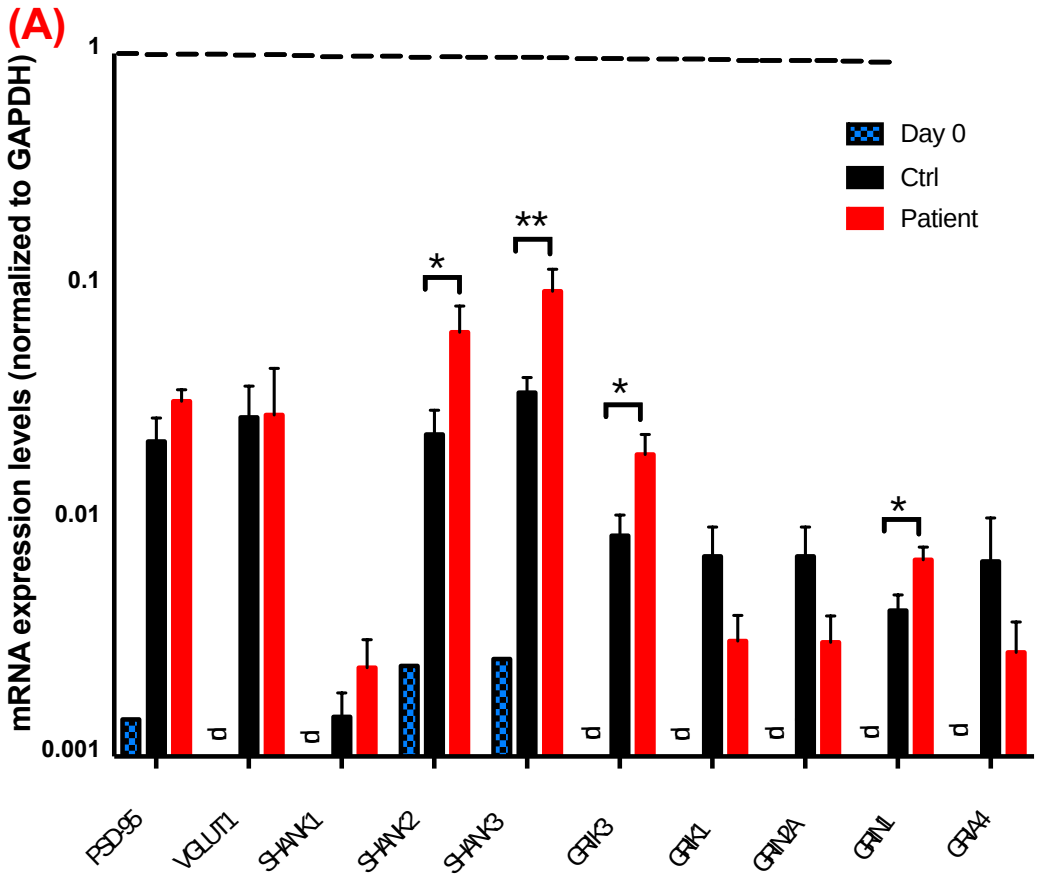
(A)
mRNA expression levels (normalized to GAPDH)
1
0.1
0.01
0.001
Day 0
Ctrl
Patient
*
**
*
*
d
PSD-95
VGLUT1
SHANK1
SHANK2
SHANK3
GRIK3
GRIK1
GRIN2A
GRIN1
GRIA4

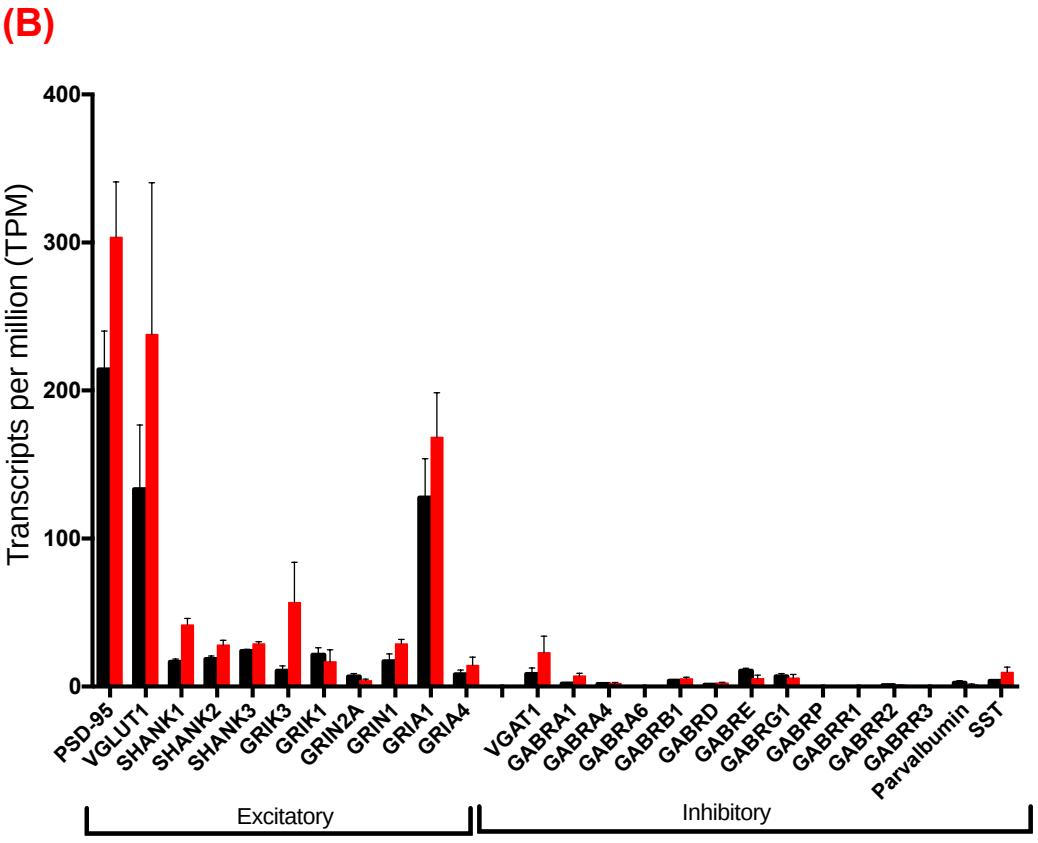
(B)
Transcripts per million (TPM)
400
300
200
100
0
PSD-95
VGLUT1
SHANK1
SHANK2
SHANK3
GRIK3
GRIK1
GRIN2A
GRIN1
GRIA1
GRIA4
VGAT1
GABRA1
GABRA4
GABRA6
GABRB1
GABRD
GABRE
GABRG1
GABRP
GABRR1
GABRR2
GABRR3
Parvalbumin
SST
Excitatory
Inhibitory

Figure 2.23. iPSC derived cortical neurons exhibit positive excitatory neuronal markers. (A) Quantitative analysis of RNA using qRT-PCR showed the expression of glutamate transporter marker (*VGLUT1*) and post-synaptic glutamatergic markers (SHANKs) and ionotropic NMDA, AMPA and kainate receptors. Day 0 indicated an iPSC line used as a negative control and n.d stands for not detected as the value was too small to be seen on the graph. (B) Transcript per million expression using RNA sequencing confirmed the expression of excitatory markers in (A) and low expression of GABA transporter (*VGAT1*) and a series of ionotropic inhibitory GABAergic receptors and inhibitory GABAergic interneurons. *SHANK1* has a significant differential expression in patients (FDR>0.05). [qRT-PCR: 1CC2, 3VCX1, 4C3, 3VC2, 2VC1, 4CX1, ND4-1C1, ND2C11, ND1C1, ND2CX1)]; [RNA-Seq: 3VCX1, 4C3, 3VC2, 2VC1, 4CX1, NCRM-1, ND2C11, ND1C1, ND2CX1, ND4-1C2] RNA were extracted from independent batches of differentiation. All data summary were means ± SEM.

2.3.8 100 days of neurons express low levels of astrocytic marker

Although the differentiation protocol used in this study was enriched for excitatory cortical neurons, other brain cells types could also exist, as neuronal rosettes might also give rise to *GFAP* positive astrocytes. To evaluate astrocytes in the 100-day culture, we have performed ICC with MAP2 for mature neurons (Red, Figure 3.24A/B) and GFAP for astrocytes (Green, Figure 3.24A/B). The data showed that the majority of the culture populations were MAP2 positive neurons (Red, Figure 2.24A/B). However, there was also a small proportion of GAFP-positive cells present in the 100-day cultures (Green, Figure 3.24A/B/C). The quantification of MAP2 immunofluorescence staining at day 100 of differentiation (Figure 2.24C) showed no significant difference between control and *NRXN1α* deletion neurons ($p<0.06$). Additionally, the expression of GFAP was also measured by both immunofluorescence (Figure 2.24C) and western blotting (Figure 2.24D) and revealed no significant effect upon *NRXN1α* deletion ($p<0.19$, $p<0.95$ respectively).

(A)

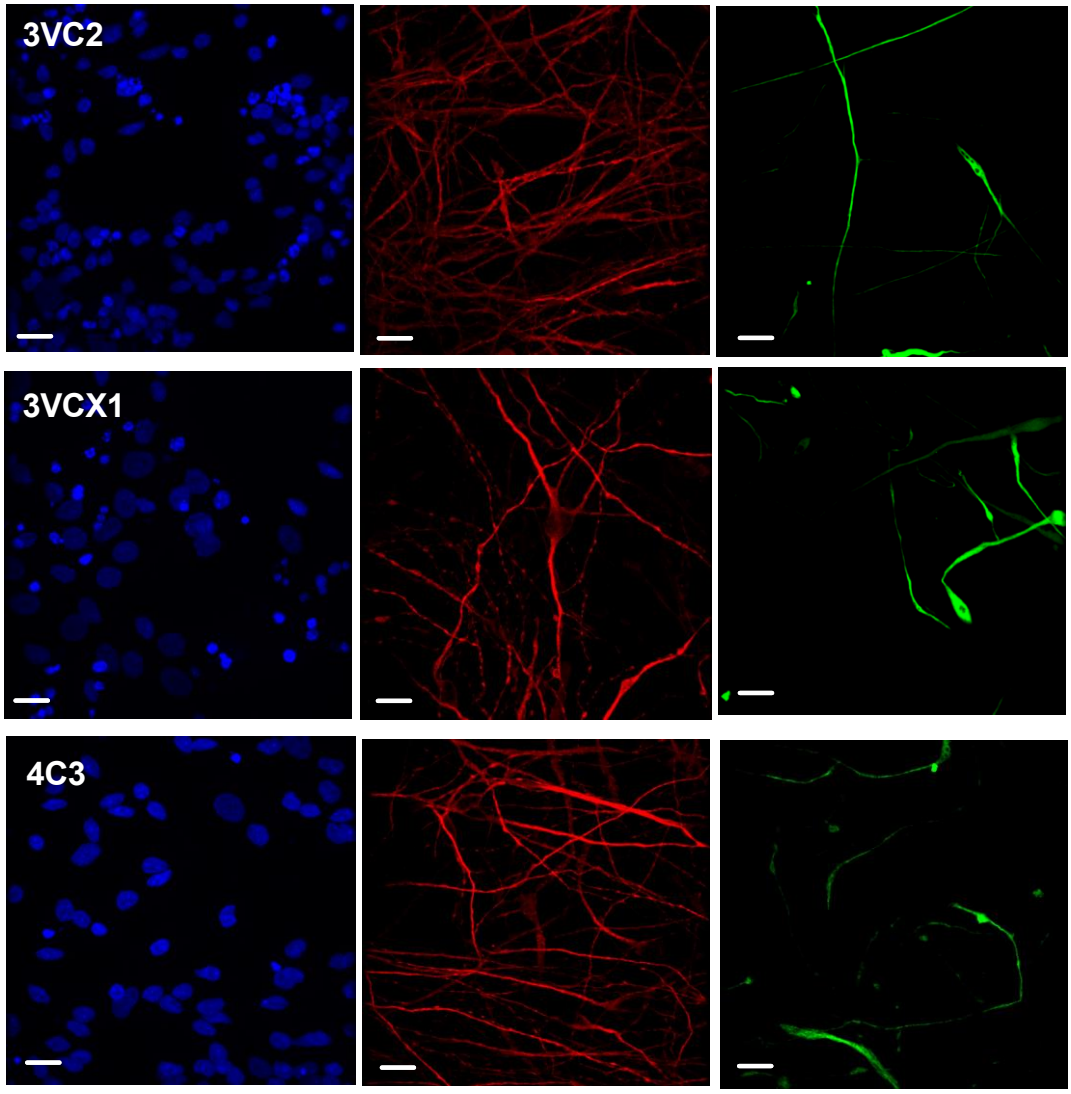

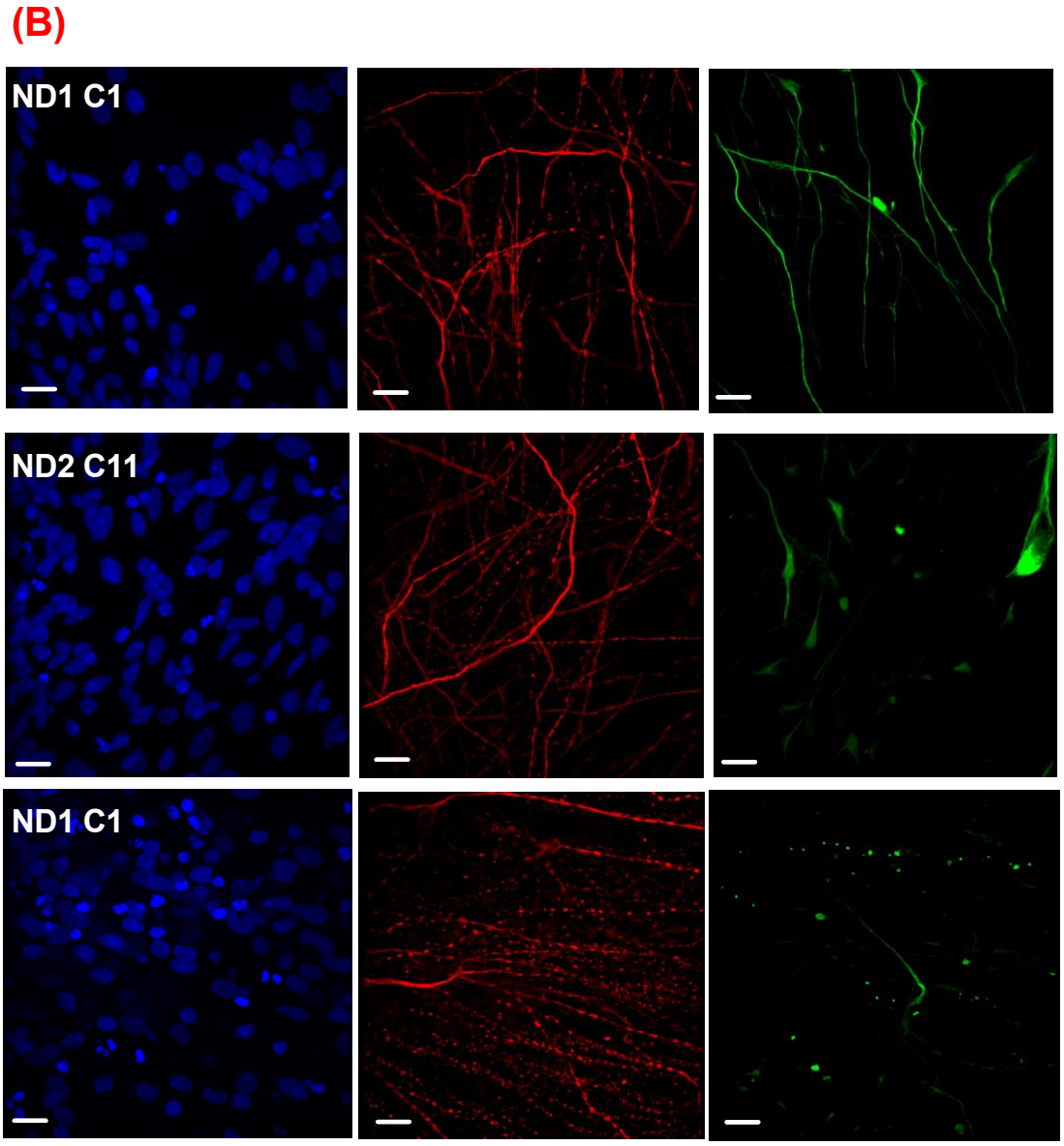
(B)
ND1 C1
ND2 C11
ND1 C1

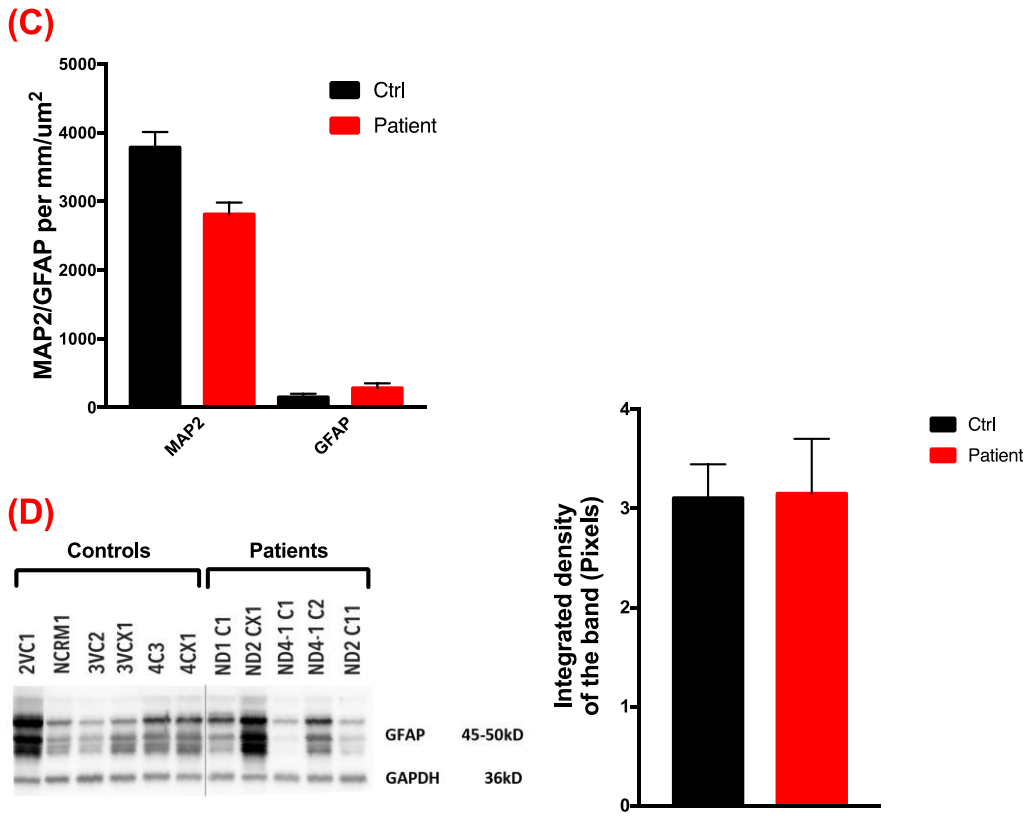

Figure 2.24. Mixed population of neurons with astrocytes at 100 days of differentiation. (A) Representative images of 3 control lines [3VCX1, 4C3, 3VC2] and three patient lines (B) [ND4-1C1, ND2C11, ND1C1] showing expression of MAP2 (red), GFAP (green) and DAPI (blue) at 100 days of iPSC-derived cortical neurons. (C) The quantitative expression of MAP2 (Control 3787±223.2 mm/µm2; Patient 2814±170.2 mm/µm2) and GFAP (Control 151.7±49.28 mm/µm2; Patient 283.7±66.78 mm/µm2) calculated as length in mm per µm2. (D) Quantitative expression of GFAP using western blotting showed no significant difference in *NRXN1α* deletion neurons (Normalized to GAPDH). This was repeated in 4 individual experiments. All data summary are means ± SEM. Scale bar is 25 µM.

Expression of TUJ1 was observed as early as day 20 of differentiation (Figure 2.25C, D). The majority of post-mitotic neurons emerge from TUJ1 positive neural progenitor cells (Luskin et al. 1997; Menezes et al. 1995). This pan-neuronal marker was also quantitatively measured at the RNA level using qRT-PCR (Figure 2.25A, B) and at the protein level using Western blotting (Figure 2.25C). There was no significant difference in either RNA ($p<0.06$) or protein expression ($p<0.97$) of TUJ1.

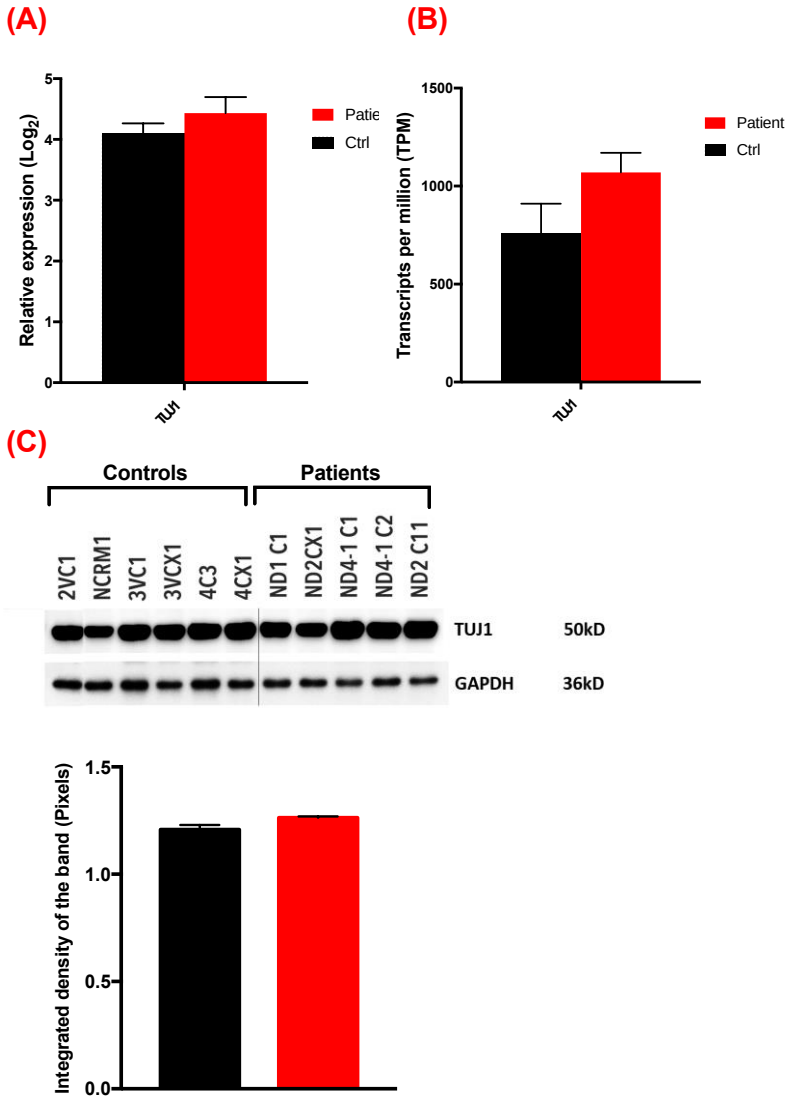

Figure 2.25. Pan-neuronal marker expression at day 100 of differentiation. (A) Comparative expression of *TUJ1* at RNA level using qRT-PCR and RNA sequencing (B) [qRT-PCR: 1CC2, 3VCX1, 4C3, 3VC2, 2VC1, 4CX1, ND4-1C1, ND2C11, ND1C1, ND2CX1)]; [RNA-Seq: 3VCX1, 4C3, 3VC2, 2VC1, 4CX1, NCRM-1, ND2C11, ND1C1, ND2CX1, ND4-1C2]. The experiments were repeated in 2 independent batches of differentiation. (C) Quantitative expression of TUJ1 in western blotting (normalized to GAPDH) and this was repeated in 4 individual experiments. All data summary are mean ± SEM.

2.3.9 100-day neurons maturity showed synaptogenesis

The maturity of 100 day cortical neurons were measured with positive expression of mature neuronal marker *MAP2* and *SYN1*, essential for synaptogenesis. This was validated at the RNA level using qRT-PCR (Figure 2.26A).

The expression of MAP2 and TUJ1 at day 100 of differentiation was quantified at the cellular level by immunocytochemical staining (Figure 2.26C). The puncta localization of SYN1 staining was observed (Figure 2.26C). Furthermore, the quantitative expression of the SYN1 protein was measured using western blotting (Figure 2.26B) which displayed no major effects of *NRXN1α* deletion on SYN1 protein expression. There was no significant difference in *NRXN1α* deletion neurons in terms of maturity *MAP2* ($p<0.07$) and synaptogenesis *SYN1* at the RNA level (Figure 2.26A, $p<0.08$).

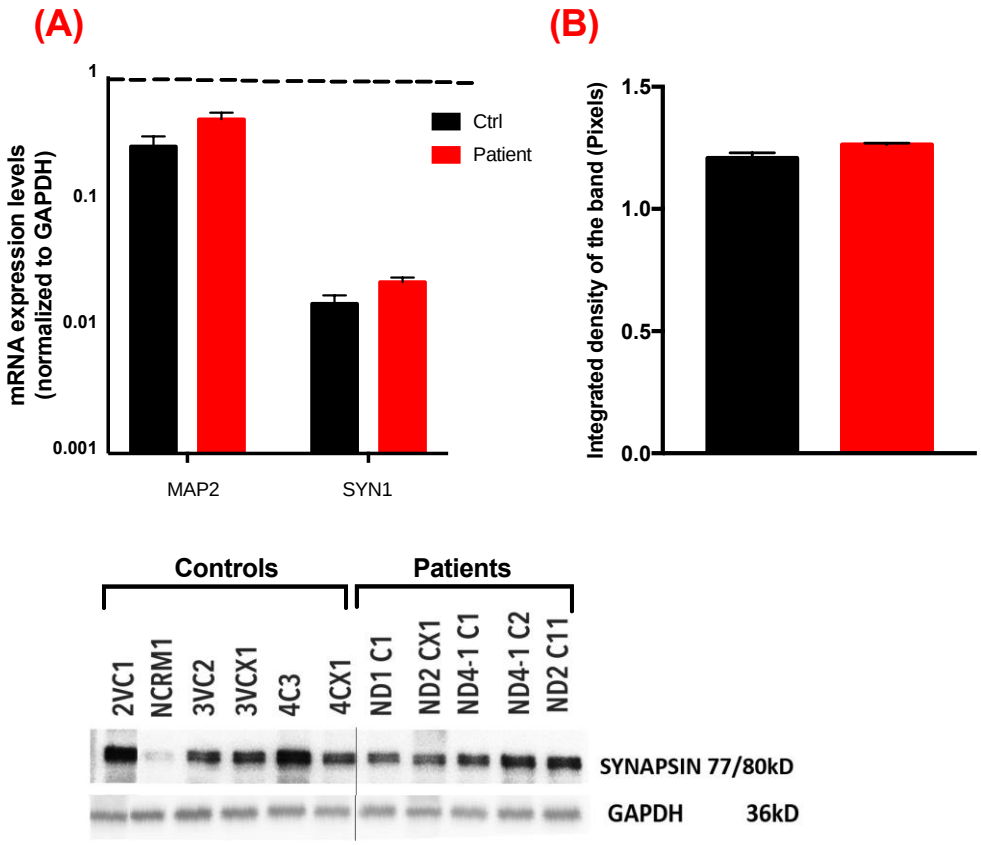

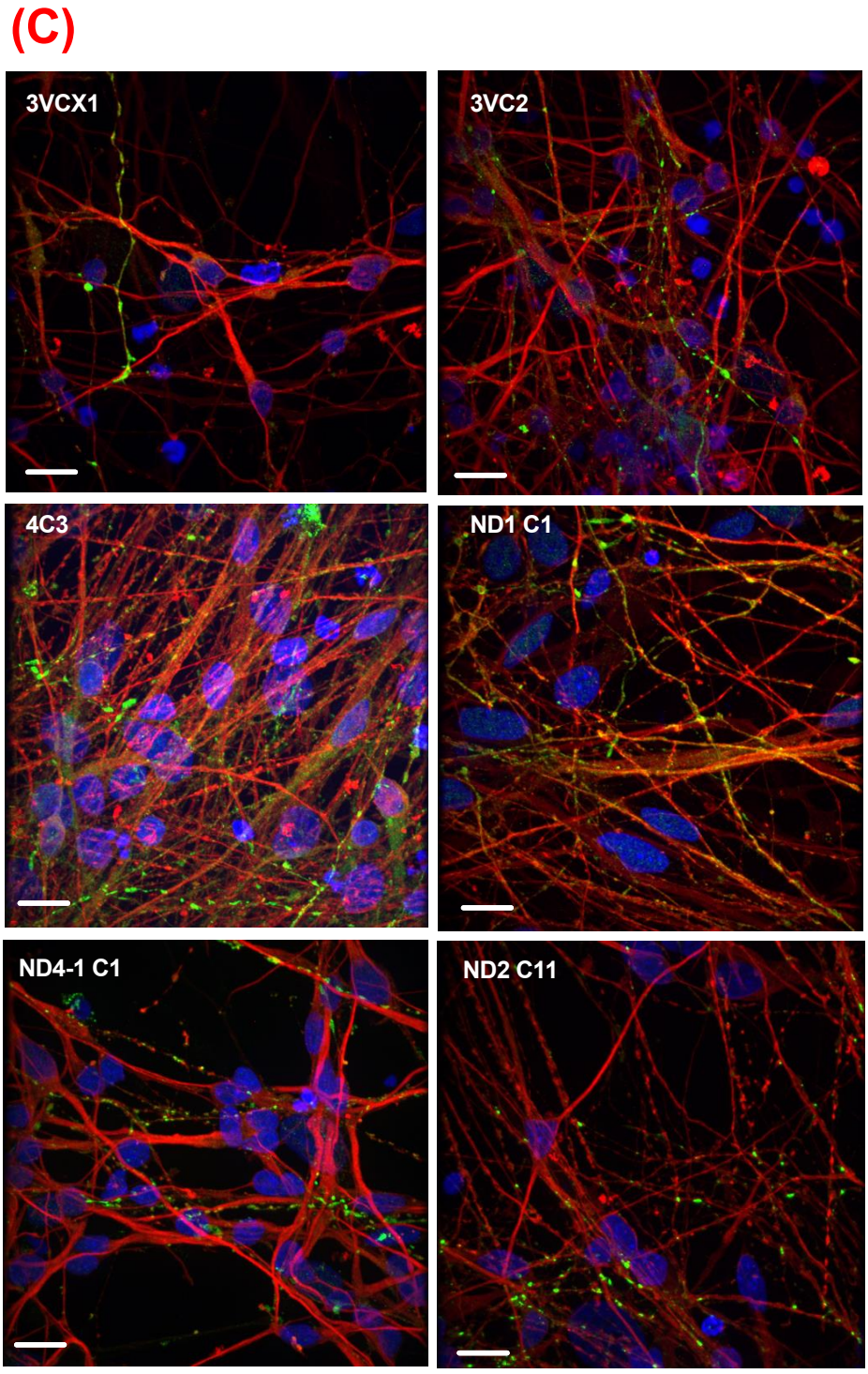

Figure 2.26. Day 100 cortical neurons exhibit maturity in a time-dependent manner. (A) Comparative analysis of *MAP2* and *SYN1* at day 100 of neurons at the RNA level using qRT-PCR [qRT-PCR: 1CC2, 3VCX1, 4C3, 3VC2, 2VC1, 4CX1, ND4-1C1, ND2C11, ND1C1, ND2CX1)]; [RNA-Seq: 3VCX1, 4C3, 3VC2, 2VC1, 4CX1, NCRM-1, ND2C11, ND1C1, ND2CX1, ND4-1C2]. (B) Quantitative expression of SYN1 proteins using western blotting showed no significant increase in *NRXN1α* deletion neurons (normalized to GAPDH). The experiments were repeated four times independently. All data summary are means ± SEM. (C) Representative images of SYN1 (green) with TUJ1 (red) and puncta staining of SYN1 staining was observed in control and patient lines. Scale bar is 25 μM.

2.3.10 100 day cortical neurons express pre-synaptic *NRXN1α* interacting partner with no significant difference in *NRXN1α* deletion patients

The iPSC-derived neurons showed expression of *NRXN1* interacting partner at the RNA level, and this was detected using qRT-PCR and RNA sequencing (Figure 2.27). The expression of *NRXN1* main interacting receptors at post-synaptic membrane NLGNs was also quantified at the RNA level (Figure 2.27). There was no significant difference at the RNA level using qRT-PCR in the expression of these genes [*MINT1* ($p<0.42$), *CASK* ($p<0.45$), *MUNC18* ($p<0.25$), *NLGN1* ($p<0.84$)].

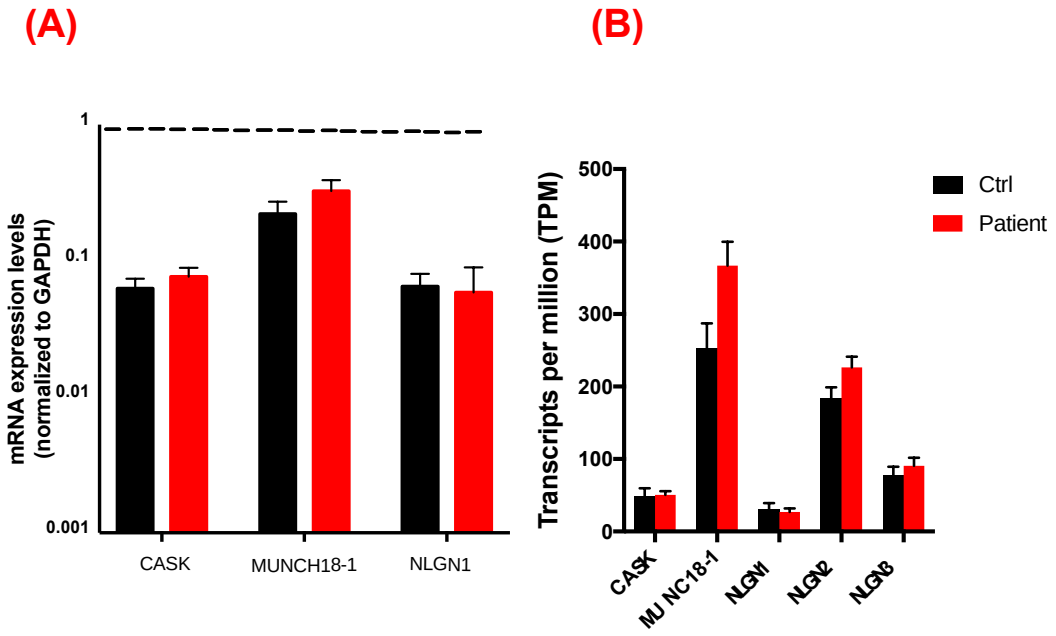

Figure 2.27. NRXN1α deletion showed no significant effect on the expression of its interacting partners. (A) Quantitative expression of *CASK, MUNC18* and *NLGN1* by qRT-PCR and RNA sequencing (B) in addition to *NLGN2* and *NLGN3*. [qRT-PCR: 1CC2, 3vcx1, 4C3, 3VC2, 2VC1, 4CX1, ND4-1C1, ND2C11, ND1C1, ND2CX1)]; [RNA-Seq: 3VCX1, 4C3, 3VC2, 2VC1, 4CX1, NCRM-1, ND2C11, ND1C1, ND2CX1, ND4-1C2]. The experiments were carried out in 2independent repeats. All data summary are means ± SEM.

2.3.11 *NRXN1* isoform expression in iPSC derived cortical neurons throughout the course of differentiation

The quantitative expression of *NRXN1α* and β isoforms were validated at the RNA level at day 20, 40, 60, 80 and 100 of differentiation in control iPSC-derived neurons (Figure 2.28A), and elevated *NRXN1* mRNA expression was seen after 40 days of differentiation. Next, the expression of *NRXN1α* and β isoforms were quantified in both control and *NRXN1α* deletion neurons at day 100 of differentiation (Figure 2.28B). The exons 1-17 are unique to *NRXN1α*, where the exon 18 is the first coding exon unique to *NRXN1β*. We designed two pairs of PCR primers flanking exon 9 and 15 respectively and carried out qRT-PCR to analyse the *NRXN1α* expression. The *NRXN1α* mRNA was reduced to ~76±28% (exon 9) and ~74±23% (exon 15), respectively, in the day 100 *NRXN1α* deletion neurons compared to healthy controls (100%). Meanwhile, the *NRXN1β* isoform was significantly upregulated by ~172±22% in the patient-derived cells. These data showed that while *NRXN1α* is heterozygously deleted in patient cells, there appeared a compensational change in the expression of the *NRXN1β* isoform, which may have functional consequences on neuronal activity.

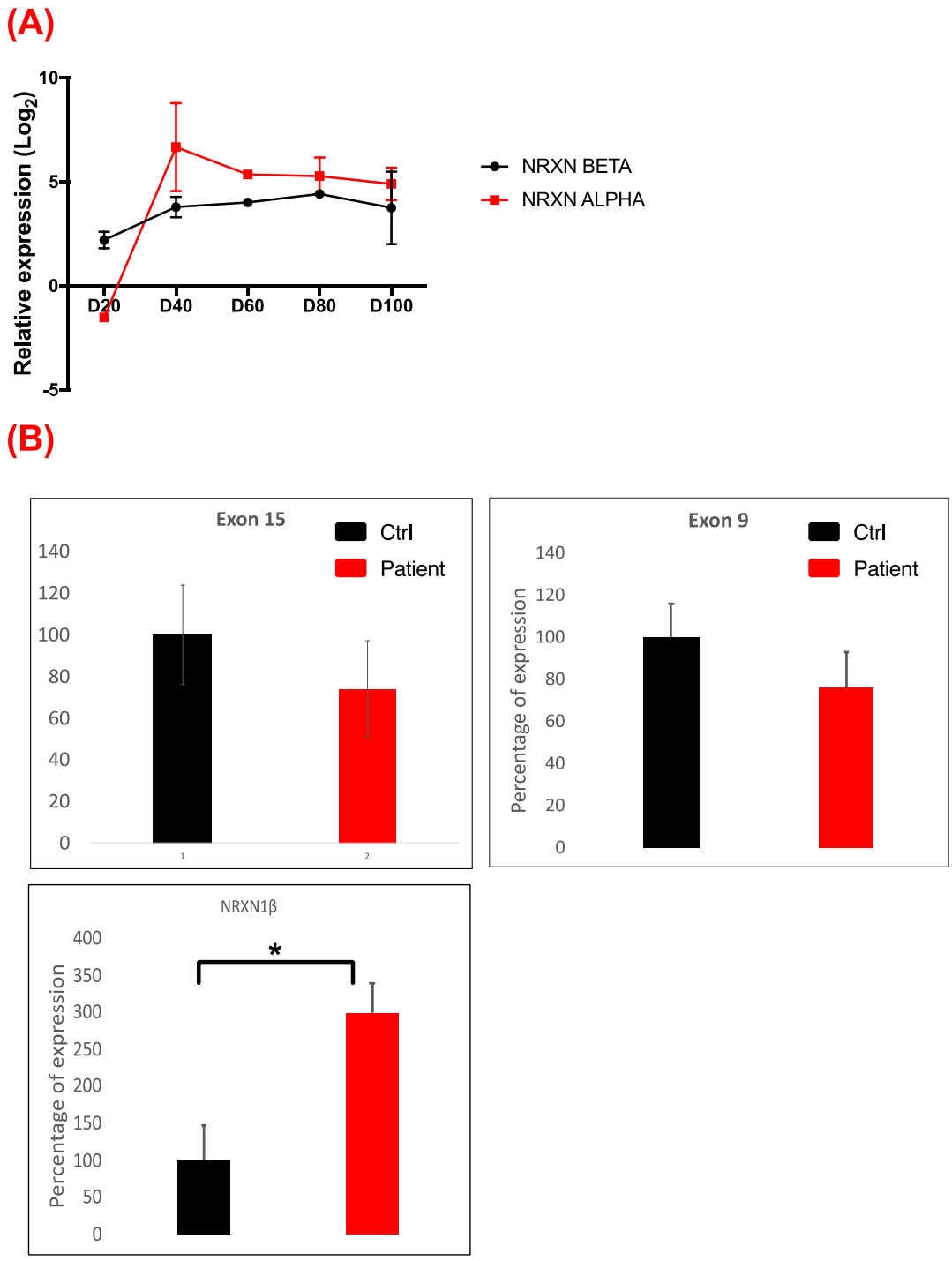

Figure 2.28. Expression of NRXN1α and NRXN1β at 100-day iPSC derived neurons. (A) The quantitative expression of *NRXN1α* and *NRXN1β* at two control lines (03VC2, 04C3) represented at time-dependent manner using qRT-PCR. Both the *NRXN1α* and *NRXN1β* were significantly upregulated at day 40 of differentiation and reached a plateau by day 60. (B) The quantitative expression using qRT-PCR shows the expression of *NRXN1α* with primers from exon 15 and exon 9 and *NRXN1β* with primers from the unique coding exon (exon 18).

2.4 Discussion

A great phenomenon in the central nervous system is the complexity of communication between neuronal cells, which is developed during synaptogenesis, and a large proportion of which occurs during the early neonatal period, which is coincided with the development of ASD. Adhesion protein systems form the essential part of physical contact between pre-synaptic and post-synaptic termini (Brose N, 1999; (Krueger et al. 2012). Neurexins are the prime example of adhesion surface proteins at the pre-synaptic terminus, the most extensively studied modulators of synaptic activity, which signal bi-directionally via binding to post-synaptic Neuroligins (Brose N 1999; Ushkaryov *et al.* 2009). Deletions of a gene encoding Neurexins, *NRXN*1, have been associated with many neurodevelopmental and psychiatric disorders including ASD (Schaaf et al. 2012; Marshall et al. 2008; Ching et al. 2010; Dabell et al. 2013). The hypothesis is that *NRXN1* influences neuronal excitation and inhibition and deletions of the *NRXN1* may disturb an imbalance of excitatory and inhibitory synaptic transmission (Chubykin et al. 2007).

There has been great amount of work on studying *NRXN1α* deletion in animal models with various phenotypic characteristics (Missler et al. 2003; Etherton et al. 2009; Pak et al. 2015; Aoto et al. 2013; Aoto et al. 2015; Chen et al. 2017; Grayton et al. 2013; Zhang et al. 2005). Deletion of α isoform of *NRXN1/2/3* genes have a consequence on vesicle release in knockout animal models, emphasising the coupling mechanism of neurexins in synaptic transmission and presynaptic release machinery (Missler et al. 2003; Kattenstroth et al. 2004).

In a mixed genetic background of an SV129/C57b16 mouse model of *Nrxn123α* knock out, Missler and colleagues have discovered a significant decrease in both spontaneous and evoked frequency of mEPSCs in cultured slices from neocortex and acute slices from the brainstem. While there was no change in amplitude of mEPSCs of either GABA or AMPA mediated post-synaptic responses, but there were a significant alteration and decrease in amplitude of evoked inhibitory and excitatory postsynaptic responses (Missler et al. 2003). This has indicated that there is a reduction in the probability of neurotransmitter release (Missler et al. 2003). This impairment in neurotransmitter release has been found to be directly related to a

reduction in presynaptic Ca^{2+} currents (Missler et al. 2003). In a subsequent study, the triple knock out of all α-neurexins (SV129/C57b16 mouse model) resulted in an alteration only on NMDA receptor-dependent mEPSCs currents (but not AMPA) without a change in their protein level (Kattenstroth et al. 2004). These results are consistent with an incline in whole cell Ca^{2+} currents, presumably mediated by postsynaptic calcium channels (Missler et al. 2003; Kattenstroth et al. 2004). These recent studies have suggested that α-neurexins might exert both pre and postsynaptic effects, involving in controlling of both pre and post-synaptic dynamics (Missler et al. 2003; Kattenstroth et al. 2004). More recent study has also shown that deletion of *Nrxn3αβ* in excitatory hippocampal synapses caused a selective reduction in AMPA receptors, leaving the presynaptic release unchanged (Chen et al. 2017). This further suggests a link between neurexins and both pre and post-synaptic functionality. It is worth mentioning that using either a mouse model with mixed or pure genetic background have significantly affected the behavioural phenotypes in *NRXN1α* (Etherton et al. 2009; Laarakker et al. 2012; Grayton et al. 2013). While in mixed genetic background of C57BL6/SV129, an increased repetitive grooming behaviour, as well as increased response to novelty, were observed (Etherton et al. 2009; Laarakker et al. 2012), an opposite result was found in pure genetic background, observing a reduction in locomotor activity in novel situations (Grayton et al. 2013). This was the first behavioural study linking altered social behaviours seen in humans with ASD to *Nrxn1α* deletion in a mouse model (Grayton et al. 2013). The severity of the phenotype has been shown to be stronger in human ESC model of *NRXN1* deletion (Pak et al. 2015). Pak *et al*. identified no phenotype in heterozygous and homozygous deletion of Nrxn1 deletion in cultured mouse cortical neurons. However, the induced mutation in ESCs showed impairment in the frequency of mEPSCs in ESC-derived cortical neurons (Pak et al. 2015). Thus, iPSC technology was used in this study to investigate the more precise function of *NRXN1α* in cortical neurons, investigating the effect of *NRXN1α* in early and late development, including any potential alteration in the level of series of molecules at both pre and post-synaptic membrane.

The iPSC technology offers great promise in the field of disease modelling by providing an unlimited number of patient-specific stem cells with particular genetic aberrations for most disease cell types. In an attempt to elucidate how *NRXN1α*

deletion predispose to the clinical phenotypes, four iPSC lines from 3 *NRXN1α* deletion patients and six iPSC lines from sex, age and ethnic-matched controls, were differentiated into cortical excitatory neurons in this study.

We have derived iPSCs from fibroblasts, a reliable and efficient starting material. One of the advantages of using fibroblasts as somatic adult cells is that it only requires a 3-mm punch of biopsy, and it can survive at normal room temperature for days. Adult dermal fibroblasts require very low maintenance, and they can emerge from a small punch of biopsies after only a few days. The success rate of growing was overwhelmingly high in our laboratory, and of biopsies from 60 donors (patients and controls), only one biopsy from a newborn baby did not produce fibroblasts for the iPSC projects. In contrast to other sources of cells, i.e., mononuclear cells from blood samples or keratinocytes from hair follicles, which may meet some levels of challenges. The iPSCs in the current study were reprogrammed using lentiviral and Episomal techniques. All generated iPSCs were validated and characterized for expression of pluripotency genes, three germ layer differentiation potentials, and whole genome CNVs. Then, we successfully used these iPSC lines to generate cortical excitatory neurons which is related to ASD disease, as excitation and inhibition balance is considered as a central for normal brain physiology and the imbalance is proposed as neuropathology for a number of neurodevelopmental disorders.

There are many lines of evidence for using dual SMAD differentiation strategy and serum-free defined factors to drive cortical neuronal differentiation (Ying et al. 2003). Several studies in *Xenopus laevis* have demonstrated that inhibitors of BMPs have an essential role during neuronal development (Smith and Harland 1992). A small molecule SB431542 has been shown to induce neuronal differentiation through inhibition of TGFβ, further inhibiting the downstream SMAD signalling (Chambers et al. 2009; Patani et al. 2009). The dual action of BMP and TGFβ inhibitors have shown to be critical for neuronal induction process (Chambers et al. 2009; Shi, Kirwan and Livesey 2012). This strategy has been used to generate iPSC-derived neurons from heterozygous *NRXN1α* deletion patients to investigate the disease phenotype in this project.

The dual SMAD inhibition with SB431542 and LDN193189 were used for directional programming of iPSCs to become neural progenitor cells of cerebral cortical neurons. Using this approach, the expression of transcription factor *PAX6* was significantly increased during the first ten days of neural induction whereas the pluripotent marker *OCT4* was significantly decreased (Figure 2.15B). This defined the efficient generation of neural progenitors, as well as morphological differences from big round nucleus of iPSCs into the columnar-shaped small nucleus of neural progenitors (Figure 2.15A). Furthermore, the appearance of neuronal rosettes was the signature of the development of neural progenitors. Cortical NSCs and NPs were further characterised at day 20 by the expression of *PAX6, NESTIN, FOXG1* and *NGN2* at the RNA level. PAX6 expression was found in over 87% of the stained cells at 20 days of induction, elucidating the cortical identity of the NP cells in the majority of cells (Figure 2.16B, C). Relative expression of these essential markers was quantitatively measured by qRT-PCR between control and patients. There was no significant difference for the expression of NP markers at day 20, suggesting that *NRXN1α* deletion does not significantly affect the initiation of the neural induction (Figure 2.16A) or production of NSCs in ASD patients.

Both macrocephaly or microcephaly were reported as ASD phenotypes (Courchesne et al. 2001). An increase in gray and white matter volume has been reported in 6-12% in adolescents and adults with ASD (Vaccarino et al. 2009). An increase in the cortical grey matter could be mainly due to an increase in a number of neurons or glial cells (McCaffery and Deutsch 2005). Although there was no obvious increase/decrease of head circumference in the ASD patients recruited in our study; we further validated the proliferation capability of NPs with a proliferating marker Ki67, which showed no significant difference between control (n=3) and patients (n=3) in 20 days of cultures. A similar proliferation rate of NPs was obtained at the early stage of differentiation between control, and ASD derived iPSCs.

Changes in cell body size have also been reported in post-mortem studies (Courchesne et al. 2011). The cell body size ratio was also measured in our study, with no significant difference in *NRXN1α* deletion TUJ+ neurons at day 30 (Figure 2.20B). These results suggest that neurogenesis was not grossly affected by *NRXN1α* deletion. This is consistent with the phenotype of *Nrxn1* knockout mice, which showed no major

neuroanatomical defects (Missler et al. 2003). This is also consistent with Mariani and colleagues' study in which proliferation of iPSC derived neurons from ASD individuals remained unchanged (Mariani et al. 2012).

The decreased PAX6 expression and increased expression of post-mitotic neuronal marker DCX marked the progression of neuronal differentiation from day 20 to day 30 under the current differentiation protocol (Figure 2.18A, B). This process was intended for NP expansion but was also accompanied by the birth of new-born neurons (DCX^+). In the same time, the expression of TUJ1 was also significantly increased (Figure 2.18C). Most of the post-mitotic neurons in cerebral cortex emerge from TUJ1 positive progenitors cells (Luskin et al. 1997; Menezes et al. 1995), and TUJ1 is therefore used as a pan-neuronal maker during neuronal development and maturation (Menezes and Luskin 1994). We quantified the percentages of cells becoming DCX^+ and cells remaining as $Ki67^+$ neural stem cells at day 30 of early differentiation, and the results showed no significant alteration in *NRXN1α* deletion neurons (Figure 2.19). TUJ1 and DCX are all microtubule-associated proteins in which alteration in their expression associated with brain development (Gleeson et al. 1998). They are the integral components of brain connectivity. Mutations in tubulins or MAPs can cause significant abnormalities in brain development which contribute to developmental delay and epilepsy (Mutch et al. 2016). Furthermore, mutations in tubulin genes have been associated with white matter anomalies (Poirier et al. 2013). In our study, the RNA and protein expression of tubulin and microtubule-associated protein remained unchanged in *NRXN1α* deletion neurons, suggesting *NRXN1α* haploinsufficiency does not grossly alter neuronal migration and formation of white matter by axonal extension.

Complete cortical neurogenesis occurs over 100 days period in humans (Caviness et al. 1995) and only six days in mice (Takahashi et al. 1996). Glutamatergic neurons in the adult cerebral cortex are generated in a temporal order and defined by expression of different transcriptional factors. Layer 6 projection neurons are *TBR1* positive, layer five subcortical neurons are CTIP2 positive, and layer 2-4 neurons are *BRN2* and S*ATB2* positive cells (Arlotta et al. 2005; Alcamo et al. 2008). These factors were used as markers in our study for day 100 of differentiated cortical neurons. The similar time frame has been used to generate glutamatergic cortical neurons from iPSCs and

ESCs in vitro (Shi, Kirwan, Smith, et al. 2012). The expression of *TBR1, CTIP2, BRN2* and *SATB2* were quantified at the RNA level (Figure 2.22A). The expression of CTIP2 and TBR1 were also quantified at the cellular level, showing 23.35% of $TBR1^+$ and 36.18% of $CTIP2^+$ (Figure 2.22C) cortical neurons were present in 100-day cultures. Transcriptome analyses showed that *BRN2*, a marker for upper layer cortical neurons, has shown a comparable number of mRNA (TPM) expression in comparison to *CTIP2* mRNA (Figure 2.22B). These data together showed that both upper and low layers of excitatory cortical neurons are abundantly present in our 100-day neuronal cultures.

We examined the expression of inhibitory GABAergic receptors and GABA interneurons (Parvalbumin and SST), and they remained at considerable low levels in 100-day neuronal cultures (Figure 2.23B). The population of astrocytes were also evaluated at 100-day of differentiation, and GFAP positive cells were quantified by immunocytochemistry and showed no significant difference in *NRXN1α* deletion neurons (Figure 2.24). This is different from Zeng *et al.* study, in which they observed reduced astrocyte differentiation in *NRXN1* knocked down iPSC and ESC cells (Zeng et al. 2013), by a reduction in generation of *GFAP* cells. One reason to explain this difference is that they used shRNA in human iPSC and ESCs which could affect both *NRXN1α* and *NRXN1β*, whereas our cohort of samples are *NRXN1α* deletion only. The second difference is that they performed spontaneous differentiation, whereas we carried out directional differentiation with a very small population of astrocytes.

The implication of glutamatergic receptors has been observed in autism (Purcell et al. 2001; Fatemi et al. 2011). For example, increased expression of metabotropic receptor density or decreased expression of AMPA receptor density has been observed in cerebellar samples or post-mortem tissue samples of autism people, respectively (Purcell et al. 2001; Fatemi et al. 2011). One post-mortem study found a significant difference in subunit one protein level of NMDA receptors, while others found no difference in NMDA receptor expression (Blatt et al. 2001; Purcell et al. 2001). Furthermore, the deletion of *Nrxn3α/β* has been shown to have a significant effect on upregulation of AMPA receptors (Aoto et al. 2013). In our study, the expression of various ionotropic and metabotropic glutamatergic receptors was examined at the RNA level, and significant upregulation was identified for some of them. These results have firstly validated and confirmed the expression of excitatory neurons using dual

SMAD differentiation protocol. The quantitative expression of the vesicular glutamate transporter (*vGLUT1*) also confirmed the excitatory differentiation protocol against the very low expression of inhibitory GABA vesicular transporter (*VGAT*) (Figure 2.23B). Secondly, it illustrates that the *NRXN1α* deletion may have a downstream effect on expression of glutamatergic neurons, as the expression of *GRIK3* and *GRIN1* were significantly increased in *NRXN1α* deletion neurons (Figure 2.23A).

The scaffold proteins SHANKS are expressed at the post-synaptic density of excitatory synapses, and their mutation and duplication have been implicated in ASD (Durand et al. 2007; Pinto et al. 2010). They are essential for synaptic development and function (Sheng and Hoogenraad 2007). Mutations in SHANKs have displayed phenotypic characteristics similar to ASD (Jiang and Ehlers 2013). *Shank1* knockout mice also showed decreased vocal communication, increased anxiety and alteration in long-term memory (Hung et al. 2008). Furthermore, *Shank2* and *Shank3* knockout mice show increased anxiety, repetitive behaviours, as well as deficits in social communication (Schmeisser et al. 2012; Peça et al. 2011). In our study, the expression of *SHANK2* and *SHANK3* has been identified as a significant upregulation in *NRXN1α* deletion neurons (Figure 2.23A). SHANK proteins directly interact with glutamatergic receptors at post-synaptic membrane such as NMDA and AMPA receptors. Therefore, an alteration in SHNAKs expression level may also change the post-synaptic level of NMDA and AMPA. This suggests that *NRXN1α* deletion has a consequence on post-synaptic density by regulating the expression of glutamatergic receptors and scaffolding protein SHANKs.

Over expression of glutamatergic receptors as well as SHANK proteins in post-synaptic density may suggest over-excitation on *NRXN1α* deletion neurons, suggesting that *NRXN1α* is essential for inhibitory synaptic transmission. This is further investigated at a functional level using electrophysiology and calcium imaging in Chapter 3 and 4, respectively. This will allow a much closer look into single level properties of neurons in terms of neuronal excitability as well as calcium dynamics, in terms of influx and efflux of calcium and insight into neurotransmitter release and synaptic transmission.

A critical step in neuronal network development is forming synapses, and this occurs largely after birth and is coincided with the ASD development. The formation the physical synapses at day 100 of differentiation were quantified at the protein level by expression of SYN1 using western blot (Figure 2.26B) and by immunocytochemistry. This was further quantified at the RNA level using qRT-PCR (Figure 2.26A). The localization of SYN1 was observed as puncta staining at the protein level using immunostaining in both controls, and ASD derived neurons (Figure 2.26C). There was no significant difference in the quantity of the SYN1 expression in our *in vitro* cell model. Pak and colleagues also demonstrated no significant change on synaptogenesis in ESC *NRXN1* mutation (Pak et al. 2015).

The effect of *NRXN1α* deletion on the maturity of 100-day cortical neurons was also validated by the presence of microtubule-associated protein MAP2. MAP2 are a family of proteins which have a key role in stabilizing microtubules, with MAP1 and MAP2 primarily seen in neurons (Cassimeris and Spittle 2001). The presence of MAP2 was quantified using immunostaining with no significant difference in *NRXN1α* deletion neurons (Figure 2.24A, B). This neuronal maturity was also quantified with the parentage of cells generating spontaneous calcium transients, which significantly increased in a time-dependent manner (Figure 4.3). Moreover, spontaneous and evoked action potentials, as well as the presence of voltage-gated sodium and potassium current, were observed during electrical examination of neurons (Chapter 3). All these data above showed the maturity of neurons at 100-day of differentiation which was generated using dual SMAD inhibition molecules, but we did not observe haploinsufficiency of *NRXN1α* on the maturation of iPSC-derived neurons.

In summary, we explored the molecular basis of iPSC derived neurons in *NRXN1α* and control progenitor at 20/30 days, and mature neurons at 100-days of differentiation, respectively. We tested for gene expression alteration in mRNA and proteins that are critical for synaptic signalling, interaction, adhesion and function. We demonstrated increased expression of excitatory postsynaptic glutamate receptors as well as postsynaptic density SHANKs. We demonstrated elevated expression of SHANKs and some of the glutamatergic receptors. This strongly indicates an over-excitation in *NRXN1α* patient's cells, which may cause significant alteration in

electrical properties and neuronal excitability (Chapter 3). This strongly supports our hypothesis that the balance between excitatory and inhibitory is disturbed in *NRXN1α* ASD patients. At the same time, the mutations did not alter neurogenesis or synaptic numbers. It is worthy to mention that iPSCs derived from patients have a genetic background. The normal ESCs and isogenic mutant lines with the same background may have an advantage in dissecting the effects of a given gene, however, how will such a discovery be readily able to apply to patients of different genetic background remain to be validated. In our study, ND1 and ND4 patients have a history of seizures and/or epilepsy, and we cannot exclude the potential un-identified genetic background may contribute to the overall cellular phenotype. It is reasonable to state that using iPSCs derived from patients may have potential advantages in finding the potential role of NRXN1. However, it is almost necessary to consider few facts; firstly NRXN1 deletions predispose to a variety of clinical phenotypes from ASD, intellectual disability, developmental delay, mental retardation to schizophrenia and epilepsy (Møller et al. 2013; Autism Genome Project Consortium et al. 2007; Glessner et al. 2009; Marshall et al. 2008; Béna et al. 2013; Ching et al. 2010; Gregor et al. 2011). Co-factors as un-identified genetic background may exist in different individuals which leads to different clinical symptoms of NRXN1 deletions. Also, NRXN1 is a large gene, and different individuals may involve in different regions of deletions. The deletion borders may not precisely have defined by copy number variation studies, and the nature of the deletion transcripts are still unknown.

While the characterisation of neurons in the Chapter was essential, it is not sufficient to conclude the functionality in neuronal networks, which will be discussed in the following chapters.

Chapter 3. *NRXN1α* deletion impairs the electrical excitability in iPSC-derived neurons

3.1 Introduction

Neurons are the workhorses of the nervous system, providing a platform for rapid and complex communication algorithms, over long (meters) and short distances (nanometers). Neurons are excitable cells, they can rapidly (1-4ms) and reversibly change membrane potential from a resting value of -80mV to a peak of +30 mV. This rapid spike in membrane voltage is termed an action potential (AP), and is the basis of neuronal communication.

Hodgkin and Huxley originally proposed a model to explain the ionic mechanisms underlying the initiation and propagation of action potentials in squid giant axon (Hodgkin and Huxley 1952b). Adapting the voltage clamp technique proposed by Cole in 1949 and taking advantage of the relatively large size of the squid axon, they used long slender intracellular electrodes to record membrane potential changes. They quantitatively recorded action potentials and demonstrated the involvement of Na^+ in the rising (depolarization) phase of an action potential. They also uncovered the role of voltage-gated ion channel kinetics in the initiation and propagation of action potentials. To date, the Hodgkin and Huxley model is still the basis of our understanding of single cell electrophysiology in the study of modern neurophysiology.

Investigating the electrophysiology properties (ionic flux, membrane conductance and voltage-gated properties) of neurons is essential when characterising any model of neurodevelopmental or neurodegenerative disease in terms of neuronal function. The electrophysiological properties demonstrate the fundamental functional phenotypes of neurons and the neuronal circuits. Moreover, these types of studies provide a better understanding of the effectiveness of the differentiation protocols employed, focusing on the maturity of neurons.

The iPSC technology has been widely used in the generation of functional neurons providing important model systems for enhancing our understanding of neurobiology and neuronal signalling in specific neuronal cell types. Specifically, excitatory pyramidal cells represent the majority of the population of the cerebral cortex, where they integrate information between the extra-cortical inputs and disparate cortical

structures. These neuronal structures provide the executive function of the human brain, and its malfunctions are associated with many disease states such as ASD, epilepsy and Alzheimer's disease (Shi, Kirwan, Smith, et al. 2012; Chambers et al. 2009; Mariani et al. 2012).

In the developing cortex, the appearance of embryonic synapse formation coincides with the development of spontaneous electrical activity in the developing neurons (Katz and Shatz 1996). Human cortical neurogenesis starts at a round week 5 of gestation and continues for over 70 days (Caviness et al. 1995). The development of synapses starts at around week 9/10 of human foetal development (Huttenlocher et al. 1982). Glutamatergic and functional deep layer neurons such as layer 5 and six are found to be present at early stages of differentiation (Kirwan et al. 2015). The function of these neurons changes over time, reflecting their development *in vivo* (Kirwan et al. 2015). The neuronal network within the cerebral cortex undergoes stages of oscillatory activity during foetal development. These oscillations and bursting network activity begin approximately halfway through the gestation up to birth (Dreyfus-Brisac and Larroche 1971). The characterization of cerebral cortex neuronal networks derived from human iPSCs requires weeks/months of differentiation before cells acquire functional firing properties (Shi, Kirwan, Smith, et al. 2012). It has been shown that action potential height increases and resting membrane potential decrease through the progressive maturation *in vitro* (105 days in culture) of the cortical neurons (Prè et al. 2014; Kirwan et al. 2015).

The expression of voltage-gated ion channels during neuronal development provides the essential machinery for neuronal excitability. The expression of these voltage-gated ion channels is the primary source of neuronal depolarization and repolarization. Their gating properties and the ion species selectivity determine the kinetics of changes in membrane potential. Subtypes of various Na^+ and K^+ channels are expressed in different brain regions and have a range of physiological property. They all comprise of 6 transmembrane segments (S1-S6), which are divided into two modular domains, the voltage-sensing domain (S1-S4) and the pore-forming domain (S5-S6). The S4 segment acts as the main voltage sensor and responds to changes in electrical potential by inducing a conformation change, resulting in the opening of the channel (Jogini and Roux 2007).

The magnitude of the inward Na^+ current is noted to increase over developmental time, in line with neuronal maturation and sensitivity to the channel blocker tetrodotoxin (TTX) (Prè et al. 2014; Song et al. 2013). On the other hand, K^+ current has been reported to remain unchanged throughout neuronal development (Belinsky et al. 2011).

In this chapter I have explored the passive and active properties of 100-day iPSC-derived neurons from *NRXN1α* deletion patients and controls. We have applied voltage and current clamp recording to investigate the electrical excitability of neurons. We report here the detailed characterization of the functional neurons. These data serve to validate firstly the maturity and functional network activity of neurons in an *in vitro* human cell model and secondly to uncover new insights into the effects of *NRXN1α* deletion on non-synaptic properties of neurons.

3.2 Material & methods

3.2.1 Cell culture

The iPSC-derived neurons were cultured on 15-mm round coverslips (Thermo Fisher Scientific 12362138) in 12-well plates, which were previously coated with poly-D-lysine (see Methods section Chapter 2). Cells were cultured in N2B27 medium, which was refreshed every two days until the day of the analysis.

3.2.2 Whole cell patch clamp recording method

Whole cell patch clamp configuration was used to record from 98 neurons (Control n=54, Patient n=39, and median of 10 cells recorded per line for both control and patients) at day 100 of differentiation in all cases. All recordings were performed at room temperature (approx. 18-20^{o}C) in warm extracellular bath solution, with140 mM NaCl (Sigma-Aldrich 71387), 5 mM KCl (Sigma-Aldrich P9333), 2 mM $CaCl_2$ (Sigma-Aldrich C5670), 2 mM $MgCl_2$ (Sigma-Aldrich M8266), 10 mM HEPES sodium salt (Sigma-Aldrich H7006) and 10 mM glucose at pH 7.4. Single cells were selected for recordings based on a pyramidal morphology and bright, clear cell body.

Additionally, each selected cell had at least 2/3 neurites, imaged under Zeiss Axiovert 200 at 40X magnification.

Patch pipettes were pulled from borosilicate glass capillaries (Harvard apparatus GC150TF-7.5) using a Zeitz DMZ puller (Werner Zeitz, Germany). The glass pipettes were filled with intracellular solution (123 mM $C_6H_{11}KO_7$, 10 mM KCL, 1 mM MgCl2, 10 mM HEPES potassium salt (Sigma-Aldrich H0527), 1 mM EGTA, 0.1 mM CaCl2, 1.5 mM adenosine 5'-triphosphate magnesium salt (Sigma-Aldrich A9187), 0.2 mM guanosine 5'-triphosphate sodium salt hydrate (Sigma-Aldrich 51120), 4 mM glucose) with resistance of 4.0-5.5 MΩ.

Recordings were made using HEKA EPC10 patch clamp amplifier. Voltage-dependent Na^+ and K^+ currents were recorded in voltage clamp mode from a holding potential of -70 mV; voltage step depolarization was applied to +20 mV in 10 mV increments and recorded for 200 ms. Additional recordings were performed in the presence of 1 µM TTX (alomone labs, T-550) and 10 mM tetraethylammonium (TEA) (Sigma Aldrich, 140023) to block Na^+ and K^+ currents respectively. All data was recorded unfiltered for voltage and current clamp recording at 50.0 kHz and 20.0 kHz, respectively.

Currents were normalized to maximum conductance ($G_{max}= I/(V-V_r)$ and plotted against the voltage steps. This was done first by calculating the reversal (V_r) potential by plotting a tangent line and calculate the intercept ($V_r=I/V$). Then the conductance (G) was calculated by dividing the desired voltage step over the V_r. Finally, the G/G_{max} was normalized against maximal conductance value for the ion of interest. Intrinsic firing properties of neurons were recorded in current clamp mode, with step current injections from a holding value of -5 pA up to +45 pA, for 500 ms, in 10 pA increments. Spontaneous action potentials were recorded in current clamp mode at zero current injection (resting membrane potential) just after whole cell configuration was achieved.

Data analysis was performed using patchmaster (HEKA) and fitmaster (HEKA). The following electrophysiological parameters were examined: resting membrane potential, input resistance, amplitude of the negative peak of inward Na^+ currents, amplitude of the peak of outward K^+ currents, sodium channel maximal conductance

(G/G_{Max}), I/I_{Max}, action potential height, time to the peak of action potential, time to the threshold of the action potential, threshold of the action potential, repolarisation slope and time.

3.2.3 Statistical analysis

All data were expressed as mean ±SEM. Each data was tested for normality using Shapiro-Wilk normality test. Statistical analysis was performed using non-parametric Mann Whitney U test with a level of significance set for $p<0.05$.

3.3 Results

3.3.1 Passive membrane properties remain unchanged in 100-day neurons with *NRXN1α* deletion

The presence of voltage-gated ion channels in neurons and their gating properties are an important determinant of membrane input resistance. We derived 100-day neurons from iPSCs of control and ASD patients with *NRXN1α* deletions and recorded the input resistance and resting membrane potential by whole cell recordings. There was no significant difference between the control and *NRXN1α* deletion neurons in input resistance (Control 688.00±46.36 MΩ; Patient 852.00±96.64 MΩ, $p<0.21$) and resting membrane potential (Control 34.11±0.90 mV; Patient 35.95±0.84 mV, $p<0.24$) (Figure 3.1). This suggests that the passive properties of neurons remain largely unchanged in *NRXN1α* deletion neurons.

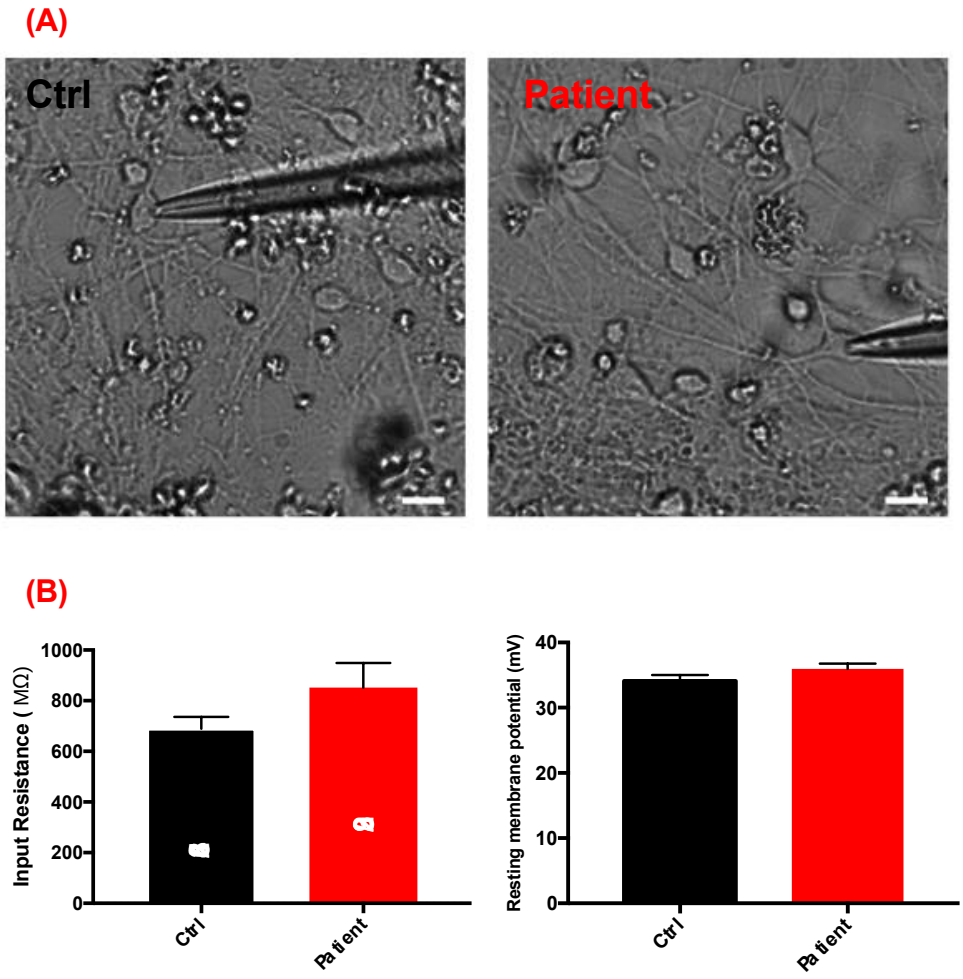

Figure 3.1. Passive membrane properties of iPSC-derived neurons. (A). Representative images of control and *NRXN1α* deletion neurons typically patched. (B) Input resistance and resting membrane potential from whole cell recordings of control and *NRXN1α* heterozygous deletion patients. All data summary were presented with mean ± SEM (numbers in bars/brackets represent a number of cells/number of coverslips used).

3.3.2 Active membrane properties are significantly changed in *NRXN1α* deletion 100-day neurons

Single cell electrophysiology, voltage clamp or current clamp recordings were used to determine the active membrane properties of the iPSC-derived neurons. The majority (96%, 94 out of 98 cells tested) of patched cells produced classical inward and outward currents typical of functional Na^+ and K^+ channels, respectively, showing that the majority of cells patched were mature neurons. The 100-day-old neurons derived iPSCs produced voltage-dependent, fast inward currents that are activated at membrane potentials of approx. -50 mV and deactivated at -30 mV.

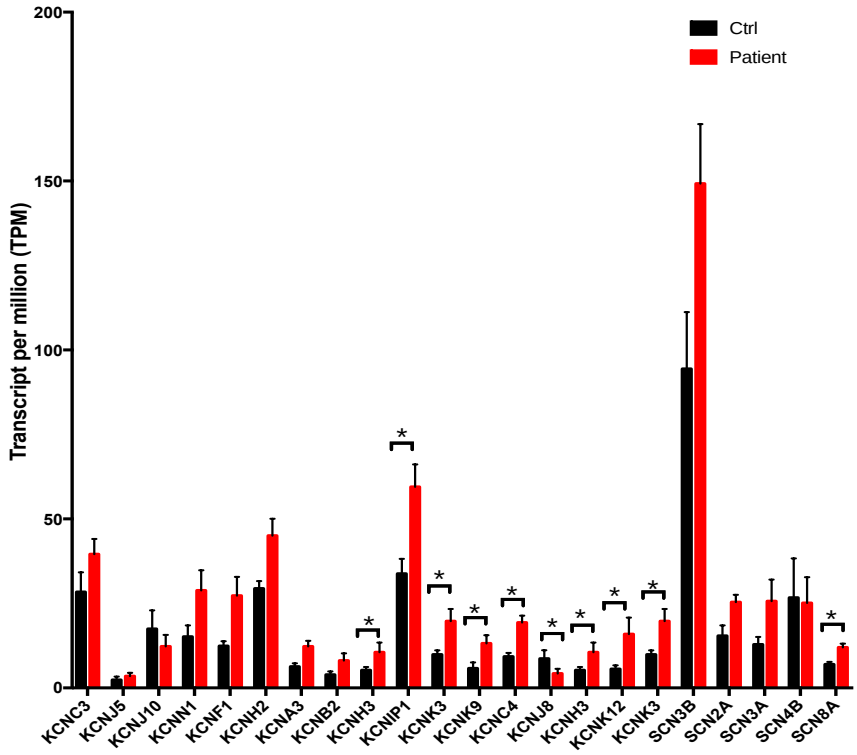

Figure 3.2. Expression of voltage-gated ion channels was elevated in neurons associated with NRXN1α deletion. Quantitative expression of voltage-gated K^+ channels (VGKCs) and voltage-gated Na^+ channels (VGSCs) at the RNA level was determined using RNA sequencing (* for FDR <0.05). Nine classes of K^+ channels and one class of Na^+ channel were significantly changed in *NRXN1α* deletion neurons, respectively.

Transcriptome analysis form 100-day iPSC-derived neurons indeed showed positive expression of various voltage-gated Na^+ and K^+ channels (VGSCs and VGKCs, Figure 3.2). The quantitative expression of these ion channels was measured at 100-day neurons using RNA sequencing. The significantly differentially expressed genes included a range of VGKCs (*KCNIP1, KCNK12, KCNA3, KCNB2, KCNC4, KCNF1, KCNH3, KCNJ8*) and one type of VGSC (*SCN8A*) at FDR of less than 0.05 (Figure 3.2).

In normal development, the electrophysiological properties of the cell membrane correlate with the appearance of ion channels (Spigelman et al. 1992). The appearance of rectifying K^+ current is a key aspect of the excitable membrane, where currents increase in amplitude at increasingly positive membrane potentials. Our data showed that 98% of iPSC-derived neurons displayed rectifying currents, with 54 of 57 of cells from control iPSCs and 39 of 41 cells from Patient iPSCs (Figure 3.3C & 3.3D).

Maximal currents of 572.50±45.98 pA and 696.70±49.49 pA ($p<0.001$) were obtained from Control and Patient iPSC lines, respectively, at +20 mV. Outward current was activated at approx. – 20 mV (Figure 3.3A & 2B). The current response as a function of applied voltage (Figure 3.3C & 3.2D) showed the voltage dependence of the inward and outward currents.

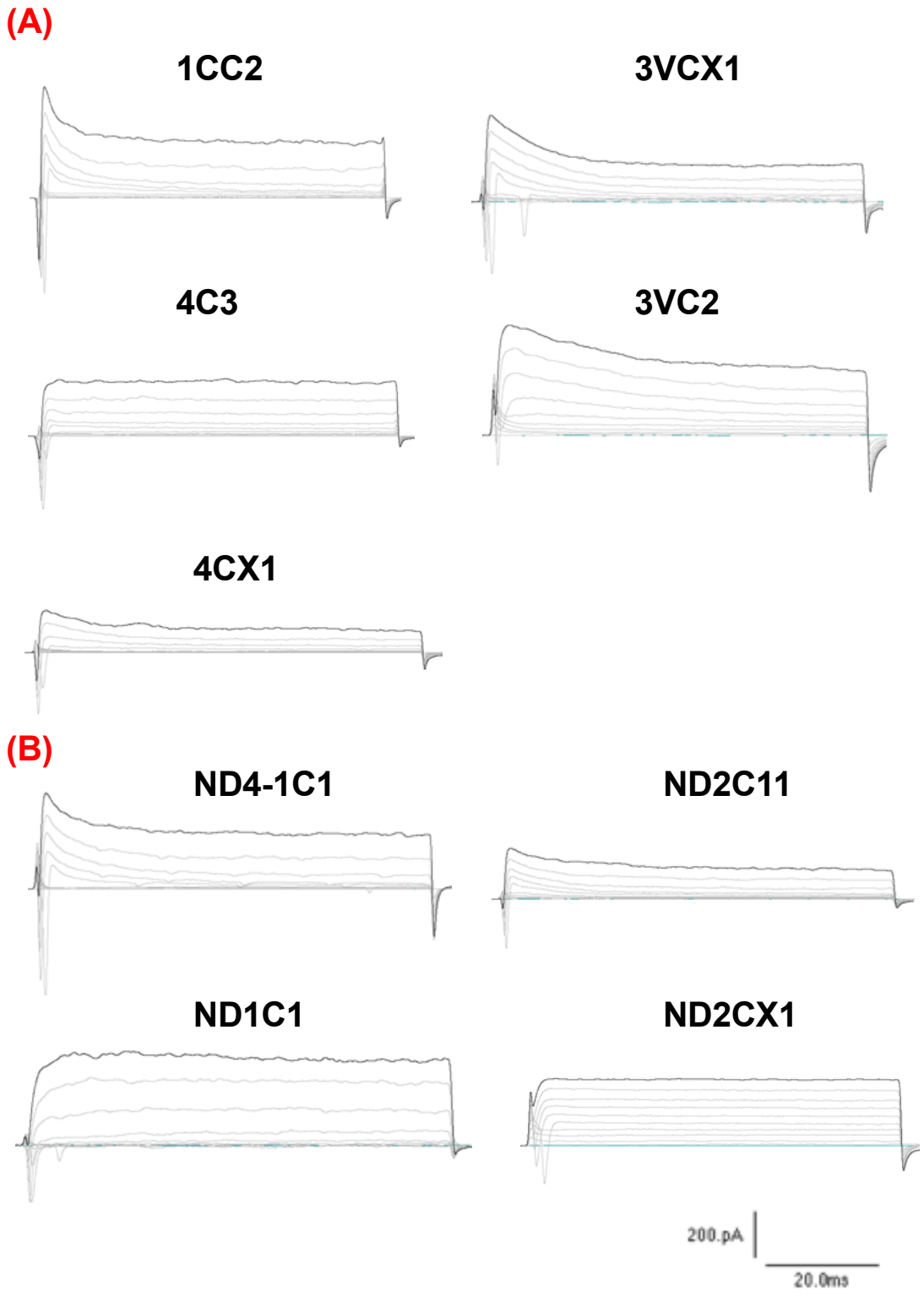
(A)
1CC2
3VCX1
4C3
3VC2
4CX1
(B)
ND4-1C1
ND2C11
ND1C1
ND2CX1
200.pA
20.0ms

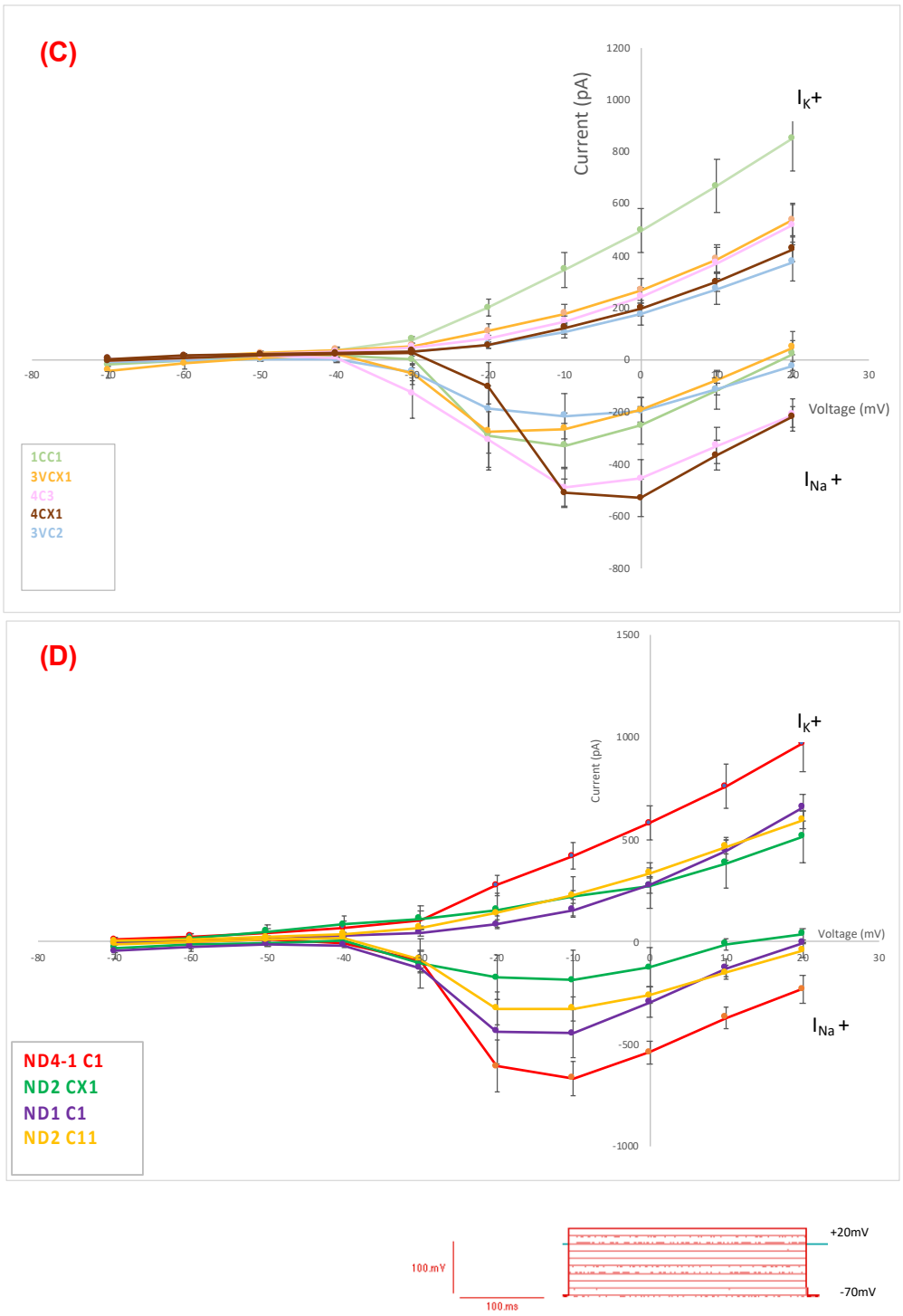

Figure 3.3 Voltage gated Na+ and Potassium Current in iPSC-derived neurons. (A) Representative traces of voltage clamp recording from each iPSC-derived neurons from both control (1CC2 n=10 cells/8 coverslips; 3VCX1 n=12/7; 4C3 n=12/6; 3VC2 n=5/3; 4CX1 n=5/2) and patients (B) (ND4-1C1 n=10/6; ND2C11 n=13/8; ND1C1 n= 10/7; ND2CX1 n=4/2), showing fast inward currents followed by outward currents. Average currents form both Na^+ and K^+ in both controls (C) and patients (D), showing slight variability between different iPSC clones but still in a defined range of physiological functionality. All data summary are mean ± SEM (The n numbers in bars/brackets represent number of cells/number of coverslips used).

Our data show that voltage-gated Na^+ and K^+ currents were significantly increased in *NRXN1α* patient cell lines. The inward Na^+ current showed a significant increase at -50 mV ($p<0.02$; Control 10.85 ±3.31 pA, Patient 3.97 ±4.19 pA), -40 mV ($p<0.03$; Control 12.91 ±5.75 pA, Patient 2.04 ±5.28), -30 mV ($p<0.001$, Control -53.35 ±27.52 nA, Patient -101.3 ±23.37) and -20 mV ($p<0.03$; Control -261.00 ±48.23, Patient -411 ±61.84) (Figure 3.4A). The most significant difference in *NRXN1α* lines was at -30 mV ($p<0.001$). The normalised maximal Na^+ conductance (G/Gmax) increased significantly at -30 mV ($P<0.005$), -20 mV ($p<0.02$) and -10 mV ($p<0.01$) (Figure 3.4C) in *NRXN1α* patient-derived cells. There was a significant increase in outward K^+ current in *NRXN1α* mutant neurons at -20 mV ($p<0.026$,Control 113.8 ±13.31 pA, Patient 162.2 ±19.63 pA), -10 mV ($p<0.024$, Control 198.10 ±22.74 pA, Patient 257 ±26.56 pA), 0 mV ($p<0.016$, Control 300.80 ±30.02 pA, Patient 376.33 ±33.14 pA), +10 mV ($p<0.020$, Control 432.80 ±38.21 pA, Patient 526.50 ±40.33 pA) and +20 mV ($p<0.01$, Control 572.50 ±45.98 pA, Patient 696.70 ±49.19 pA) (Figure 3.4B). The most significant difference in *NRXN1α* lines was at -20 mV.

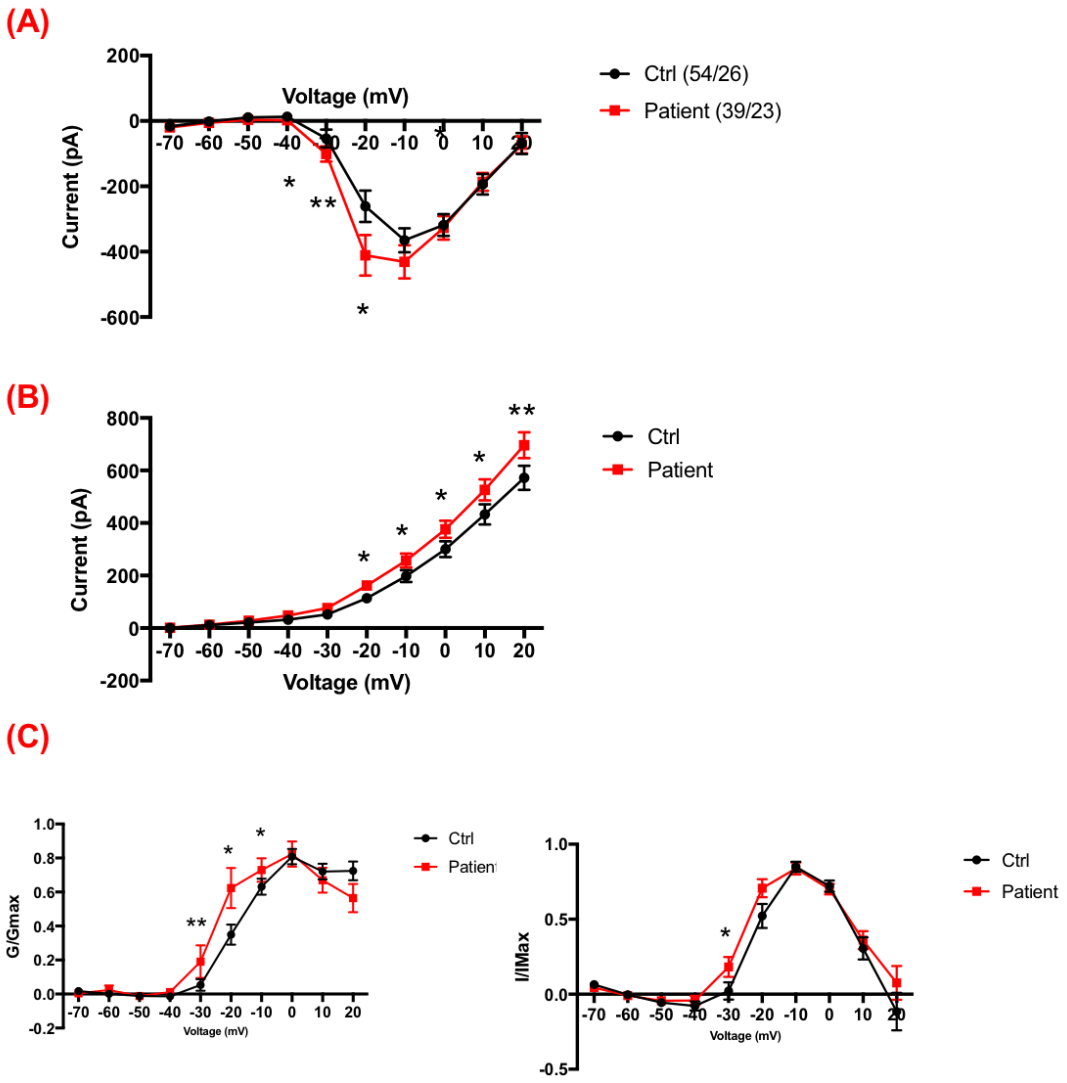

Figure 3.4 NRXN1α deletion significantly impairs voltage-gated sodium and potassium currents. *NRXN1α* deletion significantly increases the inward Na^+ (The n numbers in brackets represent number of cells/number of coverslips used) (A) and outward K^+ (B) voltage dependent current. (C) Using the data from panel B, the normalized maximal Na^+ conductance was plotted against voltage steps, with significant increase at -30, -20 mV and -10 mV. All data summary are mean ± SEM. Statistical significance (* $p<0.05$, ** $p<0.005$) were evaluated using Mann Whitney U test.

To confirm the involvement of voltage-gated Na^+ and K^+ channels in the recorded current, selective Na^+ channel and K^+ channel blockers were applied. Addition of 10 mM TEA suppressed all outward currents, demonstrating that the outward current is predominately a K^+ current in our iPSC-derived neurons (Figure 3.5). In addition, the inward current was completely abolished by the application of 1 µM TTX, confirming that voltage-gated Na^+ channels were responsible for the fast-inward currents (Figure 3.5).

3.3.3 *NRXN1α* deletion significantly impairs the electrical excitability of the neurons

The expression of voltage-gated K^+ and Na^+ channels drives the spatial and temporal dynamics of action potentials in neurons. As neurons become mature, the capability of Na^+ channels to generate action potentials following depolarization becomes greater. Consistent with previous studies, if cells are not mature, they are not able to produce action potentials (Belinsky et al. 2011). In addition, the increases in Na^+ currents (Figure 3.4A) and K^+ currents (Figure 3.4B) may have a consequence on action potential depolarisation and repolarisation characteristics, respectively. In this study, three different step current injection protocols were examined to assess the activation of action potentials in the iPSC-derived neurons (Figure 3.6). Approx. 87% of cells tested (83% from Control and 92% from Patient cells) responded to injected currents and produced action potentials.

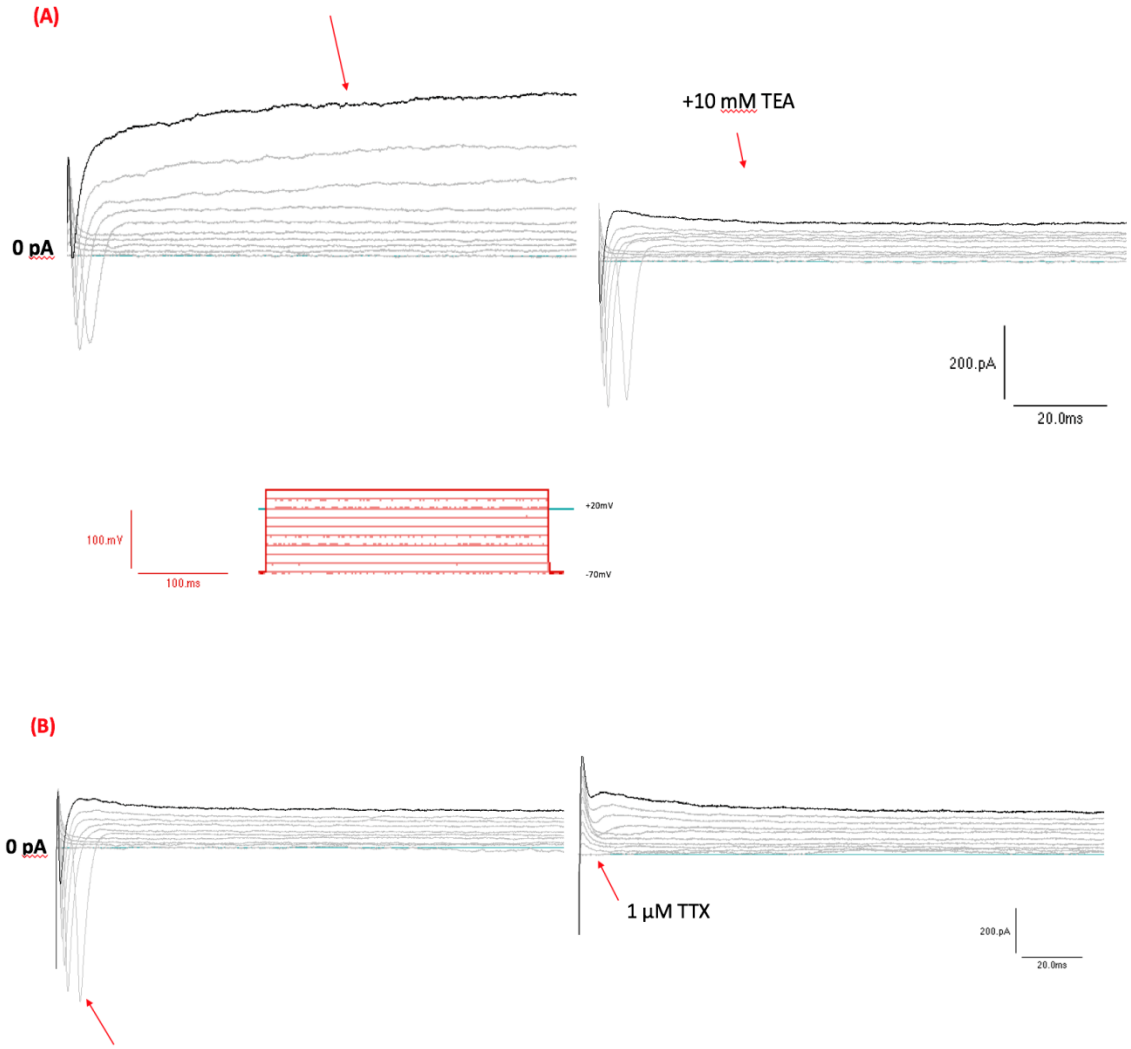

Figure 3.5. Confirming the identity of fast voltage activating and inactivating Na+ depolarizing currents and outward slower repolarizing K+ currents using pharmacological blockers. (A) Exemplar current traces from a control line (4C3 n=4/2), showing the application of 10 mM TEA and 1µM TTX with a voltage protocol shown in red (B). The "n" numbers in bars/brackets represent number of cells/number of coverslips used.

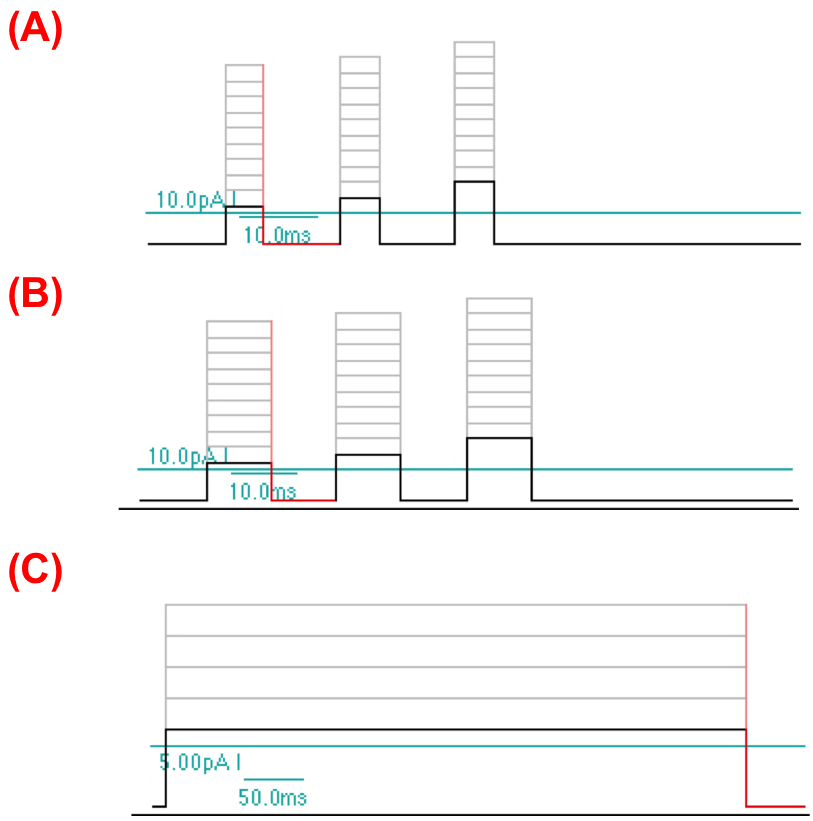

Figure 3.6. Step current injection protocols. Action potential generation occurred using step current injection of one of these protocols to the patched cell. All induced with 10 mV voltage increments.

In protocol C, the injected current was increased from 5 pA to 45 pA with a 10 pA increments (Figure 3.6C). Under these conditions, the time to reach action potential firing threshold was decreased as the injected currents increased (Figure 3.6C). Results for evoked action potential were compared between control and *NRXN1α* deletion neurons. Our results showed that the threshold voltage for action potential firing was significantly increased at 5 and 45 pA by 18.23% ($p<0.01$, Control 26.11±1.29 mV, Patient 30.87±1.35) and 20.53% ($p<0.03$, Control 22.02±122 mV, Patient 26.54±1.80 mV), respectively, in *NRXN1α* deletion neurons (Figure 3.8A), and that the action potential amplitude was significantly increased by 21.98% ($p<0.006$, Control 41.76±3.49 mV, Patient 50.94±1.76 mV) at 5 pA and by 34.85% ($p<0.006$, Control 43.44±3029 mV, Patient 58.58±3.99 mV) at 45 pA in *NRXN1α* deletion neurons (Figure 3.8B). The increase observed in Na^+ currents of *NRXN1α* deletion neurons may explain the great alteration in threshold voltage and hence the action potential height.

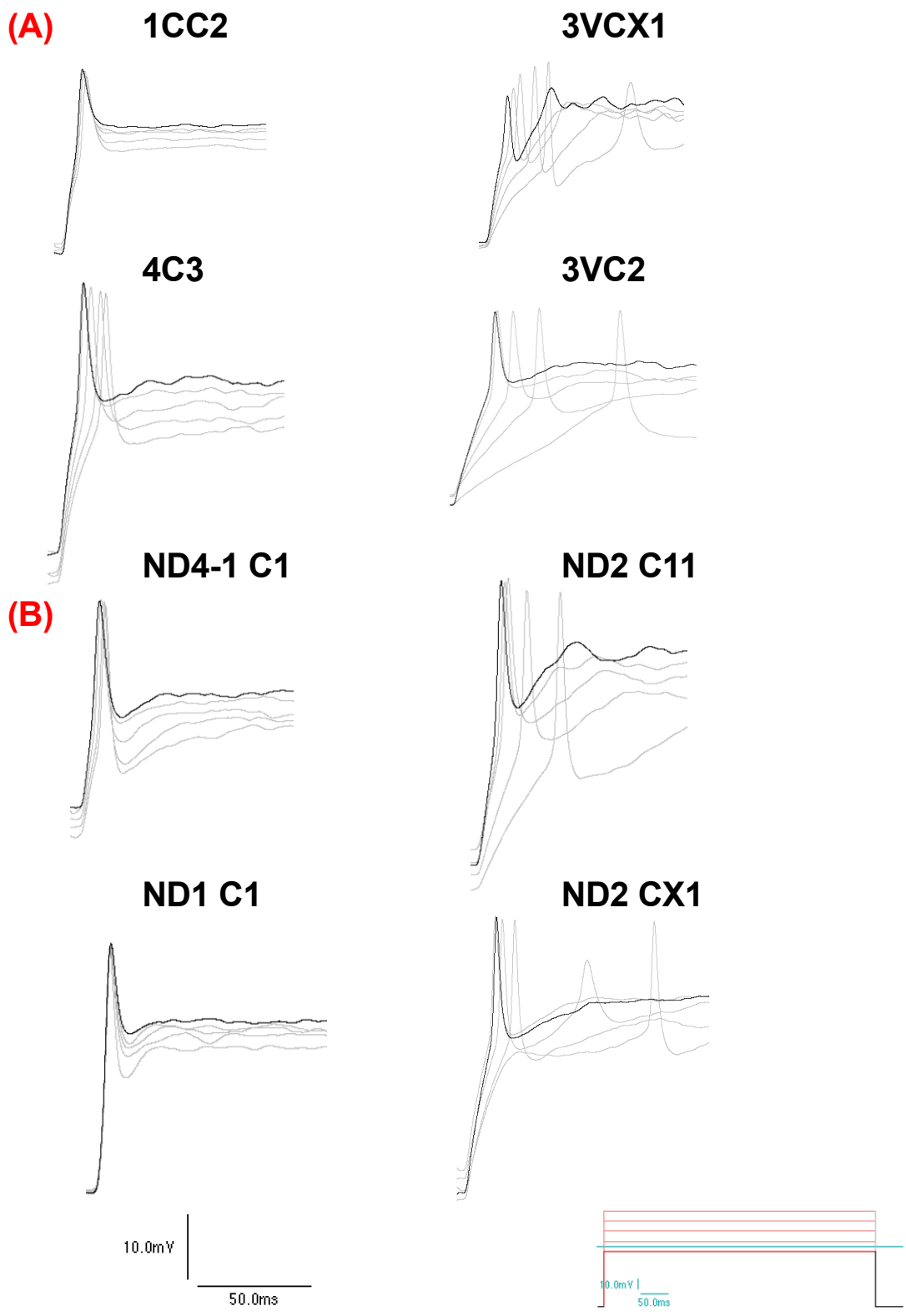
(A)
1CC2
3VCX1
4C3
3VC2
ND4-1 C1
(B)
ND2 C11
ND1 C1
ND2 CX1
10.0mV
50.0ms
10.0mV
50.0ms

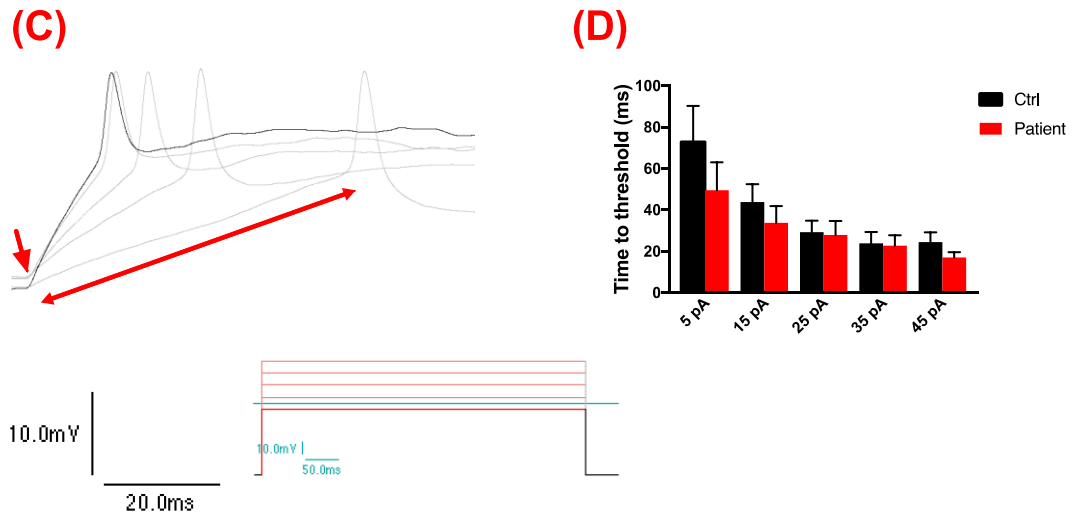

Figure 3.7. Characteristics of action potentials in iPSC derived neurons. (A) Representative traces of control and patient (B) action potentials in response to step current injections (-5 pA to +45 pA) in 10 mV voltage increments at day 100 of differentiation (protocol C from the table). (C) A representative trace from a control neuron shows the different injected current and the time to the threshold of the action potential. (D) This represents that the time decreases as the current becomes stronger. All data summary are mean ± SEM.

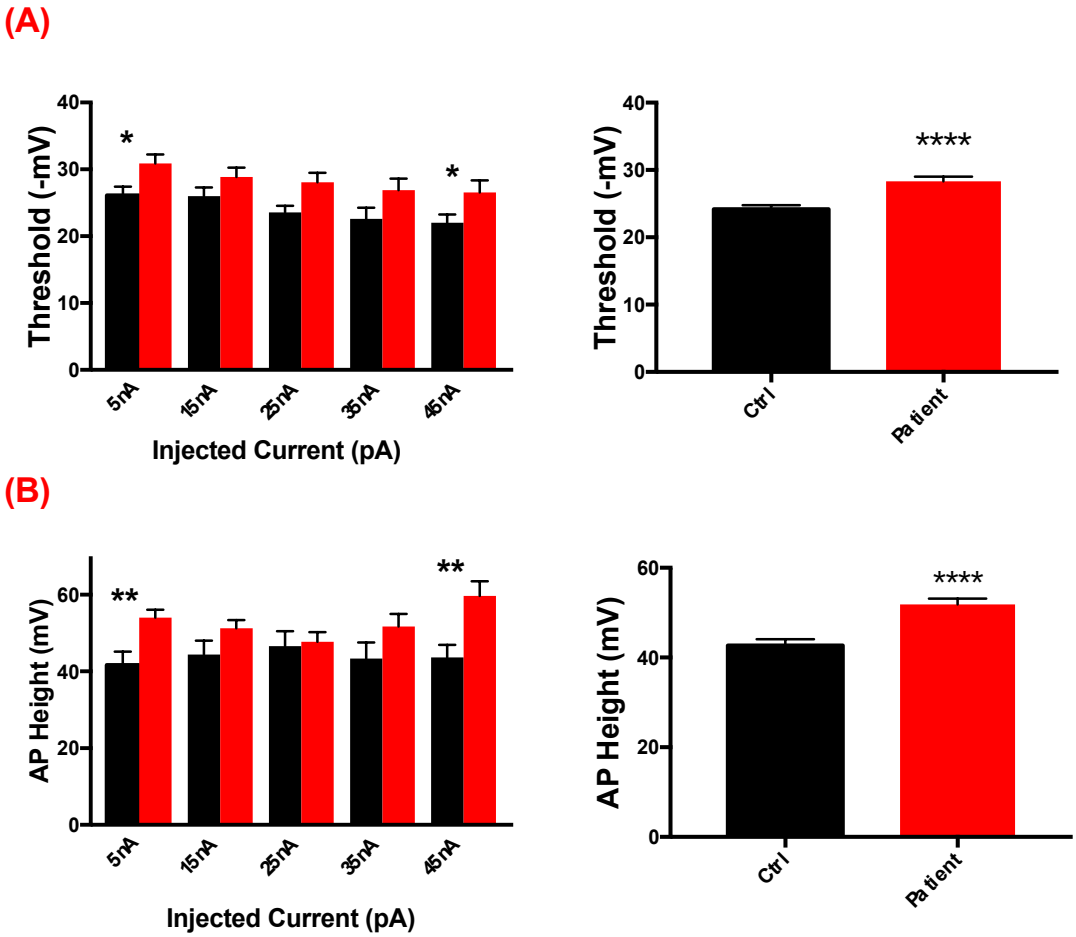

Figure 3.8. Neuronal depolarization is impaired in NRXN1α deletion patient cells. (A) The threshold of action potentials generated by step current injections (-5 nA to +45 nA) was significantly increased in *NRXN1α* deletion neurons, at -5 and +45 nA injected currents. The graph on the right represented the average threshold of all action potentials in control (n=21) and patient cells (n=23). (B) Action potential height in response to step current injections (-5 nA to +45 nA) in current clamp mode increased at the lowest (-5 nA) and the highest (+45 nA) injection. The graph on the right showed the mean of action potential from all injected currents in control and patient cells. All data summary are mean ± SEM. Statistical significance (* $p<0.05$, ** $p<0.001$, **** $p<0.0001$) were evaluated using Mann Whitney U test.

In addition, the repolarisation slope (Figure 3.8A, B) was significantly increased by 75.75% ($p<0.0006$, Control 3.01±0.63 V/s, Patient 5.29±0.37 V/s), 70.85% ($p<0.002$, Control 2.95±0.41 V/s, Patient 5.04±0.41 V/s) and 40.18% ($p<0.007$, Control 3.31±0.33 V/s, Patient 4.64±0.44) at 5, 15 and 25 pA, respectively, in *NRXN1α* deletion neurons (Figure 3.9C). Furthermore, the repolarisation time was significantly decreased in *NRXN1α* deletion neurons by 56.28% ($p<0.003$, Control 19.16±2.55 s,

Patient 12.26±0.93 s) and 30.95% ($p<0.04$, Control 15.02±1.83 s, Patient 11.47±0.62 s) at 5 and 15 pA, respectively (Figure 3.9D). An alteration in repolarisation characteristics was a consequence of changed K^+ current.

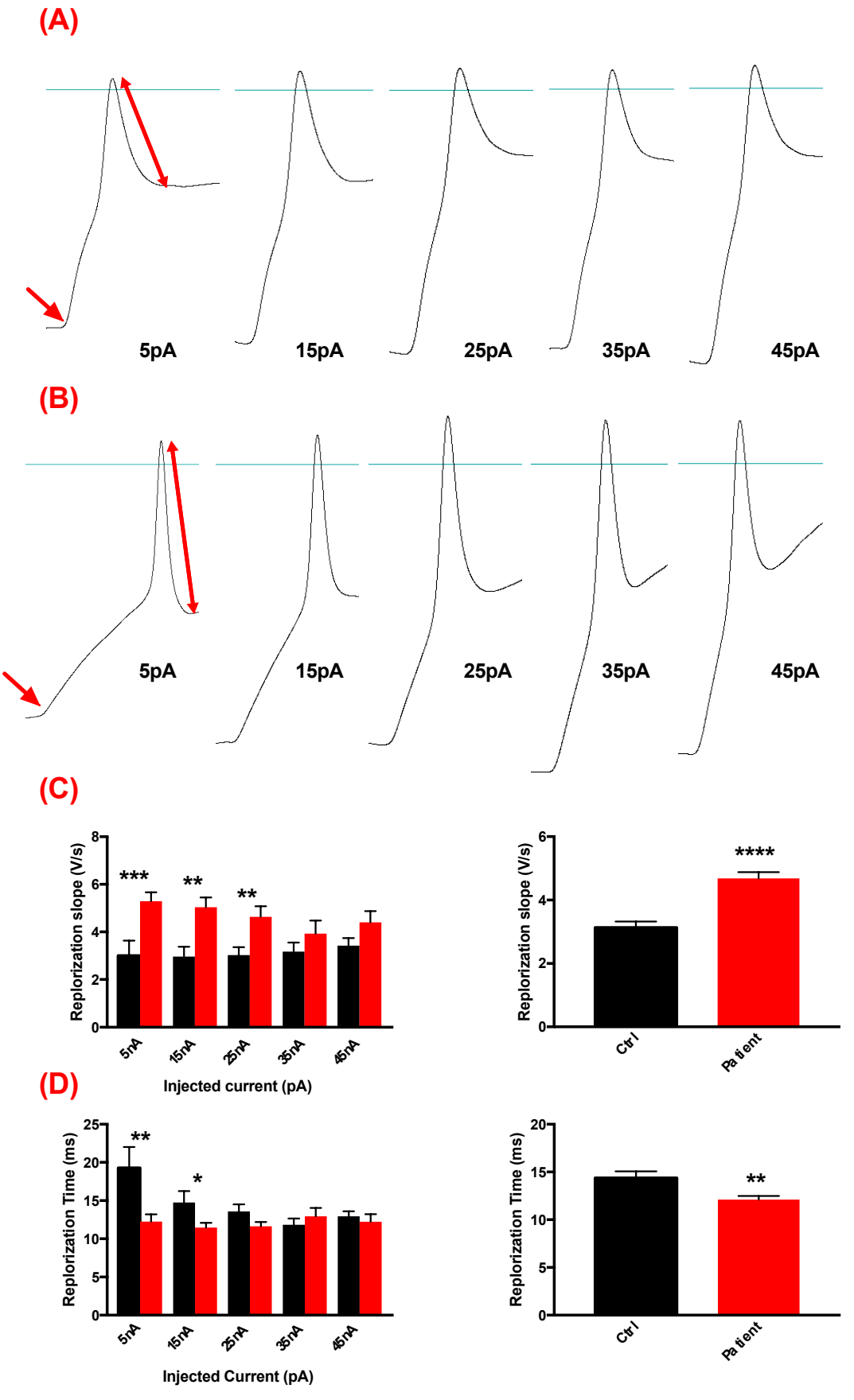
(A)
5pA
15pA
25pA
35pA
45pA
(B)
5pA
15pA
25pA
35pA
45pA
(C)
Replorization slope (V/s)
***
**
**
5nA
15nA
25nA
35nA
45nA
Injected current (pA)
Replorization slope (V/s)
****
Ctrl
Patient
(D)
Replorization Time (ms)
**
*
5nA
15nA
25nA
35nA
45nA
Injected Current (pA)
Replorization Time (ms)
**
Ctrl
Patient

Figure 3.9. NRXN1α deletion neurons are altered in the excitability by impaired depolarisation and repolarization properties of evoked action potentials. (A) Representative traces of action potential current clamp of the protocol (-5 nA to +45 nA) from a control line 1CC2 and patient line ND2C11 (B). (C) Repolarization slope was increased significantly at 5 to 25 nA in *NRXN1α* deletion patients. The graph on the right is the mean of all controls and patients (D) Repolarization time was decreased significantly at 5, and 15 nA injected current in *NRXN1α* iPSC-derived deletion neurons-. The graph on the right is the mean of all controls (n=17) and *NRXN1α* iPSC derived deletion neurons (n=16). All data summary are mean ± SEM. Statistical significance (* $p<0.05$, ** $p<0.001$, **** $p<0.0001$) were evaluated using Mann Whitney U test.

3.3.4 The 100-day iPSC-derived neurons exhibit spontaneous activity

Spontaneous action potentials were also observed in current clamp mode with zero applied current (i.e. cells were held at the resting membrane potential) (Figure 3.10). The action potential characteristics were similar to evoked action potentials.

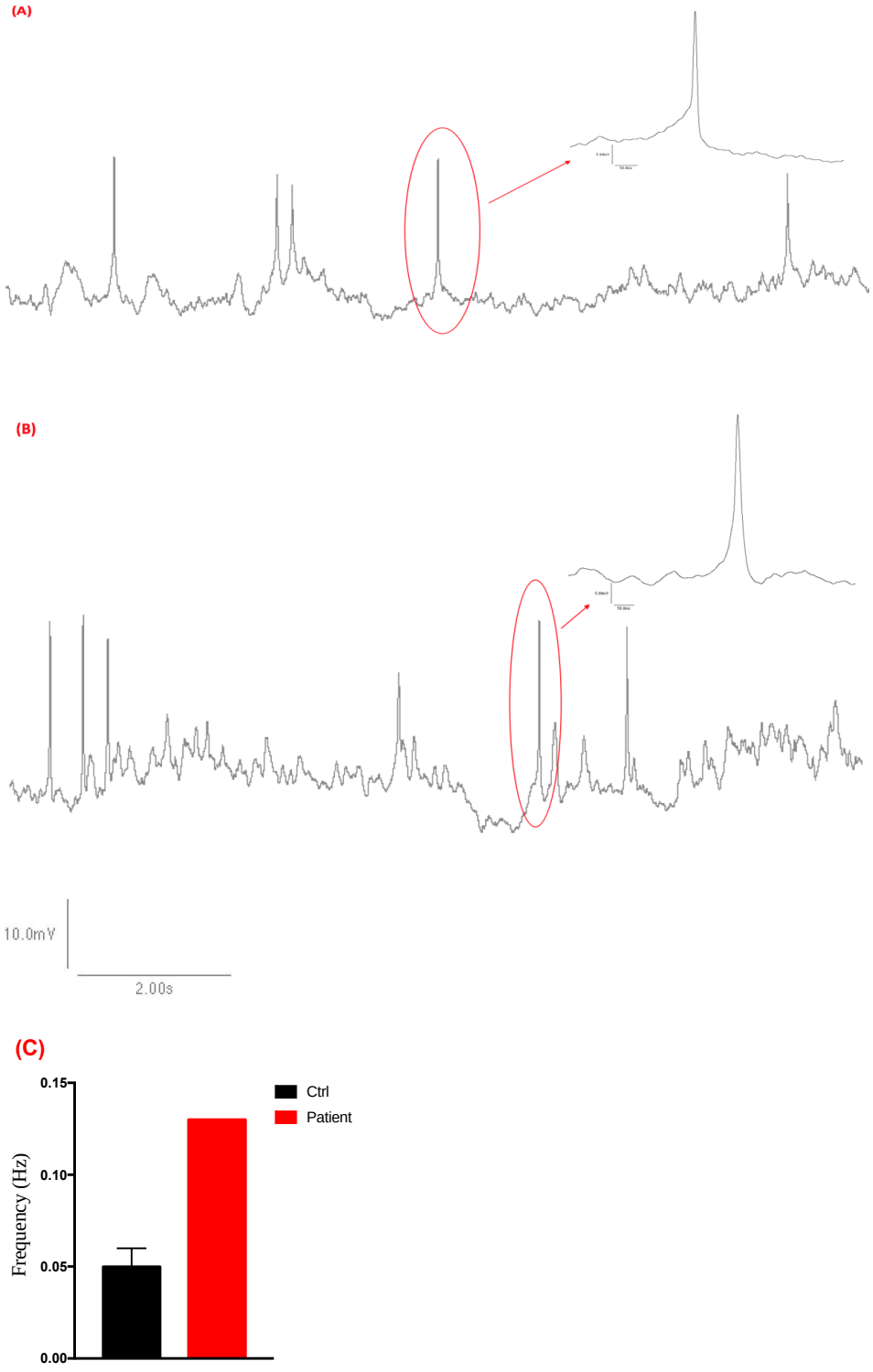

Figure 3.10. Spontaneous activity observed in iPSC-derived neurons showed similar action potential characteristics. (A) Representative traces of spontaneous action potentials recorded at resting membrane potential showing similar characteristics to evoked action potentials, from individual cells of both control (3VCX1) and *NRXN1α* deletion patient (ND2C11) (B) (n=3/3). (C) The mean frequency of spontaneous action potentials. All data summary are mean ± SEM.

3.4 Discussion

NRXN-NLGN signalling is known to couple both neuronal excitation and inhibition. *NRXN1* copy number variation is widely associated with neurodevelopmental disorders of ASD, schizophrenia, intellectual disability, epilepsy and language delay. However, how *NRXN1α* copy number variation affects brain development and/or neuronal function in patients is unknown. In this study, we have carried out whole cell patch clump on 100-day neurons derived from control and ASD patient iPSCs with *NRXN1α* heterozygous deletions. Differential electrophysiological properties were detected between the control and *NRXN1α* deletion neurons. These included significantly increased inward Na^+ current and outward K^+ current, lower threshold voltage and higher amplitude of action potential, altered firing patterns with increased repolarisation slope but decreased repolarisation time. Furthermore, transcriptome analysis of the 100-day neurons revealed significant upregulation of voltage-gated potassium channels (*KCNIP1, KCNK12, KCNA3, KCNB2, KCNC4, KCNF1, KCNH3, KCNJ8*) and a voltage gated-sodium channel (SCN8A). This is the first time to our knowledge to demonstrate that *NRXN1α* deletions are associated with altered functionality in human iPSC-derived neurons from patients.

Under currently established protocols, the differentiation and maturation of iPSC-derived neurons require several weeks to months of culture *in vitro* to acquire mature functional properties (Shi, Kirwan, Smith, et al. 2012). Differentiation protocols employed in this thesis clearly resulted in the expression of markers reflecting neural development and neuronal maturity, including the early neural stem cell markers NESTIN & PAX6, pan-neuronal marker TUJ1, and mature neuronal markers like MAP2 and SYN1 (Shimada et al. 2009; Moe et al. 2005; Gingras and Champigny. 2007). In Chapter 2, the maturity and developmental profile of the excitatory cerebral cortical neurons were validated at the cellular and molecular levels. At the start of the time course, neural progenitors were 87% and 82% $NESTIN^+$ and $PAX6^+$ cells, respectively. Differentiated 100-day neurons were shown to express neuronal marker MAP2, SYN1 and TUJ1. Significant proportions of cells were positive for different layers of cortical neuronal markers, including $TBR1^+$/$CTIP2^+$ for deep layers, and $SATB2^+$/$BRN2^+$ for upper layer cortical neurons, thus demonstrating the successful derivation of the excitatory cortical neurons.

However, these characterizations of neurons were not sufficient to demonstrate their functionality. In this Chapter, the electrophysiological properties of the neurons have been examined, as this is central to their function in neuronal networks. The ability to generate rapid dynamic changes in membrane potential or action potentials in response to a suprathreshold stimulus is an important developmental milestone in neuronal maturation. In a similar way to the passive properties of developing neurons, active properties are determined by the expression of voltage-gated ion channels in the neuronal membrane (Spigelman et al. 1992). As neurons become mature, the expression of Na^+ and K^+ voltage-gated ion channels coincides with a shift in the resting membrane potential to more negative voltages (Spitzer 1994). The 100-day iPSC-derived neurons from this study exhibited comparable resting membrane potential, with 34.11±0.90 mV (n=54 cells) in controls and 35.95±0.84 mV (n=39 cells) in patients-derived neurons, respectively. These values are very similar to other mature iPSC or ESC-derived cortical neurons (Pak et al. 2015).

The passive properties of neurons alter as neurons mature over time (Prè et al. 2014). This includes input resistance in which its value decreases over time during maturation (Prè et al. 2014). The input resistance of neurons at 100-day differentiation in this study was 668.7 MΩ in control and 852.1 MΩ in patient's cells, respectively. The assessment of these properties was not tested in a time-dependent manner. However the data presented here were very similar to other iPSC/ESC-derived forebrain/excitatory mature cortical neurons (Prè et al. 2014; Pak et al. 2015). These results also showed that there was no significant difference regarding their passives membrane properties between control and *NRXN1α* deletion neurons (Figure 3.1B).

While the presence of Na^+ and K^+ ion channels are essential for inducing action potential, hence the active properties on neurons were investigated. During neuronal maturation, the expression of voltage-gated Na^+ channels increases over time (Kawaguchi et al. 2007). The increase in a number of voltage-gated sodium channels is reflected in the average peak current (Prè et al. 2014). On the other hand, it has been reported that the peak current of K^+ current does not change significantly throughout the maturation stages in iPSC-derived forebrain neurons (Prè et al. 2014; Belinsky et al. 2011). However, this was very much dependent on the time of analysis and

differentiation protocol adopted, which was noted by other laboratories (Walton et al. 1993).

In our study, in the voltage clamp mode, the Na^+ and K^+ currents were measured, and 96% of cells responded in a voltage-dependent manner, and their currents increased as a function of applied voltage step (-70 mV to +20 mV). The Na^+ currents were activated at -30 mV with the highest sodium entry at -10 mV. Meanwhile more slowly activating K^+ outward currents were activated initially at -30 mV and had a slow and smooth activation with the highest amplitude at +20 mV voltage step. The amplitude of the peak of Na^+ and K^+ currents from the current study are similar to mature forebrain neurons studied by Prè D et al. (Prè et al. 2014). The presence of voltage-gated sodium channels was confirmed using TTX, a sodium channel blocker. When 1 µM of TTX was applied, it resulted in a total block of inward currents (Figure 3.4B). Meanwhile, the application of 10 mM TEA, a known blocker of voltage-gated K^+ channels, significantly abolished the outward currents, confirming that K^+ currents were responsible for the outward currents in the 100-day neurons (Figure 3.4A).

The variability of Na^+ current among different clones and donors were more noticeable in comparison to K^+ current in both control and patient iPSC-derived neurons (Figure 3.2C, D). These variations may explain that different neurons even from the same type of synapses express different proportions of sodium channel isoforms. For example, increased expression of $Na_v1.1$ was reported in cortical organoids from probands with ASD, which made substantial cell to cell variations in the voltage-dependence activation (Mariani et al. 2015). Mariani and colleagues demonstrated that this increase was consistent with increased expression of GABAergic neurons, as this isoform was preferentially expressed in GABAergic interneurons (Cheah et al. 2012; Han et al. 2012). Interestingly, variation in voltage-gated sodium channel was also observed in *NRXN1α* deletion neurons (Figure 3.2), which may have a functional consequence on sodium currents and action potential properties. However, we have little GABAergic neurons present in the 100-day cultures (see below).

Both the voltage-dependent Na^+ and K^+ currents showed significant alterations in the *NRXN1α* deletion neurons. The magnitude of voltage-gated Na^+ currents was significantly different at a range of membrane potentials, with a significantly increased

Na^+ current in *NRXN1α* deletion neurons. Voltage-gated K^+ current was also altered at a range of membrane potentials. These data suggest that loss of one *NRXN1α* allele in iPSC-derived neurons leads to an alteration in the measured non-synaptic properties of human neurons. It was demonstrated earlier that deletion of all three *Nrxnα* genes in mice in part altered the calcium influx during an action potential (Missler et al. 2003). This also suggests an underlying impairment in the action potential properties associated with *NRXN1α* lesions. While in our study, an alteration was identified in Na^+ and K^+ currents in *NRXN1α* deletion cortical neurons, this was not reported in the earlier study using human ESC-induced cortical neurons with mutated *NRXN1* (Pak et al. 2015).

The potential consequence of impairment in voltage-gated Na^+ and K^+ currents was subsequently investigated in evoked action potential kinetics. Action potential characteristics are directly influenced by the kinetics of depolarization and repolarization, i.e. by the opening and closing of voltage-gated sodium and potassium channels. The average action potential amplitude was 42.66±1.42 mV in control, and this was increased by 21.47% in patient iPSC-derived neurons (51.82±1.32 mV, $p<0.0001$). Subsequently, the threshold for action potentials was -24.2±0.60 mV in control but decreased by 17.02% in patient iPSC-derived neurons (-28.32±0.70 mV, $p<0.0001$).

These results clearly state the consequences of an increase in Na^+ currents by propagating stronger action potential. In addition, the repolarization slope and repolarization time were altered between control and *NRXN1α* deletion neurons. The average repolarization slope was significantly increased by 49.52% ($p<0.0001$, Control 3.13±0.19 V/s, Patient 4.68±0.20 V/s) in *NRXN1α* deletion neurons, whereas the repolarization time was significantly decreased by 15.66% ($p<0.001$, Control 14.37±0.68 s, Patient 12.12±0.38 s). Outward K^+ currents induce repolarization of the membrane, and thus these data suggest that an impairment in repolarization kinetics is directly influenced by the increased K^+ currents. The threshold of the action potential is the major determinant of excitability in neurons (Bean 2007). The threshold of action potential determines its initiation, shape and activation, and governs under sodium channel availability. Alterations in cortical neuronal

excitability were proposed as one of the fundamental properties of individuals with ASD (Rubenstein 2010).

What is the mechanism underlying this phenotype in heterozygous *NRXN1α* iPSC-derived cortical neurons? As mentioned previously, these electrophysiological properties were absent in ESC-induced *NRXN1* mutation (Pak et al. 2015). However, there is a clear difference between our studies. We believe, this is the first study investigating the role of *NRXN1α* mutations in patient iPSC-derived neurons, instead of using ESC in Pak *et al*. study. There is a possibility of genetic background effect in both cases, and we cannot exclude the possible contribution of this factor in our data. While the human ESC was based in H1 line, our study was resulted from the statistical analyses of six control lines and four mutant lines, with a minimum of statistically required donors in each group.

The second difference is that the exonic α isoform deletions are associated with our patients while both α/β isoforms have been genetically manipulated in Pak *et al.* study. *NRXN1α* and β isoforms have different interactions with their post-synaptic binding partners, and hence the deletion in each isoform may lead to failure of a different protein function (Chih et al. 2006). The first homozygous knockout mouse model of *Nrxn1α* showed a small impairment in excitatory synaptic transmission without alteration in synapse number or the quantal size of postsynaptic receptor numbers (Etherton et al. 2009). Later on, Pak et al. study showed that either homozygous or heterozygous deletion of *Nrxn1α* in mice had no change in spontaneous miniature excitatory postsynaptic currents of cultured cortical neurons (Pak et al. 2015). The discrepancies in these studies could be due to different brain regions and preparations in which electrophysiological properties have been recorded. This phenomenon has been reported and strongly suggested in Südhof research group in various studies (Aoto et al. 2015; Chen et al. 2017; Südhof 2017). They have proposed that Neurexins may perform the same canonical functions but may have different patterns of redundancy, depending on alternative splicing and different Neurexin variant studies (Aoto et al. 2015; Chen et al. 2017; Südhof 2017). This evidence further elucidate that differences in Neurexin variants may significantly alter the physiological roles of Neurexins.

In summary, data from our study show that *NRXN1α* deletion can influence the active properties of the neurons, and the electrical excitability of neurons is affected. We clearly observed an impairment in action potential properties in *NRXN1α* deletion neurons in comparison to control iPSC-derived neurons. These data suggest that the E/I balance might have been effected in the *NRXN1α* deletion neurons, a key mechanism implicated in ASD (reviewed by (Won et al. 2013). It is worthy of mention that the neuronal age and maturity differs throughout the neuronal development and it is essential to compare the same type of cells between control and *NRXN1α* deletion neurons. The resting membrane potential clearly indicate the maturity stage of neurons. The resting membrane potential becomes more negative over time during neuronal maturation (Prè et al. 2014). The frequency distribution of resting membrane potential in our study lies between 35 mV to 42 mV which reflect the fact that the neurons were on the same maturity level during recording.

Electrical excitability of neurons is dependent on and governed by various factors. The distribution and number of voltage-gated ion channels can determine the degree and rate of action potential firing. Electrical excitability has been increased by dysregulation of Na^+ channels in a mouse model of Fragile X, suggesting a major role of Na^+ channels in neuronal excitability (Deng and Klyachko 2016). Interestingly, this neuronal excitability was associated with the decreased AP threshold in the Fragile X mouse model (Deng and Klyachko 2016).

We have identified that a series of voltage-gated potassium and one member of voltage-gated sodium channel are significantly increased in the ASD *NRXN1α* deletion neurons (Figure 3.2). This may suggest a potential molecular mechanism which contribute to the overall clinical phenotypes of the ASD patients. The transcriptome results will be further discusse in RNA sequencing Chapter (Chapter 5).

Chapter 4. *NRXN1α* deletion impairs calcium dynamics in 100-day iPSC-derived cortical excitatory neuron

4.1 Introduction

Calcium ion is a ubiquitous and versatile intracellular signalling mechanism across a range of cellular systems. The concentration of calcium ions in the cytosol is tightly controlled. It is normally found at very low concentrations in the order of 50-100 nM, rising to 10 μM or higher during active signalling. Intracellular calcium is distributed and sequestered in the intracellular organelles such as the endoplasmic reticulum (ER) and mitochondria. The maintenance of a low level of calcium ions in the cytosol is achieved by either sodium-calcium exchange across the mitochondrial membrane, or via calcium ATPase pumps across the plasma membrane or internal ER store membranes (Berridge et al. 2000). Mitochondria act as an important calcium buffer system, aiding in homeostasis, by taking up calcium during periods of high cytosolic calcium concentration (Duchen 1999). The ER stores high levels of calcium filled by the Sarco-/ER calcium ATPase (SERCA). The release of calcium from these intracellular stores, mostly from ER, is regulated through inositol triphosphate and/or ryanodine receptors (Berridge et al. 2000).

In neurons, there are many sources of calcium for signalling, the intracellular concentration is determined by the balance between calcium influx (incoming) from and efflux (outgoing) to the outside of the cell, as well as the release from internal stores. Calcium influx occurs most commonly through voltage-gated calcium channels (VGCCs), ionotropic glutamate receptors and nicotinic acetylcholine receptors (Fucile 2004; Catterall and Few 2008). There is a broad range of VGCCs in neuronal tissues, and the L-type VGCCs are reported as the major channels in cortical neurons (Tang et al. 2003).

At the pre-synaptic terminus, a transient rise (up to 100x) in calcium concentration during electrical excitation triggers exocytosis of neurotransmitter-containing vesicles and subsequent release of neurotransmitters (Collins et al. 2002). The vesicle release machinery is complex and dynamic. It is made up of a large number of pre-synaptic proteins. The machinery includes SNARE complexes, synaptotagmins, syntaxin and synaptobrevin. Neurexins also have an important role in coupling VGCCs to the release machinery (Missler et al. 2003). Post-synaptically, the L-type VGCCs are

involved in activity-dependent synaptic plasticity (Zucker 1999; Neher and Sakaba 2008). The synchronous quantal release of neurotransmitter is induced by the arrival of action potentials and subsequent activation of VGCCs (Neher 1998; Stanley 1993).

Aside from its role in synaptic transmission in mature neurons, brief elevations of the intracellular calcium level, known as calcium transients, have been implicated in neuronal development, differentiation, proliferation and maturation. The timing and frequency of calcium transients play an important role in driving differentiation and maturation of neuron (Rosenberg and Spitzer 2011; Gu and Spitzer 1995). During brain development, there is a large population of neurons generating action potentials which contribute to calcium transients. These are considered as an integral part of forming functional mature synapses (Rosenberg and Spitzer 2011). The amplitude and frequency characteristics of these calcium transients are essential determinants for the function of intracellular calcium signals.

Calcium imaging is a powerful and sensitive technique which has been developed to quantify the calcium signals, and which has been widely used to measure calcium dynamics during neuronal activity *in vivo* and *in vitro* (Greenberg et al. 2008; Chen et al. 2011). One of the first calcium indicators was the bioluminescent calcium-binding proteins (Ashley and Ridgway 1968; Shimomura et al. 1962). Next, an absorbent dye, such as arsenazo III, was used as a calcium indicator by changing its absorption spectrum after binding to calcium (Brown et al. 1975). While the use of these calcium indicators was beneficial, their implementation, especially the dye delivery, was often tedious. Then in 1980, Roger Tsien and colleagues made a breakthrough by the discovery of much more powerful calcium florescent indicators (Tsien 1980). Since then, the investigation of calcium signalling, with the aid of the fluorescent indicators, have widely been adopted by scientists, allowing simultaneous recording from a large population of excitable cells, including neurons.

The florescent indicators developed by Tsien and colleagues for Ca^{++} signalling include quin-2, fura-2, indo-1 and fluo-3 (Tsien 1980). The first fluorescent dye used in biological experiments was quin-2 with excitation of ultraviolet light at 339 nm (Tsien et al. 1982). While quin-2 was a very good indicator, it was not particularly bright and had to be used at a very high intracellular concentration (Tsien 1989). Four years later, a superior replacement called Fura-2 became popular among

neuroscientists, overcoming the disadvantages caused by quin-2 (Grynkiewicz et al. 1985). Fura-2 has an excitation at 350 and/or 380 nm and allows more quantitative measurement of calcium involved in the rationing of the signals (Neher 1995). Many more calcium indicators have been introduced since then, in which Fluo-4 dye families have been widely used, due to its easy implementation and large signal to noise ratio (Paredes et al. 2008).

In this study, we recorded spontaneous and evoked calcium transients in iPSC-derived 100-day neurons using Fluo-4 dye, as a parameter for the functional mature neurons in the cultures. We have compared the Ca^{++} imaging between the neurons derived from iPSCs of healthy controls and of ASD patients with *NRXN1α* deletions and made a novel observation that an increasing Ca^{++} activity was associated with the *NRXN1α* deletion neurons.

4.2. Materials and Methods

4.2.1 Cell culture

The iPSC-derived neurons were cultured on 15-mm round coverslips in 12-well plates (Thermo Fisher Scientific 12362138), which were pre-coated with poly-D-lysine (Chapter 2). Cells were cultured in N2B27 medium and refreshed every two days until the day of the analysis.

4.2.2 Calcium imaging and data acquisition

Fluo-4AM (Thermo Fisher scientific F14201) was solubilised in DMSO to yield a 1mM stock solution. The Fluo-4AM was diluted to a final concentration of 2 µM in artificial cerebrospinal fluid (ACSF) containing140 mM NaCl (Sigma-Aldrich 71387), 5 mM KCl (Sigma-Aldrich P9333), 2 mM $CaCl_2$ (Sigma-Aldrich C5670), 2 mM $MgCl_2$ (Sigma-Aldrich M8266), 10 mM HEPES sodium salt (Sigma-Aldrich H7006), and 10 mM glucose, pH 7.4. The dye was loaded by removing the culture medium, and the neurons were washed with ACSF and then incubated with a Fluo-4AM solution for 20 minutes at 37°C. Excess dye was removed by washing with ACSF and finally replaced with culture medium for 20 minutes at 37°C. The culture medium was then replaced with warm ACSF solution, and cells were immediately

placed in an imaging chamber (Warner instruments/perfusion chamber RC-26GLP) on a Zeiss Axiovert 200 microscope under 10X magnification. Images were captured at room temperature with a Hamamatsu ORCA284 at 1 Hz frame rate for 3-5 minutes and stored as uncompressed image sequences.

Reagents/drugs were added to the ACSF solution as required, i.e., TTX (Alomone labs, T-550, 1μM) to block Na^+ channels; CNQX (Alomone labs, C-140, 50 μM) to block AMPA/Kainate receptors; DL-AP5 (Alomone labs, D-140, 50 μM) to block NMDA receptors; Nifedipine (Alomone labs, N-120, 50 μM) to block L-type calcium channels; glutamate (Sigma-Aldrich, G8415, 60 mM) and ionomycin (Sigma-Aldrich, I0634,20 μM) to raise intracellular Ca^{2+} concentration; γ-Aminobutyric (Sigma-Aldrich, A2129, 60 mM).

4.2.3 Data analysis using FluoroSNNAP

FluoroSNNAP software is a fluorescence analysis package in MATLAB (MathWorks, Inc.), which was developed for the analysis of calcium imaging data in single neuron and neuronal network (Patel et al. 2015). FluoroSNNAP can be used for simple visualization from an individual neuron, or network synchronisation analysis to indicate different patterns of activity over time.

The general workflow is outlined in Figure 4.1, and all the steps are detailed below. These include: (1) Time-lapse analysis of neurons in specified time, (2) identification of cell somata using batch segmentation, (3) automated processing to calculate a time-varying fluorescence trace for each individual neuron, (4) identification and computation of the calcium transient onset and quantification of their characteristics, and (5) network property analysis such as synchronisation (Figure 4.1).

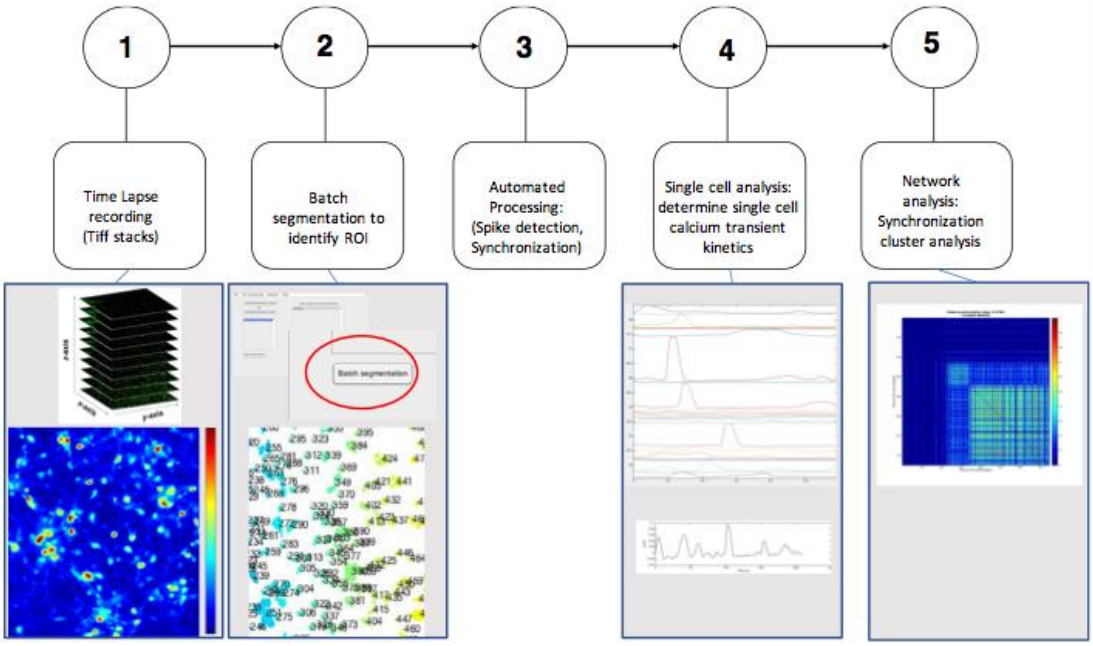

Figure 4.1. Workflow for the analysis of time-lapse calcium imaging recording. 1) Live calcium imaging was performed by acquiring stacks of images for 200-400 seconds. 2) Identifying cell bodies as the region of interests (ROI). 3) Spike detection and synchronization detection. 4) Inspecting the florescence intensity of single neurons by determining their calcium transients. 5) Properties of network cluster analysis such as neuronal synchronicity.

The first step in analysing calcium imaging video is to identify the regions of interest (ROI), which is challenging by manually drawing around large numbers of single cells. FluoroSNNAP uses an algorithm to identify sources of fluorescence variations. Throughout this Chapter, an active cell is defined as of at least 5% change in fluorescent intensity which also refer to as spontaneous calcium transient.

The active counter method is used to automatically select ROIs that delineate neurons from the background. After identifying an ROI, the second step is to detect the single neuron fluorescence event. The software computes fluorescence-versus-time trace for each ROI (=cell). $\Delta F/F$ is calculated firstly by making an average of all the pixels in the ROI to give a single time. Secondly, subtract each value by the mean of the lower 50% of previous 10 seconds values and finally, dividing it by the same value (Figure 4.2).

This software uses a previously described template matching algorithm with defined calcium transient wave forms to detect events, to identify all ranges of transients, independent of amplitudes. The software uses a correlation coefficient that

corresponds to the onset of calcium transients. We applied a threshold of 0.05 for ΔF/F amplitudes, and ΔF/F<0.05 is regarded as noise or background.

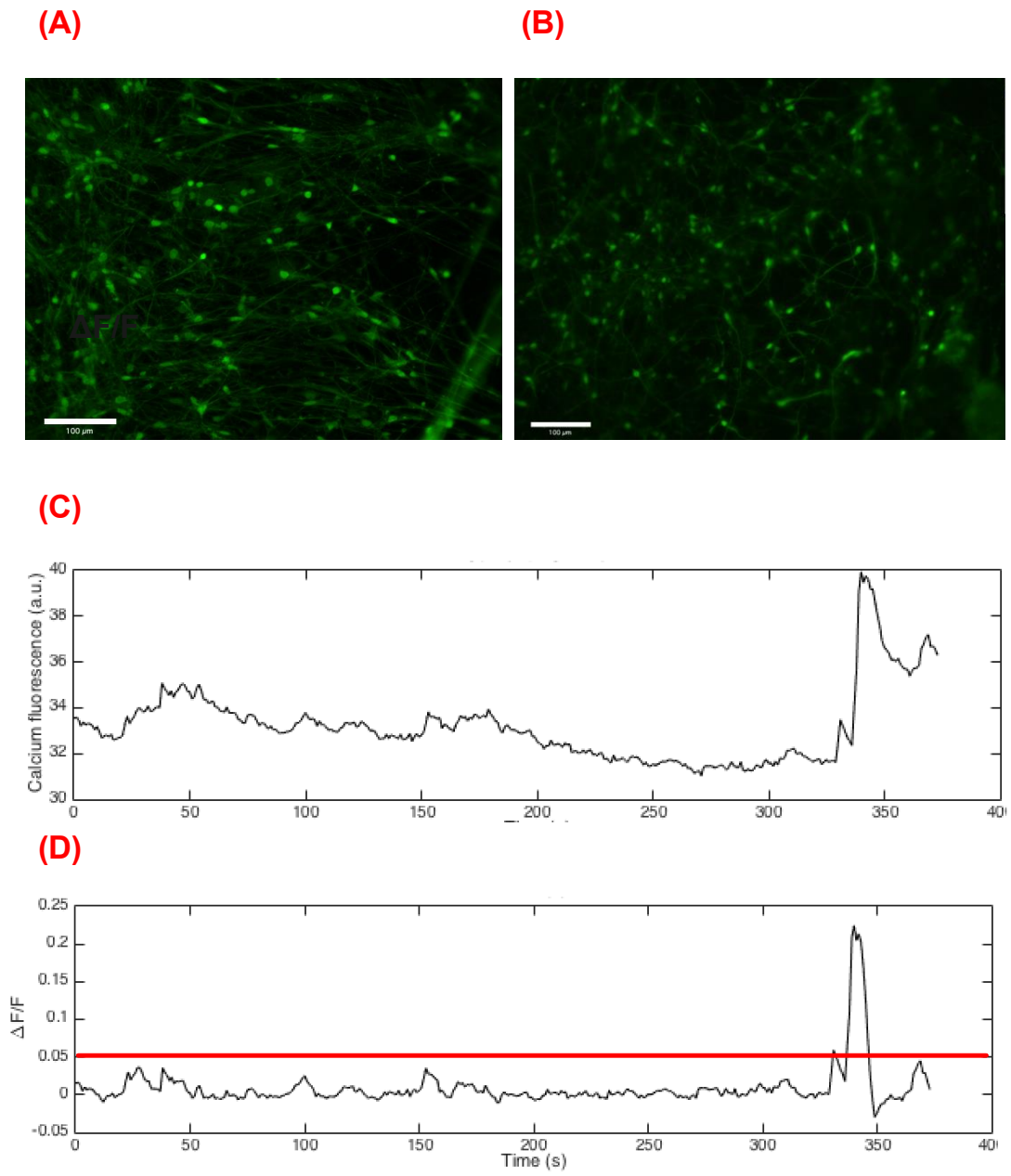

Figure 4.2. Detecting single neuron fluorescence detection. (A) Representative images of day 100 iPSC-derived neurons from control (A) and heterozygous *NRXN1α* deletion patient (B). (C) A representative trace from control. The top trace is from one ROI (neuron) where a fluorescence-versus time is shown. ΔF/F is then computed with applying a threshold of 0.05 (red line) as true calcium transient on the trace at the bottom.

We used FluoroSNNAP to measure baseline fluorescence and frequency of spontaneous and evoked calcium transients. Baseline fluorescence is an indication of free intracellular calcium concentration, which has an association with the resting

membrane potential of a neuron (Patel et al. 2015). Finally, the amplitude of spontaneous calcium transients were determined by a coding script in R-software. This software also has the capability to identify groups of neurons, which have similar patterns of activity and hence quantifying their synchronicity.

4.2.4 Statistical analysis

All data were expressed as mean ±SEM. Each data was tested for normality using Shapiro-Wilk normality test. Statistical analysis was performed using non-parametric Mann Whitney U test with a level of significance set at $p<0.05$.

4.2.5 Immunoblotting

Western blotting for protein quantification of CACNA2D1 (Santa Cruz Sc-271697) was applied as described in Chapter 2. GAPDH was used as housekeeping gene, and protein quantification was carried out using ImageJ program.

4.3. Results

4.3.1 Assessment of spontaneous calcium transients in iPSC-derived neurons

The firing pattern and frequency of neurons play a key role during cortical development. In this study, calcium transients were investigated in iPSC-derived neurons at day 50 and day 100 of differentiation. The proportion of spontaneously active cells with calcium transients grew over time. In comparison to neurons at day 50 of differentiation (Figure 4.3B, C), the day-100 iPSC-derived neuronal cultures displayed significantly higher proportion of cells with spontaneous calcium transients in both the Control group (203% up, $p< 0.006$; from Day 50 11.2±2.1%, Day 100 34.0±2.9%) and Patient cell group (253% up, $p<0.001$; Day 50 8.6±1.0%, Day 100 40.32±4.5%), showing that a substantial proportion of neurons were matured after subsequent 50 days of culture.

As the neurons further matured from day 50 to day 100 (Figure 4.3B, C), there was also a significant increase in the frequency of calcium transients per cell, which went up 65% in the Control group ($p<0.000$; Day 50 4.8±0.3 mHz, Day 100 7.9±0.3 mHz) and 112% in the Patient cell group ($p<0.0001$; Day 50 4.9±0.7 mHz, Day 100 10.4±0.6 mHz), respectively. In addition, the average amplitude of calcium transients was increased by 25.0% in the Control cells ($p<0.04$; Day 50 0.08±0.005 ΔF/F, Day 100 0.10±0.003 ΔF/F) and by 43% in the Patient-derived cells ($p<0.001$; Day 50 0.07±0.006 ΔF/F, Day 100 0.10±0.003 ΔF/F. The increases in the number, frequency and amplitude of calcium transients suggest that during the period of day 50-100, the *in vitro* culture system supports further neuronal maturation. There was no significant difference, however, between the control and patient neurons in the properties of spontaneous calcium transients at day 50 of differentiation.

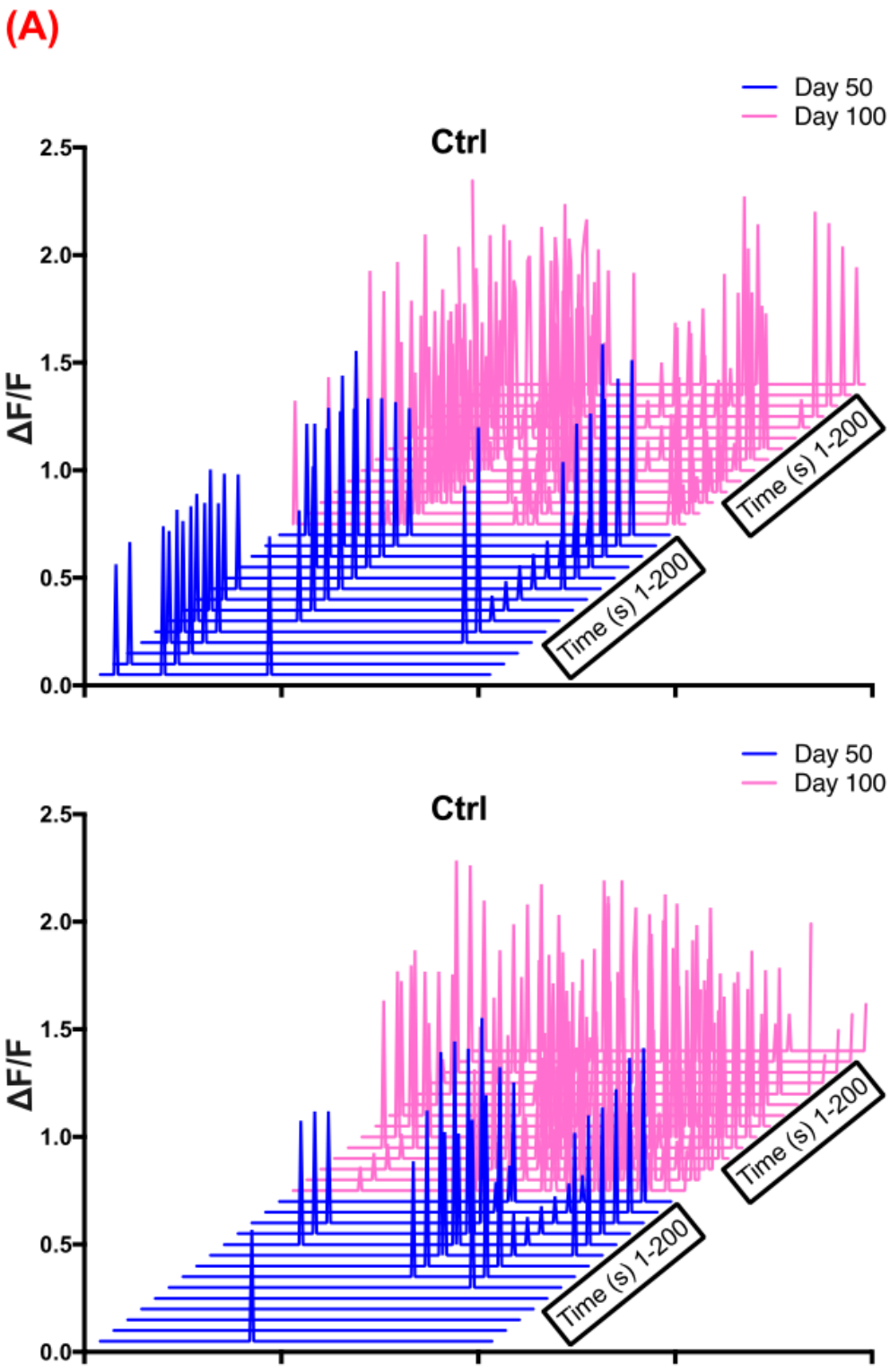
(A)
Day 50
Day 100
Ctrl
2.5
2.0
1.5
1.0
0.5
0.0
ΔF/F
Time (s) 1-200
Time (s) 1-200
Day 50
Day 100
Ctrl
2.5
2.0
1.5
1.0
0.5
0.0
ΔF/F
Time (s) 1-200
Time (s) 1-200

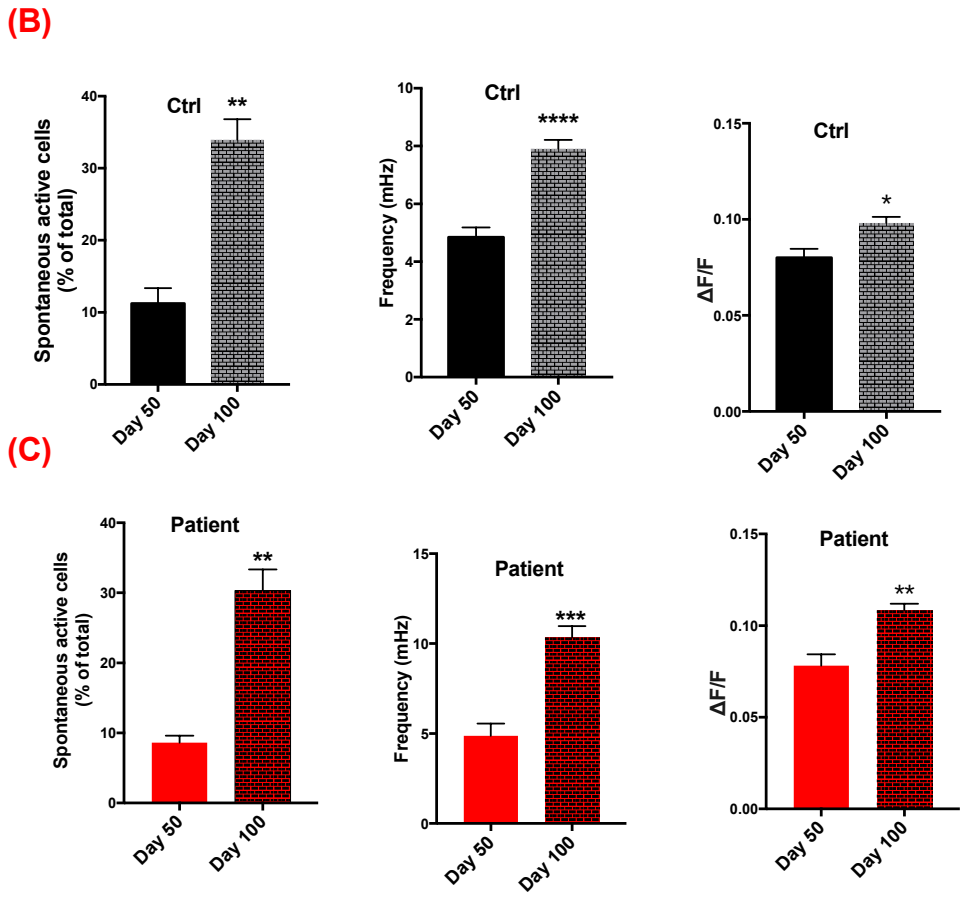

Figure 4.3. Spontaneous calcium transient properties were altered in iPSC-derived neurons during the course of day 50 to 100 differentiation. (A) Representative waterfall traces of 28 cells from day 50 and day 100 in both control and patient derived cells. Blue trace represents day 50 neurons in 200 seconds, and pink trace represents day 100 neurons in 200 seconds of recording. (B+C) Neurons exhibit a significant increase in proportion (%) of spontaneous active cells, the frequency (mHZ) and the amplitude (ΔF/F) of Ca2+ transients at day 100, in comparison to day 50 (Ctrl day 100 n=74 recordings/26 coverslips, Ctrl day 50 n= 9 recordings/3 coverslips; Patient day 100 n=35 recordings/15 coverslips, patient day 50 n=6 recordings /2 coverslips). Active cell is defined as of at least 5% change in fluorescent intensity. The data were analysed from 6 control iPSC lines and 4 ASD *NRXN1α* iPSC lines and expressed as mean ± SEM. The total numbers of ROI (cells) examined in Control were n=34,746 cells, and in Patient n=15,079 cells. Statistical significance (**p<0.01, ***p<0.001, ****p<0.0001) were evaluated using Mann Whitney U test).

The active cells with spontaneous calcium transients were defined as cells with >5% of changes in fluorescent intensity during the time course recording. To confirm that the calcium transients observed during 100-day differentiation were events associated with membrane depolarizations, 1 μM of tetrodotoxin (TTX), the voltage-gated sodium channel blocker, was applied. TTX was able to effectively abolish 88% of spontaneous calcium transients in the day 100 of iPSC-derived neuron cultures, suggesting that the

majority of the spontaneous calcium transients were mediated by the voltage-gated sodium channels through action potential.

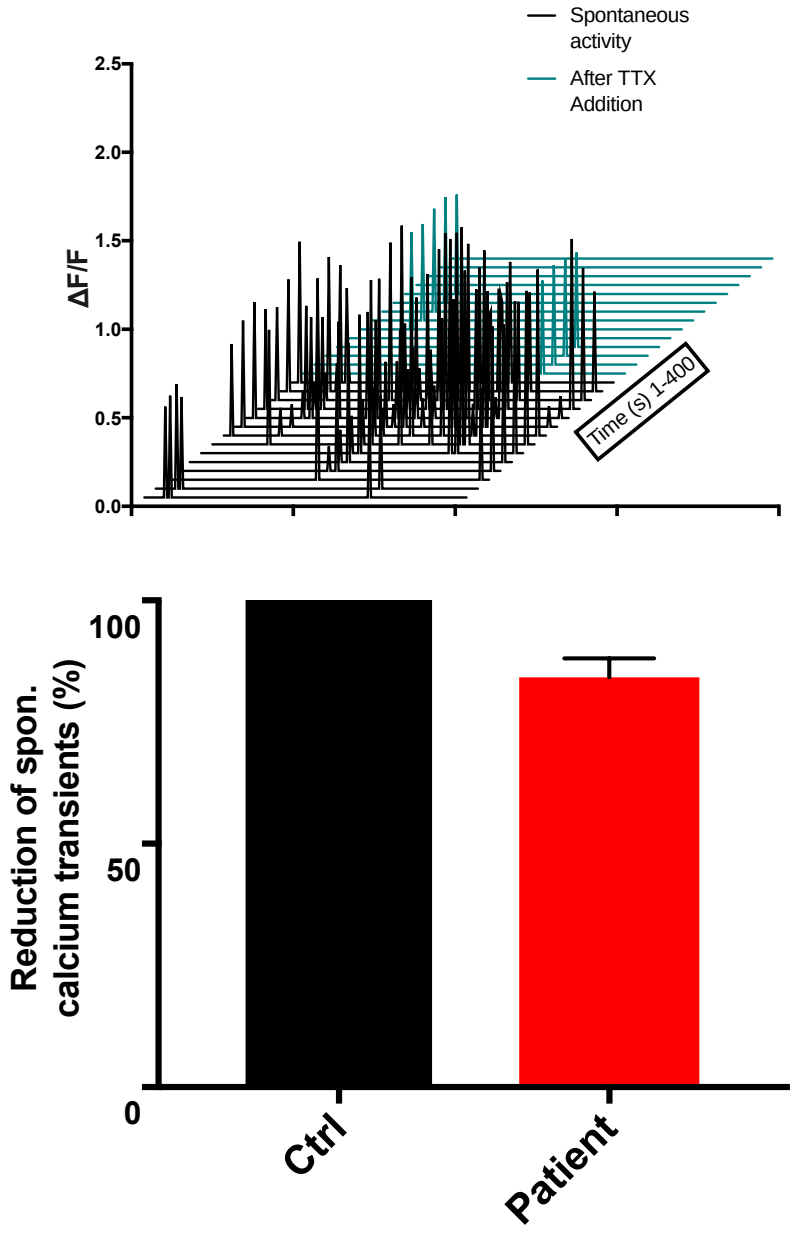

Figure 4.4. Spontaneous calcium transients are action potential dependent. (A) Representative spontaneous Ca2+ transients of 28 cells at day 100 in 400 seconds of imaging and application of 1μM TTX in 200 seconds of the recording. The average number of spontaneous Ca2+ transients was dramatically reduced after addition of TTX (Ctrl n=1 recording/1coverslip; Patient n=3 recordings/2coverslips). Active cell is defined as of at least 5% change in fluorescent intensity. The iPSC cell lines used in this experiment were Ctrl n=1 and Patient n=2). The total number of ROI (cells) examined was Control n=433 cells and Patient n=1526 cells. All data summary are presented as mean ± SEM.

4.3.2 Ca^{2+} transients are mediated primarily by voltage-gated calcium channels

Voltage-gated calcium channels (VGCC) are activated upon membrane depolarisation and facilitate the entry of calcium in response to action potentials arriving at the presynaptic membrane, and thereby initiate synaptic transmission. Having identified the role of depolarizations in driving calcium transients, we then set out to identify the calcium channels involved. To identify the channels mediating the calcium transients, we first applied the L-type calcium channel blocker, Nifedipine (50 μM), which resulted in a reduction of the number of spontaneous calcium transients in 77.80±8.2% of the control cells and in 56.60±11.9% of the Patient cells (Figure 4.5B). Additionally, the average remaining spontaneous calcium transients (Nifedipine insensitive transients) was reduced to 30.8% (with 34.80±13.0% in Control neurons and 26.80±4.2% in Patient neurons, Figure 4.5C). Control and patients' neurons appeared equally sensitive to Nifedipine ($p<0.24$), and for the remaining insensitive neurons after the Nifedipine treatment, there was no significant difference on their frequency ($p<0.92$), whereas the amplitude of the remaining calcium transients was slightly reduced (control cells 6.5%; patient cells 1.8%), although there was no significant difference between control and patient cells ($p<0.45$, Figure 4.5D).

To confirm the positive expression of VGCCs at the protein level in 100-day neurons, the quantitative expression of the gene encoding a common subunit of VGCCs, CACNA2D1, was measured using immunoblotting (Figure 4.5E). All different lines of neurons were positive for CACNA2D1 protein expression, but there was no significant difference in the amount of CACNA2D1 protein expression between the control and patient cell groups ($p<0.21$).

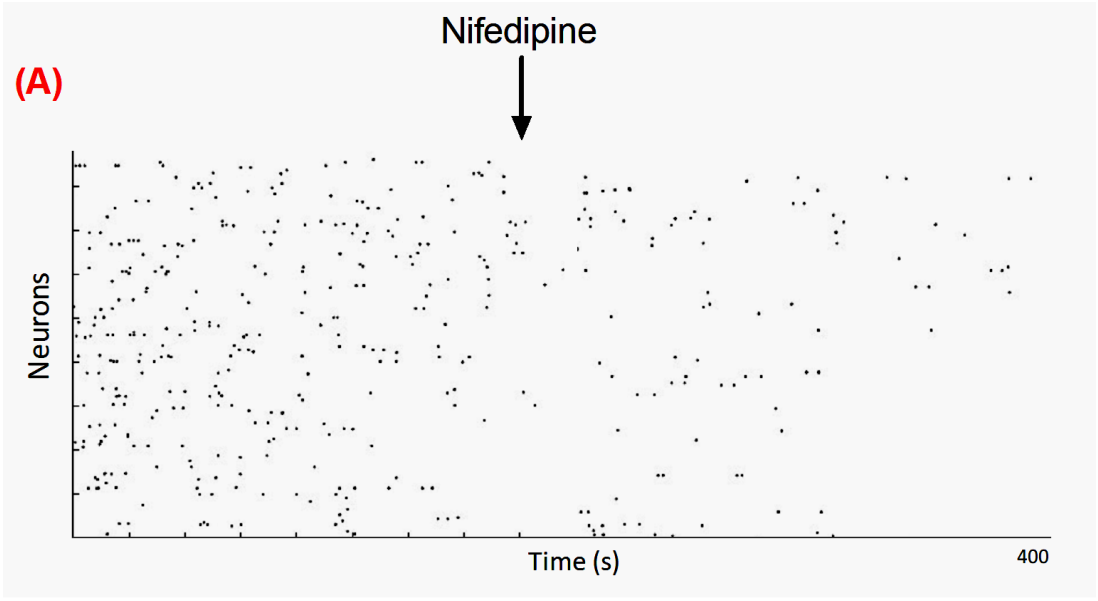
(A)
Nifedipine
Neurons
Time (s)
400

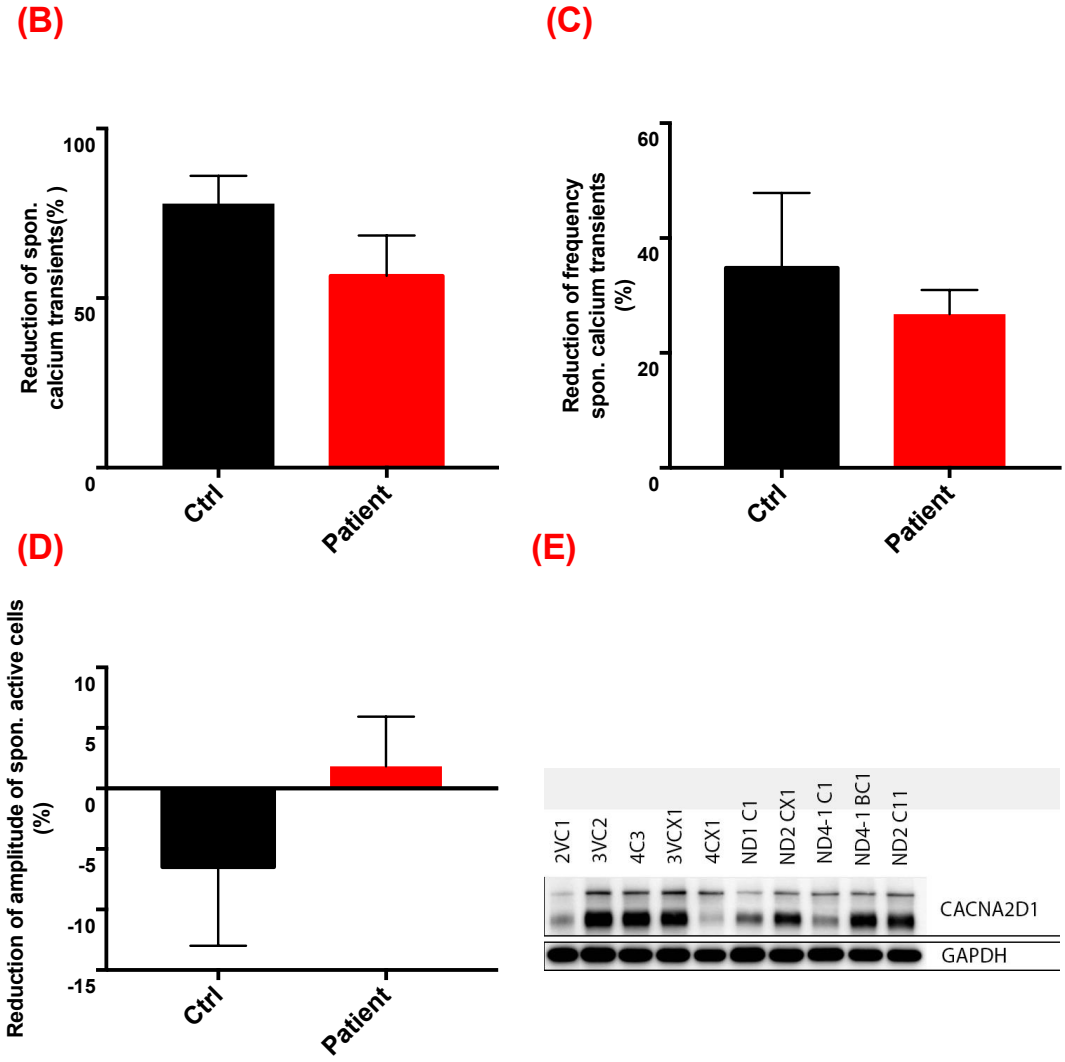
(B)
(C)
Reduction of spon. calcium transients(%)
100
50
0
Ctrl
Patient
Reduction of frequency spon. calcium transients (%)
60
40
20
0
Ctrl
Patient
(D)
(E)
Reduction of amplitude of spon. active cells (%)
10
5
0
-5
-10
-15
Ctrl
Patient
2VC1
3VC2
4C3
3VCX1
4CX1
ND1 C1
ND2 CX1
ND4-1 C1
ND4-1 BC1
ND2 C11
CACNA2D1
GAPDH

Figure 4.5. Ca2+ transients are partially mediated by the L-type VGCCs in 100-day neurons. (A) Representative trace of calcium transient from a control line. This raster plot represents the activity of each cells by showing each calcium transient as a "dot" in 400 second of recording on the x-axis, with the application of 50 μM Nifedipine at 200 seconds (black arrow). (B) Ca2+ transients were blocked partially by application of Nifedipine (Control n=12 recordings/7 coverslips; Patient n=11 recordings /5 coverslips). The IPSC lines used in this experiment was Ctrl n=3 and Patient n=3. The total number of ROI (cells) examined in Ctrl n=4883 cells and Patient n=5437 cells. (C) The remaining active cells showed reduced frequency after application of Nifedipine, while their amplitude slightly reduced (D). (E) Quantification of CACNA2D1 protein levels (MW:152KDa) in control and *NRXN1α* iPSC-derived neurons showed no significant difference (normalized to 37 KDa GAPDH). All data summary are mean ± SEM.

We subsequently investigated the potential involvement of P/Q voltage-gated calcium channels in a few cell lines (Figure 4.6A). The specific P/Q channel blocker, Agatoxin (500 nM), resulted in a large reduction of 73% (Controls 84.0%±3.1; Patients 62.0%±17.1) in the number of spontaneous calcium transients with no significant difference observed between the controls and *NRXN1α* deletion neurons ($p<0.12$, Figure 4.6B). A reduction was also observed in the frequency of the remaining Ca^{2+} transients (controls 20.5%±8.3; patients 11.4%±2.7, $P<0.2$), again with no difference between control and patient cell groups (Figure 4.6C).

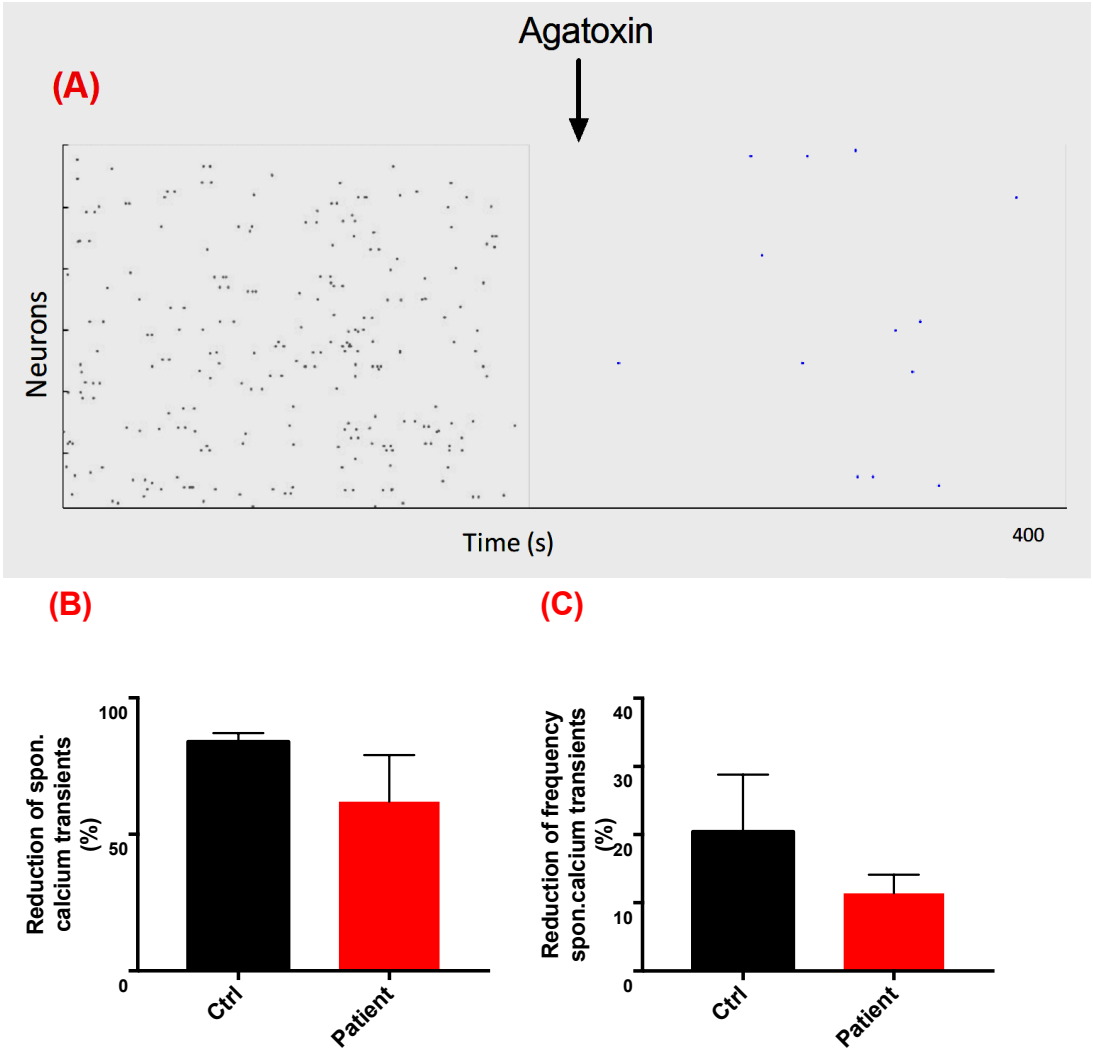

Figure 4.6. Calcium transients are also mediated by P/Q VGCC in 100-day neurons. (A) Representative trace of spontaneous calcium transients from a control line. This raster plot represents the activity of each cells by showing each spontaneous calcium transient as a "dot" in 400 second of recording on the x-axis with the application of 500 nM agatoxin at 200 seconds (black arrow). (B) Ca2+ transients were blocked partially by application of 500 nM agatoxin (Control n=10 recordings/5 coverslips; patient 2 recordings/1 coverslips. (Ctrl n=2 and Patient n=1 for iPSC lines. The total number of ROI (cells) examined was in Ctrl n=4,074 and Patient n=1,181 cells. (C) The remaining active cells showed reduced frequency. Numbers in brackets/bar represent the number of recording/number of coverslips. All data summary are mean ± SEM.

4.3.3 Ca^{2+} transients are synaptically coupled to excitatory neurons

To examine whether the observed calcium transients are associated with excitatory synaptic transmission, we applied NMDA (DL-AP5, 50 μM) and AMPA/Kainate (CNQX, 50 μM) type glutamate receptor antagonists to the day 100 cultures. The AMPA/Kainate receptor antagonist CNQX attenuated the calcium transient activity by 66.8% ($p<0.33$; Control 52.6±14.3%; Patient 81.1±9.4%) (Figure 4.7E). In a similar manner, the NMDA receptor blocker DL-AP5 abolished calcium transient activity by 97.8% (Figure 4.7E). These data strongly suggest that the calcium transients in the iPSC-derived neurons are driven by glutamatergic synaptic transmission.

CNQX specifically blocks AMPA type glutamate receptor GRIA1, and DL-AP5 blocks NMDA type glutamate receptors GRIN1 and GRIN2A. Quantitative analysis using the whole genome RNA sequencing showed that not only the expression of these subtypes of glutamatergic receptors, but also other ionotropic and metabotropic glutamate receptors were highly expressed in the day-100 cultures (Figure 4.7D).

To further evaluate whether the excitatory synapses was driven calcium transient activity, we applied 60 mM glutamate to the culture and observed 87.2% increase in percentage of active cells with transient activity (Control 82.3±7.2%; Patient 92.0±1.3%) with no significant difference between controls and patient on the response ($p<0.43$) (Figure 4.7A). On the other hand, addition of 60 mM GABA showed only a 2.3% increase change in transient activity (Figure 4.7A). In consistent with this, the mRNA encoding the GABAergic receptors (*GABRA1*, *GABRA6*, *GABRD*, *GABRE*, *GABRG3*, *GABRP*, *GABRR1* and *GABRR2*) was detected in the iPSC-derived cortical cultures. However, their abundance was extremely low (Figure 4.7D). These data together demonstrated that the majority of the cells in the iPSC-derived neurons are excitatory cortical neurons.

Large concentrations of KCl (60 mM) are known to evoke presynaptic depolarization, and the compound ionomycin can rapidly raise intracellular Ca^{2+} concentration in excitable cells by increasing transport of Ca^{2+} across the plasma membrane and by transport of Ca^{2+} from the intracellular store into the cytosol. When we challenged the

day 100 cultures with 60mM KCl, 95.5% of cells were shown to be highly responsive ($p<0.30$; Control 82.3±7.2%, Patient 91.9±1.3%). When 20 µM of ionomycin was applied to the solution, 98.6% of cells displayed Ca^{2+} flux (Figure 4.7F). These data further confirmed the functionality of the neurons in the day 100 cultures.

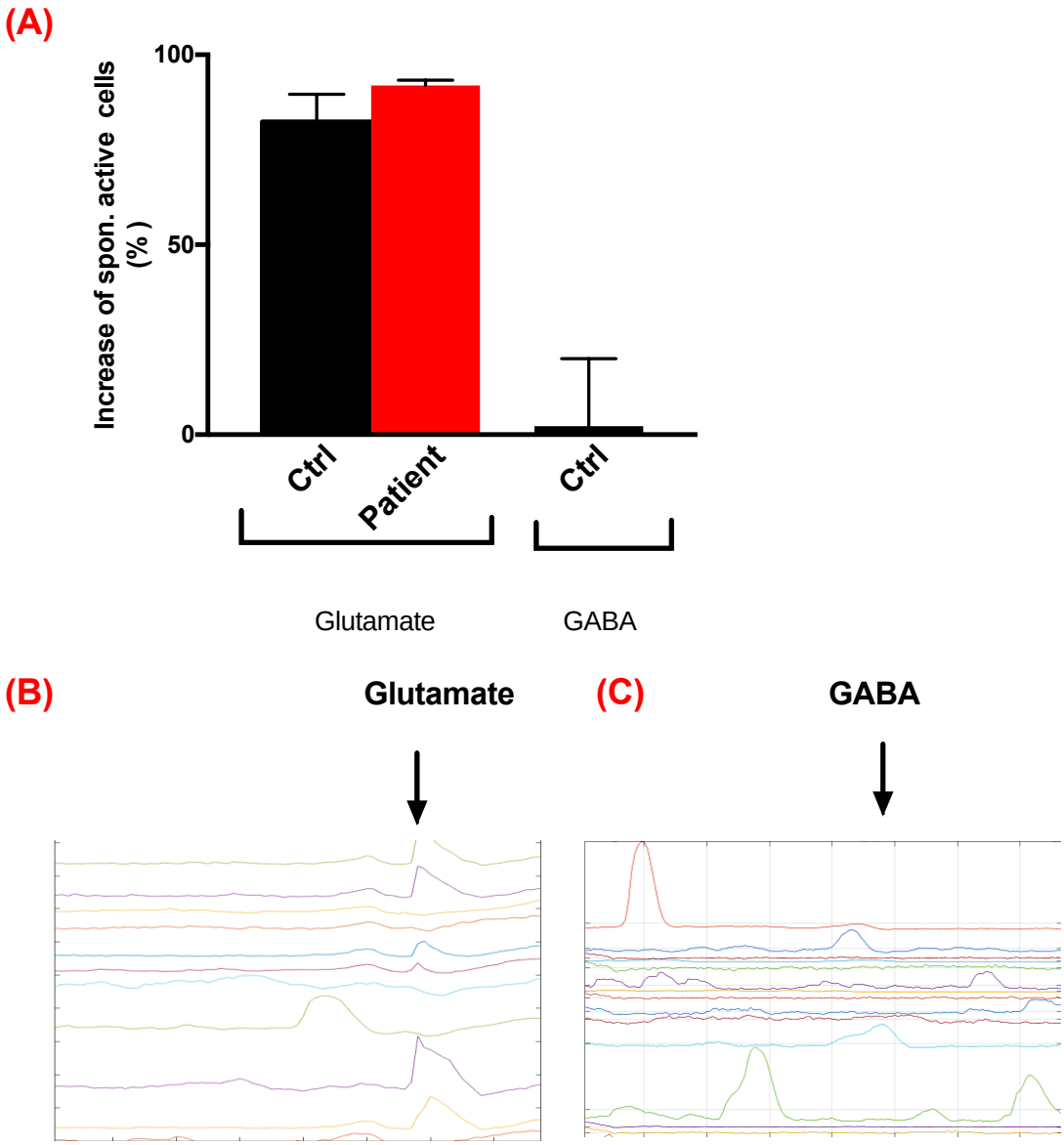

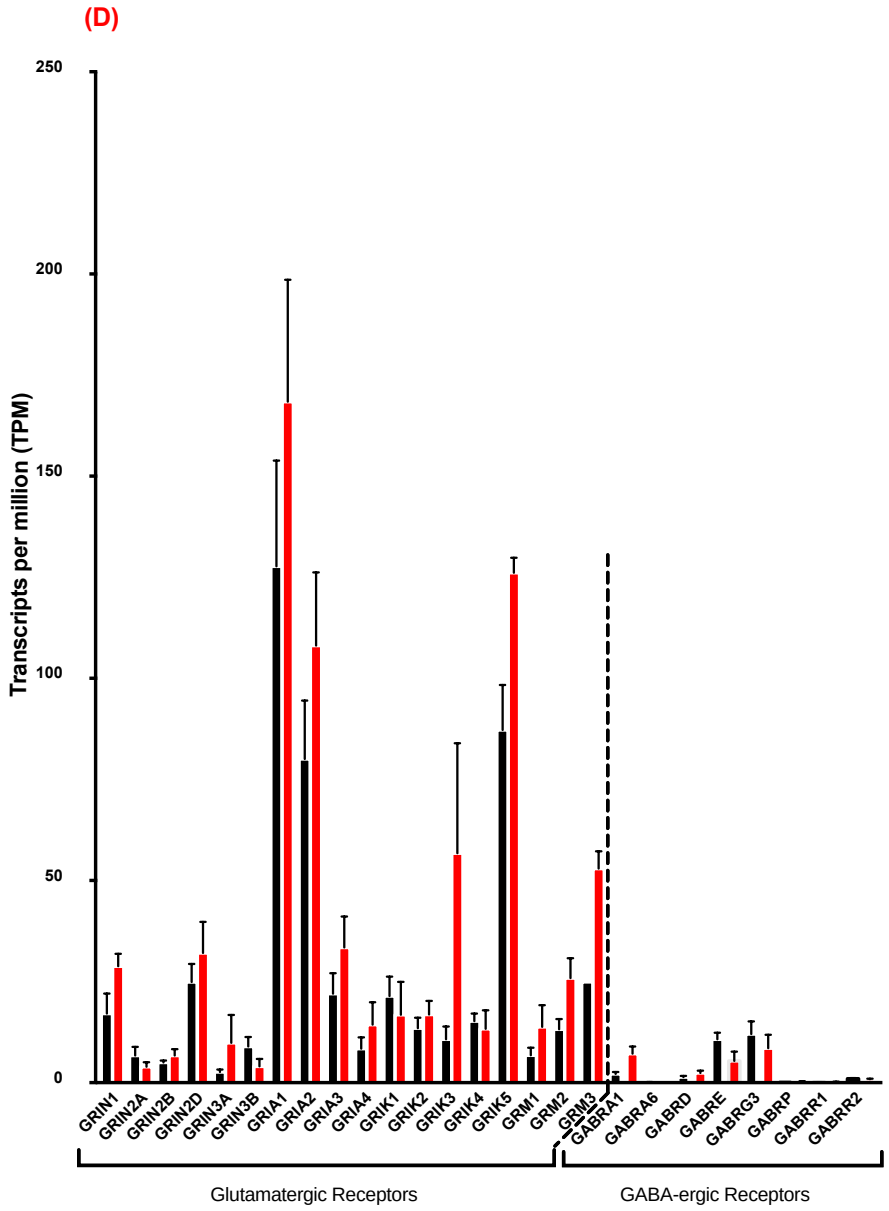
(D)
Transcripts per million (TPM)
250
200
150
100
50
0
GRIN1
GRIN2A
GRIN2B
GRIN2D
GRIN3A
GRIN3B
GRIA1
GRIA2
GRIA3
GRIA4
GRIK1
GRIK2
GRIK3
GRIK4
GRIK5
GRM1
GRM2
GRM3
GABRA1
GABRA6
GABRD
GABRE
GABRG3
GABRP
GABRR1
GABRR2
Glutamatergic Receptors
GABA-ergic Receptors

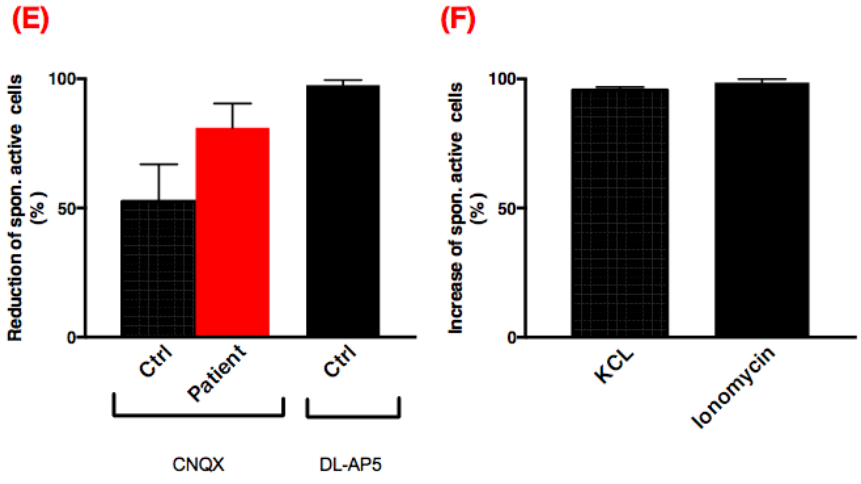
(E)
Reduction of spon. active cells (%)
100
50
0
Ctrl
Patient
Ctrl
CNQX
DL-AP5

(F)
Increase of spon. active cells (%)
100
50
0
KCL
Ionomycin

Figure 4.7. iPSC-derived neurons are coupled to glutamatergic neurons with a positive response to pharmacological reagents. (A) Cells responded with an increase in spontaneous calcium transient activity after addition of 60 mM glutamate (Control n=6 recordings/6 coverslips; Patient n=4 recordings/4 coverslips) but displayed no significant increase of activity in response to 60 mM GABA (Control n=2 recordings/2 coverslips. (Ctrl n=4; Patient n=3 for iPSC lines); (Total number of ROI (cells) examined in Ctrl n=2170; Patient n=1946). (B) Representative trace of cells responding to glutamate or GABA (C). (D) Quantitative RNA transcriptome analyses demonstrated abundant expression of GRIN1, GRAI1, GRIN2A as well as other ionotropic and metabotropic glutamate receptors, but low expression of GABAergic receptors (Ctrl n=6; Patient n=4 iPSC lines). (E) The average number of spontaneous calcium transients decreased in the presence of glutamate receptor blocker AMPA/kainate-type (CNQX) and NMDA type blocker (DL-AP5) (Ctrl iPSC lines n=2; Patient iPSC lines n=1, Control n=4 recordings/4coverslips; patient 2 recordings/2 coverslips); (Total number of ROI (cells) examined in Ctrl n=1,127; Patient n=508). (F) Functional neurons responded positively to 20 μM ionomycin (Control n=2 recordings/2 coverslips) with increasing intracellular level of Ca^{2+} and positively to high extracellular 60 mM KCL (Control n=4 recordings /3 coverslips; patient n=2 recordings /2 coverslips); (Ctrl iPSC lines n=2; Patient iPSC lines n=2) (Total number of ROI (cells) examined in Ctrl n=1746; Patient n=598). All data summary are mean ± SEM.

4.3.4 Heterozygous *NRXN1α* deletion increases the frequency of spontaneous calcium transients in iPSC-derived cortical neurons

Normal functioning of the brain requires synchronous network activity comprised of large-scale action potential firing and calcium transients, which partly regulate the balance of neuronal excitation and inhibition. The characteristics of these calcium transients play an important role in neurotransmitter release. To determine the effects of *NRXN1α* gene deletion on spontaneous fluctuations of calcium transients in iPSC-derived cortical neurons, we analysed spontaneous calcium transients during a 3~5-minute interval and compared 34,746 control neurons with 15,079 patient-derived neurons which displayed spontaneous calcium transients over our indicated threshold (5%). The average calcium transients recorded in each recording period was 463 to 419 cells in control and patient cell lines, respectively.

The characteristics of spontaneous calcium transients were evaluated in 6 control iPSC lines (Figure 4.8A) and 4 ASD patient iPSC lines (Figure 4.8B). Interestingly, the frequency of calcium transients was significantly increased by 30.8% in the *NRXN1α* deletion neurons ($p<0.0004$; Control 7.9±0.3 mHz; Patient 10.4±0.6 mHz, Figure 4.8C). We next measured the duration of the calcium transients, from where the transient crossed the 5% threshold level to the peak and back to 5% threshold. The

duration of the calcium transients was significantly longer in the *NRXN1α* deletion neurons ($p<0.0004$; Control 6.30±0.2 s; Patient 7.70±0.3 s, Figure 4.8D). Furthermore, the amplitude of calcium transients also significantly increased in *NRXN1α* deletion neurons (Control 0.098±0.003 ΔF/F; Patient 0.108±0.004 ΔF/F, $p<0.006$) (Figure 4.8E). While the calcium transient properties significantly differed in the *NRXN1α* deletion neurons, however, the number of spontaneous active cells remained unchanged ($p<0.2$; Control 34.0±2.8%; Patient 40.32%±4.5%, Figure 4.8F).

Alterations in calcium transient properties suggest an impaired neuronal function, increased the abundance of VGCCs and the influx of calcium upon neuronal depolarization. The function and abundance of L type and P/Q type voltage-gated calcium channels were examined in the previous section and are further discussed in Chapter 5 in connection with the transcriptome changes.

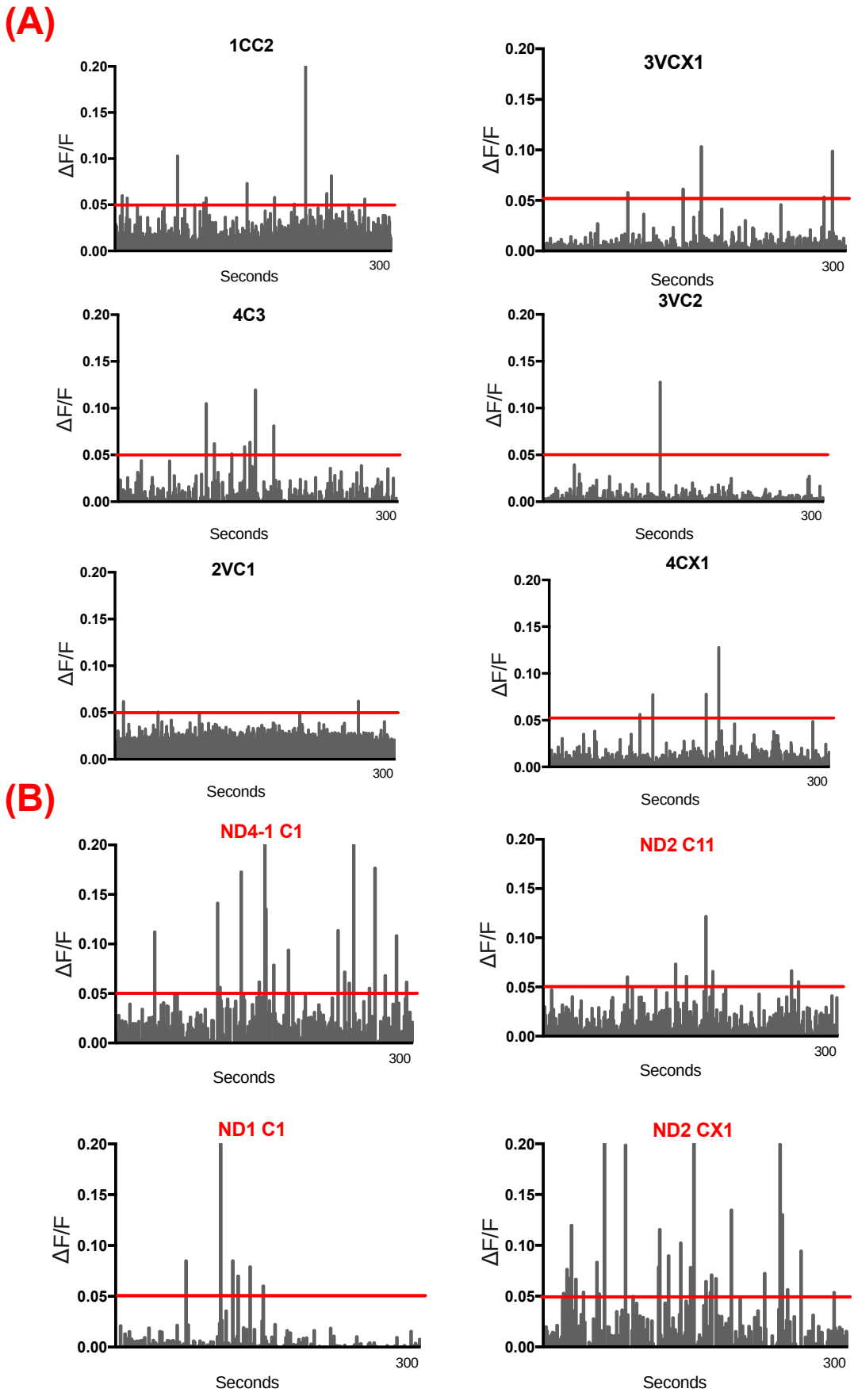
(A)
1CC2
3VCX1
4C3
3VC2
2VC1
4CX1
(B)
ND4-1 C1
ND2 C11
ND1 C1
ND2 CX1
ΔF/F
0.20
0.15
0.10
0.05
0.00
300
Seconds

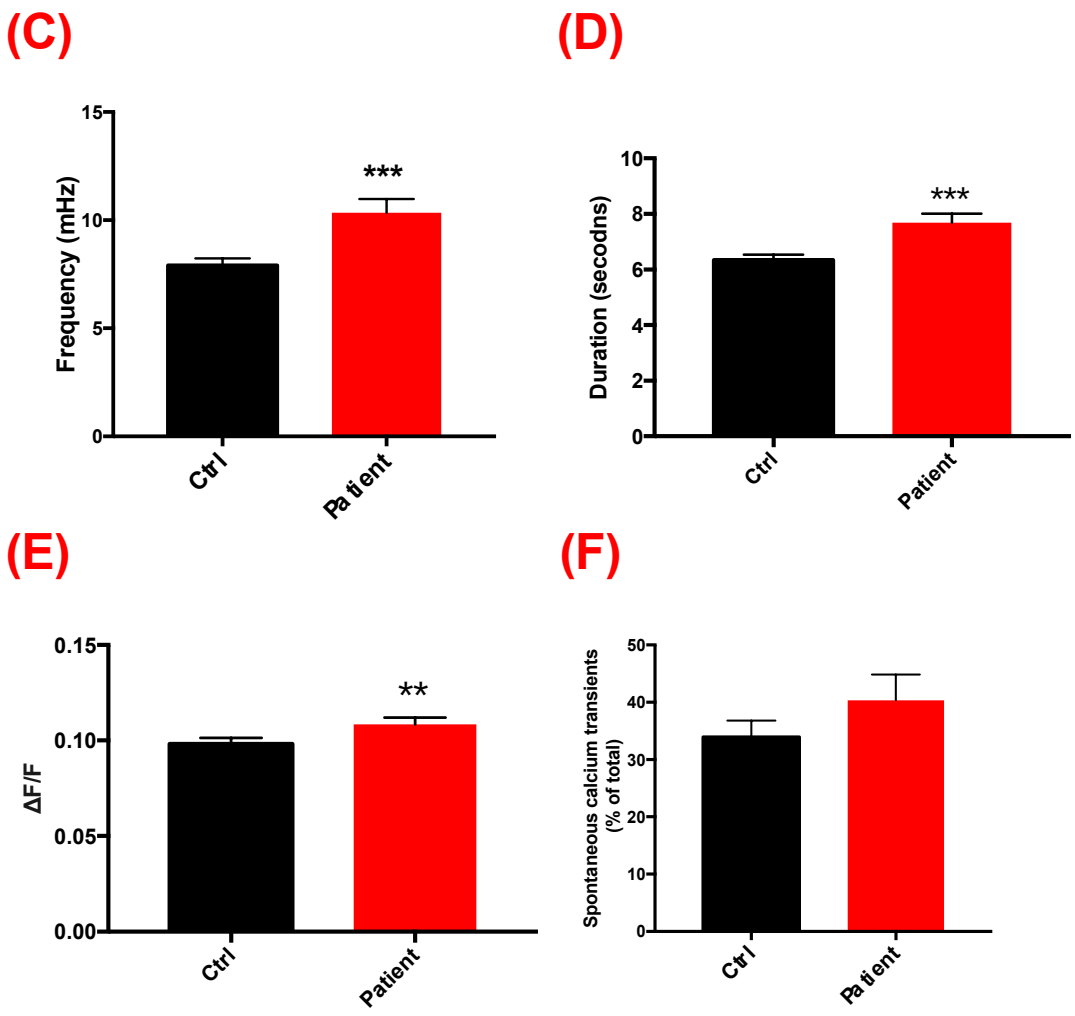

Figure 4.8. Spontaneous calcium transient properties were significantly altered in the day 100 neurons derived from ASD NRXN1α deletion patients. (A) Representative traces of Fluo-4 spontaneous Ca^{2+} transients from one individual neuron for each control (A) and (B) patient iPSC lines. The red line indicated the threshold level of 5% fluorescence intensity. (C) The frequency of spontaneous Ca^{2+} transients was significantly increased in the *NRXN1α* deletion patient cells. (D) The duration of calcium transients was significantly longer in the *NRXN1α* deletion patient cells. (E) The amplitude of spontaneous Ca^{2+} transient was significantly increased in the *NRXN1α* deletion patient cells and the percentage of spontaneous Ca^{2+} transients remained unchanged between two groups (F). (Control n=74 recording /26 coverslips, Patient n=35 recording /15 coverslips). Ctrl n=6 iPSC lines; Patient n=4 iPSC lines. The total number of ROI (cells) examined in Ctrl n=34746; Patient n=15079. Statistical significance (**p<0.01, ***p<0.001, ****p<0.0001) were evaluated using Mann Whitney U test). All data summary are mean ± SEM.

While the exact Ca^{2+} concentration inside the cell cannot be calculated by using Fluo-4AM dye, the relative fluorescence intensity can be taken as an indicator of calcium abundance inside the cell (Patel et al. 2015). The intracellular calcium abundance of each individual neuron can be quantified by the average fluorescence trace at 2

seconds before and 10 seconds after the onset of all calcium transients (Patel et al. 2015). This baseline fluorescence intensity showed no significant difference between control and the *NRXN1α* deletion neurons ($p<0.40$; Control 55.9±3.8, Patient 52.4±2.6, Figure 4.9).

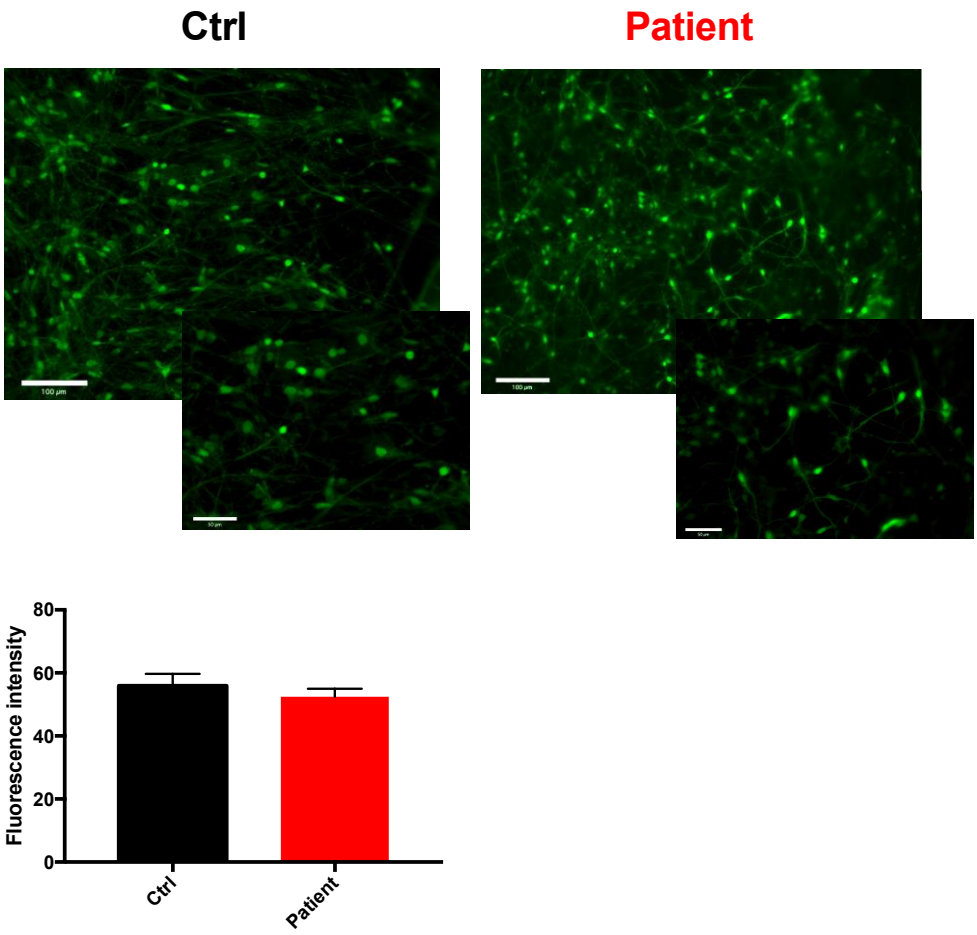

Figure 4.9. The fluorescence intensity remained unchanged in the NRXN1α deletion neurons. The representative images of both control and patient cells loaded with fluo-4AM, displaying a dense network of neurons in day 100 neuronal cultures. The baseline intracellular Ca^{2+} concentration remained unchanged in *NRXN1α* deletion patients. The data were based on Control n=74 recordings from 26 coverslips, Patient n=35 recordings from 15 coverslips; The Control n=6 and Patient n=4 iPSC lines. The total number of ROI (cells) examined in Ctrl n=34,746; Patient n=15,079. All data summary are mean ± SEM.

4.3.5 Synchronicity of neurons remained unchanged in *NRXN1α* deletion

During development, a large scale of cortical neurons develops synchronised activity patterns, which results from bursts of action potentials and associated calcium events. To determine the network activity patterns of in 100-day iPSC-derived neurons, we used FluoroSNNAP to generate a synchronisation index, which indicates the level of synchronicity, with a FluoroSNNAP score of 1 being the most synchronised network and 0 being the least. The iPSC-derived neurons in this study showed a very low level (2.8%) of synchronicity in our cultures (Figure 4.10A). On the other hand, asynchronous activity was observed in 97.2% of the recordings from both the control and patient groups (Figure 4.10B). The level of neuronal synchronisation *in vitro* appeared not affected by heterozygous *NRXN1α* deletion ($p<0.51$; Control 0.15±0.04%; Patient 0.10±0.03%, Figure 4.5B).

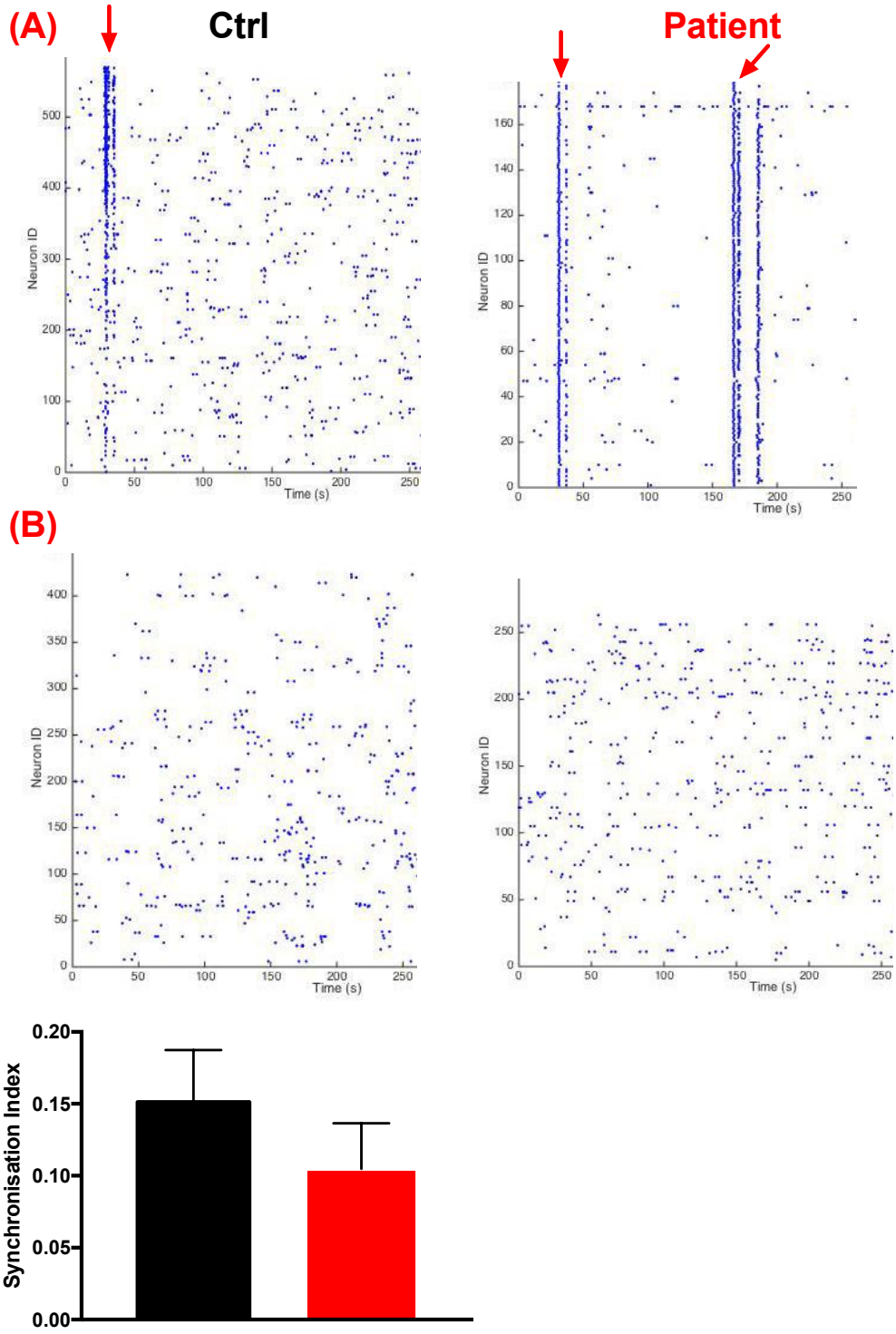

Figure 4.10. Synchronous and asynchronous Ca^{2+} transient activity of iPSC-derived neurons. (A) Representative raster plots showed the spontaneous Ca2+ transient activity of the cells. The synchronized activity (the red arrow) was only observed in a limited number of recordings. The raster plot showed the duration of recording in seconds (x-axis) versus a number of active neurons (on Y-axis). Each dot shows the presence of calcium transient activity. (B) Representative raster calcium plot is showing asynchronous firing on day 100 of iPSC-derived neurons from control and patient cells. There is no significant difference in iPSC-derived neurons between control and *NRXN1α* deletion patient cells. The data were analysed from Control n=74

recordings from26 coverslips, and Patient n=35 recordings from 15 coverslips. The iPSC lines used were Ctrl n=6 and Patient n=4. The total number of ROI (cells) examined in Ctrl n=34,746; Patient n=15,079. All data summary are mean ± SEM.

4.4 Discussion

Neurexin1α was first discovered as a receptor for a component called α-latrotoxin from the black widow spider venom which resulted in massive stimulation of neurotransmitter release in a calcium-dependent manner (Ushkaryov et al. 1992; Geppert et al. 1998). Südhof and colleagues, later on, discovered that neurexins couple voltage-gated calcium channels to the release machinery and vesicle exocytosis in presynaptic terminus (Missler et al. 2003).

Neuronal excitability can directly cause calcium influx and a change in calcium transient activity in presynaptic terminals. The literature reports show that high-frequency spontaneous calcium transients are observed in developing and postnatal cortical neurons (Yuste et al. 1992; Mao et al. 2001). Calcium transients are the main regulatory element of synaptic transmission. The arrival of an action potential at the axon terminus triggers calcium influx through VGCCs, which results in neurotransmitter release. Calcium transients are an essential part of brain development and maturation of functional synapses (Rosenberg and Spitzer 2011).

Moreover, the frequency of calcium transients is shown to regulate the neurite extension during nervous system development (Gu and Spitzer 1995). By using an appropriate florescent dye, Fluo4-AM in this study, we analysed the cellular Ca^{2+} spontaneous activity in iPSC-derived 100-day neurons. Unexpectedly, our results showed that *NRXN1α* deletion altered the Ca^{2+} signalling in the day 100 neurons derived from ASD patients.

The culture system we have used in this study supports *in vitro* maturation of iPSC derived neurons. Spontaneous calcium transients were observed as early as day 50 of iPSC neuronal differentiation, although the control and patient-derived neurons displayed no significant difference in Ca^{2+} dynamics at this time point. As the neurons matured, the proportion of cells presenting with spontaneous calcium transients increased, and the frequency of Ca^{2+} transients increased in cultures. The timing and frequency of calcium transients play an essential role in driving neuronal

differentiation (Rosenberg and Spitzer 2011; Prè et al. 2014). However, we have observed no significant difference in terms of neural progenitor proliferation at day 20, or early neuronal differentiation at day 30 (Chapter 2), or Ca^{2+} transients at day 50 in this Chapter, suggesting the *NRXN1α* dosage does not play a major role in early neurogenesis.

At 100 days of neuronal differentiation, the percentage of active cells with spontaneous calcium transients was increased by 203% in control and 253% in patients in comparison to day 50 neurons. These changes were accompanied by an increased frequency of spontaneous calcium transients, by 65% and 112% in control and patient iPSC derived neurons. Furthermore, the average amplitude of Ca^{2+} transients was also increased by 25% and 43% in control and patient neurons, respectively. These observations agree with other previous work in iPSC-derived human neurons (Prè et al. 2014) that spontaneous calcium transients with various frequency are present in iPSC-derived cortical neurons, and that individual cortical neurons acquire mature calcium transient properties over several weeks/months *in vitro* differentiation (Prè et al. 2014). Additionally, asynchronous activity in 100 days iPSC-derived neurons in this study are similar to day-108 iPSC-derived cortical neurons in Kirwan *et al.* study (Kirwan et al. 2015). However, there were no significant alterations between the control and ASD patient cell groups, during the maturation process. These data together further confirmed that the maturity of human iPSC-derived neurons required months in culture. However, human neurons also require a lengthy time of development *in vivo*, considering major network development in the first 2 years of the postnatal period after 40 weeks of pregnancy, when clinical symptoms of ASD start to appear.

To explore the *NRXN1α* dosage in the functionality of neurons, we investigated Ca^{2+} dynamics in this study. We applied VGSCs blocker with TTX, which resulted in a reduction of 88% in calcium transients, and this supported that calcium transients were due to action potential arrival at the presynaptic terminal, and Na^{+} channels were essential to drive calcium transients in our cultures.

VGCCs are the primary signal transducer of electrical excitability in neurons facilitating calcium entry, and in a study by Dolmetsch *et al.*, they observed that the

L-type VGCCs was the most abundant VGCCs in cortical neurons (Dolmetsch et al. 2001). We showed that 50 μM Nifedipine, L-type VGCC blocker, reduced calcium transients by 67.30% in controls and 62.02% in patient cell lines. Approximately 30.8% (34.8% in Control; 26.8% in Patient) of calcium transients remained as Nifedipine-insensitive. However, they did not show a significant difference in the 100-day neurons between two groups. The quantitative protein expression of L-type VGCCs investigated using CACNA2D1 antibody also revealed no apparent difference in *NRXN1α* deletion neurons, however, immunoblotting was known to be a less sensitive method, and variation of CACNA2D1 expression existed between lines. This suggests that L-type VGCCs play a part in the impairment in Ca^{2+} transients of *NRXN1α* deletion neurons.

We next investigated the P/Q type VGCCs in 2 control and one patient lines. Application of 500 nM of agatoxin, a P/Q type VGCC blocker, reduced calcium transients by 84.03% and 61.96% in control and patient neurons, respectively. Again, there was no significant difference between the control and *NRXN1α* deletion neurons. However, the effect of P/Q VGCCs was examined in limited samples, and samples need to be increased for validation. Current data suggest that both L-type and P/Q types of VGCCs are present in day 100 neurons, and they both can contribute to the altered calcium transients in the *NRXN1α* deletion neurons.

While these results show the contribution of VGCCs in spontaneous calcium transient activity, a question rises that whether Nifedipine and agatoxin have dual actions on VGCCs. However, we shall rule out this possibility as both Nifedipine and agatoxin selectively abolish the L-type and the P/Q type channels respectively. It shall be noted that P/Q type VGCCs are predominantly expressed in presynaptic termini, while L-type VGCCs are located in the cell body. This shows that the location of these VGCCs are distinctive in neurons and therefore the effect of channel blockers are non-relevant to each other. Furthermore, the function of these channels is different from each other. The P/Q type VGCCs are responsible for neurotransmitter release while L-type VGCCs have an essential function in the modulation of intercellular calcium homeostasis (Qian and Noebels 2001; Davare and Hell 2003). Double immunocytochemical staining with antibodies against both classes of the VGCCs may validate this point in a future study.

The protocol we used was aimed for differentiation of enriched excitatory cortical neurons. To demonstrate if the spontaneous calcium activity was dependent on functional excitatory synapses, we tested NMDA and AMPA/kainate glutamate receptor antagonists which blocked spontaneous calcium transients by 98.30% and 61.20% respectively. This was further validated by 87.80% of cells responded to glutamate with increased spontaneous calcium transient activity. These results suggested that the majority of the population of cells in this culture system were glutamatergic and that the calcium transients were driven by glutamatergic synaptic activity. The transcriptome analyses indeed showed high levels of expression of a series of NMDA type (*GRIN1*, *GRIN2A*, *GRIN2B*, *GRIN2C*, *GRIN2D*, *GRIN3A*, *GRIN3B*), AMPA type (*GRIA1*, *GRIA2*, *GRIA3*, *GRIA4*) and Kainate type (GRIK1, *GRIK2*, *GRIK3*, *GRIK4*, *GRIK5*), ionotropic and metabotropic (*GRM1*, *GRM2*, *GRM3*, *GRM4*, *GRM5*, *GRM6*, *GRM7*, *GRM8*) glutamate receptors in the iPSC-derived neurons.

The presence of GABAergic receptors in iPSC-derived cortical cultures has been reported to be essential for normal synaptic function (Kirwan et al. 2015). However, in this study, whereas a very low level of GABAergic receptors (*GABRA1*, *GABRA6*, *GABRD*, *GABRE*, *GABRG3*, *GABRP*, *GABRR1*, *GABRR2*) was detected, application of GABA only resulted in a neglectable change (approx. 2.3%) of calcium transient activity. This means that GABAergic neurons were not the major cell population in the cultures and did not contribute much to the network oscillation in this iPSC-derived neuronal network and was consistent with the excitatory cortical differentiation protocol we have used.

After evaluating the characteristics of calcium transients at two different developmental stages, we next compared the important properties of spontaneous Ca^{2+} activity between the control and *NRXN1α* deletion 100-day neurons. At day 50 of neuronal differentiation, there was no major difference in terms of spontaneous Ca^{2+} transient activity. The frequency of calcium transient activity was significantly increased in *NRXN1α* deletion neurons (control 7.9 mHz; patient 10.4 mHz, $p<0.0004$, Figure 4.8C). The amplitudes of these calcium transients were also significantly altered and increased in *NRXN1α* deletion neurons (Control 0.098±0.003 ΔF/F; Patient 0.108±0.004 ΔF/F, Figure 4.8E). The difference was also observed in the

duration of calcium transients with a significant increase in *NRXN1α* deletion neurons (Control 6.1 s; patient 7.5 s, $p<0.0004$, Figure 4.8D).

Alterations in calcium transients' frequency, amplitude and duration could be related to the density of VGCCs. The frequency of calcium transients is responsible and essential for conveying information about the stimulus activity. The previous study showed that neurexins are essential for the organization of presynaptic termini by functionally coupling to voltage-gated calcium channels (Missler et al. 2003) to the release machinery at presynaptic termini. Deletion of *NRXN1α*, may disturb this coupling mechanism and affect the density of calcium channels at the membrane surface. This, in turn, may influence the characteristics of calcium transients including their frequency and duration. Different patterns of calcium activity can influence Ca^{2+} influx, which has a direct effect on neuronal development and plasticity. This suggests that an alteration in frequency of calcium activity may have a downstream effect on calcium entry, binding and neurotransmitter release. It will be interesting to determine neurotransmitter release in related ASD patients.

Our current study with human *NRXN1α* patient-derived neurons showed different results from the triple knockout mouse models. A severe reduction in neurotransmitter release was observed in mice with multiple α-neurexins deficiency, and this was assumed as results of an impairment in VGCCs (Missler et al. 2003). However, it was unclear which neurexin gene/isoform was associated and which VGCCs were impaired. A subsequent study by the same research group showed that transgenic neurexin 1α but not 1β was able to rescue the release and the reduced Ca^{2+} current phenotype (Zhang et al. 2005). Interestingly, in both the transgenic and knockout mouse models, α-neurexins only affected the neurotransmitter release based on the N and P/Q type VGCC and not L-type VGCCs (Zhang et al. 2005). In the human *NRXN1α* deletion neurons, it is more likely that both L-type and P/Q type VGCCs collectively contributed to the observed phenotype. In addition, the observed phenotypes in calcium dynamics may not be solely dependent on VGCCs but also other molecular mechanism of actions, such as master regulators of neurotransmitter release, synaptotagmins (Südhof 2013) or other calcium-binding proteins such as SNARE complexes, that have an essential role in vesicle exocytosis and fusion.

The Neurexins were initially suggested to promote the formation of synapses and differentiation of postsynaptic receptors (Scheiffele et al. 2000; Dean et al. 2003), but this was challenged by the study that cultured hippocampal neurons from *Nrxn1α* knockout mouse model only showed a discrete change in synaptic change with no alteration in neurotransmitter release (Etherton et al. 2009). In addition, heterozygous and homozygous deletion of *Nrxn1α* knockout mouse model in cultured cortical neurons showed no synaptic or non-synaptic phenotype (Pak et al. 2015). Thus, the mouse *Nrxn* models have been challenged by the lack of consistent phenotype relevant to human clinical symptoms of a range of neurodevelopmental disorders associated with *NRXN1* deletions.

Human are more sensitive to genetic alteration as a whole. Haploinsufficiency in humans often presents more severe phenotype than in heterozygous mice (Pandolfi et al. 1995; Van Esch and Devriendt 2001; Bi et al. 2002; Zhang and Baldini 2008). Induced *NRXN1* mutations in a human ESC line did show an impairment in evoked neurotransmitter release by altering the EPSC amplitude (Pak et al. 2015). It is difficult to compare knockout animal and human induced mutation in ESC models to our study.

Our current study showed a difference in Ca^{2+} transient activity in day 100 neurons, not in day 50 neurons, between the six control iPSC lines and 4 ASD *NRXN1α* deletion iPSC lines. The changes in calcium transient activity and subsequent results from chapter 3 in our present data suggests there could be an increased neuronal excitation and neurotransmitter release associated with *NRXN1α* in human patients and derived cells. This is consistent with the current knowledge that *NRXN1α* is involved in both excitation and inhibition, while *NRXN1β* is mainly engaged with excitation. Therefore, the balance is expected to have reduced inhibition, for which *NRXN1α* is responsible. Furthermore, *NRXN1α* deletion is also associated with our ASD patients and comorbidity of epilepsy. Our quantitative analysis of whole genome RNA sequencing has also demonstrated genome-wide molecular changes related to our observed phenotypes (See Chapter 5).

In summary, we carried out functional analyses of iPSC-derived neurons via calcium imaging. We showed that *NRXN1α* deletion impaired calcium dynamics and an increased frequency and amplitude of calcium transients were observed in ASD

patient-derived neurons. This novel finding suggests that a disturbed calcium signalling may be the cause of abnormal neurotransmitter release and neuronal dysfunction in ASD patients with co-morbidity of epilepsy.

Chapter 5. Transcriptome analyses of 100-day cortical excitatory neurons from iPSCs of healthy controls and *NRXN1α* deletion patients

5.1 Introduction

5.1.1 RNA sequencing background

Genetic information is stored in double helix DNA packages on chromosomes inside the nucleus of a cell (Crick 1970; Crick 1958). All cells in a body are derived from a fertilized egg which in theory should pass identical genetic information if no genetic alteration occurs during embryonic development or after birth. The genetic information is converted from DNA to RNA, known as transcription, and from RNA to protein, known as translation (Crick 1970; Crick 1958).

The ultimate transcription of DNA into complementary RNA molecules, defined as transcriptome, is the functional interpretation of the genome. The human genome consists of around 20,000 to 25,000 coding genes including microRNAs and pseudogenes. A proportion of these genes are essential for normal function and survival of all cells, but the activation or inactivation of subsets of these genes will favour towards a specific organ.

A proportion of them are commonly required by every cell for basic cell function, survival and house-keeping. However, it is the selective genome-wide activation/inactivation of special subsets of genes, which are essential for the specification of different cell types, the formation of different organs, and proper physiological function of an organism. An appropriate amount of these genes are critical for the normal/abnormal physiological function.

There are different RNA quantification methods for evaluation of RNA transcriptions. Northern blotting were initially developed to hybridize a defined amount of RNA on a blot using radioactive DNA probe. Polymerase chain reaction (PCR) was developed afterwards, in which DNA fragments amplified in test tubes on the PCR machine (Mullis 1994). RNA can be converted into complementary DNA (cDNA) by reverse transcription (RT) in tubes with reverse transcriptase purified from RNA viruses.

By going through series of steps of denaturing, annealing, extension and cycling, using PCR machine, hundred base pairs of DNA fragments can be synthesized that are visible by naked eye on an agarose gel, from as little as <50ng of DNA templates of

$6x10^9$ bp genome size. To quantify the gene expression quantitative RT-PCR is commonly used in laboratories. However, it can only detect a limited number of genes with housekeeping genes in one 96/364 well PCR plate. Therefore, it is difficult to relate to other genes on a large scale.

Over the last two decades, a wide range of methods has been evolved for genome-wide quantification of gene expression. The first transcriptomic method was developed by Schena et al. (Schena et al. 1995) using hybridisation-based microarray, which can be used to quantify genome-wide gene expression. However, this technology is not very advantageous as there is only limited number of transcripts available in one array system as well as the G/C contents of individual transcripts and/or their non-bias amplification during the cDNA/probe synthesis.

Another display system was further developed for RT-PCR by using random primers. High-resolution silver staining will be then used for analyzing the subsets of cDNA in desaturation polyacrylamide gel electrophoresis (Liang and Pardee 1992). This technology can also be limited by generating similar sizes of cDNA bands having the same sequence identity.

High throughput RNA sequencing technology has revolutionized genome-wide transcriptomics allowing the entire transcriptome to be quantified in a high-throughput manner (Wang et al. 2009). This method has high advantages over other previously developed methods by enabling investigation of a complex aspect of transcriptomics, e.g. allele-specific expression, alternative splicing, the discovery of candidate mutations in the coding regions of the RNA and importantly the differential expression of genes among different conditions.

Now researchers have commonly started to quantitatively analyze gene expression profiles to assess an appropriate disease model genome-wide (Bock et al. 2011; Lin et al. 2011; Lin et al. 2016). With the use of this approach, researchers can generate a quantitative index of transcriptomes, which can provide a robust profile of quantitative measurements. Comparison of the healthy controls with disease cells/tissues can thus provide a whole picture of cellular changes at the molecular and genome levels, which can provide molecular and cellular mechanisms to evaluate/interpret the functional differences between patients and controls.

Most neuropsychiatric and neurodevelopmental disorders are rarely caused by single genetic alteration, but associated with hundreds of genetic risk factors, each with a low prevalence. Although personalized medicine is a fashionable proposal, the application of a treatment based on a single gene target will have a high cost. This may not apply to patients in which their clinical phenotypes are caused by more than one genetic alterations. In addition, it is still unknown how alterations in different genetic risk factors lead to the same phenotype and or disease. A systematic analysis may lead to the identification of molecular pathways of diseases, which may subsequently lead to the development of therapeutic drugs and intervensions.

NRXN1 is a major drug target for a number of brain disorders including ASD, schizophrenia, intellectual disability, epilepsy and developmental delay. *NRXN1* gene does not encode a transcriptional factor which may affect a small number of genes by transactivation and/or repression. Instead, it encodes numerous synaptic neuro-adhesion proteins by differential splicing. The Neurexin proteins are partially located on axonal terminals which form complexes with post-synaptic molecules, such as Neuroligins, thereby initiating neuronal inhibition and excitation bi-directionally.

In this part of the study, the whole genome RNA sequencing was used to characterize the gene expression profiles, in 100-day cortical excitatory neurons directionally differentiated from iPSCs of healthy controls and ASD patients with heterozygous *NRXN1α* gene deletion. The purpose of this approach is not aimed at the identification of a small number of genes leading to the disease, but to identify genome-wide molecular changes and pathways associated with *NRXN1α* lesion, which are critical for the determination, differentiation, specification and function of the iPSC-derived neurons, and to understand how their alterations are associated with changes in cell function and to develop ASD model in culture dishes.

5.1.2 Voltage-gated ion channels

One of the functional characteristics of a mature neuron is its ability to fire. The initiation and propagation of electrical signals in nerves have fascinated physiologists for centuries. The basis of electrical signalling was laid down by Hodgkin & Huxley using the voltage-clamp technique (Hodgkin and Huxley 1952a), in which they propose the association of sodium and potassium current in the rising and falling phases of an action potential respectively. In an excitable cell such as a neuron, transmission of signals occurs due to a flow of Na^+ and K^+ ions, which propagate an action potential and an electrical spike (Hodgkin and Huxley 1952b). All voltage-gated ion channels share the same structure, a common four subunits which comprise of six transmembrane segments, with S1-S4 responsible for voltage sensor and S5-S6 as a pore-forming domain (Yu and Catterall 2004).

The Na^+ gradient across the plasma membrane is dependent on the influx of sodium through Voltage-gated Na^+ channels (VGSCs). VGSCs are macromolecular complexes compromising of a pore-forming α subunit and one or more β subunits (Isom et al. 1992; Morgan et al. 2000). Both the α and β subunits of VGSCs are expressed in excitable cells and cortical neurons (Isom et al. 1992; Morgan et al. 2000; Shah et al. 2001; Qu et al. 2001). The transcription of these channels is developmentally regulated and tissue-restricted. Furthermore, the electrical activity can also influence their transcription. Above statements suggest that an essential determinant of resting membrane potential across the neurons is associated with voltage-gated sodium and potassium channels.

In Chapter 3 and 4, our results showed that the electrical excitability and calcium dynamics are impaired in *NRXN1α* deletion neurons. Electrical activity drives each action potential, and this activity arises from the association of Na^+/K^+ ion channels and membrane proteins that allow the influx and efflux of ions. Consequently, calcium entry through voltage-gated calcium channels (VGCCs), on the cell membrane, in response to membrane depolarization, is responsible for many physiological processes and the process of neurotransmitter release. These statements suggest that there might be an underlying molecular mechanism disturbing voltage-gated ion channels resulting in impairment at the functional level.

5.2 Material & Methods

5.2.1 RNA extraction

The 100-day neurons were derived from differentiation of the iPSCs as described in Chapter 2. The iPSC lines were derived from controls [1CC1, 2VC1, 3VC2, 3VCX1, 4C3, 4CX1, NCRM, NCRM5], and patient lines [ND1C1, ND2C11, ND2CX1, ND4-1C1, ND4-1C2] and were differentiated to excitatory cortical neurons using dual SMAD inhibition (Table 5.1). Neurons were cultured for 100 days in N2B27 medium and positively validated for mature neuronal marker MAP2, cortical neuronal marker CTIP2, TBR1, post-synaptic glutamatergic markers PSD-95, SHANKs and various ionotropic and metabotropic glutamate receptors such as GRIK1 and GRIA1 (Figure 2.23A?). The 100-day neuronal cultures were washed with DPBS, and total RNA was extracted using the RNeasy Mini Kit (74104, Qiagen) according to the manufacturer's instructions. Their quality was determined initially by OD260/280 ratios from ND-1000 Nanodrop, and all samples had A260: A280 ratio above 1.8 and A260: A230 above 2.0. Subsequently, 1µg RNA of each sample was sent to BGI for whole genome RNA sequencing (Hong Kong, China).

Table 5.1. Quality control test at BGI using BioAnalyzer 2100 (Agilent)

Sample Name	RIN	28s/18s	Library type
1CC1	9.5	1.8	BGISEQ-500RS RNA-Seq
2VC1	9.5	1.9	BGISEQ-500RS RNA-Seq
3VC2	8.5	1.4	BGISEQ-500RS RNA-Seq
3VCX1	9.0	2.3	BGISEQ-500RS RNA-Seq
4C3	10	2.0	BGISEQ-500RS RNA-Seq
4CX1	9.3	1.7	BGISEQ-500RS RNA-Seq
NCRM1	8.2	1.0	BGISEQ-500RS RNA-Seq
NCRM5	9.3	1.8	BGISEQ-500RS RNA-Seq
ND1C1	9.3	1.6	BGISEQ-500RS RNA-Seq
ND2CX1	8.6	1.7	BGISEQ-500RS RNA-Seq
ND4-1C2	6.2	2.5	BGISEQ-500RS RNA-Seq
ND4-1C1	3.7	0.3	BGISEQ-500RS RNA-Seq

*Samples were filtered for sequencing using RIN number based on the ribosomal band ratios. The Sample ND4-1C1 was excluded from the sequencing due to its low RIN (labelled in red).

RNA quality was independently monitored using BioAnalyzer 2100 (Agilent), which creates an RNA Integrity Number (RIN) between 1 and 10, with 10 being the highest

quality sample. The RIN was calculated from the ratio of 28S and 18S ribosomal bands on an electrophoresis gel. One sample (ND4-1C1) with a low RIN of 3.7 (<6) was therefore excluded from the further RNAseq analysis, as it would lead to erroneous biological conclusions (Table 5.1).

Total RNA was incubated with oligo (dT) magnetic beads, which bind to the polyA tail of mRNA. This was followed by purification to obtain the target mRNA. The mRNA was then reversely transcribed into double-stranded cDNA using N6 random primers according to the BGI protocol. The double-stranded cDNA was ligated, and two specific primers were used to amplify the ligation products. Finally, the PCR products were denatured by heat and single-stranded DNA was amplified using splint oligo and DNA ligase. Each step of the experiment process (like sample test, library construction and sequencing) influence data quality and quantity, and then directly affect bioinformatics results. To get highly reliable sequencing data, we carry out strict quality control in each experiment step. The experiment pipeline is described in Figure 5.1.

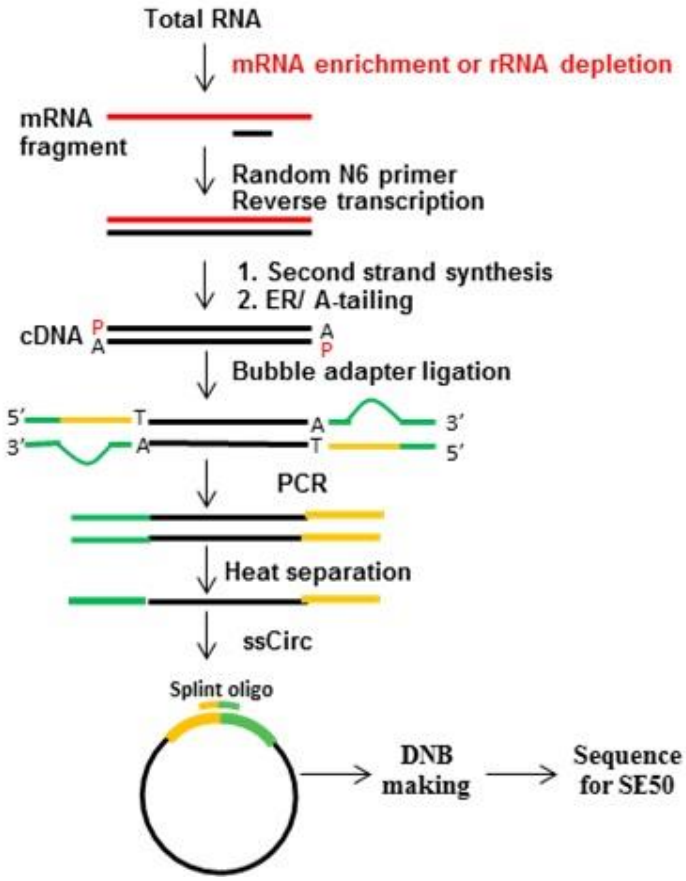

Figure 5.1. RNA-Seq experimental process. 1) There are two methods to enrich mRNA from the total RNA. Total RNA can be treated with Oligo (dT) magnetic beads to bind mRNA with polyA tail and then to pull down the mRNA. The total RNA can also be hybridized with a DNA probe for the rRNA, digested the DNA/RNA hybrid strand, and then treated with DNase I to remove DNA probe. Then the target RNA can be obtained after purification. 2) The target RNA is then reversely transcribed to double-strand cDNA (dscDNA) by the N6 random primer. 3) End repair the dscDNA with phosphate at 5' end and stickiness 'A' at 3' end, then adaptor with stickiness 'T' at 3' end can be ligated to the dscDNA. 4) Two specific primers are used to amplify the ligation product. 5) The PCR products are denatured by heat, and the single strand DNA was cyclized by splint oligo and DNA ligase. 6) Sequencing was performed on the prepared library.

5.2.2 Library Preparation methods

Following RNA extraction, quality control check and cDNA generation, the RNA-sequencing libraries were created. This can be varied by the selection of RNA species and the desired RNA molecules. In this study, BGI constructed BGISEQ-500RS library for all the samples (Table 5.1).

5.2.3 Data Filtering

The raw data were filtered to remove the low-quality, "dirty", reads. "Dirty" reads were defined as reads which contained a high content (>10%) of unknown bases. This is essential to detect and remove data noise which affects the downstream analysis. After noise filtering, the remaining reads were defined as "clean" reads, which account for the average of 99.75% of the total reads (Table 5.2).

Table 5.2. Summary of RNA sequencing data cleaning from BGI.

Cell line	Raw data size (bp)	Raw reads number	Clean data size (bp)	Clean reads number	Clean data rate (%)*
1CC1	1,144,374,900	22,887,498	1,140,751,350	22,815,027	99.68
2VC1	1,154,115,000	23,082,300	1,150,699,450	23,013,989	99.70
3VC2	1,151,120,750	23,022,415	1,149,645,450	22,992,909	99.87
3VCX1	1,142,378,400	22,847,568	1,140,938,350	22,818,767	99.87
4C3	1,160,236,500	23,204,730	1,158,646,800	23,172,936	99.86
4CX1	1,160,239,650	23,204,793	1,157,133,700	23,142,674	99.73
NCRM1	1,162,272,050	23,245,441	1,158,732,300	23,174,646	99.69
NCRM5	1,156,510,550	23,130,211	1,152,301,25	23,046,025	99.63
ND1C1	1,144,491,650	22,889,833	1,141,428,550	22,828,571	99.73
ND2C11	1,153,834,000	23,076,680	1,150,303,500	23,006,070	99.69
ND2CX1	1,158,493,900	23,169,878	1,154,750,150	23,095,003	99.67
ND4-1C2	1,163,835,250	23,276,705	1,162,319,050	23,246,381	99.86

***This Table shows the raw and clean data size, raw and clean reads number and the clean data reads for each sample (Clean data rate (%) = Clean reads number/Raw reads number).**

The clean reads were mapped to reference human genome (GRCh37/hg19), using HISAT/Bowtie tool with an average genome mapping ratio of 94.96% after evaluating the quality of the sequencing data. The alignment was performed by BGI, and all samples passed the test by clean reads average of 97.15% (Table 5.3). The average mapped ratios were calculated using HISAT/Bowrie2 for each sample (Table 5.3).

Table 5.3. Alignment statistics of reads mapped to reference genome.

Cell line	Total Reads	Total mapped reads (%)	Total unmapped (%) reads
1CC1	22,815,027	94.71	5.29
2VC1	23,013,989	94.91	5.08
3VC2	22,992,909	95.27	4.72
3VCX1	22,818,767	95.09	4.91
4C3	23,172,936	94.91	5.09
4CX1	23,142,674	95.19	4.81
NCRM1	23,174,646	94.93	5.07
NCRM5	23,046,025	94.58	5.42
ND1C1	23,006,070	94.91	5.09
ND2C11	22,828,571	94.78	5.22
ND2CX1	23,095,003	94.89	5.10
ND4-1C2	23,246,381	95.37	4.62

BGI also used sequencing saturation to measure the depth of sequencing for informatics analysis (Table 5.3). The number of identified genes reaches a threshold (saturation) level when their growth curves flatten (Figure 5.2).

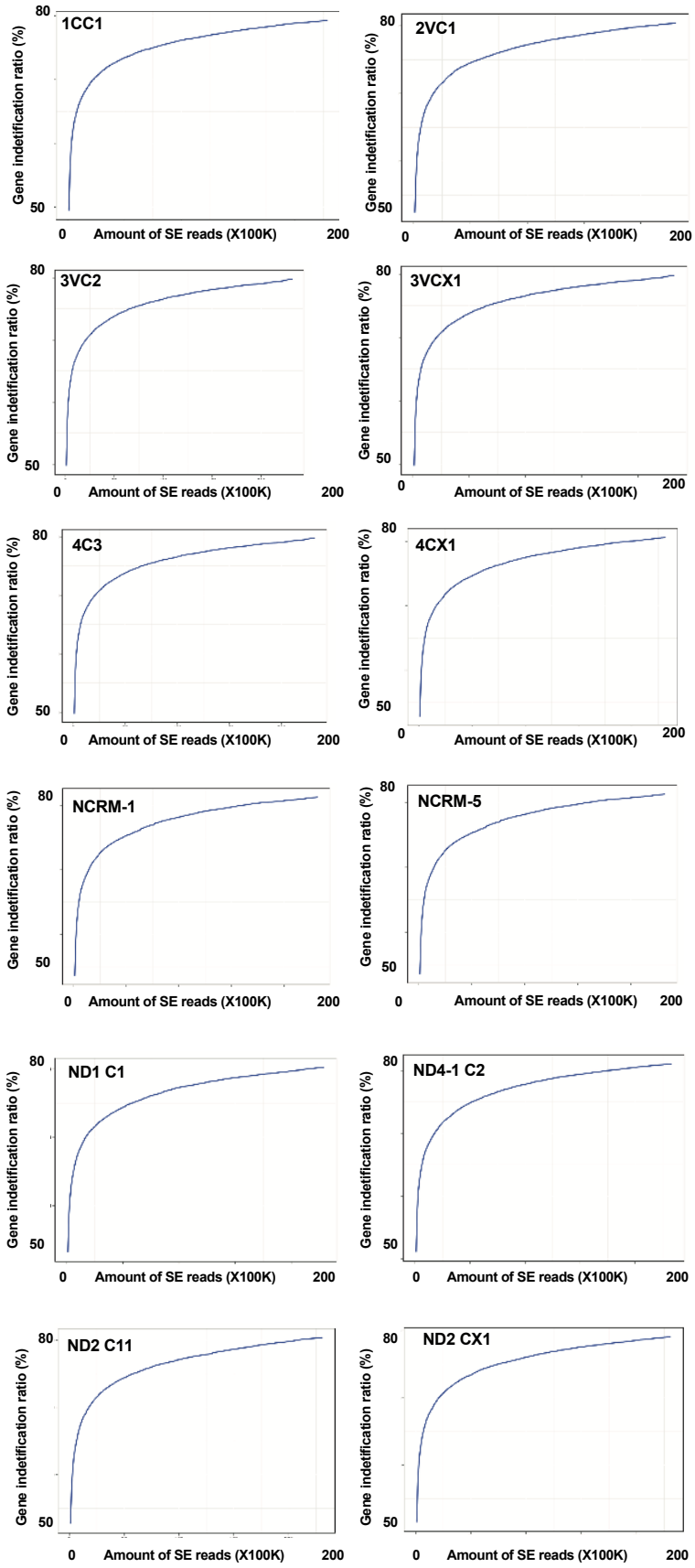

Figure 5.2. Sequencing saturation curve. The number of identified genes reaches a threshold level called saturation growth curve. The x-axis represents the number of clean read and y-axis shows the ratio of identified genes to total genes reported in the database.

The NIH iPSC lines of NCRM-1 and NCRM-5 were recommended by experts in the field as a control IPSC line, however, the two control lines behave very differently. Among the control lines, we have used, the NCRM-5 (red arrows, Figure 5.3) and 1CC1 (green arrows, Figure 5.3) lines were excluded for the final analysis. Differentiation of NCRM-5 line resulted in enhanced non-neuronal differentiation with very low expression of major neuronal markers. These included major mature neuronal markers *MAP2*, *SYN1*, *NeuN*, *PSD-95* and synaptophysin (Figure 5.3A), postsynaptic receptors and sodium/potassium voltage-gated channels such as NMDARs, *GRIA2, GRIN1, KCNQ2* and *SCN3B* (Figure 5.3B). Furthermore, other neuronal markers such as hippocalcin (*HPCA*), a major neuron-specific calcium-binding protein, synuclein beta (*SNCB*) with functionality in neuronal plasticity, calcium-dependent exocytosis of secretory vesicle synaptotagmin 4 (*SYT4*), neurofilament medium (*NEFM*) which has a major role in intracellular transport to axons and dendrites and *TBR1* which is a major lower layer cortical neuronal marker showed very low expression level (Figure 5.2C). On the other hand, expression of non-neuronal markers such as *SMOC2*, a major regulator of endothelial cell proliferation and migration, *CFAP126* that has a role in cilia formation of multiciliated lung cells, and fibulin (*FBLN5*) which notably expressed in intimal vascular smooth muscle cells and endothelial cells showed very high expression level (Figure 5.3D). This decreased expression of neuronal markers and increases expression of non-neuronal markers have also been observed in 1CC1 line (green arrows, Figure 5.3) in most of the cases. Meanwhile, the other golden iPSC line (NCRM-1) showed the similar gene expression along with other lines.

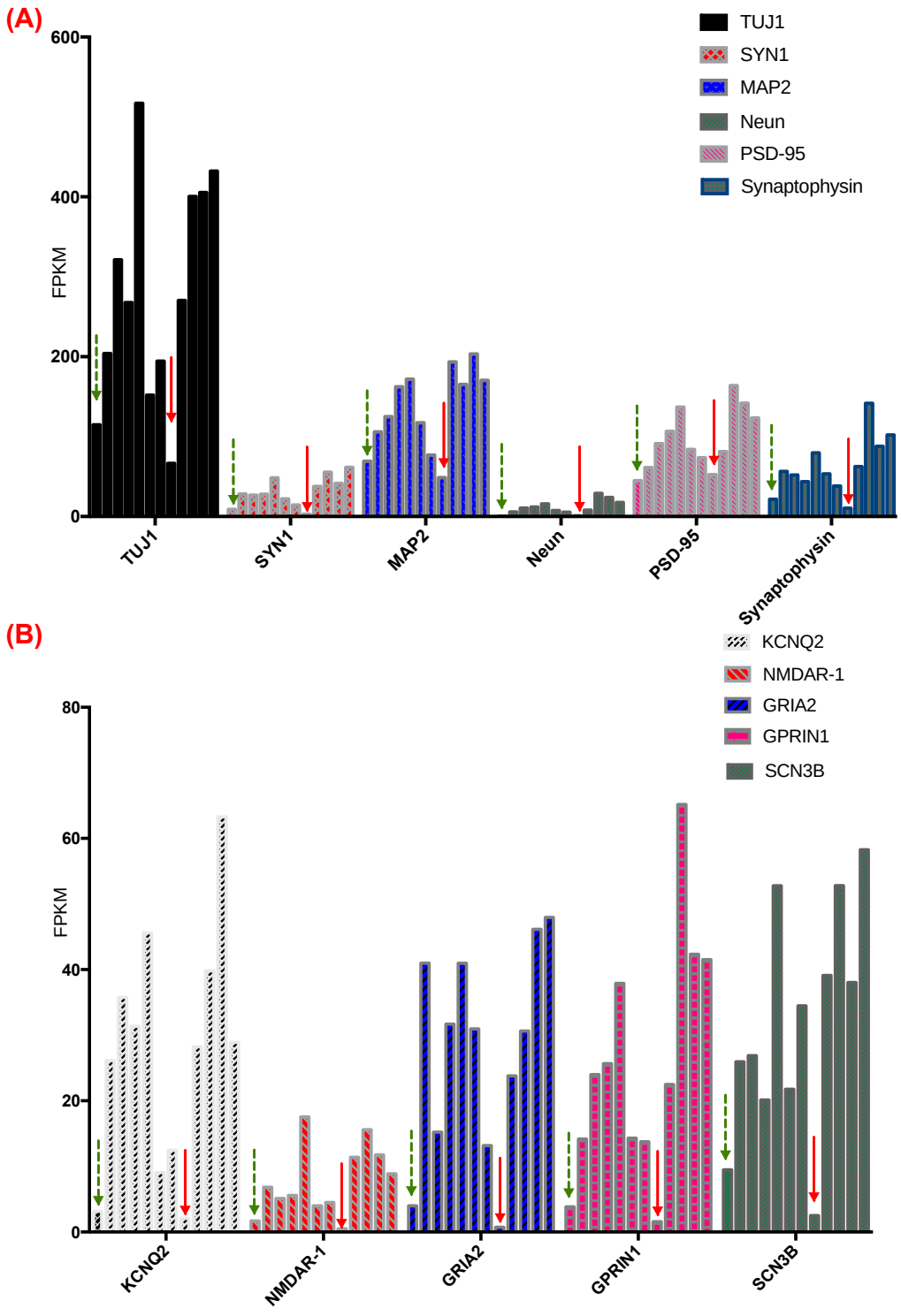
(A)
TUJ1
SYN1
MAP2
Neun
PSD-95
Synaptophysin
FPKM
600
400
200
0
TUJ1
SYN1
MAP2
Neun
PSD-95
Synaptophysin
(B)
KCNQ2
NMDAR-1
GRIA2
GPRIN1
SCN3B
FPKM
80
60
40
20
0
KCNQ2
NMDAR-1
GRIA2
GPRIN1
SCN3B

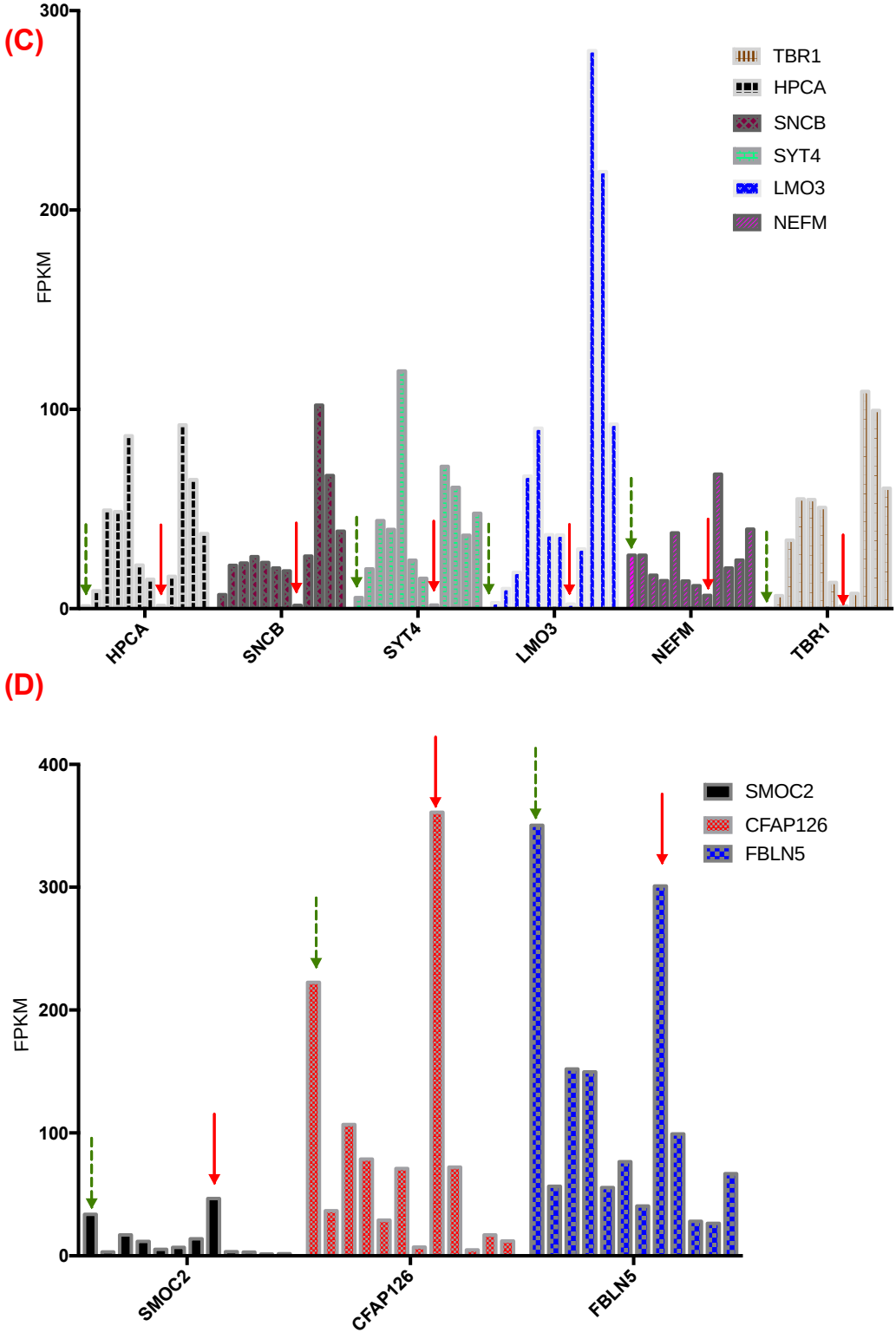

Figure 5.3. NCRM-5 showed very low expression for the majority of neuronal markers in whole genome RNA sequencing. (A) The expression of major mature neuronal markers *SYN1*, *MAP2, NeuN, PSD-95* and synaptophysin across all lines showed low expression in 1CC1 and NCRM-5. (B) The expression of a group of neuronal receptors, channels along with other major markers essential for plasticity, vesicle exocytosis, calcium binding (C) showed very low in NCRM-5 and almost all of 1CC1. (D) Endothelial cell proliferation marker

and multiciliated lung cells cilia formation showed very high expression in comparison to other lines. Red arrows indicated NCRM-5 and dashed green arrow represent 1CC1. The order of lines is 1CC1, 2VC1, 3VC2, 3VCX1, 4C3, 4CX1, NCRM-1, NCRM-5, ND1C1, ND2C11, ND2CX1, ND4-1C1.

Surrogate variable analyses (SVA) were further used for identifying the unknown source of variations such as batch effects and conditions. In any scientific research, great care must be taken to evaluate and understand the correlation between the two identified variables. These variables are, for example, sex, age, disease condition severity etc. It is impossible to control every single variable present in our experiments due to the complexity of our genomes and environment which may have an effect on the genes expressed. It has been shown that SVA is very useful in large-scale gene expression studies (Leek and Storey 2007). SVA has the capability to estimate, utilize and correct the components of "expression heterogeneity" (Leek and Storey 2007). The SVA analysis on our data clearly showed that the presence of 1CC1 even after SVA correction has a disruption effect on clustering of control and patient samples (Figure 5.4A). Furthermore, multi-dimensional scaling (MDS) which indicates how closely the samples are related to each other, has identified a similar pattern of disruption. MDS analysis showed that in the presence of 1CC1, the control and patient samples have spread across heat map (Figure 5.4B). When 1CC1 removed, the SVA and MDA analysis were performed again, and a much greater result observed (Figure 5.4C, D). The results showed that the presence of 1CC1 creates a huge variability and disruption which may have a strong effect on our differential gene expression analysis. It should be noted that MDS analysis of samples without 1CC1 still showed a distance between ND1C1 and the rest of deletion lines. One reason to explain this is that ND1C1 has the larger deletion region in comparison to other *NRXN1α* deletion lines, i.e. ND2CX1, ND2C11 and ND4-1C2.

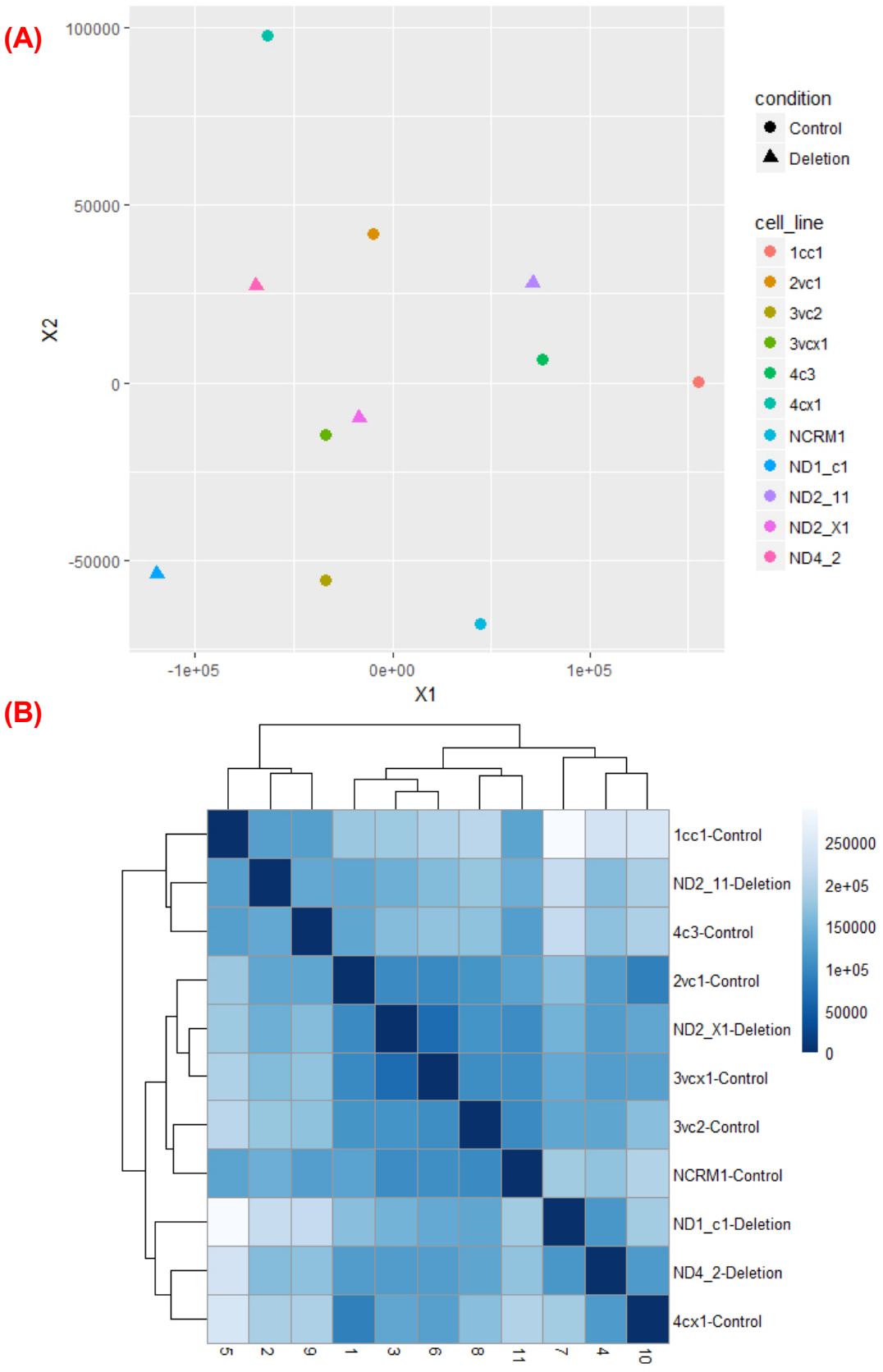
(A)
100000
50000
0
-50000
X2
-1e+05
0e+00
1e+05
X1
condition
Control
Deletion
cell_line
1cc1
2vc1
3vc2
3vcx1
4c3
4cx1
NCRM1
ND1_c1
ND2_11
ND2_X1
ND4_2
(B)
1cc1-Control
ND2_11-Deletion
4c3-Control
2vc1-Control
ND2_X1-Deletion
3vcx1-Control
3vc2-Control
NCRM1-Control
ND1_c1-Deletion
ND4_2-Deletion
4cx1-Control
5
2
9
1
3
6
8
11
7
4
10
250000
2e+05
150000
1e+05
50000
0

(C)

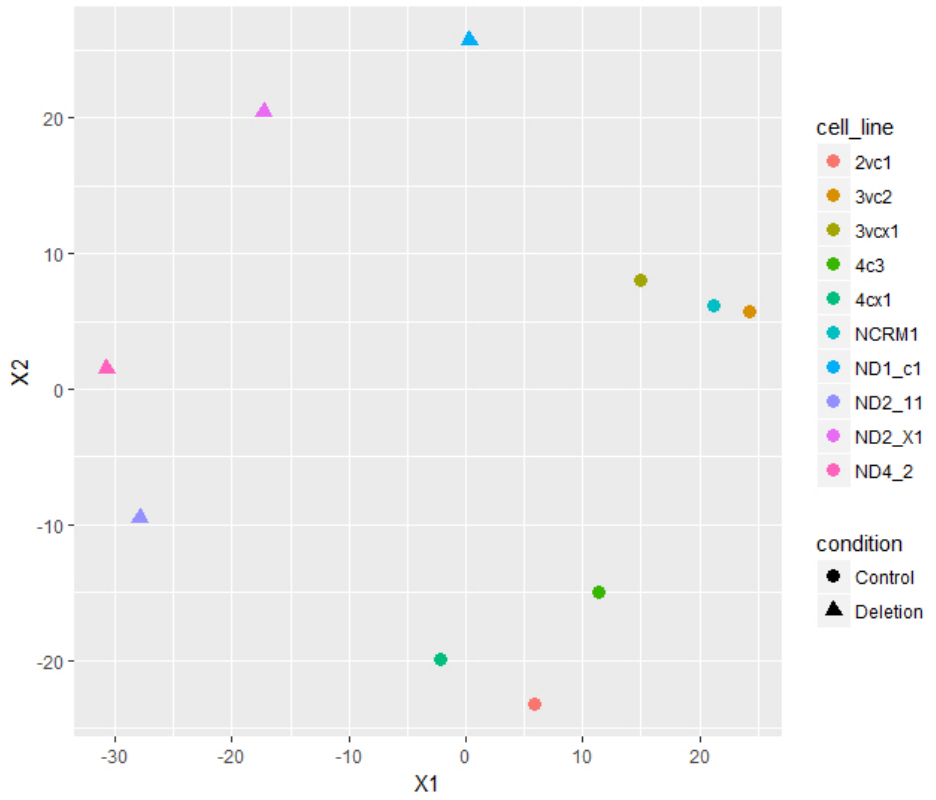
X2
X1
20
10
0
-10
-20
-30
-20
-10
0
10
20
cell_line
2vc1
3vc2
3vcx1
4c3
4cx1
NCRM1
ND1_c1
ND2_11
ND2_X1
ND4_2
condition
Control
Deletion

(D)

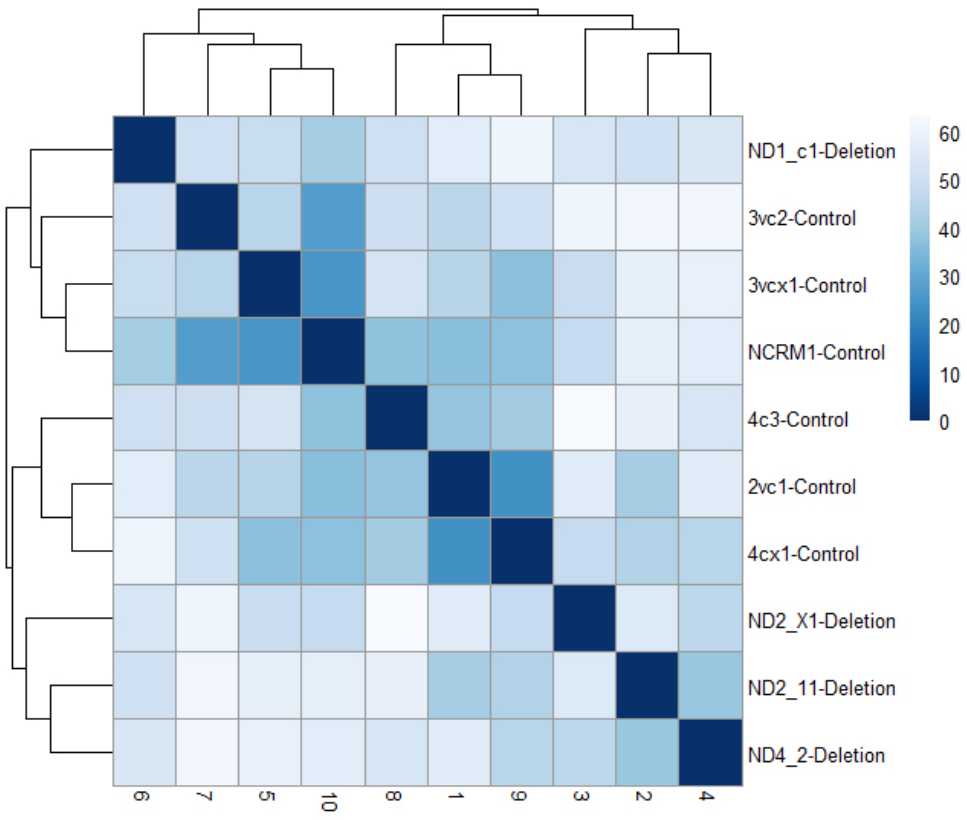
ND1_c1-Deletion
3vc2-Control
3vcx1-Control
NCRM1-Control
4c3-Control
2vc1-Control
4cx1-Control
ND2_X1-Deletion
ND2_11-Deletion
ND4_2-Deletion
9
7
5
10
8
1
6
3
2
4
60
50
40
30
20
10
0

Figure 5.4. SVA and MDS analysis with and without 1CC1. (A) SVA correction with 1CC1 showed a disruption in clustering of control and patient lines. Furthermore, the MDS heatmap showed that the distance between the controls and patient lines were disturbed (B). (C) With the exclusion of the 1CC1 line, SVA correction nicely clustered and grouped all deletion lines close to each other with the controls lines also clusters together. The MDS heat map also showed a short distance between patient's lines and control lines separately (D). It is noted that ND1-C1 displayed a high distance from other deletion lines which could be due to its larger deletion region

5.2.4 RNA sequencing analysis

Whole genome RNA sequencing was performed to quantitatively identify global transcription of iPSC-derived cortical neurons from 4 control donor participants of 6 lines (2VC1, 3VCX1& 3VC2, 4C3&4CX1, NCRM-1] and 3 *NRXN1α* deletion patients of 4 lines (ND1C1, ND2C11& ND2CX1, ND4-1C2). Transcripts from 27,163 genes (Figure 5.2A) were identified using Dseq2 analysis (with help from Jamie Reilly in the lab). The FASTQ files in Kallisto (v0.43.1) were used for quantification of the transcriptome (based on GRCH37/hg19) and gene abundance, and the gene expression was converted into Transcripts Per Million (TPM). Differential gene expression between control and *NRXN1α* deletion neurons, was then calculated using the Dseq2 package in R. The control and patient groups were compared and analyzed with FDR (false discovery rate) and adjusted multiple P value.

5.2.5 Shortlist criteria for differentially expressed genes

An FDR of <0.05 was firstly applied to the transcriptome of 27,163 transcripts, which were quantitatively sequenced from 6 control and four patient IPSC lines. This identified 1487 differentially expressed genes between the control and patient groups. We hypothesized that a gene would require a detectable level of expression to play a role in cellular function, and therefore applied TPM value of 2 to filter out extremely low abundance genes. The ratios of gene expression between the patient and control groups were calculated using the average TPM of the patient group over the average TPM of the patient group. Haploinsufficiency is a common interpretation for human genetic alterations without dominant effect, and we, therefore, applied 50% or higher reduction to further narrow down the shortlist, and this resulted in a total of 259 down-regulated genes. *NRXN1α* is a neuronal adhesion molecule, not a transcription

activator or repressor; we therefore anticipated an equivalent amount of targets upregulated. We, therefore, chose 1.7-fold or more increase in the patient group as the criteria, and this led to the shortlist with 271 upregulated genes. This finalized the differentially expressed genes to a list 530 genes. The list of significantly differentially expressed genes was then analysed using the STRING and GSEA database.

5.2.6 STRING analyses

STRING is a database which has been used for predicting either direct or indirect protein-protein interactions and associations. The 530 significant differential expressed genes were analysed in STRING to investigate potential significant GO group (molecular function, biological processes, cellular processes) in our study.

5.2.7 GSEA analyses

Gene set enrichment analysis (GSEA) is a computation method which has been used to show a statistically significant enriched set of genes. The 530 significant differential expressed genes were analyzed in GSEA to investigate the most overlapped genes across all GO groups (molecular function, biological processes, cellular processes). Additionally, KEGG pathways analysis were used to identify the significant pathways involved in our study.

5.3 Results

5.3.1 Differential gene expression between controls and ASD cases with heterozygous *NRXN1α* deletion

In this study, 100-day neuronal differentiation was performed with six iPSC control lines (2VC1, 3VCX1&3VC2, 4C3&4CX1, NCRM-1) from 4 healthy independent donors and four iPSC lines (ND1C1, ND2C11&ND2CX1, ND4-1C2) from three ASD patients with *NRXN1α* deletion. Transcriptome analyses were carried out by whole genome RNASeq and differential gene expression between the control, and patient groups were analyzed by using the Dseq2 package in R, which resulted in a list of 530 genes with FDR <0.05, TMP>2. The list included 259 genes with >50% downregulation of the gene expression in the ASD group, and 271 genes with >1.7-fold of upregulation in the *NRXN1α* deletion neurons, as illustrated by the volcano plot (Figure 5.5B) and heatmap (Figure 5.5C).

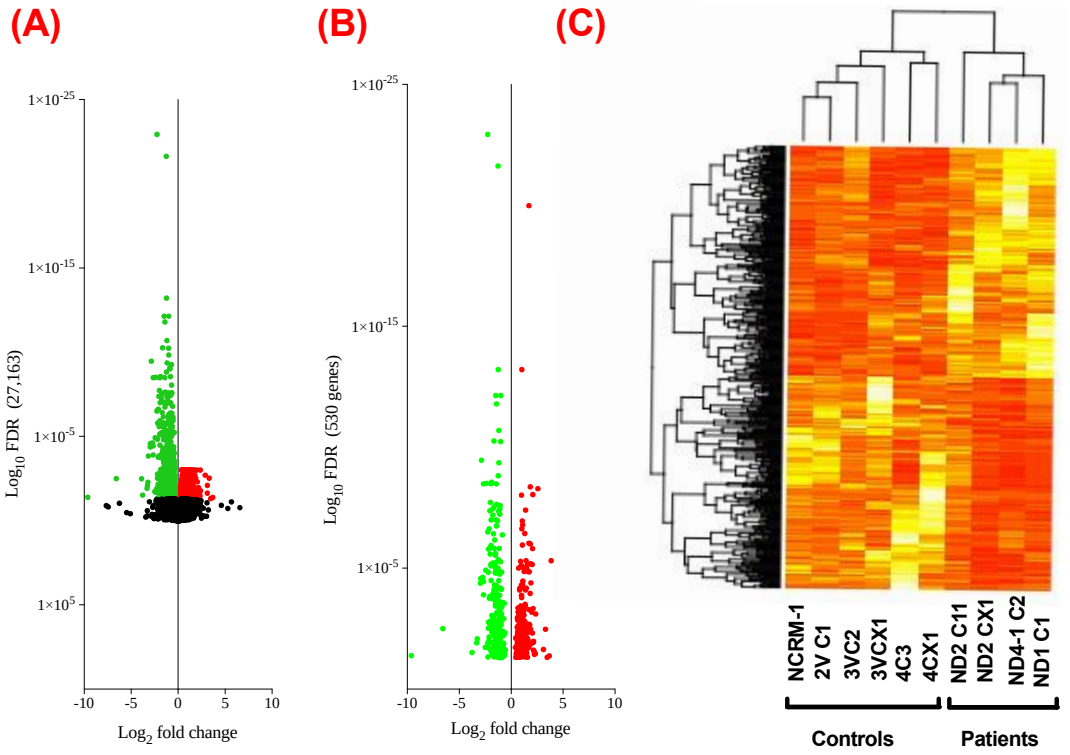

Figure 5.5. Differential expression between control and NRXN1α deletion of iPSC derived neurons. (A) Volcano plot of FDR on the y-axis and Log2 fold change in the x-axis of all 27,163 genes. Among them, 1487 genes were identified to have FDR of 0.05 or less in which 948 genes were downregulated (green dots), and 539 genes were upregulated (red dots). (B) Volcano plot of Log10 FDR on the y-axis and Log2 fold changes on the x-axis of significantly differentially expressed in *NRXN1α* heterozygous deletion neurons. Among the 530 genes, 254 were downregulated (green dots) and 276 were upregulated (red dots) below the FDR 0.05. (C) Bivariate clustering of samples (Columns) of the 530 differentially expressed genes at FDR 0.05 or less (rows). The colour ranges from red (upregulated genes) to white (downregulated genes) based on TPM values.

The shortlisted 530 differentially expressed genes were analyzed on STRING to investigate the protein-protein interactions. Among them, 429 proteins were recognized by the STRING with 487 edges and PPI (protein-protein interaction) enrichment P value of less than 1.0x10E-16 (Figure 5.6).

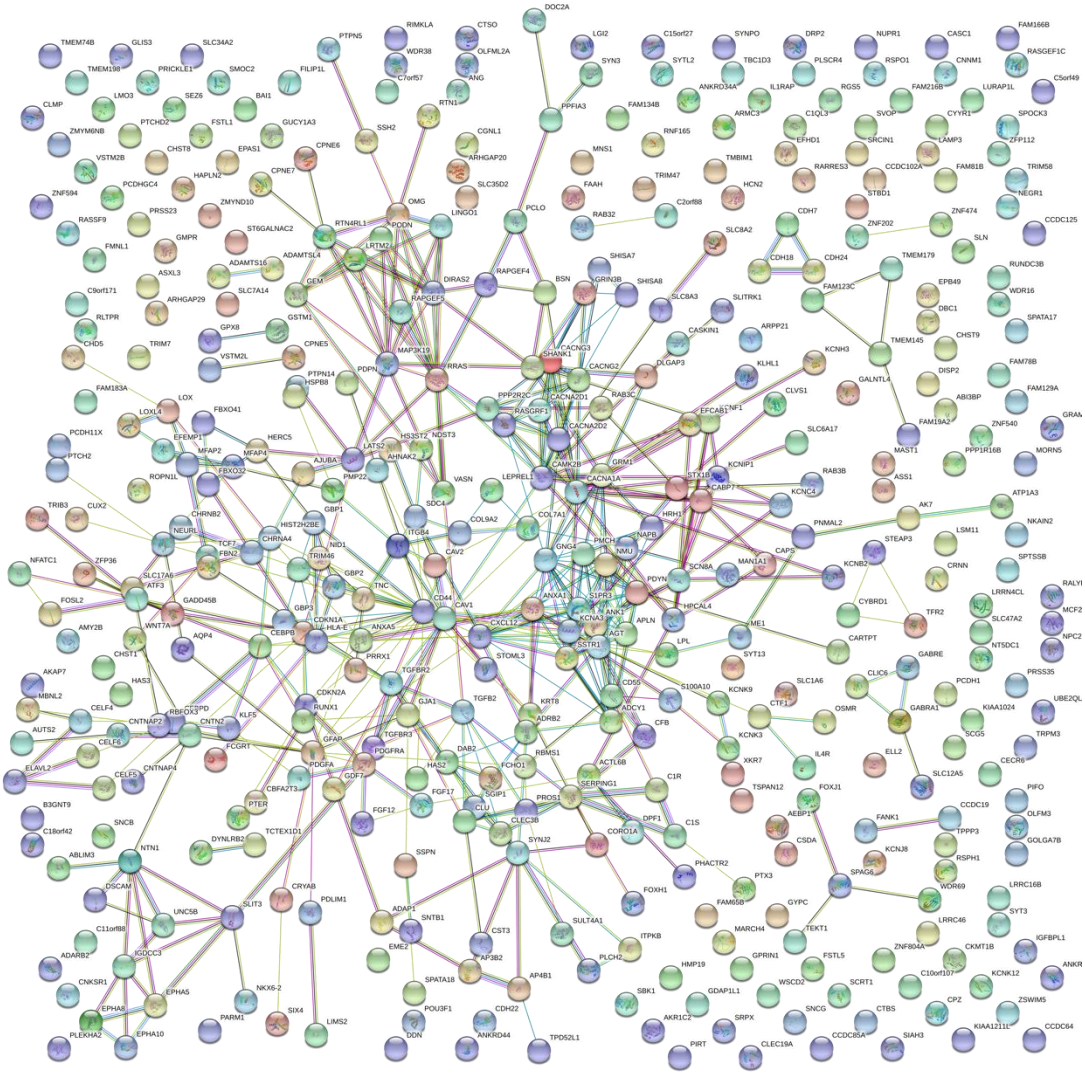

Figure 5.6. Summary view of the protein-protein interaction network of NRXN1α targets. 530 *NRXN1a* targets were input into the STRING program, and 429 proteins were recognized. The figure represented an overview of the protein-protein interaction of the *NRXN1a* targets after hiding the disconnected proteins.

The outcome of the STRING analyses included: 103 biological processes (GO, FDR<0.05), 56 cellular components (GO, FDR<0.05) and 16 molecular functions (GO, FDR<0.05), with 2 KEGG Pathways (GO, FDR<0.05).

Among the 103 biological processes, the synaptic transmission was the most enriched pathway with 45 genes dysregulated (FDR of 2.12E-011) (Table 5.4). The 103 biological processes can be categorized as synaptic transmission, ion transport and neuronal activity, neurotransmitter secretion, cell communication, CNS development and behaviour, and others.

Table 5.4. The Biological Processes (GO) groups from the 429 differentially expressed genes in *NRXN1α* heterozygous deletion neurons.

Pathway ID	Pathway description	Gene	FDR
	Synapses		
GO.0007268	synaptic transmission	45	2.12E-11
GO.0050804	modulation of synaptic transmission	18	1.39E-03
GO.0050808	synapse organization	12	6.77E-03
GO.0050807	regulation of synapse organization	10	1.51E-02
GO.0050803	regulation of synapse structure or activity	15	7.78E-03
GO.0016079	synaptic vesicle exocytosis	8	1.14E-02
GO.0048489	synaptic vesicle transport	9	3.95E-02
	Ion transport and neuronal activity		
GO.0051049	regulation of transport	66	7.69E-05
GO.0034765	regulation of ion transmembrane transport	27	4.90E-05
GO.0043269	regulation of ion transport	34	5.63E-05
GO.0034220	ion transmembrane transport	31	4.59E-02
GO.0030001	metal ion transport	33	1.09E-04
GO.0098660	inorganic ion transmembrane transport	27	9.27E-03
GO.0098662	inorganic cation transmembrane transport	23	2.19E-02
GO.0006812	cation transport	30	4.03E-02
GO.0051952	regulation of amine transport	8	1.36E-02
GO.0006816	calcium ion transport	15	7.78E-03
GO.0006813	potassium ion transport	11	3.35E-02
GO.0042391	regulation of membrane potential	16	2.62E-02
GO.0051899	membrane depolarization	7	3.35E-02
	Neurotransmitter secretion		
GO.0046903	secretion	29	2.27E-03
GO.0032940	secretion by cell	25	3.96E-03
GO.1903530	regulation of secretion by cell	25	4.73E-02
GO.0006887	exocytosis	18	6.77E-03
GO.0023061	signal release	14	6.77E-03
GO.0006836	neurotransmitter transport	14	8.73E-04
GO.0007269	neurotransmitter secretion	12	1.67E-03
GO.0050433	regulation of catecholamine secretion	6	2.36E-02
	Cell communication		
GO.0007154	cell communication	128	1.76E-02
GO.0023052	signaling	126	1.63E-02
GO.0007267	cell-cell signalling	51	1.25E-07
GO.0007155	cell adhesion	35	4.17E-02
GO.0030155	regulation of cell adhesion	26	1.51E-02
GO.0045785	positive regulation of cell adhesion	18	2.53E-02
GO.0030198	extracellular matrix organization	25	9.05E-05
GO.0085029	extracellular matrix assembly	5	5.33E-03
GO.0019220	regulation of phosphate metabolic process	48	4.74E-02
GO.0060389	pathway-restricted SMAD protein phosphorylation	4	1.65E-02

	CNS development		
GO.0007399	nervous system development	75	3.28E-05
GO.0022008	neurogenesis	56	1.51E-04
GO.0007417	central nervous system development	33	2.65E-02
GO.0051960	regulation of nervous system development	28	2.92E-02
GO.0051962	positive regulation of nervous system development	21	1.76E-02
GO.0048699	generation of neurons	50	1.94E-03
GO.0030182	neuron differentiation	38	9.27E-03
GO.0048666	neuron development	33	1.11E-02
GO.0045664	regulation of neuron differentiation	24	7.78E-03
GO.0030030	cell projection organization	45	1.06E-04
GO.0031344	regulation of cell projection organization	27	2.41E-04
GO.0031175	neuron projection development	30	6.65E-03
GO.0010975	regulation of neuron projection development	21	1.67E-03
GO.0010976	positive regulation of neuron projection development	13	4.15E-02
	Behaviour		
GO.0007610	behavior	29	3.04E-04
GO.0030534	adult behaviour	15	2.61E-04
GO.0008344	adult locomotory behaviour	9	1.43E-02
GO.0007626	locomotory behaviour	14	1.21E-02
	From cell to system development		
GO.0048731	system development	104	1.11E-03
GO.0048856	anatomical structure development	115	1.78E-03
GO.0022603	regulation of anatomical structure morphogenesis	42	7.69E-05
GO.0032502	developmental process	123	7.75E-03
GO.0050793	regulation of developmental process	71	6.13E-04
GO.0051094	positive regulation of developmental process	46	5.60E-04
GO.0051093	negative regulation of developmental process	32	4.29E-02
GO.0048639	positive regulation of developmental growth	12	1.63E-02
GO.0042127	regulation of cell proliferation	51	7.78E-03
GO.0031099	regeneration	13	3.15E-03
GO.0048468	cell development	61	2.15E-04
GO.0060284	regulation of cell development	33	5.51E-03
GO.0010720	positive regulation of cell development	23	1.03E-02
GO.0030154	cell differentiation	86	2.59E-02
GO.0045595	regulation of cell differentiation	51	7.78E-03
GO.0045597	positive regulation of cell differentiation	33	1.14E-02
GO.0048869	cellular developmental process	91	1.36E-02
GO.0051128	regulation of cellular component organization	74	2.61E-04
GO.0022604	regulation of cell morphogenesis	27	6.13E-04
GO.0010769	regulation of cell morphogenesis involved in	19	3.23E-03
GO.0010770	positive regulation of cell morphogenesis involved in	11	4.17E-02
GO.0048518	positive regulation of biological process	130	6.89E-03
GO.0048522	positive regulation of cellular process	112	2.94E-02
GO.0032879	regulation of localization	82	3.49E-05

GO.0051130	positive regulation of cellular component organization	43	7.76E-03
	Others		
GO.0061041	regulation of wound healing	10	3.35E-02
GO.0061045	negative regulation of wound healing	7	3.06E-02
GO.0006956	complement activation	6	3.98E-02
GO.0006958	complement activation, classical pathway	5	4.74E-02
GO.0030193	regulation of blood coagulation	8	4.17E-02
GO.0030195	negative regulation of blood coagulation	6	4.48E-02
GO.0070482	response to oxygen levels	17	1.90E-02
GO.0001666	response to hypoxia	15	4.74E-02
GO.0042698	ovulation cycle	9	3.74E-02
GO.0007275	multicellular organismal development	113	3.41E-03
GO.2000026	regulation of multicellular organismal development	53	6.77E-03
GO.0051240	positive regulation of multicellular organismal process	51	1.39E-03
GO.0051241	negative regulation of multicellular organismal process	35	4.36E-02
GO.0051239	regulation of multicellular organismal process	79	2.61E-04
GO.0044700	single organism signaling	125	2.25E-02
GO.0044767	single-organism developmental process	122	7.78E-03
GO.0044708	single-organism behaviour	22	5.50E-03

For the Cellular Components, The GO analyses identified 56 pathways, of which Neuron Part being the most enriched pathway (FDR 2.89E-08) with 57 genes involved (Table 5.5). The affected cellular components include neuron projection, synapse, cell membrane, channels and transporters, extracellular matrix and Golgi.

Table 5.5. Cellular components GO groups for 429 differentially expressed gene in *NRXN1α* heterozygous deletion.

Pathway ID	Pathway description	Gene Count	FDR
	Neuron		
GO.0042995	cell projection	69	4.35E-07
GO.0043005	neuron projection	43	3.12E-06
GO.0097458	neuron part	57	2.89E-08
GO.0043025	neuronal cell body	28	2.97E-06
	Synapse		
GO.0045202	synapse	35	5.48E-06
GO.0044456	synapse part	30	1.53E-05
GO.0030672	synaptic vesicle membrane	6	2.14E-02
GO.0098793	presynapse	13	4.57E-04
GO.0048788	cytoskeleton of the presynaptic active zone	2	1.46E-02
GO.0098831	presynaptic active zone cytoplasmic	2	1.46E-02
GO.0098794	postsynapse	20	1.33E-03
GO.0030425	dendrite	22	2.83E-03

GO.0036477	somatodendritic compartment	33	1.91E-05
GO.0097440	apical dendrite	3	2.88E-02
GO.0008021	synaptic vesicle	10	8.03E-03
GO.0031982	vesicle	100	4.67E-03
GO.0044433	cytoplasmic vesicle part	27	5.86E-04
GO.0031988	membrane-bounded vesicle	99	2.57E-03
GO.0016023	cytoplasmic membrane-bounded vesicle	38	5.15E-03
	Membrane		
GO.0016020	membrane	206	1.33E-03
GO.0044425	membrane part	158	5.51E-03
GO.0005886	plasma membrane	142	2.97E-07
GO.0044459	plasma membrane part	82	5.02E-06
GO.0009986	cell surface	28	1.44E-02
GO.0098805	whole membrane	55	3.98E-02
GO.0031224	intrinsic component of membrane	140	1.11E-02
GO.0031226	intrinsic component of plasma membrane	65	1.68E-06
GO.0016021	integral component of membrane	136	1.67E-02
GO.0005887	integral component of plasma membrane	64	1.16E-06
GO.0098797	plasma membrane protein complex	32	3.80E-07
GO.0098796	membrane protein complex	40	2.20E-04
GO.0005604	basement membrane	10	9.79E-04
GO.0030054	cell junction	43	9.57E-04
GO.0043235	receptor complex	18	1.30E-03
GO.0098802	plasma membrane receptor complex	12	2.73E-03
	Channels and transporters		
GO.1902495	transmembrane transporter complex	23	5.02E-06
GO.0034702	ion channel complex	22	3.12E-06
GO.0034703	cation channel complex	14	2.20E-04
GO.0034705	potassium channel complex	8	7.58E-03
GO.0008076	voltage-gated potassium channel complex	9	1.69E-03
GO.0005891	voltage-gated calcium channel complex	5	2.65E-02
	Extracellular matrix		
GO.0044421	extracellular region part	102	6.44E-03
GO.0005576	extracellular region	115	1.46E-02
GO.0031012	extracellular matrix	28	5.64E-07
GO.0044420	extracellular matrix component	13	8.05E-05
GO.0005578	proteinaceous extracellular matrix	25	3.22E-06
GO.0005615	extracellular space	47	1.33E-03
GO.0005614	interstitial matrix	4	5.15E-03
	Golgi		
GO.0005794	Golgi apparatus	46	1.42E-02
GO.0044431	Golgi apparatus part	31	1.46E-02
GO.0000139	Golgi membrane	25	2.48E-02
	Others		
GO.0071944	cell periphery	144	2.97E-07
GO.0044297	cell body	29	5.48E-06

GO.0042383	sarcolemma	11	1.02E-03
GO.0072562	blood microparticle	8	4.98E-02
GO.0001527	microfibril	3	2.88E-02

In molecular function GO, groups, there were 16 significant pathways with voltage-gated ion channel activity (FDR 7.30E-06) and calcium ion binding being the most enriched ones (FDR 7.30E-06) (Table 5.6). The 16 significant pathways are centred on channel activities, calcium signalling and transporter activities.

Table 5.6. Molecular function GO groups of 429 differentially expressed genes in *NRXN1α* heterozygous deletion.

Pathway ID	Pathway description	Gene Count	FDR
	Channel activity		
GO.0005244	voltage-gated ion channel activity	19	7.30E-06
GO.0005216	ion channel activity	21	7.20E-03
GO.0022843	voltage-gated cation channel activity	16	5.69E-05
GO.0005261	cation channel activity	18	7.20E-03
GO.0015267	channel activity	23	2.88E-03
GO.0022838	substrate-specific channel activity	22	3.99E-03
GO.0022836	gated channel activity	25	7.30E-06
GO.0005249	voltage-gated potassium channel activity	9	2.27E-02
	Calcium signalling		
GO.0005509	calcium ion binding	40	7.30E-06
GO.0015085	calcium ion transmembrane transporter activity	10	4.92E-02
GO.0005245	voltage-gated calcium channel activity	6	4.92E-02
	Transporter activity		
GO.0046873	metal ion transmembrane transporter activity	24	1.20E-03
GO.0015075	ion transmembrane transporter activity	31	3.19E-02
GO.0022891	substrate-specific transmembrane transporter activity	33	2.29E-02
GO.0022857	transmembrane transporter activity	34	3.73E-02
GO.0005215	transporter activity	40	4.92E-02

In order to narrow down the number of GO pathways and identify the most significant pathways with most overlapped genes, the 530 *NRXN1α* targets were evaluated by the Gene Set Enrichment Analysis (GSEA). The top 10 GO pathways were identified by GSEA were presented in Table 5.7, and they were largely clustered around membrane protein signalling, transport and synapse signalling. Some of the top genes which overlap the most among these pathways included *CACNA1A* (90%), *SHANK1* (80%) and KCNC4 (80%).

Table 5.7. The top 10 GO pathways from GSEA.

Gene Set Name	Genes in overlap	FDR
Intrinsic component of plasma membrane	84	1.16E-31
Plasma membrane protein complex	43	1.06E-23
Cell cell signalling	49	4.76E-22
Neuron part	71	5.26E-29
Regulation of transport	83	1.42E-28
Cell development	68	8.73E-24
Cell projection	73	5.16E-22
Synapse	50	3.33E-23
Synapse signalling	38	6.61E-22
Synapse part	43	6.56E-21

The Kyoto Encyclopedia of Genes and Genomes (KEGG) pathway analysis of the 530 genes by the GSEA showed that MAPK signalling, calcium signalling and neuroactive ligand-receptor interaction are the top three significant pathways (Table 5.8). Taken together, different bioinformatic analyses collectively showed that synapses, ion channels and transporter activity, calcium signalling, MAPK pathways are the major pathways associated with *NRXN1α* deletions.

Table 5.8. KEGG pathway analysis in GSEA.

Gene Set Name	Genes in Overlap	Name of the overlapped genes	FDR
MAPK signalling	17	*CACNA1A, CACNA1I, CACNA2D1, CACNA2D2, CACNG2, CACNG3, FGF12, FGF17, GADD45B, PDGFA, PDGFRA, PLA2G4A, PTPN5, RASGRF1, RRAS, TGFB2, TGFBR2*	3.50E-07
Calcium signalling	13	*ADCY1, ADRB2, CACNA1A, CACNA1I, CAMK2B, CD38, CHRM2, GRM1, HRH1, ITPKB, PDGFRA, SLC8A2, SLC8A3*	2.83E-06
Neuroactive ligand receptor interaction	14	*CACNA1A, CACNA1I, CHRNA4, CHRNB2, F2RL2, GABRA1, GABRE, GRIN3B, HCRTR2, HTR1D, PDGFRA, S1PR3, SSTR1*	4.21E-05
Complement and coagulation cascades	7	*C1R, C1S, C6, CD55, CFB, PROS1, SERPING1*	2.24E-04
Pathways in cancer	14	*CDKN1A, CDKN2A, EPAS1, FGF12, FGF17, PAX8, PDGFA, PDGFRA, PTCH2, RUNX1, TCF7, TGFB2, TGFBR2, WNT7A*	2.24E-04

5.3.2 *NRXN1α* deletion disrupts the ion channels/transporter activity in iPSC derived neurons

There are a series of pathways which are disrupted in Biological Processes (GO) groups. Among these, the regulation of ion channels and transporter activity are strongly associated. These included: regulation of ion transmembrane transport (GO.0034765, FDR 4.90E-05, 27 genes), regulation of ion transport (GO.0043269, FDR 5.63E-05, 34 genes), metal ion transport (GO.0030001, FDR 1.09E-04, 33 genes), calcium ion transport (GO.0006816, FDR 7.78E-03, 15 genes), inorganic ion transmembrane transport (GO.0098660, FDR 9.27E-03, 27 genes), potassium ion transport (GO.0006813, FDR 3.35E-02, 11 genes), ion transmembrane transport (GO.0034220, FDR 4.59E-02, 31 genes) and ion transport (GO.0006811, FDR 4.79E-02, 39 genes).

There were a total of 60 genes associated with these eight pathways. Among them, 16 genes were upregulated, and 44 genes were downregulated in *NRXN1α* deletion neurons (Figure 5.7C). Some genes were overlapped genes among the eight pathways (Figure 5.7B), and the most overlapped genes were *KCNK12*, *KCNJ8*, *KCNIP1*, *KCNH3*, *KCNF1*, *KCNC4*, *KCNB2*, *KCNA3*, *CACNG3*, *CACNG2*, *CACNA2D1*, *SCN8A* and *HCN2*. They were all linked to potassium, calcium or sodium voltage-gated channel activity (Figure 5.7B). Surprisingly, only *KCNJ8* was down-regulated and all other 12 mostly shared genes were up-regulated, suggesting an increased ion transport activity.

(A)

Pathway ID	Pathway description	Gene Count	FDR
GO.0034765	regulation of ion transmembrane transport	27	4.90E-05
GO.0043269	regulation of ion transport	34	5.63E-05
GO.0030001	metal ion transport	33	1.09E-04
GO.0006816	calcium ion transport	15	7.78E-03
GO.0098660	inorganic ion transmembrane transport	27	9.27E-03
GO.0006813	potassium ion transport	11	3.35E-02
GO.0034220	ion transmembrane transport	31	4.59E-02
GO.0006811	ion transport	39	4.79E-02

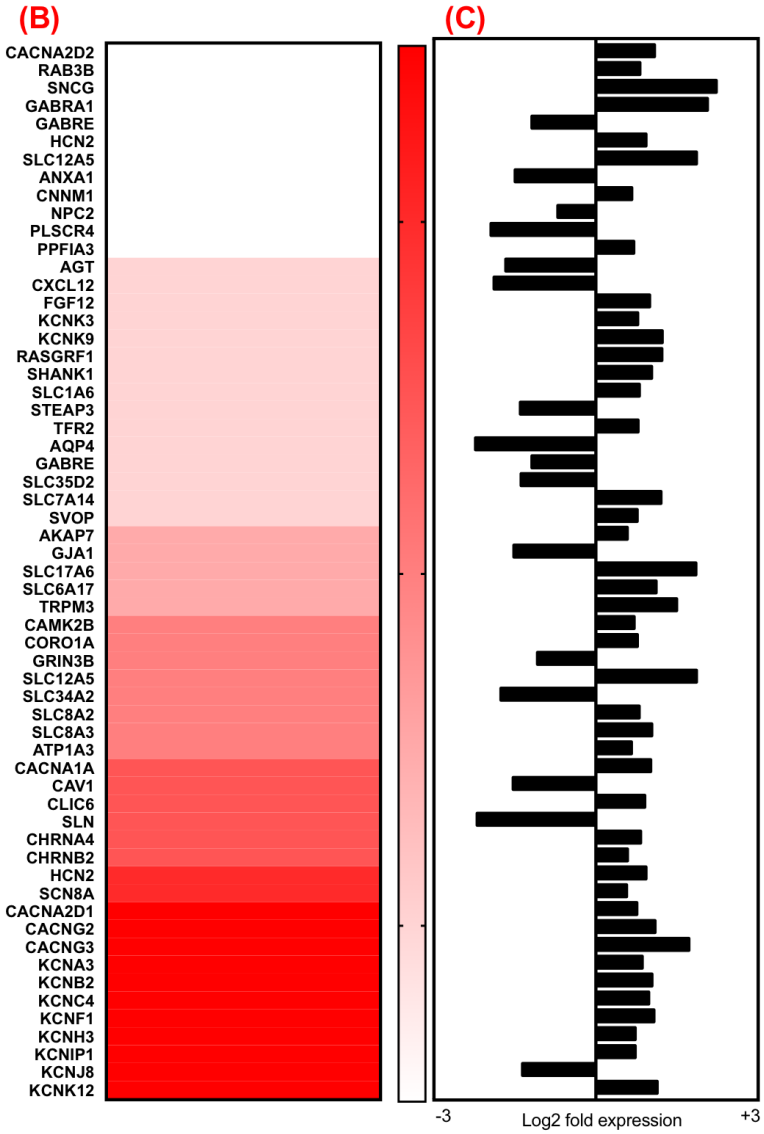

Figure 5.7. Significant pathways associated with ion transport in NRXN1α deletion neurons. (A) The listed eight pathways involved in Biological Processes of (GO) group that was linked to ion transport with their FDR and observed number of genes. (B) The heatmap represented all genes which were linked to the eight pathways. The colour showed the most overlapped genes (darker red) to non-overlapped genes (white) among the pathways. (C) Upregulation (on the right) and downregulation (on the left) of genes were shown with Log_2 fold expression.

Ion channel transporter activity was also impaired in *NRXN1α* deletion neurons. Almost 94% of pathways (15 out of 16 pathways) disrupted in Molecular Function GO groups were involved in ion transporter activity (Figure 5.8A). There were 42 genes that were involved and associated with these pathways, in which 86% of them overlapped among pathways (Figure 5.8B). Genes associated with voltage-gated potassium (*KCNK12, KCNJ8, KCNIP1, KCNH3, KCNF1, KCNC4, KCNB2, KCNA3, HCN2*), sodium (*SCN8A*) and calcium (*CACNA1A, CACNG3, CACNG2, CACNA2D1, CACNA2D1*) ion channels are the most overlapped genes (Figure 5.8B). Remarkably, out of the 16 most overlapped genes, 15 (*KCNK12* 2.2x, *KCNIP1* 1.7x, *KCNH3* 1.7x, *KCNF1* 2.1x, *KCNC4* 2.0x, *KCNB2* 2.0x, *KCNA3* 1.8x, *HCN2* 1.9x, *SCN8A* 1.5x, *CACNA1A* 2.02x, *CACNG3* 3.29x, *CACNG2* 2.13x, *CACNA2D1* 1.69x, *CACNA2D2* 2.18x) were upregulated and only 1 gene (*KCNJ8*, 50%) was downregulated (Figure 5.8C). These results suggest that there is a disruption in the balance of the influx or efflux of ions across the membrane.

Among the most enriched genes associated with voltage-gated potassium transport and transporter activity, only *KCNJ8* was downregulated, whereas other associated members of voltage-gated potassium channels (*KCNA3, KCNB2, KCNC4, KCNF1, KCNH3, KCNIP1*) were upregulated. The *SCN8A* is a voltage-gated sodium channel, essential for membrane depolarization and neuronal excitability.

In terms of voltage-gated calcium channels (VGCCs), five of the members (*CACNA2D1, CACNA2D2, CACNA1A, CACNG2, CACNG3*) enriched in both transport and transporter activity were significantly upregulated in *NRXN1α* deletion (Figure 5.8B). Consistently, an impairment in regulation of ion transport (FDR 1.42E-28) has also been observed among the top 10 overlapped GO pathways (Table 5.7).

(A)

Pathway ID	Pathway description	Gene Count	FDR
GO.0005244	voltage-gated ion channel activity	19	7.30E-06
GO.0005509	calcium ion binding	40	7.30E-06
GO.0022836	gated channel activity	25	7.30E-06
GO.0022843	voltage-gated cation channel activity	16	5.69E-05
GO.0046873	metal ion transmembrane transporter activity	24	1.20E-03
GO.0015267	channel activity	23	2.88E-03
GO.0022838	substrate-specific channel activity	22	3.99E-03
GO.0005216	ion channel activity	21	7.20E-03
GO.0005261	cation channel activity	18	7.20E-03
GO.0005249	voltage-gated potassium channel activity	9	2.27E-02
GO.0022891	substrate-specific transmembrane transporter activity	33	2.29E-02
GO.0015075	ion transmembrane transporter activity	31	3.19E-02
GO.0022857	transmembrane transporter activity	34	3.73E-02
GO.0005215	transporter activity	40	4.92E-02
GO.0005245	voltage-gated calcium channel activity	6	4.92E-02
GO.0015085	calcium ion transmembrane transporter activity	10	4.92E-02

(B)

(C)

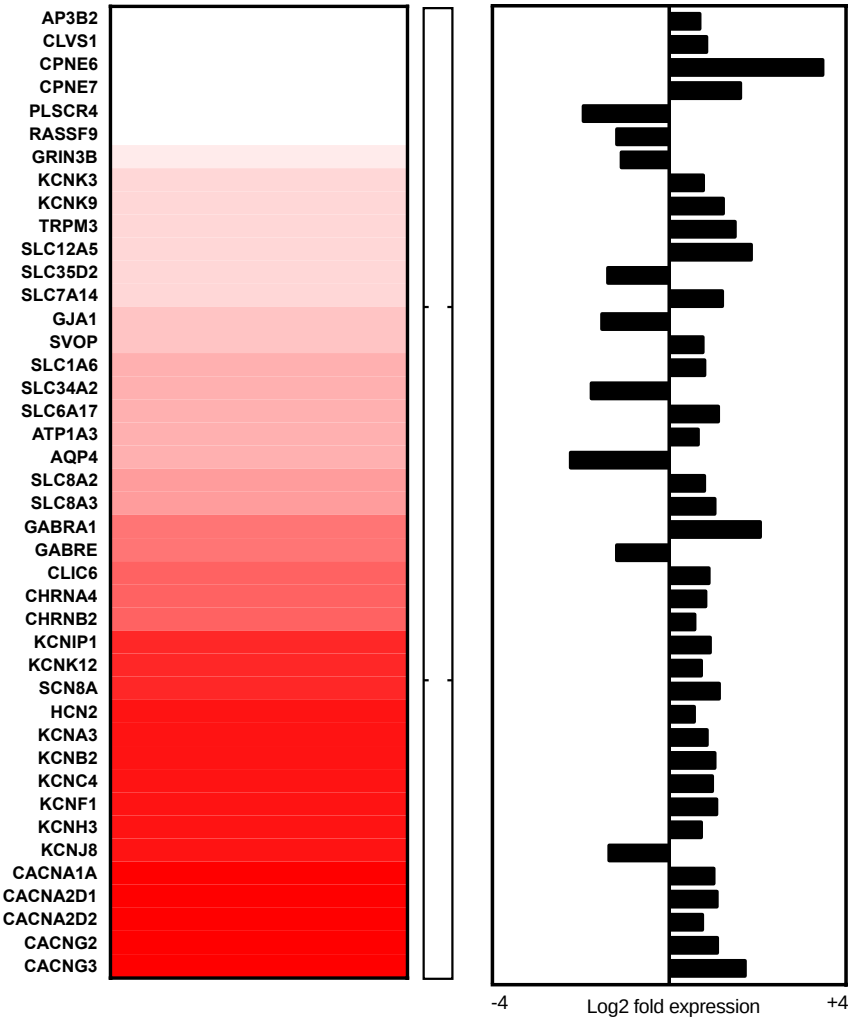

Figure 5.8. Significant pathways associated with ion transporter activity in NRXN1α deletion neurons. (A) The 16 listed pathways in Molecular Function of GO groups are linked to ion transporter activity with their FDR and observed number of genes. (B) The heatmap represents all genes which are linked to the 16 pathways. The colour shows the most overlapped genes in dark red and with no overlapped genes in white. (C) Upregulation (on the right) and downregulation (on the left) of genes associated with these pathways are shown with Log_2 fold expression.

Results from both ion transport and their transporter activity reveal that potassium, sodium and calcium voltage-gated ion channels are disrupted in *NRXN1α* deletion neurons. Among the all 24 pathways, the most overlapped genes included *KCNK12* (20/24 overlapped pathways), *KCNJ8* (20/24 pathways), *KCNIP1* (20/24 pathways), *KCNH3* (20/24 pathways), *KCNF1* (20/24 pathways), *KCNC4* (20/24 pathways), *KCNB2* (20/24 pathways), *KCNA3* (20/24 pathways), *HCN2* (19/24 pathways, *SCN8A* (18/23 pathways),*CACNA1A* (19/23 pathways), *CACNG3* (21/23 pathways), *CACNG2* (21/23 pathways), *CACNA2D1* (21/23 pathways) and *CACNA2D2* (15/23 pathways). Among the 14 shared molecules, only *KCNJ8* was downregulated, and all other 13 *NRXN1α* targets were upregulated, suggesting an important role of *NRXN1α* dosage effects on ion transport activity and potential disruption in electrophysiological function in *NRXN1α* deletion neurons.

Change in Na^+ and K^+ transport and transporter activity would lead to an impairment in exchange of ions across the membrane. Na^+ and K^+ ions are the key elements in propagation and initiation of action potentials. Hence a change in expression of regulatory sodium and potassium ion channel transmembrane transporter activity would cause an alteration in membrane potential. Single cell electrophysiology recording from Chapter 3 showed that there was an apparent alteration in voltage-gated sodium and potassium current in *NRXN1α* deletion neurons. This could result in alterations of action potential characteristics. RNA-Seq results of this study thus showed consistently that the regulation of membrane depolarization was significantly impaired in *NRXN1α* heterozygous deletion neurons.

5.3.3 *NRXN1α* deletion impair the membrane depolarization pathway in iPSC derived neurons

Membrane depolarization (GO.0051899, FDR 3.35E-02, 7 genes) and regulation of membrane potential (GO.0042391, 2.62E-02, 16 genes) were detected as the

significantly altered pathways in Biological Processes (Figure 5.9A). This pathway modulates the establishment of electrical excitability across the membrane. There are five genes which are upregulated in *NRXN1α* deletion neurons (*CHRNB2* 1.5x, *CHRNA4* 1.8x, *CACNG2* 2.1x, *CACNA1A* 2.0), while two genes (*CDKN2A* 28%, CAV1 39%) are downregulated (Figure 5.9B). This gene-ontology term is underneath the "parent" class of "regulation of membrane potential (GO:0042391)" , with 16 differentially expressed genes, with downregulated ADRB2 (27%), *CAV1* (39%), *CDKN2A* (28%) and *GJA1* (22%), and upregulated *AKAP7* (1.7-fold), *TMEM266* (2.2-fold), *CACNA1A* (2.2-fold), *CHRNA4* (2.4-fold), *FGF12* (2.0-fold), *HCN2* (2.1-fold), *KCNH3* (2.0-fold), *KCNK12* (2.8-fold), *KCNK3* (2.0-fold), *KCNK9* (2.3-fold), *SEZ6* (2.1-fold), SLC1*A6* (1.9-fold) in the *NRXN1α* deletion neurons.

(A)

Gene symbol	Full gene name	FDR	log_2 fold
CACNA1A	Calcium Voltage-Gated Channel Subunit Alpha1 A	1.200E-02	1.013
CACNG2	Calcium Voltage-Gated Channel Auxiliary Subunit	1.107E-06	1.093
CAV1	Caveolin 1	3.654E-04	-1.53
CDKN2A	Cyclin Dependent Kinase Inhibitor 2A	2.597E-06	-2.008
CHRNA4	Cholinergic Receptor Nicotinic Alpha 4 Subunit	1.200E-02	0.824
CHRNB2	Cholinergic Receptor Nicotinic Beta 2 Subunit	1.800E-02	0.581
TMEM266	Transmembrane protein 266	1.612E-02	1.11

(B)

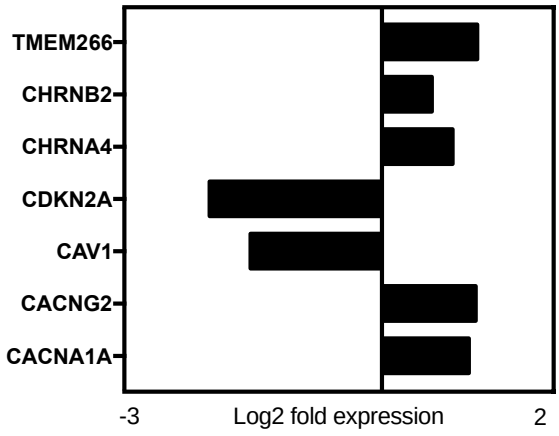

Figure 5.9. Membrane depolarization pathway is affected in NRXN1α deletion neurons. (A) Six gene was found to be significantly and differentially expressed in *NRXN1α* deletion iPSC derived neurons relating to membrane depolarization pathway. (B) Upregulation (on the right) and downregulation (on the left) of genes associated with this pathway are shown with Log2 fold expression.

CACNA1A is a voltage-gated calcium channel that plays an essential role in the influx of calcium ions and an essential role in neurotransmitter release and is also associated with membrane depolarization. In addition, *CACNA1A* also appears as one of the most enriched genes in ion transporter activity in *NRXN1α* deletion neurons. *CACNG2* is also voltage-gated calcium channel, in which the protein encoded by this gene in AMPA receptor regulatory proteins that have a role in AMPA transmembrane trafficking and gating. This result suggests that alteration in expression of post-synaptic glutamatergic receptors i.e. AMPA may have a consequence on posy-synaptic response and hence the depolarization of the presynaptic membrane.

5.3.4 *CACNA1A* is the most overlapped gene in gene enrichment analysis among all pathways

The STRING Pathway analysis showed an association of *NRXN1α* deletion neurons with voltage-gated calcium channels (*CACNA1A*, *CACNA2D1*, *CACNA2D2*, *CACNG2*, *CACNG3*) in ion transport and transporter activity (Figure 5.8). In the GSEA analysis, among the all biological processes, molecular function and cellular components (Figure 5.10A), *CACNA1A* is identified as the most overlapped genes in the top 20 pathways (Figure 5.10B). This confirms that *CACNA1A* is a core regulator of various neuronal pathways.

(A)

Gene Set Name	Genes in Overlap	FDR
GO-Neuron part	71	5.26E-29
GO- Cell projection	73	5.16E-22
GO-Neuron projection	52	8.09E-21
GO- Somatodendritic compartment	40	1.74E-17
GO- Neurogenesis	58	1.44E-17
GO- Synaptic signaling	38	6.61E-22
GO- Synapse	50	3.33E-23
GO- Synapse part	43	6.56E-21
GO-Modulation of synaptic transmission	30	1.87E-18
GO- Regulation of transport	83	1.42E-28
GO-Metal ion transport	38	1.97E-17
GO- Calcium ion binding	44	1.28E-19

GO-Intracellular vesicle	56	2.94E-18
GO-Cell development	68	8.73E-24
GO- Regulation of cell differentiation	60	1.28E-17
GO- Cell cell signaling	49	4.76E-22
GO- Intrinsic component of plasma	84	1.16E-31
GO- membrane protein complex	52	2.42E-19
GO- Plasma membrane protein complex	43	1.06E-23
GO- Response to endogenous stimulus	60	3.41E-18

(B)

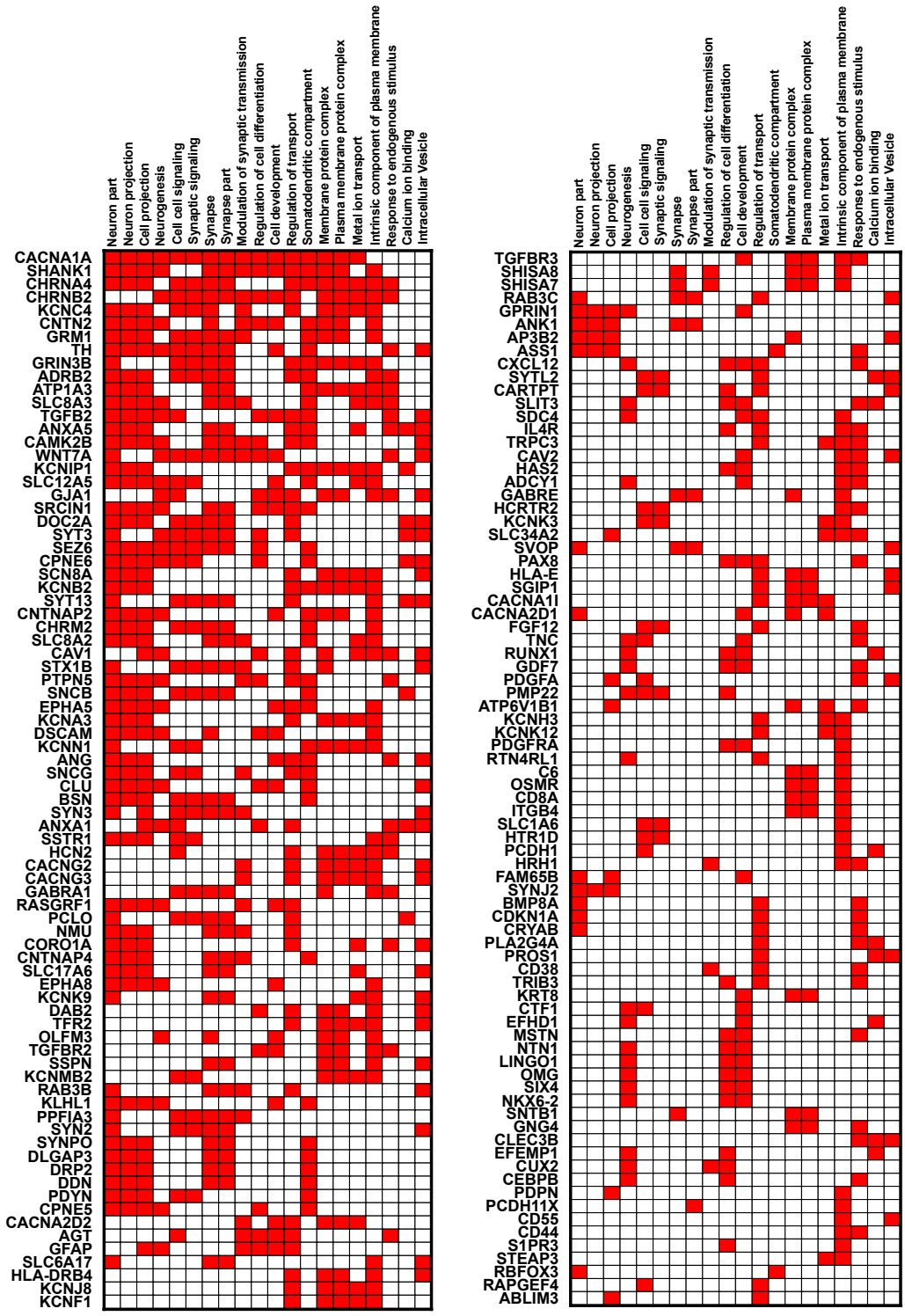
Neuron part
Neuron projection
Cell projection
Neurogenesis
Cell cell signaling
Synaptic signaling
Synapse
Synapse part
Modulation of synaptic transmission
Regulation of cell differentiation
Cell development
Regulation of transport
Somatodendritic compartment
Membrane protein complex
Plasma membrane protein complex
Metal ion transport
Intrinsic component of plasma membrane
Response to endogenous stimulus
Calcium ion binding
Intracellular Vesicle
CACNA1A
SHANK1
CHRNA4
CHRNB2
KCNC4
CNTN2
GRM1
TH
GRIN3B
ADRB2
ATP1A3
SLC8A3
TGFB2
ANXA5
CAMK2B
WNT7A
KCNIP1
SLC12A5
GJA1
SRCIN1
DOC2A
SYT3
SEZ6
CPNE6
SCN8A
KCNB2
SYT13
CNTNAP2
CHRM2
SLC8A2
CAV1
STX1B
PTPN5
SNCB
EPHA5
KCNA3
DSCAM
KCNN1
ANG
SNCG
CLU
BSN
SYN3
ANXA1
SSTR1
HCN2
CACNG2
CACNG3
GABRA1
RASGRF1
PCLO
NMU
CORO1A
CNTNAP4
SLC17A6
EPHA8
KCNK9
DAB2
TFR2
OLFM3
TGFBR2
SSPN
KCNMB2
RAB3B
KLHL1
PPFIA3
SYN2
SYNPO
DLGAP3
DRP2
DDN
PDYN
CPNE5
CACNA2D2
AGT
GFAP
SLC6A17
HLA-DRB4
KCNJ8
KCNF1
TGFBR3
SHISA8
SHISA7
RAB3C
GPRIN1
ANK1
AP3B2
ASS1
CXCL12
SYTL2
CARTPT
SLIT3
SDC4
IL4R
TRPC3
CAV2
HAS2
ADCY1
GABRE
HCRTR2
KCNK3
SLC34A2
SVOP
PAX8
HLA-E
SGIP1
CACNA1I
CACNA2D1
FGF12
TNC
RUNX1
GDF7
PDGFA
PMP22
ATP6V1B1
KCNH3
KCNK12
PDGFRA
RTN4RL1
C6
OSMR
CD8A
ITGB4
SLC1A6
HTR1D
PCDH1
HRH1
FAM65B
SYNJ2
BMP8A
CDKN1A
CRYAB
PLA2G4A
PROS1
CD38
TRIB3
KRT8
CTF1
EFHD1
MSTN
NTN1
LINGO1
OMG
SIX4
NKX6-2
SNTB1
GNG4
CLEC3B
EFEMP1
CUX2
CEBPB
PDPN
PCDH11X
CD55
CD44
S1PR3
STEAP3
RBFOX3
RAPGEF4
ABLIM3

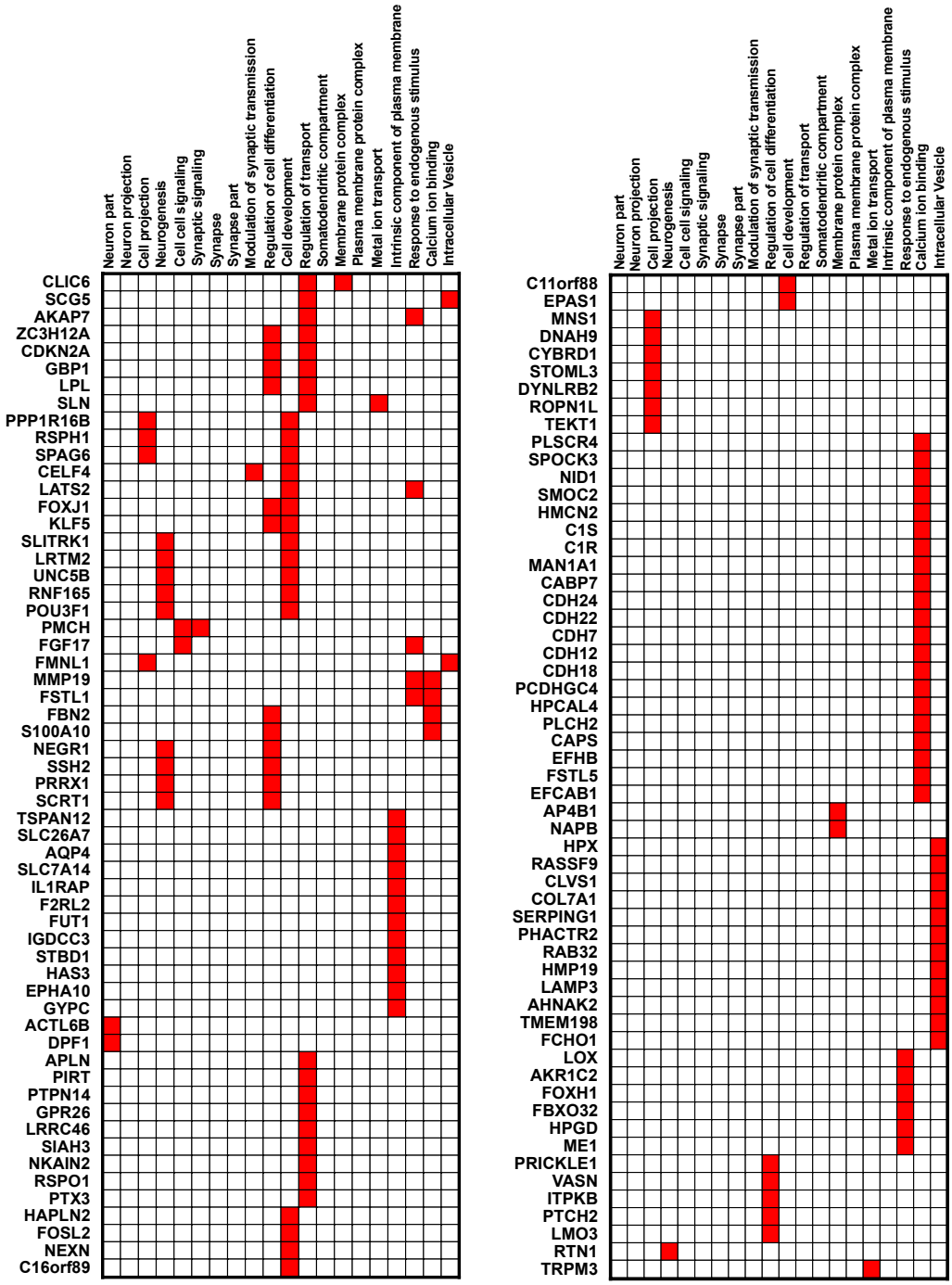

Figure 5.10. Gene enrichment analysis by GSEA among all biological processes, molecular function and cellular component. (A) The top 20 overlapped significant pathways identified by GSEA from 530 differential expressed genes in *NRXN1α* deletion neurons. (B) *CACNA1A* was identified as the most overlapped genes among the top 20 pathways with 275 overlapped genes. In the heatmap, the genes appeared in the pathway were filled in red and genes not appeared in the pathways are indicated in white.

5.3.5. *NRXN1α* deletion impair synaptic vesicle exocytosis and neurotransmitter release

A series of pathways were disrupted in biological processes and cellular components which were associated with vesicle release and neurotransmitter release and secretion (Figure 5.11A). There are 104 genes which are involved in these pathways. Among them *SYT3* (2.02-fold) is the most overlapped gene and contributes to all ten pathways. This is followed by RAB3B (1.75-fold), and *RAB3C* (2.04-fold), associate in 90% of pathways and *SYTL2* (-3.07fold), *SYT13* (2.17-fold), *PCLO* (1.87-fold) and *DOC2A* (1.59-fold) contribute in 70% of the pathways (Figure 5.11B, C).

(A)

Pathway ID	Pathway description	Gene Count	FDR
GO.0044433	cytoplasmic vesicle part	27	4.540E-04
GO.0006836	neurotransmitter transport	14	7.720E-04
GO.0007269	neurotransmitter secretion	12	1.510E-03
GO.0031982	vesicle	99	4.420E-03
GO.0008021	synaptic vesicle	10	7.720E-03
GO.0016079	synaptic vesicle exocytosis	8	1.100E-02
GO.0006887	exocytosis	17	1.390E-02
GO.0030672	synaptic vesicle membrane	6	1.950E-02
GO.0048489	synaptic vesicle transport	9	3.750E-02
GO.0097479	synaptic vesicle localization	9	3.980E-02

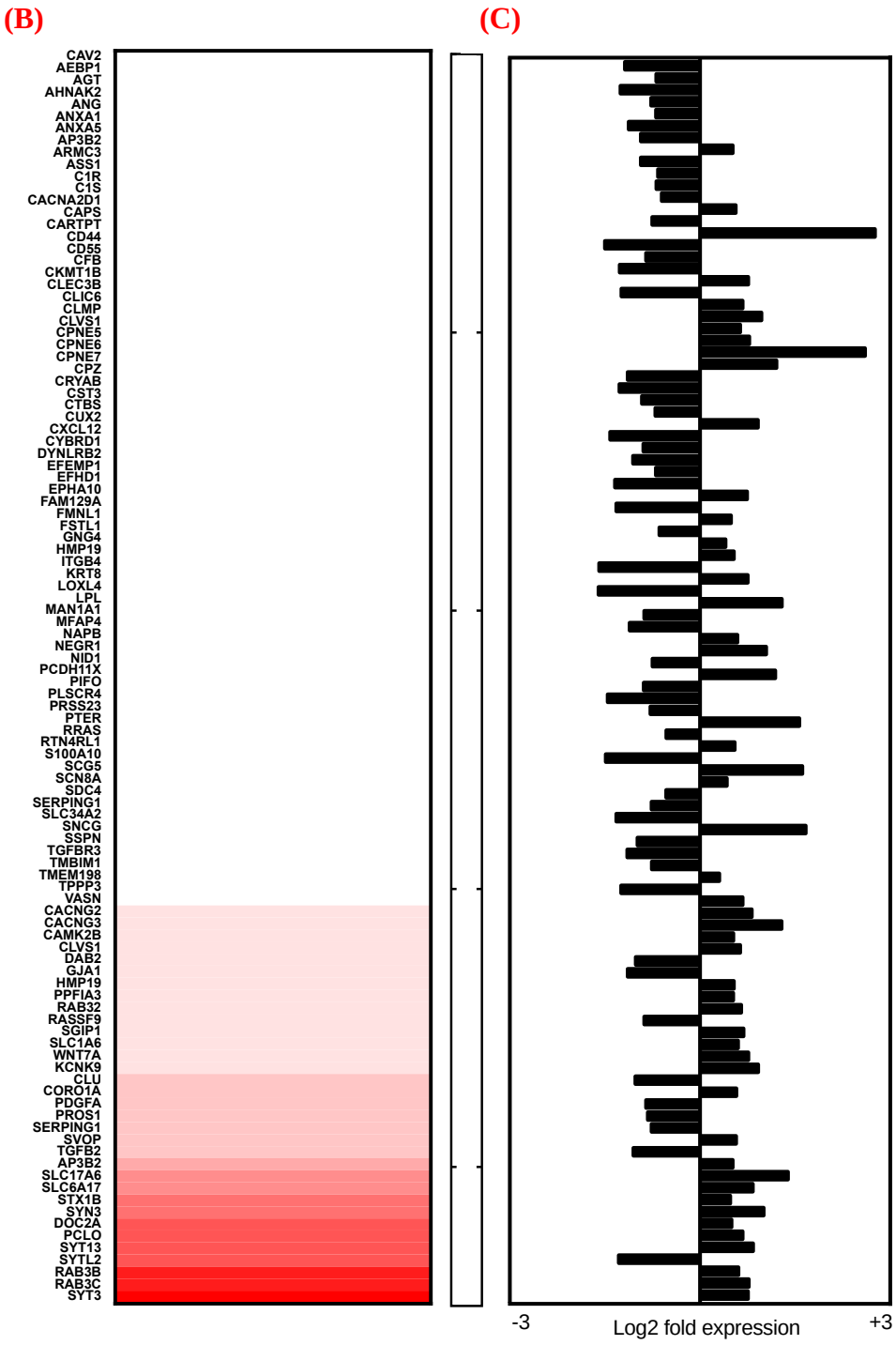

Figure 5.11. Significant pathways associated with vesicle exocytosis in NRXN1α deletion neurons. (A) The ten listed pathways in Biological Function and Cellular Components of GO groups are linked to vesicle exocytosis with their FDR and observed number of the gene. (B) The heatmap represents all genes which are linked to the ten pathways. The colour shows the most overlapped genes in dark red and with no overlapped gene in white. (C) Upregulation (on the right) and downregulation (on the left) of genes associated with these pathways are shown with Log2 fold expression.

KEGG pathway analysis by the GSEA showed that MAPK, calcium signalling, and neuroactive ligand-receptor interaction are the top three significant pathways. Interestingly, *CACNA1A* (Calcium Voltage-Gated Channel Subunit Alpha1 A), *CACNA1I* (Calcium-channel-voltage-dependent-T-type subunit 1I) and *PDGFRA* (Platelet Derived Growth Factor Receptor Alpha) are the only genes overlapped between these MAPK and calcium signalling pathways (Figure 5.12A).The calcium and neuroactive ligand-receptor interaction pathways shared 4 *NRXN1* targets of *GRM1* (Glutamate Metabotropic Receptor 1), *CHRM2* (Cholinergic Receptor Muscarinic 2), *ADRB2* (beta2-adrenoceptor)) and *HRH1* (Histamine Receptor H1) (Figure 5.12).

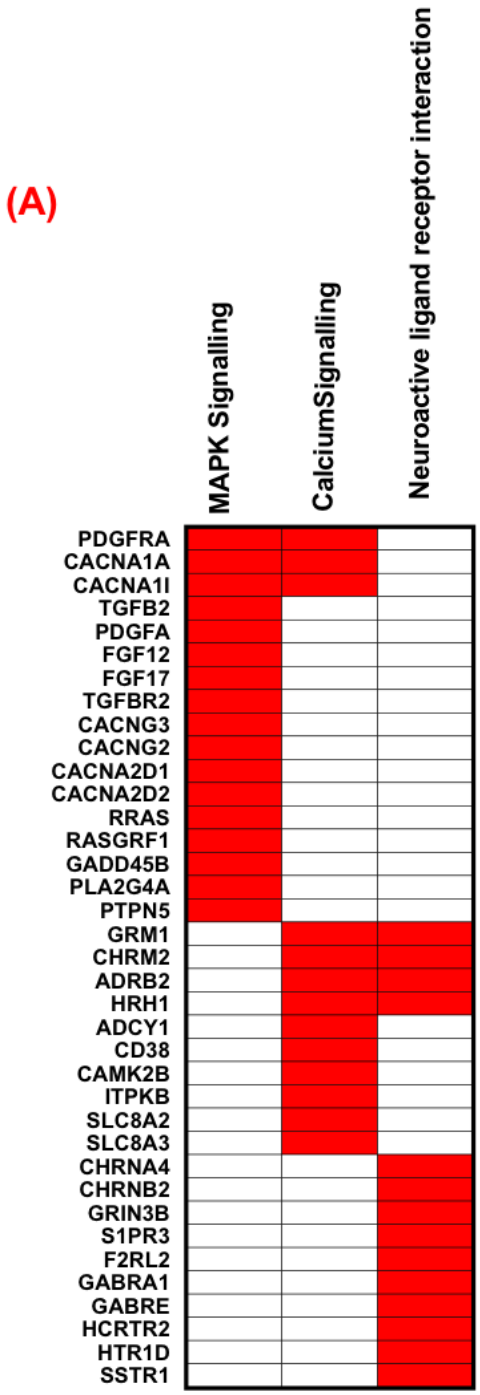

Figure 5.12. KEGG pathway analysis in GSEA. (A) MAPK, calcium signalling, and neuroactive ligand-receptor interaction pathways were identified as the significant pathways impaired in *NRXN1α* deletion neurons. In the heatmap, the genes appeared in the pathway were filled in red and genes not appeared in the pathways are indicated in white. The MAPK and calcium signalling pathways shared three targets of *CACNA1A, CACNA1I* and *PDGFRA*. The calcium signalling and neuroactive ligand-receptor interaction pathways shared 4 *NRXN1* targets of *GRM1, CHRM2, ADRB2* and *HRH1*.

5.3.5 Transcriptome analysis showed an association with important ASD genes

The 530 differential gene expression in *NRXN1α* deletion neurons were compared with the SAFARI database and this led to the identification of 42 ASD risk genes that were previously reported as ASD associated genes (Table 5.9). Among the 42 genes, three (*CACNA1A, CACNA1I* and *SCN8A*) are voltage-gated ion channels. The protein-protein interaction analysis of the 42 genes in STRING indeed showed that calcium imaging (FDR 3.50E-04) as the most significant pathway in KEGG pathways, with 6 genes involved (*ADRB2, CACNA1A, CACNA1I, CAMK2B, CD38, GRM1*) (Figure 5.10). Furthermore, the KEGG pathway analysis in GSEA also shows calcium signalling as the most enriched and significant pathway (FDR 2.32E-06). In addition, four genes are identified to be involved in Adrenergic signalling (*ADRB2, ATP1A3, CAMK2B, RAPGEF4*, FDR=0.026) and three in the GABAergic synapse (*CACNA1A, GABRA1, SLC12A5*, FDR=0.035) (Figure 5.10). The cellular components pathways are largely centred on synapses and cell membrane functions including ion channels, transporter activity and membrane signalling molecules. The major pathways of the Biological Process (GO) are clustered around behaviour, neurogenesis, hormonal response and calcium signalling which are related to ASD dysfunctions.

Table 5.9. The intersection of differential gene analysis with SAFARI genes.

Gene name	FDR	Log2 fold change
ADRB2	2.68E-02	-1.942
ANXA1	2.56E-06	-1.494
ASS1	3.96E-04	-0.884
CD38	1.28E-02	-1.365
CD44	1.90E-08	-1.998
CGNL1	2.36E-02	-0.868
GADD45B	1.67E-02	-1.316
SLIT3	2.42E-02	-0.559
ASXL3	5.66E-03	0.675
ATP1A3	3.62E-02	0.654
AUTS2	2.90E-03	0.981
BRINP1	9.36E-04	0.837
CACNA1A	1.18E-02	1.013
CACNA1I	2.41E-02	1.015
CAMK2B	2.27E-02	0.705
CDH22	4.77E-03	1.559
CELF4	6.80E-05	0.820
CELF6	6.19E-04	0.770
CHD5	4.96E-06	1.427
CNTNAP2	1.11E-07	1.084
CNTNAP4	7.09E-06	2.021

CNTNAP5	2.08E-03	1.724
DLGAP3	9.36E-03	0.869
DSCAM	8.27E-06	0.925
ELAVL2	1.43E-04	1.008
GABRA1	1.56E-06	2.060
GRM1	1.26E-02	1.255
GSTM1	4.64E-02	0.89
HS3ST5	7.91E-03	1.562
LPL	9.26E-07	1.722
PCDH11X	1.11E-02	1.583
PRICKLE1	3.66E-04	0.931
RAPGEF4	8.56E-04	0.943
SCN8A	2.06E-02	0.566
SHANK1	2.37E-07	1.028
SLC12A5	4.33E-09	1.857
SYN2	3.58E-02	0.867
SYN3	3.15E-04	1.342
SYT3	5.95E-04	1.013
TH	1.20E-02	2.083
ZNF804A	7.54E-04	1.174
ZSWIM5	2.22E-02	0.816

Table 5.10. STRING analyses of 42 ASD risk factors shared by NRXN1α deletion neurons and the SAFARI ASD genes.

Pathway ID	**KEGG pathway description**	**Gene count**	**FDR**	**Matching proteins in your network (labels)**
4020	Calcium signaling pathway	6	3.50E-04	*ADRB2, CACNA1A, CACNA1I, CAMK2B, CD38, GRM1*
4261	Adrenergic signaling in cardiomyocytes	4	2.58E-02	*ADRB2, ATP1A3,CAMK2B,RAPGEF4*
4727	GABAergic synapse	3	3.53E-02	*CACNA1A, GABRA1,SLC12A5*
Pathway ID	**Cellular components (GO pathways)**	**Gene count**	**FDR**	**Matching proteins in your network (labels)**
GO.0030425	dendrite	10	9.88E-06	*ADRB2,CACNA1A,CNTNAP2,CNTNAP4,DLGAP3,GRM1,SCN8A,SHANK1,SLC12A5,TH*
GO.0036477	somatodendritic compartment	11	9.98E-06	*ADRB2, ASS1, CACNA1A,CNTNAP2,CNTNAP4,DLGAP3,GRM1,SCN8A,SHANK1,SLC12A5,TH*
GO.0043005	neuron projection	12	1.86E-05	*ADRB2,ASS1,CACNA1A,CNTNAP2,CNTNAP4,DLGAP3,DSCAM,GRM1,SCN8A,SHANK1,SLC12A5,TH*
GO.0044456	synapse part	9	1.35E-04	*ADRB2, CAMK2B,CNTNAP4,DLGAP3,GABRA1,GRM1,SHANK1,SYT3,TH*
GO.0045202	synapse	9	3.08E-04	*ADRB2,CAMK2B,CNTNAP4,DLGAP3,GABRA1,GRM1,SHANK1,SYT3,TH*
GO.0098794	postsynapse	7	4.46E-04	*ADRB2,CAMK2B,DLGAP3,GABRA1,GRM1,SHANK1,SYN3*
GO.0014069	postsynaptic density	5	2.64E-03	*CAMK2B,DLGAP3,GRM1,SHANK1,SYN3*
GO.0097481	neuronal postsynaptic density	3	1.73E-02	*CAMK2B,SHANK1,SYN3*
GO.0030424	axon	5	3.47E-02	*ADRB2,CNTNAP2,DSCAM,SCN8A,TH*
GO.0097458	neuron part	13	2.29E-05	*ADRB2,ASS1,CACNA1A,CAMK2B,CNTNAP2, DLGAP3,DSCAM,GRM1,SCN8A,SHANK1,SLC12A5,SYT3,TH*
GO.0043025	neuronal cell body	8	2.05E-04	*ADRB2,ASS1,CACNA1A,CNTNAP2,DLGAP3, SCN8A,SLC12A5,TH*

GO.0044459	plasma membrane part	16	2.73E-04	*ADRB2,ANXA1,ATP1A3,CACNA1A,CACNA1I,CNTNAP2,CNTNAP4,DLGAP3,DSCAM,GABRA1,GRM1,PCDH11X,SCN8A,SHANK1,SLC12A5,TH*
GO.1902495	transmembrane transporter complex	7	2.73E-04	*ATP1A3,CACNA1A,CACNA1I,CNTNAP2,GABRA1,SCN8A,SHANK1*
GO.0034702	ion channel complex	6	1.15E-03	*CACNA1A,CACNA1I,CNTNAP2,GABRA1,SCN8A,SHANK1*
GO.0098797	plasma membrane protein complex	7	2.34E-03	*ATP1A3,CACNA1A,CACNA1I,CNTNAP2,GRM1,SCN8A,SHANK1*
GO.0005887	integral component of plasma membrane	11	7.10E-03	*ADRB2,ATP1A3,CD44,CNTNAP2,DSCAM,GABRA1,GRM1,PCDH11X,SCN8A,SHANK1,SLC12A5*
GO.0030054	cell junction	9	1.35E-02	*ANXA1,CD44,CGNL1,CNTNAP4,DLGAP3,GABRA1,SHANK1,SYN3,SYT3*
GO.0005886	plasma membrane	19	1.42E-02	*ADRB2,ATP1A3,CACNA1I,CAMK2B,CD38,CDH22,CNTNAP2,CNTNAP4,DLGAP3,DSCAM,GABRA1,GRM1,LPL,PCDH11X,RAPGEF4,SCN8A,SHANK1,SYT3,TH*
GO.0034703	cation channel complex	4	1.47E-02	*CACNA1A,CACNA1I,CNTNAP2,SCN8A*
GO.0043235	receptor complex	5	1.47E-02	*ADRB2,CD44,GABRA1,GRM1,SHANK1*
GO.0098590	plasma membrane region	8	1.47E-02	*ADRB2,ANXA1,CD44,CNTNAP2,CNTNAP4,DLGAP3,GABRA1,SHANK1*
GO.0098796	membrane protein complex	8	1.73E-02	*ATP1A3,CACNA1A,CACNA1I,CNTNAP2,GABRA1,GRM1,SCN8A,SHANK1*
Pathway ID	**Biological processed (GO) pathways**	**Gene count**	**FDR**	**Matching proteins in your network (labels)**
GO.0007610	behavior	11	2.61E-05	*ADRB2,ATP1A3,AUTS2,CACNA1A,CNTNAP2,DSCAM,GRM1,SCN8A,SHANK1,SLC12A5,TH*
GO.0007626	locomotory behavior	6	5.55E-03	*ATP1A3,CACNA1A,DSCAM,GRM1,SCN8A,TH*
GO.0071625	vocalization behavior	3	5.55E-03	*AUTS2,CNTNAP2,SHANK1*
GO.0030534	adult behavior	5	8.04E-03	*ATP1A3,CACNA1A,CNTNAP2,SCN8A,SHANK1*
GO.0035176	social behavior	3	4.49E-02	*CNTNAP2,SHANK1,TH*
GO.0060004	reflex	3	8.04E-03	*AUTS2,CACNA1A,SHANK1*
GO.0060013	righting reflex	2	4.49E-02	*AUTS2,SHANK1*
GO.0022008	neurogenesis	11	1.94E-02	*ANXA1,CACNA1A,CACNA1I,CAMK2B,CHD5,CNTNAP2,DBC1,SHANK1,SLIT3,SYT3,TH*
GO.0007612	learning	6	6.28E-04	*ADRB2,ATP1A3,CNTNAP2,SHANK1,SLC12A5,TH*
GO.0007399	nervous system development	14	7.83E-03	*ANXA1,CACNA1A,CACNA1I,CAMK2B,CDH22,CHD5,CNTNAP2,DBC1,PRICKLE1,SCN8A,SHANK1,SLIT3,SYT3,TH*
GO.0048699	generation of neurons	10	4.49E-02	*CACNA1A,CACNA1I,CAMK2B,CHD5,CNTNAP2,DBC1,SHANK1,SLIT3,SYT3,TH*
GO.0050877	neurological system process	11	8.04E-03	*ADRB2,ATP1A3,CACNA1A,CACNA1I,CAMK2B,CNTNAP2,GRM1,SCN8A,SHANK1,SLC12A5,TH*
GO.0048813	dendrite morphogenesis	3	4.49E-02	*CACNA1A,DSCAM,SHANK1*
GO.0050804	modulation of synaptic transmission	7	1.38E-03	*CACNA1A,CD38,CELF4,CNTNAP4,GRM1,SHANK1,SYN3*
GO.0007270	neuron-neuron synaptic transmission	4	7.83E-03	*ADRB2,CACNA1A,GABRA1,TH*
GO.0007268	synaptic transmission	8	8.04E-03	*ADRB2,CAMK2B,GABRA1,GRM1,SLC12A5,SYN3,SYT3,TH*
GO.0048545	response to steroid hormone	7	8.04E-03	*ADRB2,ANXA1,ASS1,ATP1A3,CD38,SLIT3,TH*
GO.0051384	response to glucocorticoid	5	8.04E-03	*ADRB2,ANXA1,ASS1,SLIT3,TH*
GO.0043627	response to estrogen	5	2.25E-02	*ADRB2,ANXA1,ASS1,CD38,TH*

GO.0050905	neuromuscular process	4	2.52E-02	*CACNA1A,CAMK2B,SCN8A,SHANK1*
GO.0032355	response to estradiol	4	4.49E-02	*ANXA1,ASS1,CD38,TH*
GO.0023061	signal release	5	1.74E-02	*ANXA1,CACNA1A,RAPGEF4,SYN3,SYT3*
GO.0007267	cell-cell signaling	9	2.25E-02	*ANXA1,CAMK2B,GABRA1,GRM1,RAPGEF4, SLC12A5,SYN3,SYT3,TH*
GO.0017156	calcium ion-dependent exocytosis	3	1.94E-02	*CACNA1A,RAPGEF4,SYT3*

5.4 Discussion

Neurodevelopmental disorders such as epilepsy, ASD and schizophrenia are multi-factorial disorders and represent a major challenge to find complex molecular mechanisms, because of genetic heterogeneity and environmental effects. The heritability in ASD probands suggests a strong association of genetic components in this disorder (Bailey et al. 1995). Forty-two genes from our differential study have been identified in SAFARI database as ASD risk factors, representing the association of ASD genetic risk factors in iPSC derived neurons from *NRXN1α* deletion patients. Clinically, 30-46% of people with ASD also display co-morbidity with some form of epilepsy (Lee et al. 2014). In this study, the clinical records showed that both the ASD probands for cell line ND1C1 and ND4-1C1 displayed a history of seizures and epilepsy in association with their *NRXN1α* gene deletion.

The iPSCs were generated from a skin biopsy of ASD cases with *NRXN1α* deletion, and 100-day neurons were derived and compared with cells from healthy controls with no *NRXN1α* lesion. 530 genes were found to be differentially expressed in *NRXN1α* deletion neurons. Different approach was additionally performed using different cut off point (i.e. 2-fold up and down-regulation) (data not shown). This were resulted to 426 differentially expressed genes in *NRXN1α* deletion neurons in which the same GO groups and pathways were identified.

The STRING Biological Processes (GO) have identified 8 and 15 pathways which are involved in the regulation of ion transport and transporter activity, respectively (Figure 5.7A, 8A). Among these pathways, some genes are essentially associated with the transport, regulation of ions and their transporter activity across the cell membrane. The most overlapped genes in both ion transport and transporter activity are *SCN8A* (FDR 2.056E-02, 1.5x), *HCN2* (FDR 1.804E-03, 1.9x), *KCNA3* (FDR 4.061E-03, 1.8x), *KCNB2* (FDR 2.400E-02, 2.0x), *KCNC4* (FDR 8.110E-03, 2.0x), *KCNF1* (FDR 3.119E-02, 2.1x), *KCNH3* (FDR 1.472E-02, 1.7x) , *KCNIP1* (2.681E-02, 1.7x), *KCNJ8* (FDR 1.572E-05, 50%), *KCNK12* (FDR 3.410E-05, 2.2x), *CACNA1A* (FDR 1.182E-02, 2.0x), *CACNG2* (FDR 1.107E-06, 2.1x) and *CACNG3* (FDR 1.881E-02, 3.3x) (Figure 5.6B, 7B). These are voltage-gated sodium (*SCN8A*, 1.7x), potassium (*KCNK12* 2.2x, *KCNJ8* 50%, *KCNIP1* 1.8x, *KCNH3* 1.7x, *KCNF1* 2.1x, *KCNC4* 2.0x,

KCNB2 2.0x, *KCNA3* 1.8x, *HCN2* 1.9x) and calcium (*CACNA1A* 2.0x, *CACNG3* 3.3x, *CACNG2* 2.1x, *CACNA2D1* 1.7x, *CACNA2D2* 2.1x) channels, respectively. The fact, that only one of these differentially expressed mRNA (*KCNJ8*) was reduced, whereas all other were upregulated, suggested an elevated ion channel/transporter activity in *NRXN1α* heterozygous neurons as a whole.

There is a mounting body of evidence that a number of ion channel genes are involved in ASD (Schmunk and Gargus 2013). The entry of ion across the plasma membrane modulates a variety of cell function, such as propagation and initiation of the action potential, vesicle release and exocytosis. Therefore, a defect in genes associated with these ion channels will have profound effects on neuronal functions. In the present work, whole genome sequencing from iPSC-derived *NRXN1α* deletion neurons and controls were compared, and data suggest Voltage-gated sodium channels (VGSCs), Voltage-gated potassium channel (VGKCs) and voltage-gated calcium channels (VGCCs) are dysregulated in *NRXN1α* deletion neurons.

Change of a voltage-gated sodium channel (*SCN8A*) in *NRXN1α* deletion neurons

Alterations in sodium channel properties have been identified in many neurological disabilities. Voltage-gated sodium channels (VGSC) are mandatory for modulating neuronal excitability by setting an action potential threshold and inducing depolarization. Our study showed that expression of *SCN8A*, a member of VGSC, was significantly (1.5-fold) increased in *NRXN1α* deletion neurons (FDR 2.056E-02).

Expression of *Scn8a* in mouse hippocampus model was increased following epilepticus, suggesting that this gene might contribute to some form of epilepsy such as temporal lope epilepsy (Wong et al. 2018). On the other hand, knockdown of *Scn8a* in mice prevented the induction of spontaneous seizures (Wong et al. 2018). Heterozygous loss of function of *SCN8A* was also found to increase the resistance to both electrically and pharmacologically induced seizures (Martin et al. 2007). Also the animal model with mutation in a member of the Scn8a family, *Scn2a*, exhibited epilepsy with repetitive behaviors (Kearney et al. 2001), whereas a subtle increase in *Scn2a* current generates a seizure in a transgenic Q54 mice model, a mutation linked to the S4-S5 domain of *Scn2a* (Kearney et al. 2001). A 10 mV shift in voltage dependence activation of a mouse model of *Scn8a* significantly modify the firing

patterns of neurons in Purkinje cells (Escayg et al. 2000; Spampanato et al. 2001). These data demonstrated a key role of VGSC in neuronal excitability and contribution to spontaneous seizure hyperactivity, and increased expression *SCN8A* as a member of VGSCs is likely to play a role in the susceptibility of ASD and associated epilepsy.

Though there is no direct association for some subunits of VGSCs with ASD, their implication in multiple forms of epileptic encephalopathies have been investigated and reported (Scheffer et al. 2010). For example, mutations in the *SCN1A*, an *SCN8A* family member, has been identified in the inherited seizure disorder, Generalized Epilepsy (Meisler et al. 2001). The current study demonstrates that overexpression of SCN8A in *NRXN1α* deletion neurons may have a significant functional consequence on the sodium current during action potential initiation. Single cell electrophysiology recording from this study shows that the sodium current in *NRXN1α* neurons is indeed significantly increased in voltage step protocol at -40 mV by 85% ($p<0.03$), -30 mV by 48% ($p<0.001$) and -20 mV by 37% ($p<0.03$).

SCN8A is abundantly expressed in neurons and located at the distal part of axons (Burgess et al. 1995). The initiation of the action potential in pyramidal cortical neurons starts from the distal part of the axons (Van Wart et al. 2007). *SCN8A* is predominantly expressed at the distal part of the axons, and the threshold activation of action potentials is lower at this part. This means that the increased expression of *SCN8A* in *NRXN1α* deletion neurons can lower the threshold activation and hence induce more excitability. Our results show that the average threshold voltage of action potential is significantly lowered in *NRXN1α* deletion neurons (Ctrl -24.2±0.60 mV and -28.32±0.70 mV). Furthermore, the action potential height also increased significantly in *NRXN1α* deletion neurons by 23% ($p<0.001$) at 5 pA and 27% ($p<0.02$) at 45 pA, elucidating the effect of increased Na^+ ion influx and currents.

It remains a challenging and complex question at this stage that how *NRXN1α* deletion can increase the expression of a subtype of VGSCs, as there is no direct interaction between neurexins and VGSCs. However, the described phenotype can result from combinational effects. Two of our probands in this study have history/diagnosis of seizures in addition of ASD. An increased expression of *SCN8A* in *NRXN1α* deletion patients may be driven by various factors and not only the deletion of *NRXN1α*

deletion.

Changes of voltage-gated potassium channels (VGKC) in *NRXN1α*-deletion neurons.

Following the influx of sodium across the membrane and initiation of the action potential, the slow activating outward potassium current is responsible for repolarization and hyperpolarization. They are key regulators of neuronal excitability and are encoded by forty different genes in 12 different sub-families (Yellen 2002). RNA sequencing from the present study shows that nine classes of voltage-gated potassium channels (*HCN2, KCNA3, KCNB2, KCNC4, KCNF1, KCNH3, KCNIP1, KCNJ8, KCNK12)* are differentially increased, except *KCNJ8*, in *NRXN1α* deletion neurons. They belong to different subtypes of voltage-gated potassium channel families.

K^+ channels are involved in EPSC, post-synaptic spike coupling and synaptic plasticity, hence providing the central nervous system with a distinct neuronal identity. An alteration in this network can have a major contribution to the excitability equilibrium of the neuronal network. Deletion or mutation of K^+ channels in animal models has shown to be associated with epilepsy and behavioural phenotypes that are similar to ASD (D'Adamo et al. 2013). There are three animal models of two sub-families of VGKSCs (*KCNJ10, KCNQ2*) which are listed in the SAFARI database in association with autism (Sicca et al. 2016; Hawkins et al. 2011). *KCNJ10* (kir4.1) is an inwardly rectifying potassium channel exclusively expressed in the brain, regulates astrocyte resting membrane potential (Nwaobi et al. 2016) and contributes to autism-epilepsy comorbidity. Although they are expressed in astrocytes, they are also an essential regulator of neuronal excitability (D'Adamo et al. 2013). Therefore when this pathway is impaired, there is high susceptibility to seizures and a great impact on motor function and cognitive development (Pereira and Furlan 2010; Seifert and Steinhäuser 2013). Conditional knockout mouse model of *KCNJ10* also resulted in brain dysfunction including seizures and ataxia (Djukic et al. 2007). Loss of function of *KCNJ10* (Kir4.1) in zebrafish recapitulated the human disease phenotypes such as epilepsy (Mahmood et al. 2013). Remarkably, a gain of function of mutations in *KCNJ10* also revealed seizures and ASD (Sicca et al. 2011), suggesting an appropriate

dose of VGKSC are essential for normal neuronal function.

In our study, a *KCNJ10* family member, *KCNJ8* (FDR 1.572E-05), is reduced by 50% in *NRXN1α* deletion neurons. KCNJ8 (kir6.1) also belongs to inwardly rectifying potassium channel (2TM). However there is no evidence of its association with ASD/epilepsy currently. They are responsible for allowing potassium ion into the cell rather than the efflux of K^+ ions. A reduction in the expression of *KCNJ8* may have a functional effect on potassium current; i.e. elevated efflux of potassium ions out of the cell and eventually increase in K^+ current. *KCNK12* (FDR 3.410E-05), on the other hand, is the most significantly increased (+2.191 fold) VGKC in *NRXN1α* deleted neurons. *KCNK12* is a two-pore domain voltage gated potassium channel (4TM) which has not been found to be a functional channel. Other identified VGKCs include 6-TM *KCNA3, KCNB2, KCNC4, KCNF1, KCNH3*, and Potassium Voltage-Gated Channel Interacting Protein 1 (*KCNIP1*), which showed increased expression by 1.808, 2.047, 1.966, 2.102, 1.653 and 1.655 –folds in *NRXN1α* deletion neurons, respectively.

How does *NRXN1α* deletion mediate the high expression and high-density clustering of VGKCs? It is clear that the localization of ion channels, cell adhesion molecules and signalling molecules are essential for normal brain function. For example, juxtaparanodal Kv1 (shaker family) channels that are clustered at high density and mediate axonal excitability interact with *Caspr2*, a member of the neurexin subfamily in the rat brain (Poliak et al. 1999). *Caspr2* is a mammalian homolog of *Drosophila* neurexin IV. This interaction between Kv1.2 and *Caspr2* is not through direct binding but requires a PDZ containing a domain (Poliak et al. 1999). This suggests that an indirect interaction of neurexins with VGKCs and clustering of these channels may happen. The altered expression of a series of voltage-gated sodium (SCN8A) and potassium (*HCN2, KCNA3, KCNB2, KCNC4, KCNF1, KCNH3, KCNIP1, KCNJ8*, KCNK12) channels implied that there could be a fundamental consequence associated with the functional of the *NRXN1*-deletion neurons, which could be elucidated by single cell functional recording.

The electrophysiology characterization by single cell voltage clamp recording indeed revealed significant alteration of VGKCs in the current study. A significant increase

in the K+ current was detected in *NRXN1α* deletion neurons, by 58% ($p<0.03$), 49% ($p<0.03$), 36% ($p<0.02$), 39% ($p<0.02$) and 22% ($p<0.001$) at -20 mV, -10 mV, 0 mV, 10 mV and 20 mV, respectively. In addition, the repolarization slope was significantly increased by 43% ($p<0.0006$), 41% ($p<0.002$) and 35% ($p<0.007$) at 5, 15 and 25 pA, respectively, in *NRXN1α* deletion patient's neurons. The repolarization time was also significantly increased by 56% ($p=0.003$) and 31% ($p=0.041$) in *NRXN1α* deletion neurons. These results demonstrated a significant change in neuronal function, as a consequence of elevated ion channel/transport expression, and as an underlying mechanism for ASD and associated epilepsy.

Changes of voltage-gated calcium channels (VGCCs) in *NRXN1α* deletion neurons.

VGCCs have a key role in synaptic transmission, converting the electrical signal from action potentials to intracellular calcium transients (Tsien 1983). This depolarization initiates calcium entry, leading to a series of events such as neurotransmitter release, gene expression and intracellular signalling. An alteration in the homeostasis of the calcium has been shown to be an underlying mechanism in diseases such as ASD and seizures (Palmieri et al. 2010). Post-mortem brain tissue analysis also revealed importance of calcium signalling in ASD (Cellot and Cherubini 2014). Furthermore, a dysfunction in the calcium signalling in a mouse model of *Cadps2*$^{-/-}$ and *Cd38*$^{-/-}$ shows autistic-like behaviour (Jin et al. 2007; Sadakata et al. 2007). This evidence strongly suggests an association of calcium homeostasis with the pathogenesis of ASD.

An alteration in the transport of ions across the membrane that affects the excitability of the neurons may have a consequence on calcium ion influx and hence vesicle exocytosis. In this study, transcriptome analysis by RNA sequencing showed impairments in calcium ion transport, transporter activity and voltage-gated channel complexes in *NRXN1α* deletion neurons. *CACNA1A*, *CACNA2D1*, *CACNA2D2*, *CACGN2*, *CACGN3* were identified as the most enriched genes in functional pathways (Figure 5.6B). They were upregulated by 2.019, 1.688, 2.177, 2.133 and 3.293-fold, respectively, in *NRXN1α* deletion neurons. Gene enrichment analysis with GSEA program also showed that *CACNA1A* was the most overlapped gene among the 16 of the top 20 pathways in biological processes, molecular function and cellular

components.

CACNA1A1 is the only voltage gated calcium gene from our study which overlaps with the VGCC gene list in SAFARI database. On the other hand, *CACNA1A, CACNA2D2, CACNG2* and *CACNG3* are all associated with epilepsy (based on CarpeDB epilepsy genetics database (Wang et al. 2017). This means that *CACNA1A* is a critical P/Q type VGCCs that have an essential role in the pathogenesis of ASD and epilepsy. *CACNA1A* is a high voltage-activated calcium channel and highly abundant in many nerve terminals (Catterall 2000).

CACNA1A is involved in both ASD and epilepsy database among the VGCCs. *CACNA1A* knockout mouse model showed an impairment in recognition memory with cognitive deficits (Mallmann et al. 2013). Previous studies showed that the mutations in *CACNA1A* on chromosome 19p13 were associated with autism and epilepsy (Rajakulendran et al. 2012; McCauley et al. 2005). Moreover, intellectual disability, the occurrence of seizures and language delay have also been identified with a *de novo* deletion on 19p13 where *CACNA1A* is located (Natiq et al. 2014). It has been reported that autism coexists with epilepsy up to 30-46% of patients (Berney 2000). These results suggest that *CACNA1A* may play a crucial role in the aetiology of the autism and/or epilepsy.

The KEGG pathway analysis of 530 differentially expressed gene by both STRING and GSEA showed that MAPK kinase and calcium signalling are the most significant pathways in *NRXN1α* deletion neurons. This means that the association of VGCCs are strongly related to *NRXN1α* functional properties. *CACNA1A, CACNA1I* and *PDGFRA* are shared by the two pathways, and *CACNA1A* and *CACNA1I* are the only VGCCs which overlaps between two pathways. Our data are consistent with a recent study, which investigated gene enrichment in the SAFARI human genes relevant to ASD and showed that calcium signalling and MAPK signalling were the most significant pathways (Wen et al. 2016). Furthermore, they revealed that VGCCs were the most overlapped and enriched genes among these two pathways, concluding them as major contributors to the pathophysiology of ASD (Wen et al. 2016). The MAPK signalling was an essential ASD signalling pathway which has also been suggested by Pinto et al. (Pinto et al. 2010; Pinto et al. 2014). Moreover, our data also support other

ASD studies, which examined the genetics variants by using genome-wide association studies (GWAS) and concluded that calcium signalling was the most significant and enriched pathway (Skafidas et al. 2014; Wen et al. 2016; Lu et al. 2012).

Our results from calcium imaging data showed that the spontaneous neuronal activity was significantly altered in *NRXN1α* deletion neurons. The frequency and timing of spontaneous calcium transients were significantly increased in NRXN1α deletion neurons. This means that the density and distribution of VGCCs have a role in calcium transient characteristics. These findings suggest that alteration and clustering of VGCCs, especially *CACNA1A*, may have a crucial role of impaired calcium signalling observed in *NRXN1α* deletion neurons. The coupling of VGCCs and synaptic vesicles are important for vesicular fusion and release probabilities (Schmidt et al. 2013). The VGCCs must be evenly distributed within the active zones for a uniform probability release of vesicles (Ermolyuk et al. 2013; Holderith et al. 2012). Our results indicated that vesicle exocytosis and neurotransmitter release was significantly affected in *NRXN1α* deletion neurons (Figure 5.11), which may couple with the changes observed in properties of calcium transients.

The synapse ultrastructure and functional relationship have been widely studied in postsynaptic membrane (Nusser et al. 1998; Takumi et al. 1999). The density of AMPA and NMDA receptors in the post-synaptic density affects the size of the postsynaptic response. The number and density of AMPA receptors are tightly correlated to postsynaptic density area, and it can be used to anticipate the response of the post-synaptic membrane (Takumi et al. 1999). Interestingly, the expression of two VGCC gamma subunit genes (*CACNG2, CACNG3*) that results in protein translation of transmembrane AMPA receptor regulatory proteins were also altered and upregulated in *NRXN1α* deletion neurons by 2.133 and 3.293-fold, respectively. They belong to voltage-gated calcium channel gamma subunits and are involved in AMPA receptor trafficking and gating.

Processes at pre- and post-synaptic membrane regulate the strength of synapses. This regulation can alter and affect the pre-synaptic calcium entry upon action potential stimulation. The glutamate receptors such as NMDA and AMPA receptors are modulated by a synaptic strength and activity (Malinow and Malenka 2002; Watt et

al. 2000). The overall properties of synaptic transmission are regulated by discrete adjustments of parameters such as pre-synaptic Ca^{2+} influx through VGCCs, the secretory components and the post-synaptic receptor-gated currents. Researchers have identified that ion channel receptors such as AMPA are functionally impaired when the expression of *Nrxn3α/β* is altered (Kattenstroth et al. 2004; Aoto et al. 2013). This is also true in pre-synaptic axon terminals. Studies have shown that the release probability correlates directly with the number of vesicles and the surface area of the active zones in hippocampal neurons (Branco et al. 2010). The density of VGCCs is essential for calcium dynamics, fusion and docking of the vesicle at synaptic zones as well as synaptic responses.

In summary, we have investigated the iPSC-derived 100-day neurons and identified major defects in electrophysiology (Chapter 3) and Ca^{++} signalling profiles (Chapter 4) as functional readouts associated with the *NRXN1α* deletion. The current transcriptome analyses have uncovered 530 differentially expressed genes in the ASD neurons. Bioinformatic analyses have underpinned the molecular mechanisms of synapses, ion channels/transport activity, calcium signalling and MAPK pathways, which are well-coupled to the functional changes of electrophysiology and Calcium transients, with altered VGSCs, VGKCs, VGCCs and MAPK pathways being the most prominent features of the *NRXN1α* deletions.

Chapter 6. Conclusion/Discussion and Future perspectives

6.1 Conclusion

ASD is a multi-factorial disease with hundreds of genetic risk factors, among which *NRXN1* gene deletion is commonly recognised as the highest risk factor. The focus of this PhD project was to develop and characterise an ASD patient-specific stem cell model with *NRXN1α* gene mutations. We anticipated that characterisation of this stem cell model during the *in vitro* differentiation process would lead us to find underlying molecular, cellular and functional phenotypes for better understanding and identification of potential pathways affected in ASD. The *NRXN1* gene is transcribed into two major class of protein isoforms, the long form of *NRXN1α* starts from exon 1, whereas the short form of *NRXN1β* starts from exon 18. The current research demonstrates that *NRXN1β* primarily engages with neuronal excitation, whereas *NRXN1α* is communicated through both excitatory and inhibitory synapses. We hypothesized that deletion of the *NRXN1α* may disturb the balance of neuronal excitation and inhibition. The experimental design of this project involves (1) derivation of iPSCs from healthy controls and ASD patients with *NRXN1α* deletion, (2) differentiation of iPSCs into 100-day neurons, (3) electrophysiological characterisation of iPSC-derived neurons via whole cell patch clump recording, (4) Ca^{2+} imaging and Ca^{2+} profile analyses, and (5) transcriptome comparison of the 100-day neurons. The major conclusions of the project are:

1. The iPSCs can be derived from both healthy controls and ASD patients with *NRXN1α* deletions. The project benefited from a lab colleague who had generated the majority of iPSC lines used in this study. *NRXN1α* deletion exhibited no major effects on the generation of the iPSCs from ASD skin biopsy as iPSC lines were successfully derived from both control and patient populations. We firstly examined the effect of *NRXN1α* deletion on iPSC proliferation (Figure 2.14) by double immunostaining with a proliferative marker Ki67 and a mitotic phase marker PH3. Quantitative analyses of the percentage of $Ki67^{+}$ or $PH3^{+}$ cells in control (n=4) and patients groups (n=3) did not show the statistically significant difference of proliferation. All iPSC lines were able to differentiate into cells of three germ layers. *NRXN1α* deletion displays no significant effect on early neurogenesis. To study the genetic aberrations of *NRXN1α*,

it was crucial to generate a homogenous population of the desired disease-specific cell type. In this project, excitatory glutamatergic cortical neurons were generated from human iPSCs derived from a skin biopsy of ASD patients with *NRXN1α* deletion. During the early neural induction stage, the day 20 neural progenitor cells (NPC) were also evaluated using Ki67, and the NPC proliferation remained unaltered in *NRXN1α* population (Figure 2.17). Subsequently, to assess the early neuronal differentiation, the day 30 cultures were characterised by Ki67/DCX/DAPI immunofluorescence staining and by qRT-PCR for DCX, TUJ1 and GFAP. There was no significant effect of *NRXN1α* on the birth of newborn neuron (DCX^+) or on different brain cell type of neurons ($TUJ1^+$) or astrocytes ($GFAP^+$) between the control and ASD groups (Figure 2.19).

2. NRXN1α heterozygous deletion has no significant effect on neuronal maturation. The next goal of this PhD thesis was to create an *in vitro* model of *NRXN1α* deletion neuronal network which has a resemblance to *in vivo* development. We have differentiated the control and *NRXN1α* iPSCs into cortical excitation neurons and investigated the maturity by neuronal excitability via recording of spontaneous calcium transients at day 50 and day 100 of differentiation (Figure 4.3). The spontaneous calcium transients and their frequency and amplitude were significantly increased at day 100 in comparison to day 50 neurons, in both populations. Neurons formed mature physical synapses as they expressed postsynaptic MAP2 and SYN1 (Figure 2.24, 2.26). Application of the AMPA/kainate and NMDA glutamatergic receptors blockers, CNQX and DL-AP5, abolished 66.8 to 97.8% of spontaneous calcium transients, respectively (Figure 4.7), suggesting that the majority of the cells are excitatory neurons and that spontaneous calcium transients were dependent on glutamatergic synaptic activity. Their functionality and neuronal excitability were also examined at the electrophysiological level in the presence of sodium and potassium currents (Figure 3.3), evoked (Figure 3.7) and spontaneous action potentials (Figure 3.10). Additionally, the transcriptome analyses revealed high abundant expression of the VGCCs, VGSCs, VGKCs and Glutamatergic receptors, as convincing signatures of excitatory/functional neurons. However, we did not observe significant effects of *NRXN1α* heterozygous deletion on the later phase of neuronal differentiation or maturation.

3. *NRXN1α* heterozygous deletion alters electrophysiology profiles of the 100-day neurons. To test whether heterozygous *NRXN1α* mutations have a phenotypic effect on human neurons, we investigated the role of *NRXN1α* in 4 cell lines from three ASD patients with exonic deletion of *NRXN1α* by comparison with six lines of healthy controls. The phenotypic effects of *NRXN1α* deletion on the function of neurons were examined via electrophysiology and calcium imaging together with RNA sequencing for underlying molecular mechanisms. At single cell recording, we identified significant alterations in voltage-gated sodium and potassium currents in *NRXN1α* deletion neurons (Figure 3.4). This increase in current significantly affected evoked action potential depolarization and repolarization characteristics (Figure 3.8, 3.9). This means that active non-synaptic properties of neurons and neuronal excitability were disrupted in *NRXN1α* deletion lines. In the subsequent experiment of RNA sequencing, the transcriptome analyses revealed a significantly disrupted expression on voltage-gated sodium and potassium ion transport and transporter activity (Figure 5.7, 5.8). This means that disruption on electrical excitability at least in part is due to an upregulation of VGSC, VGKCs and VGCCs. Overall, RNA sequencing analysis shows that in both transporter ion and transporter ion activity, VGSC and VGKCs are among the most overlapped genes which may have a strong association with our electrophysiology phenotype.

4. *NRXN1α* heterozygous deletion alters Ca^{2+} profiles in the 100-day neurons. An alteration in membrane excitability can have a direct consequence on calcium entry into the cell. We have next showed that 100-day-old patient iPSC-derived cortical neurons with *NRXN1α* deletion had significantly increased frequency of calcium transients (10.35 mHz) compared to control neurons (7.91 mHz, $p<0.0004$) (Figure 4.8C). This difference was also observed for the duration of the recorded calcium transients, where the *NRXN1α* deletion neurons had transients of longer duration (7.70 s) compared to control neurons (6.30 s, $p<0.0004$) (Figure 4.8D). The spontaneous calcium transients were effectively abolished by an average of 88% in the presence of tetrodotoxin (TTX), supporting the role of voltage-gated sodium channels in driving calcium transients (Figure 4.4). The observed differences in calcium transient frequency and duration in the *NRXN1* deletion neurons could be related to either an alteration in the expression of VGCCs or changes in calcium signalling machinery.

Transcriptome analysis of RNA sequencing showed impairments in calcium ion transport, transporter activity and voltage-gated channel complexes in *NRXN1α* deletion neurons. *CACNA1A*, *CACNA2D1*, *CACNA2D2*, *CACGN2*, *CACGN3* were identified as the most enriched genes in functional pathways (Figure 5.7, 5.8), and they were upregulated by 2.02, 1.69, 2.18, 2.13 and 3.29-fold, respectively, in *NRXN1α* deletion neurons. Gene enrichment analysis with the GSEA program also showed that *CACNA1A* was the most overlapped gene (16 out of 20) among the top 20 pathways in all biological processes, molecular function and cellular components. *CACNA1A* was also listed in the SAFARI database as an associated gene with ASD. On the other hand, *CACNA1A*, *CACNA2D2*, *CACNG2* and *CACNG3* are all considered to be associated with epilepsy based on CarpeDB epilepsy genetics database.

5. *NRXN1α* heterozygous deletion shows transcriptome changes in relation to the genetics of ASD pathways. As mentioned above, the RNA sequencing showed supporting data in molecules involved in electrophysiology and Ca^{2+} signalling. In addition, the pathways of synapses, exocytosis and MAPK kinase are altered significantly affected in the *NRXN1* deletion neurons.

Overall, our results suggest that there are alterations in electrical excitability of neurons, which are coupled with the changes in calcium transients and/or VGCC abundance and distribution. This is accompanied by a change in important presynaptic regulatory elements of neurotransmitter release, not to forget about the post-synaptic alteration in few key molecules (*SHANKs, GRIN1*). The deletion of neurexins produced large effects on post- synaptic receptor expression and pre-synaptic release probability in previous studies, elucidating the importance of neurexins in synaptic transmission. Our results have provided additional novel sight into the role of *NRXN1* in human iPSC-derived ASD model.

6.2 General Discussion

Autism spectrum disorder (ASD) is a devastating neurodevelopmental disorder with limited symptom-based treatment. Current care of ASD is mostly associated with education and behavioural interventions, focusing on improving their social interactions and behaviours (Myers et al. 2007).

It is generally believed that the lack of human disease models in the field of neurodevelopmental and neuropsychiatric diseases was the major impediment for drug discovery and therapeutic interventions. It has been shown that the lack of specific human models, especially in the early phase of drug screening, significantly associated with the failure of many clinical trials. Therefore, it is vital to understand the pathophysiology of ASD to target the core deficits contributed to ASD.

A significant technological breakthrough was made in 2006, making it possible to use induced pluripotent stem cells (iPSCs) to model brain diseases in a dish to direct use of brain tissue which was difficult to access otherwise (Takahashi and Yamanaka 2006). With the iPSC technology, it is possible to convert a patient's biopsy into ESC-like iPSCs, which can be then differentiated into different disease cell types, including different brain cells. In comparison to healthy controls, it is possible to study disease progression, pathology and mechanisms, to establish patient-derived human disease model in a dish, to identify phenotypes with potential development of drug screening assays, to use iPSC models for toxicity test, to manipulate and/or to rescue the genetic alterations in iPSCs for the generation of isogenic rescued cells, and all of these are anticipated to pave the way towards treatment and drug discovery.

Which subgroup of patients shall be the priority for the iPSC study? We have turned this question to the genetics of ASD. ASD has been affected by a very complex genetic aberrations, and over 100 genetic risk factors have been identified. Many of them are identified for ASD by recurrent copy number variations that comprise a large array of genes so far. The costs for more advanced technologies such as exome and whole genome sequencing are much higher, and these studies are in progress, which will further validate the current genetic discoveries.

The genetic risk factors identified so far largely fall into two categories of functions; genes that contribute to synaptic structure and function, i.e., *SHANKs* and *NRXNs*, and genes that predominantly control transcription and translation processes of gene expression, i.e., *PTEN* and *MECP2*. As mentioned previously in Chapter 1, the meta-analysis of genetic data by combination studies of copy number variation and single nucleotide polymorphism showed that *NRXN1* and *SHANK2* are the two common genetic factors overlapped by all studies (Pinto et al. 2010; Pinto et al. 2014). Presynaptic *NRXNs* bind to postsynaptic *NLGNs* which are associated with GABA

receptors for inhibitory signalling, or with glutamatergic receptors and *SHANKs* for excitatory signalling. The above genetic meta-analysis suggests that the *NRXN1*-mediated excitatory synaptic pathway may play a significant role in associated ASD.

Glutamate dysfunction and glutamate receptor impairment have been central in neurotransmitter involvement in autism (Carlsson 1998; Fatemi 2008). There have been evidence of the implication of glutamate receptors including NMDA receptor subunit *GRIN2B* and kainate receptor subunit GlurR6 in ASD. (Tarabeux et al. 2011; Yoo et al. 2012; Jamain et al. 2002). These evidences on excitatory neurotransmission dysfunction in autism are related to cell adhesion proteins, i.e. neurexins and neuroligins (Ching et al. 2010). Glutamatergic signalling is implicated in ASD, and *NRXN1* is known to signal bi-directionally through excitation and inhibition. *NRXN1α* is deleted in a proportion of ASD patients, and how *NRXN1α* deletion affects patient's excitatory neuronal function *in vivo* and/or *in vitro* is entirely unknown. Therefore, the ability to model cortical development with the control *NRXN1α* deletion iPSCs in cultures, from cortical neural induction to synapse formation to functionality of glutamatergic neurons, would enable us to examine the disease progression, the stage of neuronal development and function of the neurons affected by *NRXN1α* lesions, eventually leading to the generation of an ASD disease model.

Furthermore, *NRXN1* is a genetic risk factor for many neurodevelopmental disorder which implicates an impairment in cortical development (Jenkins et al. 2016). A protocol is developed to generate glutamatergic cortical neurons using combinational effect of two molecules which inhibit BMP and TGFβ pathways, leading to an efficient and robust production of population of neurons that can recapitulate the cortical development *in vitro* (Chambers et al. 2009; Shi, Kirwan, Smith, et al. 2012).

This protocol generates almost 100% population of the neuronal progenitor, being PAX6 and NESTIN positive (Figure 2.16). Neuronal progenitor rosettes generation in this phase is a critical step in differentiating iPSCs towards cortical neurons (Shi, Kirwan and Livesey 2012) (Figure 2.15). Brain size i.e. macrocephaly and microcephaly have both been reported in patients with *NRXN1* deletion (Marshall et al. 2008; Ching et al. 2010; Gregor et al. 2011; Schaaf et al. 2012; Béna et al. 2013; Curran et al. 2013; Dabell et al. 2013) (Figure 6.1). The study by Schaaf *et al*. has

reported that macrocephaly is highly correlated with *NRXN1β* deletion (Schaaf et al. 2012), but the implication of brain size including macrocephaly have also been reported in intronic and alpha isoform region. Hence, we investigated the association of *NRXN1α* at iPSC and neuronal progenitor level. We examined the proliferation capability of iPSCs and neuronal progenitor using proliferating marker Ki67 as well as early-born neuronal marker DCX. We have no supporting evidence that *NRXN1α* deletion affects neural proliferation, differentiation or neurogenesis or brain size (Chapter 2).

Table 6.1. Clinical features (micro/macrocephaly) of individuals with the *NRXN1* mutation.

Reference	Patient ID	Deletion region	Macro/ microcephaly	Other head circumference/ mutation
(Ching et al. 2010)	Number 2	Exon 1-22	x	Plagiocephaly
(Ching et al. 2010)	Number 10	Intron 5	x	Dolichocephaly
(Ching et al. 2010)	Number 12	Intron 5	Macrocephaly	x
(Gregor et al.	N2	Exon 1-18	Macrocephaly	x
(Schaaf et al.	E11	Exon 6-18	Macrocephaly	x
(Schaaf et al.	E12	Exon 6-18	Macrocephaly	x
(Schaaf et al.	E13	Exon 17-18	Macrocephaly	x
(Schaaf et al.	E14	Exon 19-20	Macrocephaly	x
(Schaaf et al.	E15	Exon 20-24	Macrocephaly	x
(Schaaf et al.	E16	Exon 23-24	Macrocephaly	x
(Schaaf et al.	E17	Exon 23-24	Macrocephaly	x
(Béna et al. 2013)	E13	Exon 3-18	Macrocephaly	x
(Béna et al. 2013)	E19	Exon 1-5	Macrocephaly	x
(Curran et al.	Number 2	Exon 1-5	Microcephaly	x
(Curran et al.	Number 13	Exon 4-5	Microcephaly	x
(Curran et al.	Number 17	Intron 5	Microcephaly	x
(Curran et al.	Number 18	Intron 5	Microcephaly	x
(Dabell et al.	Number 32	Exon 6-8	x	Plagiocephaly
(Dabell et al.	Number 24	Exon 1-5	x	Encephalopathy
(Dabell et al.	Number 31	Exon 9-11	x	Encephalopathy
(Dabell et al.	34a	Exon 19-20	Macrocephaly	x
(Dabell et al.	34b	Exon 19-20	Macrocephaly	x
(Dabell et al.	Not identified	Not Identified	Microcephaly	x
(Dabell et al.	Not identified	Not Identified	Microcephaly	x
(Agha et al. 2014)	MRQ12	Exon 3-19	Microcephaly	x
(Agha et al. 2015)	Dutch female	Exon 1	Microcephaly	x

Following the establishment of neuronal progenitor rosettes, the fundamentals of the cortical neuronal development progressed into projection pyramidal excitatory neurons. The neurogenesis of cortical neurons takes around 100 days *in vivo* in comparison to only six days in a mouse (Caviness et al. 2003). The generation of projection excitatory cortical neurons in this system approximates that seen in previous literature: generation of deep layer 5 and 6 neurons, as well as upper layer neurons (Figure 2.22) (Shi, Kirwan, Smith, et al. 2012). It is noteworthy that we did not detect any GABA-ergic interneurons in our culture. Generation of GABA-ergic interneurons requires additional ventralizing morphogens from cortical rosettes. The transcriptome analyses from RNA sequencing did not show significant levels of GABAergic gene expression (Figure 2.23). Furthermore, the addition of GABA in calcium imaging showed very little change in spontaneous transient activity for the GABAergic population as a whole (Figure 4.7). In summary, we have thus validated the differentiation protocol, with the cortical neuronal markers, the presynaptic and post-synaptic markers, the excitatory glutamatergic markers, and the maturity and the functionality of the neurons.

Despite a significant body of work and the many studies investigating the role of neurexin and its isoforms in synaptic function, the precise role of neurexin remains unknown. What is known is that heterozygous *NRXN1* mutations are the most frequently observed single gene mutation correlating with ASD and other neuropsychiatric disorders (Doherty et al. 2012; Südhof 2008; Ching et al. 2010). The functional consequences of neurexin mutations differ dramatically in different experimental paradigms. *Nrxn1α* deletion mutation in mice resulted in the impairment of both evoked and spontaneous neurotransmitter release, by impairing the Ca^{2+} influx upon the initiation of an action potential (Missler et al. 2003). In culture, cortical neurons from a hetero and homozygous mouse model of *Nrxn1α* deletion showed no significantly different phenotype (Pak et al. 2015), while the same mutation resulted in a reduction in mEPSC frequency in excitatory hippocampal slices (Etherton et al. 2009).

Current results showed that different neurexins performed different functions, depending on a given synapse, alternative splicing and specific brain region. For example, the *Nrnx3α/β* mutation in the mouse was associated with increased

postsynaptic AMPA receptor expression at excitatory synapses in hippocampal neurons (Aoto et al. 2015). The hippocampal phenotype was rescued only with *Nrnx3β*, not by *Nrnx3α*. In inhibitory olfactory neurons, the same *Nrnx3α/β* mutation resulted in a reduction in presynaptic release probability (Aoto et al. 2015). The long form of *Nrxn3α* was required to rescue the inhibitory presynaptic release of olfactory bulb phenotype. These phenotypes were also highly regulated by alternative splicing. The increased expression of AMPARs was corrected by isoforms with the excision of the SS4 exon, suggesting that presynaptic alternative splicing of *Nrnx3β* govern the abundance of AMPARs in hippocampal neurons (Aoto et al. 2013). However, the same manipulations of *Nrnx3β* alternative splicing did not affect excitatory or inhibitory transmission of olfactory bulb neurons (Aoto et al. 2015). This discrepancy was also observed in Chen and colleagues' study in which conditional knockout of all neurexins (*Nrxn1/2/3*) in mice resulted in two distinct phenotypes (Chen et al. 2017). The number of parvalbumin interneurons was decreased without a change in synaptic transmission of remaining synapses, while the number of somatostatin interneurons remained unchanged, but a significant reduction in Ca^{2+} influx, leading to a decrease in release probability of somatostatin, was observed (Chen et al. 2017). It is unknown whether three different neurexins in the triple *Nrxn1/2/3* knockout studies have similar or distinct functions towards the phenotypes. At present, only Nrxn3 has been more extensively investigated (Aoto et al. 2013; Aoto et al. 2015) as discussed above. Therefore, the data to date support a role of neurexin in synaptic function which may differ based on alternative splicing, type of synapse and brain regions.

Therefore, the animal data are inconclusive and sparse. It is unclear what are the precise roles of neurexin in normal neurophysiology, how *NRXN1* mutations predispose individuals to the clinical phenotypes observed in humans, and whether there is a more severe human-specific effect of *NRXN1* mutation when compared to animal models. Pak *et al*. compared the hetero- or homozygous *NRXN1α* deletion in mouse and human H1 ESC model of cortical neurons, and found a dramatic effect in human cortical neurons, with much more pronounced phenotype than in mouse cells (Pak et al. 2015). They identified that in the mouse model there is no impairment in synaptic transmission, but in human H1 ESC induced model, there was a severe alteration in neurotransmitter release probability due to a reduction in mEPSCs frequency and evoked EPSC amplitude. Importantly human models are lacking.

In our study, we observed a change in both sodium and potassium current with subsequent change in depolarization and repolarization characteristics. This disruption was not reported in Pak *et al.* study, the only human cortical neuron derived from *NRXN1* deletion using H1 ESCs (Pak et al. 2015). One reason to explain this is that our study is based on iPSCs from patients with *NRXN1α* deletions, while in Pak *et al.* study, recombinant adeno associated viruses were introduced to generate a conditional mutation on ESCs and were used as a *NRXN1* cortical neuronal model. This conditional knockout caused the deletion of both α and β isoform in ESCs. (Pak et al. 2015). It is argued that genetic manipulation may have potential functional consequences.

Second reason to explain this is that our deletion lines only have α isoform mutation on exon 1-5 in ND2 and ND4 and exon 6 -13 in ND1, while in Pak *et al.* study, two conditional mutations on exon 19 and 24, which resulted in deletion of both α and β isoforms (Pak et al. 2015). *NRXN1α* and *NRXN1β* isoforms interact with different post-synaptic binding partners (NLGNs) and hence the deletion in each isoform may lead to failure of a different protein function (Chih et al. 2006). Both *NRXN1α* and *NRXN1β* share the same transmembrane and intracellular domain, whereas the extracellular domains of both isoforms are different (chapter 1, Figure 3A). Deletion of the promoter regions, i.e. exon 1, inhibits the transcription/translation of the *NRXN*1α isoform, but the translation of the β isoform remains intact. However, deletions in the C-terminal region results in the formation of a C-terminal truncated protein with a signal polypeptide as a secretory protein if the truncated protein is stable. The cytoplasmic C-terminal tail is essential for forming a stable interaction with intracellular proteins, hence synaptic vesicle release and function. The PDZ domain of the cytoplasmic tail of *NRXN1α/β* isoform is essential for interaction with scaffolding proteins. These sequential steps are essential for the assembly of presynaptic active zones (Dean et al. 2003). All the above statements suggest that there might be phenotypic differences between patient iPSCs and genetically manipulated ESCs with *NRXN1α* and/or *NRXN1α/β* isoform deletion.

VGSCs have an essential role in the excitability of neurons by generating and propagating the action potentials (Goldin et al. 2000; Yu and Catterall 2003). It is strongly suggested that significant negative reduction in threshold activation of

evoked action potentials correlated to upregulation of *SCN8A* ($Na_v1.6$), a VGSC gene. One reason to explain this finding is that *SCN8A* is predominantly expressed at the distal part of the axon initial segment (AIS), where action potentials are initiated in pyramidal cortical neurons (Burgess et al. 1995; Van Wart et al. 2007). Predominant expression of Nav1.6 at the distal part of AIS of cortical neurons have shown to significantly reduce the threshold of the action potential in comparison to the proximal part of the AIS, suggesting their role in lowering the threshold (W Hu et al. 2009).

This increased expression of *SCN8A* in our study might contribute to lowering the threshold of the action potential and hence more readily induce neuronal excitability. Furthermore, the overexpression of *SCN8A* may lead to excessive neuronal firing and excitability in cortical neurons (Papale et al. 2009). Clinically, a *de novo* heterozygous missense mutation of *SCN8A* was found in a 16-year-old female proband, who exhibited seizers, ASD, intellectual disability and ataxia (Veeramah et al. 2012). The functional consequences of the mutation were investigated in transfected cells, and it was shown to persistently increase the sodium current (Veeramah et al. 2012). This subsequently slowed down the non-inactivating component of the channel and increased the neuronal excitability (Veeramah et al. 2012). This elucidates that the mutant *SCN8A* channel can increase the neuronal excitability. A series of studies on *SCN8A* mutation showed that seizures were usually present by the average age of 5 months with autistic features, and intellectual disability usually appear afterwards (Larsen et al. 2015). This is a similar scenario in our study because, in ND1 and ND4, the history of seizures was identified at a very young age.

In our study, upregulation of *SCN8A* (1.5-fold increase, FDR 2.056E-02) was strongly associated with the influx of sodium currents and alteration of the action potential threshold to a more negative voltage and an increase of action potential peak height, all suggesting increasing neuronal excitability. An influential review published in 2003 in which John Rubenstein and Michael Merzenich proposed that there was an increased ratio between excitation and inhibition in autism which has resulted in hyper-excitability of the cortical neuronal network (Rubenstein and Merzenich 2003). Reduced GABAergic signalling was frequently observed in autism, as well as their tendency to develop epilepsy (Cellot and Cherubini 2014). The loss of inhibition and increase in excitatory responses could lead to enhance imprecision in learning and

cognition, one of the main characteristics in ASD. While in our study only excitatory cortical neurons were generated and investigated, but our results clearly have shown functional evidence towards increased neuronal excitability in *NRXN1α* deletion neurons. It is interesting that in RNA sequencing the membrane depolarization GO groups have been significantly disturbed in *NRXN1α* deletion neurons. This may be explained partially by the disruption of ion transport activity in VGSCs.

The neuronal excitability is further accompanied by upregulation of few classes of VGKCs in *NRXN1α* deletion neurons, including *KCNA3* (FDR 4.061E-03, 1.8-fold), *KCNB2* (FDR 2.400E-02, 2.0-fold), *KCNC4* (FDR 8.110E-03, 2.0-fold), *KCNF1* (FDR 3.119E-02, 2.1-fold), *KCNH3* (FDR 1.472E-02, 1.7-fold) , *KCNIP1* (2.681E-02, 1.7-fold), , *KCNK12* (FDR 3.410E-05, 2.2-fold) (Figure 5.7, 5.8). This means that an alteration in this network has a major impact on the excitability equilibrium of a neuronal network. Both VGSC and VGKCs are amongst the most overlapped genes associated with channel and transporter activity in RNA sequencing.

There are five classes of voltage gate potassium channels that all have been upregulated in *NRXN1α* deletion neurons (*KCNA3*/Kv1.3, *KCNC4*/Kv3.4, *KCNH3*/Kv12.2, *KCNF1*/Kv5.1, *KCNB2*/Kv2.2), all which have a role in regulation of the outward potassium current upon generation of an action potential, modulation of neurotransmitter release, as well as controlling the excitability of neurons. Increased expression of Kv channels influences the action potential repolarization by controlling the efflux of potassium currents. In our study, the potassium currents were significantly increased in patients and in turn, the repolarization time was significantly shortened (Figure 3.9D).

On the other hand, one member of inwardly rectifying potassium channel (*KCNJ8*/Kir6.1) is downregulated in *NRXN1α* deletion neurons, maintaining the resting membrane potential. The downregulation of a kir6.1 channel may enhance the excitability of neurons because the lower expression of kir channels reduces the tendency of potassium ions getting into the inside of the neurons, which may aid along with Kv channels, enhancing more potassium efflux and increasing currents.

KCNA3 (K_v1.3) belongs to Kv subfamily of VGKCs which clustered at high densities at juxtaparanodal regions of the axoglial junction (Wang et al. 1993). One of the

proteins which interact with Kv1 channels at juxtaparanodal regions is Caspr2, a member of the neurexin superfamily (Poliak et al. 1999). This might suggest that there could be an indirect interaction between *NRXN1* and VGKCs which are not known. However, it is noteworthy to mention that the association of VGKC to ASD is well-known. For example, Kv4.2 channel expression contributes to ASD by binding with Fragile X mental retardation protein (FMRP), a common cause of autism and often seizures (Garber et al. 2008). There are many direct and indirect involvement of other VGKCs with ASD. For example, direct involvement of *KCND2* and *KCNQ3* (Chen et al. 2006; Singh et al. 2006) and indirect involvement of *KCNMA1* and *KCNT1* (Bhattacharjee and Kaczmarek 2005; Deng et al. 2011).

The contribution of potassium channels has also been identified in epileptic phenotypes (Brenner and Wilcox 2012). This might be important in our study because two of our patients, ND1 and ND4, have been additionally diagnosed with epilepsy and have a history of seizures respectively. While ND1 has been diagnosed with epilepsy, ND4's father and aunt have a diagnosis of epilepsy too. It is long known that alterations in potassium ions will change excitability and result in epilepsy. Our data is the first evidence suggesting that there might be an indirect interaction between *NRXN1* and VGKCs, and these might be a link between VGKCs expression and the clinical phenotype of ND1 and ND4 regarding epilepsy and seizures. It is noteworthy to mention that the contribution of epilepsy in our observed phenotypes are not conclusive and much further experiments and validations are essential.

An alteration in action potential properties may influence the calcium influx into the presynaptic terminal. Previous studies have shown that neurexins are essential for the organization of presynaptic terminals by functionally coupling calcium channels to the vesicle release machinery at the presynaptic terminal (Missler et al. 2003). This was concluded as the whole cell calcium current was reduced and have resulted in an impairment in neurotransmitter release, affecting the frequency of both spontaneous and evoked minis (Missler et al. 2003).

Furthermore, alterations in the homeostasis of the calcium have been shown to be an underlying mechanism in diseases such as autism and seizures (Palmieri et al. 2010). Calcium level has been reported to be significantly increased in the neocortical region of autistic patients in comparison to healthy controls. Post-mortem brain tissue

analysis has revealed the importance of calcium signalling in ASD (Cellot and Cherubini 2014). Furthermore, a dysfunction in the calcium signalling in a mouse model (Cadps2$^{-/-}$) shows autistic-like behaviour (Sadakata et al. 2007). Cadps2 is a Ca^{2+} dependent activator protein for secretion 2 which has a crucial role in exocytosis of vesicles. The knockout mouse model of this gene exhibited impaired neurotropic factor release, as autistic-like behavioural phenotypes (Sadakata et al. 2007). These data strongly suggest the association of calcium homeostasis in the pathogenesis of ASD.

Subcellular localization and density of calcium ion channels significantly influence the frequency and timing of calcium transients (Rosenberg and Spitzer 2011). In normal neuronal physiology, calcium transients are the main regulatory element of synaptic transmission. The arrival of an action potential at the axon terminal results in calcium influx through VGCCs, triggering neurotransmitter release. Calcium transients have been identified as an essential part of brain development and maturation of functional synapses (Rosenberg and Spitzer 2011). Thus, we hypothesized that mutation of *NRXN*, may disturb this coupling mechanism and affect calcium signalling and its dynamics in neurons, based on the alterations on electrical excitability on neurons. Our calcium imaging results have clearly demonstrated a significant change in frequency and duration of calcium transients.

Transcriptome analysis has revealed a significant change in ion transporter activity including VGCCs. VGCCs are tetramers containing three auxiliary subunits (β/α2δ/γ) and one pore-forming α1 subunit encoded by *CACNA1A, CACNA1B, CACNA1C, CACNA1D, CACNA1E* and *CACNA1S*. Calcium influx is determined by the opening duration of the α1 subunit in response to depolarization. Consistent with our data, gain-of-function of VGCCs is implicated in a wide range of neurodevelopmental disorders. For example, Cav1.2 G406R (*CACNA1C*) causes Timothy Syndrome with ASD by delaying voltage-dependent inactivation and prolonging Cav1.2 opening (Splawski et al. 2004; Splawski et al. 2005). Knock-in mice also exhibited autistic phenotype with impaired neuronal migration (Bett et al. 2012; Kamijo et al. 2018). Exome sequencing have identified Cav1.3 A59V, G407R, A749G, V584I, Ala769Gly, S1953L and R1997H mutations (*CACNA1D*) in ASD (Iossifov et al. 2012; O'Roak et al. 2012; De Rubeis et al. 2014; Pinggera et al. 2015), V401L in ASD and epilepsy (Pinggera et al. 2017), and

Q558H in developmental delay/epilepsy (Pinggera et al. 2017). Pharmacological activation of Cav1.3 induced depressive behavior in mice (Pinggera and Striessnig 2016)[62]. A *CACNA1D* paralog, *CACNA1F* (Cav1.4), was linked to New Zealand autistic males with excessive Ca^{2+} influx (Hemara-Wahanui et al. 2005; Hope and Sharp… 2005).

CACNA1A is the most enriched and overlapped gene in the top 20 of all biological processes, molecular function and cellular components (GO) pathways. *CACNA1A* is involved in both ASD and epilepsy database among the VGCCs. *CACNA1A* is predominantly expressed in neurons and is involved in NRXN1α signaling which triggers release of fusion-ready vesicles (Brockhaus et al. 2018). *CACNA1A* rs7249246/rs12609735 were associated with Chinese ASD (Li et al. 2015), and *CACNA1A* E101Q, S218L, A420V, A713T and A1511S mutations in Epileptic Encephalopathy (Epi4K Consortium et al. 2013; Epi4K Consortium 2016). Additionally, mutations of *CACNA1B, CACNA1C, CACNA1H, CACNA1S, CACNA2D1, CACNA2D2, CACNA2D4, CACNB2* and *CACNB4* were identified as a major pathway in schizophrenia (Purcell et al. 2014; Sundararajan et al. 2018), *CACNA1C* (rs1024582) and *CACNB2* (rs2799573) as the common risks across seven brain diseases (Cross-Disorder Group of the Psychiatric Genomics Consortium 2013; Borlot et al. 2017), and *CACNB2* G167S/S197F/F240L associated with ASD (Breitenkamp et al. 2014; Soldatov 2015).

Some of the VGCC mutations in neuropsychiatric/neurodevelopmental conditions are known to be loss-of-function, i.e., *CACNA1C* rs1006737 decreases its expression in bipolar disorder (Gershon et al. 2014), *CACNA1H* R212C, R902W, W962C and A1874V reduce its activity in ASD (Gershon et al. 2014), *CACNA2D1* deleted in epilepsy and intellectual disability (Gershon et al. 2014), *CACNG2* V143L decreased its binding to GLUR1 or GLUR2 (Hamdan et al. 2011; Gershon et al. 2014), and *Cacng2* hypomorph resulted in epileptic phenotype (Gershon et al. 2014). In addition, *Cacna1a* knockout mouse model shown impairment in recognition memory and cognitive deficits (Mallmann et al. 2013). Knockout mouse model of *Cacna1a* (flanked exon 4 by LoxP sites) have shown a loss of function in reducing the EPSC amplitude, suggesting strong impairment in synaptic transmission in Schaffer collateral-CA1 synapses (Mallmann et al. 2013). CACNA1A is located on chromosome 19p, which have been suggested as a region with a strong linkage to autism (McCauley et al. 2005). For example, intellectual

disability, the occurrence of seizures and language delay have been identified in a *de novo* deletion in 19p13 detected by array comparative genomic hybridization, where *CACNA1A* gene is located (Natiq et al. 2014). These evidence supports altered VGCCs as a mechanism in ASD *NRXN1α*$^{+/-}$ neurons.

The human *NRXN1α*$^{+/-}$ phenotype reported here differs from that in triple *Nrxn1α*$^{-/-}$ *Nrxn2α*$^{-/-}$*Nrxn3α*$^{-/-}$ mice, which were neuroanatomically normal (Geppert et al. 1998; Missler et al. 2003), but exhibited different phenotypes in different neurons or synapses (Pak et al. 2015). In hippocampal presynapse, the Ca^{2+} influx was reduced with lower Cav2.1-mediated transients and elevated axonal mobility of α2δ1(Missler et al. 2003). Overexpression of *Nrxn1α* and α2δ1 was shown to rescue Ca^{2+} currents, suggesting that *Nrxn1α* modulates Ca^{2+} influx through Cav2.1-α2δ1 interaction (Brockhaus et al. 2018). However, NRXN1α also negatively regulates Cav2.2 currents through NRXN1α-Cav2.2-αδ3 interactions in transfected cells (Tong et al. 2017).

Approximately >20% of human essential genes are nonessential in mice (Pak et al. 2015) , suggesting that species differences may also exist. The penetrance of *NRXN1a*$^{+/-}$ is not 100% in humans and homozygous *NRXN1a* deletions are rare. Clinical conditions of *NRXN1a*$^{+/-}$ are diverse, and genetic background and co-factors may play a role in penetrance and/or clinical diversity. These are less likely to be revealed by *NRXN1*$^{+/-}$ neurons created from a control ES line (Pak et al. 2015). In opposite to mammals, *C. elegans* NRXN1 at acetylcholine neuromuscular synapse is located postsynaptically (Tong et al. 2017). Therefore, synapse/cell types, anatomic regions, species differences and co-factors may all contribute to the diversity of phenotypes of *NRXN1* lesions.

Our *NRXN1a*$^{+/-}$ phenotype is, however, consistent with differential roles of NRXN1α and NRXN1β: NRXN1β triggers excitation, and NRXN1α regulates both excitation and inhibition (K Ichtchenko et al. 1995; Song et al. 1999; Berninghausen et al. 2007). If there is no significant compensational change, NRXN1α deletions are anticipated to weaken the inhibition in *NRXN1α*$^{+/-}$ neurons. Interestingly, neuroligins contain Ca^{2+}-binding EF-hand domains, and NLGN-NRXN1β interaction is dependent on calcium (Tsigelny et al. 2000). Ca^{2+} transients in *NRXN1α*$^{+/-}$ neurons may therefore also enhance excitation through increased NLGN-NRXN1β interactions. Furthermore, two of our ASD patients had a history of seizures. This concurs with disrupted calcium signalling implicated in a

range of neurodevelopmental disorders including ASD and epilepsy (Krey and Dolmetsch 2007; Breitenkamp et al. 2015; Heyes et al. 2015; Zamponi 2016; Nanou and Catterall 2018; O'Connell et al. 2018).

The vesicle release probability is strongly correlated with the amount of calcium influx and the structure of the active zone (Holderith et al. 2012). The number, density and distribution of VGCCs, calcium sensors and vesicle fusion kinetics are all required for the release probability. Furthermore, the amplitude of calcium transients has a tight relationship with the release probability, which is linearly connected to the proportion of P/Q VGCC encoded by *CACNA1A* (Holderith et al. 2012). The expression of *CACNA1A* is proportional to the area of the presynaptic active zone (Holderith et al. 2012). As stated previously, studies have strongly shown that impairment of presynaptic neurotransmitter release is strongly related to *NRXN1* mutation in both mouse and human induced ESCs (Pak et al. 2015; Etherton et al. 2009).

It is noteworthy to emphasise that there are many pathways from our transcriptome analysis have shown the contribution of synaptic vesicle exocytosis disruption in *NRXN1α* deletion neurons (Figure 5.11). A significant change in VGCCs and key molecules in synaptic exocytosis clearly elucidate a disruption in neurotransmitter release, and *NRXNs* have a crucial role in this matter. For example, synaptotagmins (*SYT3, SYT13, SYTL2*) and syntaxin (*STX1B*) that have a role in docking, priming and fusion of vesicles are significantly upregulated and enriched in *NRXN1α* deletion neurons. Furthermore, the expression of *DOC2A* is significantly enriched in *NRXN1α* deletion neurons. *DOC2A* is a double C2 protein which contains two C2-like domains, involve in Ca^{2+} dependent neurotransmitter release. Copy number variations in *DOC2A* have been associated as a significantly enriched gene in association with autism (Gai et al. 2012). These results from RNA sequencing results can strongly support our conclusion towards impairment in neurotransmitter release, the main canonical function of neurexins in presynaptic release probability and hence an alteration in synaptic transmission.

KEGG pathway analysis by GSEA and STRING showed that MAPK kinase and calcium signalling are the most significant pathways in *NRXN1α* deletion neurons (Figure 5.11). This means that the association of VGCCs are strongly related to

NRXN1α functional properties. *CACNA1A* and *CACNA1I* are the only VGCCs which overlap between two pathways. A recent study investigated the gene enrichment analysis with KEGG pathway database with enriched SAFARI human genes relevant to ASD, showed calcium signalling and MAPK signalling to be the most significant pathways (Wen et al. 2016). Furthermore, they revealed that VGCCs are the most overlapped and enriched genes among these two pathways, concluding them as a major contributor to the pathophysiology of ASD (Wen et al. 2016). MAPK may phosphorylate T321 of TARP (encoded by *CACNG2/CACNG3*) which are elevated in *NRXN1α*$^{+/-}$ neurons. Phosphorylation of T321 can dissociate TARP-PSD-95 interaction and decrease activity-dependent synaptic clustering of TARP/AMPAR (Stein and Chetkovich 2010). The DEGs may also arise from calcium influx and voltage-dependent conformational changes of VGCCs. For example, Cav1.2 is shown to interact with αCaMKII, and βCaMKII is then recruited by Ca^{2+} mobilization. Voltage-dependent conformational changes can lead to α/βCaMKII activation, CREB phosphorylation and nuclear accumulation (Li et al. 2016), in addition to activation of transcription factors NFAT and MEF2 (Sheng et al. 1990; Zafra et al. 1990; Graef et al. 1999; Hardingham et al. 1999; Mao et al. 1999). Therefore, the transcriptome changes may reflect both functional features of ASD *NRXN1α*$^{+/-}$ neurons and activity-driven alterations in *NRXN1α*$^{+/-}$ neurons.

6.3 Future perspectives

In the present study, iPSCs were mostly established using an integration method lenti virus. However, in order for iPSCs to be considered in cell replacement therapy, the method used in this study must be considered. Arguably, the best method for the generation of iPSCs from fibroblast would involve the use of non-integration strategy. But the iPSCs from this project were only used as an *in vitro* disease model and it proved to be a reliable method to generate efficient iPSC colonies for this study. The heterogeneity of iPSCs is common and the current data are derived statistically viable numbers. A larger population of iPSC lines with 3-D modelling in the follow-up investigations may independently validate the discoveries of this study.

While this study investigated the association of α isoform, it will be interesting also to find out the effect of β and whole *NRXN1αβ* on iPSC derived from patients and investigate their dosage effect of different *NRXN1* isoform deletion. Moreover, to ensure that results are due to the level of *NRXN1* expression and not other inherent differences between the three patient lines, it would be valuable to see if the same gene expression effects can be reproduced using a shRNA or another knockdown strategy in the control lines. More recently in the lab, an attempt has been made to employ to generate isogenic line using CRISPR-Cas9. While CNV array analysis were perfomed to identify *NRXN1* deletion, further analysis would be beneficial to report any other variants which may present in the ASD patients' genome that are related to neuronal development or excitability.

In the view of the data collected in this PhD project so far, which demonstrated that *NRXN1α* deletion impairs the electrical excitability of neurons, one definite possible area for future study would be to investigate the synaptic properties of neurons, i.e. the frequency and amplitude of both spontaneous and evoked mEPSCs which could definitely couple to our current results. This is essential to detect any alteration and disruption in presynaptic release probability which has been strongly suggested from our calcium imaging data. mEPSCs are non-action potential driven events that can be used to quantify the readily releasable pool size. It will be valuable to record both spontaneous and miniature EPSCs to understand whether the changes in synaptic transmission are from presynaptic or postsynaptic side.

Furthermore, it would be interesting to measure the amount of intracellular calcium concentration using ratiometric calcium indicators such as Fura-2. It would be interesting to perform dual patch clamp recording and calcium imaging to further validate our discovery in single cell level. Given the presence of specific mutation site on a limited number of samples, rescue experiments would be valuable to show that the *NRXN1* mutation was responsible for the functional phenotypes observed.

Differential gene expression from RNA sequencing analysis can be further investigate by genome wide association study to find out common variants. Furthermore, it will be beneficial to perform additional statistical analysis on ASD risk factors between the samples studied in our project and SAFARI database.

Upregulation in VGKCs observed in our data may have a consequence on neuronal apoptosis because they have a role in regulating apoptosis and proliferation of neurons (Shah and Aizenman 2014). Neuronal apoptosis is strongly related to increased expression of potassium channels. Increased potassium current in *NRXN1α* deletion neurons, which means facilitation in K^+ efflux and maybe a drop in intracellular K^+. Reduction in K^+ can facilitate pre apoptotic enzymes and hence trigger apoptotic signals (Leung 2010). This is another area of future study which can be investigated.

In the view of the data collected which demonstrated an alteration in electrical excitability and calcium signaling with potential upregulation in VGSC, VGKCs and VGCCs. It would be valuable to investigate the consequence of different ion channel blockers on electrical firing of neurons as well as their calcium transient properties.

Bibliography

Aasen, T. and Izpisúa Belmonte, J.C. 2010. Isolation and cultivation of human keratinocytes from skin or plucked hair for the generation of induced pluripotent stem cells. *Nature Protocols* 5(2), pp. 371–382.

Abrahams, B.S., Tentler, D., Perederiy, J.V., Oldham, M.C., Coppola, G. and Geschwind, D.H. 2007. Genome-wide analyses of human perisylvian cerebral cortical patterning. *Proceedings of the National Academy of Sciences of the United States of America* 104(45), pp. 17849–17854.

Adolphs, R. 2001. The neurobiology of social cognition. *Current Opinion in Neurobiology* 11(2), pp. 231–239.

Agha, Z., Iqbal, Z., Azam, M., Siddique, M., Willemsen, M.H., Kleefstra, T., Zweier, C., de Leeuw, N., Qamar, R. and van Bokhoven, H. 2014. A complex microcephaly syndrome in a Pakistani family associated with a novel missense mutation in RBBP8 and a heterozygous deletion in NRXN1. *Gene* 538(1), pp. 30–35.

Agha, Z., Iqbal, Z., Kleefstra, T., Zweier, C., Pfundt, R., Qamar, R., VAN Bokhoven, H. and Willemsen, M.H. 2015. A de novo microdeletion in NRXN1 in a Dutch patient with mild intellectual disability, microcephaly and gonadal dysgenesis. *Genetics research* 97, p. e19.

Alarcón, M., Abrahams, B.S., Stone, J.L., Duvall, J.A., Perederiy, J.V., Bomar, J.M., Sebat, J., Wigler, M., Martin, C.L., Ledbetter, D.H., Nelson, S.F., Cantor, R.M. and Geschwind, D.H. 2008. Linkage, association, and gene-expression analyses identify CNTNAP2 as an autism-susceptibility gene. *American Journal of Human Genetics* 82(1), pp. 150–159.

Alcamo, E.A., Chirivella, L., Dautzenberg, M., Dobreva, G., Fariñas, I., Grosschedl, R. and McConnell, S.K. 2008. Satb2 regulates callosal projection neuron identity in the developing cerebral cortex. *Neuron* 57(3), pp. 364–377.

Amaral, D.G., Schumann, C.M. and Nordahl, C.W. 2008. Neuroanatomy of autism. *Trends in Neurosciences* 31(3), pp. 137–145.

Ananiev, G., Williams, E.C., Li, H. and Chang, Q. 2011. Isogenic pairs of wild type and mutant induced pluripotent stem cell (iPSC) lines from Rett syndrome patients as in vitro disease model. *Plos One* 6(9), p. e25255.

Anderson, G.R., Aoto, J., Tabuchi, K., Földy, C., Covy, J., Yee, A.X., Wu, D., Lee, S.-J., Chen, L., Malenka, R.C. and Südhof, T.C. 2015. β-Neurexins Control Neural Circuits by Regulating Synaptic Endocannabinoid Signaling. *Cell* 162(3), pp. 593–606.

Aoto, J., Földy, C., Ilcus, S.M.C., Tabuchi, K. and Südhof, T.C. 2015. Distinct circuit-dependent functions of presynaptic neurexin-3 at GABAergic and glutamatergic synapses. *Nature Neuroscience* 18(7), pp. 997–1007.

Aoto, J., Martinelli, D.C., Malenka, R.C., Tabuchi, K. and Südhof, T.C. 2013. Presynaptic neurexin-3 alternative splicing trans-synaptically controls postsynaptic AMPA receptor trafficking. *Cell* 154(1), pp. 75–88.

Arikkath, J. and Reichardt, L.F. 2008. Cadherins and catenins at synapses: roles in synaptogenesis and synaptic plasticity. *Trends in Neurosciences* 31(9), pp. 487–494.

Arking, D.E., Cutler, D.J., Brune, C.W., Teslovich, T.M., West, K., Ikeda, M., Rea, A., Guy, M., Lin, S., Cook, E.H. and Chakravarti, A. 2008. A common genetic variant in the neurexin superfamily member CNTNAP2 increases familial risk of autism. *American Journal of Human Genetics* 82(1), pp.

160–164.
Arlotta, P., Molyneaux, B.J., Chen, J., Inoue, J., Kominami, R. and Macklis, J.D. 2005. Neuronal subtype-specific genes that control corticospinal motor neuron development in vivo. *Neuron* 45(2), pp. 207–221.
Arstikaitis, P., Gauthier-Campbell, C., Huang, K., El-Husseini, A. and Murphy, T.H. 2011. Proteins that promote filopodia stability, but not number, lead to more axonal-dendritic contacts. *Plos One* 6(3), p. e16998.
Ascano, M., Mukherjee, N., Bandaru, P., Miller, J.B., Nusbaum, J.D., Corcoran, D.L., Langlois, C., Munschauer, M., Dewell, S., Hafner, M., Williams, Z., Ohler, U. and Tuschl, T. 2012. FMRP targets distinct mRNA sequence elements to regulate protein expression. *Nature* 492(7429), pp. 382–386.
Ashley, C.C. and Ridgway, E.B. 1968. Simultaneous recording of membrane potential, calcium transient and tension in single muscle fibres. *Nature*.
Atmaca, M., Yildirim, H., Ozdemir, H., Tezcan, E. and Poyraz, A.K. 2007. Volumetric MRI study of key brain regions implicated in obsessive-compulsive disorder. *Progress in Neuro-Psychopharmacology & Biological Psychiatry* 31(1), pp. 46–52.
Autism and Developmental Disabilities Monitoring Network Surveillance Year 2008 Principal Investigators and Centers for Disease Control and Prevention 2012. Prevalence of autism spectrum disorders--Autism and Developmental Disabilities Monitoring Network, 14 sites, United States, 2008. *MMWR. Surveillance summaries : Morbidity and mortality weekly report. Surveillance summaries / CDC* 61(3), pp. 1–19.
Autism Genome Project Consortium, Szatmari, P., Paterson, A.D., Zwaigenbaum, L., Meyer, K.J., et al. 2007. Mapping autism risk loci using genetic linkage and chromosomal rearrangements. *Nature Genetics* 39(3), pp. 319–328.
Avilion, A.A., Nicolis, S.K., Pevny, L.H., Perez, L., Vivian, N. and Lovell-Badge, R. 2003. Multipotent cell lineages in early mouse development depend on SOX2 function. *Genes & Development* 17(1), pp. 126–140.
Bacchelli, E., Blasi, F., Biondolillo, M., Lamb, J.A., Bonora, E., Barnby, G., Parr, J., Beyer, K.S., Klauck, S.M., Poustka, A., Bailey, A.J., Monaco, A.P., Maestrini, E. and International Molecular Genetic Study of Autism Consortium (IMGSAC) 2003. Screening of nine candidate genes for autism on chromosome 2q reveals rare nonsynonymous variants in the cAMP-GEFII gene. *Molecular Psychiatry* 8(11), pp. 916–924.
Bachiller, D., Klingensmith, J., Kemp, C., Belo, J.A., Anderson, R.M., May, S.R., McMahon, J.A., McMahon, A.P., Harland, R.M., Rossant, J. and De Robertis, E.M. 2000. The organizer factors Chordin and Noggin are required for mouse forebrain development. *Nature* 403(6770), pp. 658–661.
Bader, P.L., Faizi, M., Kim, L.H., Owen, S.F., Tadross, M.R., Alfa, R.W., Bett, G.C.L., Tsien, R.W., Rasmusson, R.L. and Shamloo, M. 2011. Mouse model of Timothy syndrome recapitulates triad of autistic traits. *Proceedings of the National Academy of Sciences of the United States of America* 108(37), pp. 15432–15437.
Bailey, A., Le Couteur, A., Gottesman, I., Bolton, P., Simonoff, E., Yuzda, E. and Rutter, M. 1995. Autism as a strongly genetic disorder: evidence from a British twin study. *Psychological Medicine* 25(1), pp. 63–77.
Bakkaloglu, B., O'Roak, B.J., Louvi, A., Gupta, A.R., Abelson, J.F., Morgan, T.M., Chawarska, K., Klin, A., Ercan-Sencicek, A.G., Stillman, A.A., Tanriover, G., Abrahams, B.S., Duvall, J.A., Robbins, E.M., Geschwind, D.H.,

Biederer, T., Gunel, M., Lifton, R.P. and State, M.W. 2008. Molecular cytogenetic analysis and resequencing of contactin associated protein-like 2 in autism spectrum disorders. *American Journal of Human Genetics* 82(1), pp. 165–173.

Banerjee, S., Riordan, M. and Bhat, M.A. 2014. Genetic aspects of autism spectrum disorders: insights from animal models. *Frontiers in Cellular Neuroscience* 8, p. 58.

Banovic, D., Khorramshahi, O., Owald, D., Wichmann, C., Riedt, T., Fouquet, W., Tian, R., Sigrist, S.J. and Aberle, H. 2010. Drosophila neuroligin 1 promotes growth and postsynaptic differentiation at glutamatergic neuromuscular junctions. *Neuron* 66(5), pp. 724–738.

Barkovich, A.J., Guerrini, R., Kuzniecky, R.I., Jackson, G.D. and Dobyns, W.B. 2012. A developmental and genetic classification for malformations of cortical development: update 2012. *Brain: A Journal of Neurology* 135(Pt 5), pp. 1348–1369.

Barnea-Goraly, N., Kwon, H., Menon, V., Eliez, S., Lotspeich, L. and Reiss, A.L. 2004. White matter structure in autism: preliminary evidence from diffusion tensor imaging. *Biological Psychiatry* 55(3), pp. 323–326.

Baudouin, S.J., Gaudias, J., Gerharz, S., Hatstatt, L., Zhou, K., Punnakkal, P., Tanaka, K.F., Spooren, W., Hen, R., De Zeeuw, C.I., Vogt, K. and Scheiffele, P. 2012. Shared synaptic pathophysiology in syndromic and nonsyndromic rodent models of autism. *Science* 338(6103), pp. 128–132.

Bauman, M.L. 1991. Microscopic neuroanatomic abnormalities in autism. *Pediatrics*.87(5 Pt 2).pp 791-6.

Bean, B.P. 2007. The action potential in mammalian central neurons. *Nature Reviews. Neuroscience* 8(6), pp. 451–465.

Beattie, G.M., Lopez, A.D., Bucay, N., Hinton, A., Firpo, M.T., King, C.C. and Hayek, A. 2005. Activin A maintains pluripotency of human embryonic stem cells in the absence of feeder layers. *Stem Cells* 23(4), pp. 489–495.

Belinsky, G.S., Moore, A.R., Short, S.M., Rich, M.T. and Antic, S.D. 2011. Physiological properties of neurons derived from human embryonic stem cells using a dibutyryl cyclic AMP-based protocol. *Stem Cells and Development* 20(10), pp. 1733–1746.

Béna, F., Bruno, D.L., Eriksson, M., van Ravenswaaij-Arts, C., Stark, Z., Dijkhuizen, T., Gerkes, E., Gimelli, S., Ganesamoorthy, D., Thuresson, A.C., Labalme, A., Till, M., Bilan, F., Pasquier, L., Kitzis, A., Dubourgm, C., Rossi, M., Bottani, A., Gagnebin, M., Sanlaville, D., Gilbert-Dussardier, B., Guipponi, M., van Haeringen, A., Kriek, M., Ruivenkamp, C., Antonarakis, S.E., Anderlid, B.M., Slater, H.R. and Schoumans, J. 2013. Molecular and clinical characterization of 25 individuals with exonic deletions of NRXN1 and comprehensive review of the literature. *American Journal of Medical Genetics. Part B, Neuropsychiatric Genetics* 162B(4), pp. 388–403.

Berkel, S., Marshall, C.R., Weiss, B., Howe, J., Roeth, R., Moog, U., Endris, V., Roberts, W., Szatmari, P., Pinto, D., Bonin, M., Riess, A., Engels, H., Sprengel, R., Scherer, S.W. and Rappold, G.A. 2010. Mutations in the SHANK2 synaptic scaffolding gene in autism spectrum disorder and mental retardation. *Nature Genetics* 42(6), pp. 489–491.

Berney, T.P. 2000. Autism—an evolving concept. *The British Journal of Psychiatry*.

Berninghausen, O., Rahman, M.A., Silva, J.-P., Davletov, B., Hopkins, C. and Ushkaryov, Y.A. 2007. Neurexin Ibeta and neuroligin are localized on

opposite membranes in mature central synapses. *Journal of Neurochemistry* 103(5), pp. 1855–1863.

Berridge, M.J., Lipp, P. and Bootman, M.D. 2000. The versatility and universality of calcium signalling. *Nature Reviews. Molecular Cell Biology* 1(1), pp. 11–21.

Betizeau, M., Cortay, V., Patti, D., Pfister, S., Gautier, E., Bellemin-Ménard, A., Afanassieff, M., Huissoud, C., Douglas, R.J., Kennedy, H. and Dehay, C. 2013. Precursor diversity and complexity of lineage relationships in the outer subventricular zone of the primate. *Neuron* 80(2), pp. 442–457.

Bett, G.C., Lis, A., Wersinger, S.R., Baizer, J.S., Duffey, M.E. and Rasmusson, R.L. 2012. A Mouse Model of Timothy Syndrome: a Complex Autistic Disorder Resulting from a Point Mutation in Cav1.2. *North American journal of medicine & science* 5(3), pp. 135–140.

Bhattacharjee, A. and Kaczmarek, L.K. 2005. For K+ channels, Na+ is the new Ca2+. *Trends in Neurosciences* 28(8), pp. 422–428.

Bi, W., Yan, J., Stankiewicz, P., Park, S.-S., Walz, K., Boerkoel, C.F., Potocki, L., Shaffer, L.G., Devriendt, K., Nowaczyk, M.J.M., Inoue, K. and Lupski, J.R. 2002. Genes in a refined Smith-Magenis syndrome critical deletion interval on chromosome 17p11.2 and the syntenic region of the mouse. *Genome Research* 12(5), pp. 713–728.

Blanpied, T.A. and Ehlers, M.D. 2004. Microanatomy of dendritic spines: emerging principles of synaptic pathology in psychiatric and neurological disease. *Biological Psychiatry* 55(12), pp. 1121–1127.

Blatt, G.J., Fitzgerald, C.M., Guptill, J.T., Booker, A.B., Kemper, T.L. and Bauman, M.L. 2001. Density and distribution of hippocampal neurotransmitter receptors in autism: an autoradiographic study. *Journal of Autism and Developmental Disorders* 31(6), pp. 537–543.

Bock, C., Kiskinis, E., Verstappen, G., Gu, H., Boulting, G., Smith, Z.D., Ziller, M., Croft, G.F., Amoroso, M.W., Oakley, D.H., Gnirke, A., Eggan, K. and Meissner, A. 2011. Reference Maps of human ES and iPS cell variation enable high-throughput characterization of pluripotent cell lines. *Cell* 144(3), pp. 439–452.

Böckers, T.M., Mameza, M.G., Kreutz, M.R., Bockmann, J., Weise, C., Buck, F., Richter, D., Gundelfinger, E.D. and Kreienkamp, H.J. 2001. Synaptic scaffolding proteins in rat brain. Ankyrin repeats of the multidomain Shank protein family interact with the cytoskeletal protein alpha-fodrin. *The Journal of Biological Chemistry* 276(43), pp. 40104–40112.

Borlot, F., Regan, B.M., Bassett, A.S., Stavropoulos, D.J. and Andrade, D.M. 2017. Prevalence of Pathogenic Copy Number Variation in Adults With Pediatric-Onset Epilepsy and Intellectual Disability. *JAMA neurology* 74(11), pp. 1301–1311.

Borrell, V. and Götz, M. 2014. Role of radial glial cells in cerebral cortex folding. *Current Opinion in Neurobiology* 27, pp. 39–46.

Borrell, V. and Reillo, I. 2012. Emerging roles of neural stem cells in cerebral cortex development and evolution. *Developmental Neurobiology* 72(7), pp. 955–971.

Boucard, A A, Chubykin, A.A., Comoletti, D., Taylor P.and Sudhot TC. 2005. A splice code for trans-synaptic cell adhesion mediated by binding of neuroligin 1 to α-and β-neurexins. *Neuron*.48(2).pp.229-36.

Boucard, Antony A, Chubykin, A.A., Comoletti, D., Taylor, P. and Südhof, T.C. 2005.

A splice code for trans-synaptic cell adhesion mediated by binding of neuroligin 1 to alpha- and beta-neurexins. *Neuron* 48(2), pp. 229–236.

Boucard, A.A., Maxeiner, S. and Südhof, T.C. 2014. Latrophilins function as heterophilic cell-adhesion molecules by binding to teneurins: regulation by alternative splicing. *The Journal of Biological Chemistry* 289(1), pp. 387–402.

Boyer, L.A., Lee, T.I., Cole, M.F., Johnstone, S.E., Levine, S.S., Zucker, J.P., Guenther, M.G., Kumar, R.M., Murray, H.L., Jenner, R.G., Gifford, D.K., Melton, D.A., Jaenisch, R. and Young, R.A. 2005. Core transcriptional regulatory circuitry in human embryonic stem cells. *Cell* 122(6), pp. 947–956.

Brambrink, T., Foreman, R., Welstead, G.G., Lengner, C.J., Wernig, M., Suh, H. and Jaenisch, R. 2008. Sequential expression of pluripotency markers during direct reprogramming of mouse somatic cells. *Cell Stem Cell* 2(2), pp. 151–159.

Branco, T., Marra, V. and Staras, K. 2010. Examining size-strength relationships at hippocampal synapses using an ultrastructural measurement of synaptic release probability. *Journal of Structural Biology* 172(2), pp. 203–210.

Breitenkamp, A.F., Matthes, J. and Herzig, S. 2015. Voltage-gated Calcium Channels and Autism Spectrum Disorders. *Current molecular pharmacology*.

Breitenkamp, A.F.S., Matthes, J., Nass, R.D., Sinzig, J., Lehmkuhl, G., Nürnberg, P. and Herzig, S. 2014. Rare mutations of CACNB2 found in autism spectrum disease-affected families alter calcium channel function. *Plos One* 9(4), p. e95579.

Brennand, K.J., Simone, A., Jou, J., Gelboin-Burkhart, C., Tran, N., Sangar, S., Li, Y., Mu, Y., Chen, G., Yu, D., McCarthy, S., Sebat, J. and Gage, F.H. 2011. Modelling schizophrenia using human induced pluripotent stem cells. *Nature* 473(7346), pp. 221–225.

Brenner, R. and Wilcox, K.S. 2012. Potassium channelopathies of epilepsy. In: Noebels, J. L., Avoli, M., Rogawski, M. A., Olsen, R. W., and Delgado-Escueta, A. V. eds. *Jasper's basic mechanisms of the epilepsies*. 4th ed. Bethesda (MD): National Center for Biotechnology Information (US).

Britanova, O., de Juan Romero, C., Cheung, A., Kwan, K.Y., Schwark, M., Gyorgy, A., Vogel, T., Akopov, S., Mitkovski, M., Agoston, D., Sestan, N., Molnár, Z. and Tarabykin, V. 2008. Satb2 is a postmitotic determinant for upper-layer neuron specification in the neocortex. *Neuron* 57(3), pp. 378–392.

Brockhaus, J., Schreitmüller, M., Repetto, D., Klatt, O., Reissner, C., Elmslie, K., Heine, M. and Missler, M. 2018. α-Neurexins Together with α2δ-1 Auxiliary Subunits Regulate Ca2+ Influx through Cav2.1 Channels. *The Journal of Neuroscience* 38(38), pp. 8277–8294.

Brown, J.E., Cohen, L.B., De Weer, P., Pinto, L.H., Ross, W.N. and Salzberg, B.M. 1975. Rapid changes in intracellular free calcium concentration. Detection by metallochromic indicator dyes in squid giant axon. *Biophysical Journal* 15(11), pp. 1155–1160.

Bucan, M., Abrahams, B.S., Wang, K., Glessner, J.T., Herman, E.I., Sonnenblick, L.I., Alvarez Retuerto, A.I., Imielinski, M., Hadley, D., Bradfield, J.P., Kim, C., Gidaya, N.B., Lindquist, I., Hutman, T., Sigman, M., Kustanovich, V., Lajonchere, C.M., Singleton, A., Kim, J., Wassink, T.H., McMahon, W.M., Owley, T., Sweeney, J.A., Coon, H., Nurnberger, J.I., Li, M., Cantor, R.M., Minshew, N.J., Sutcliffe, J.S., Cook, E.H., Dawson, G., Buxbaum, J.D.,

Grant, S.F.A., Schellenberg, G.D., Geschwind, D.H. and Hakonarson, H. 2009. Genome-wide analyses of exonic copy number variants in a family-based study point to novel autism susceptibility genes. *PLoS Genetics* 5(6), p. e1000536.

Buganim, Y., Faddah, D.A., Cheng, A.W., Itskovich, E., Markoulaki, S., Ganz, K., Klemm, S.L., van Oudenaarden, A. and Jaenisch, R. 2012. Single-cell expression analyses during cellular reprogramming reveal an early stochastic and a late hierarchic phase. *Cell* 150(6), pp. 1209–1222.

Burgess, D.L., Kohrman, D.C., Galt, J., Plummer, N.W., Jones, J.M., Spear, B. and Meisler, M.H. 1995. Mutation of a new sodium channel gene, Scn8a, in the mouse mutant "motor endplate disease". *Nature Genetics* 10(4), pp. 461–465.

Calahorro, F. and Ruiz-Rubio, M. 2012. Functional phenotypic rescue of Caenorhabditis elegans neuroligin-deficient mutants by the human and rat NLGN1 genes. *Plos One* 7(6), p. e39277.

Carlsson, M.L. 1998. Hypothesis: is infantile autism a hypoglutamatergic disorder? Relevance of glutamate - serotonin interactions for pharmacotherapy. *Journal of Neural Transmission* 105(4–5), pp. 525–535.

Casanova, M.F., El-Baz, A.S., Kamat, S.S., Dombroski, B.A., Khalifa, F., Elnakib, A., Soliman, A., Allison-McNutt, A. and Switala, A.E. 2013. Focal cortical dysplasias in autism spectrum disorders. *Acta neuropathologica communications* 1, p. 67.

Cassimeris, L. and Spittle, C. 2001. Regulation of microtubule-associated proteins. *International Review of Cytology* 210, pp. 163–226.

Catterall, W.A. 2000. Structure and regulation of voltage-gated Ca2+ channels. *Annual Review of Cell and Developmental Biology* 16, pp. 521–555.

Catterall, W.A. and Few, A.P. 2008. Calcium channel regulation and presynaptic plasticity. *Neuron* 59(6), pp. 882–901.

Catterall, W.A., Goldin, A.L. and Waxman, S.G. 2005. International Union of Pharmacology. XLVII. Nomenclature and structure-function relationships of voltage-gated sodium channels. *Pharmacological Reviews* 57(4), pp. 397–409.

Catterall, W.A., Perez-Reyes, E., Snutch, T.P. and Striessnig, J. 2005. International Union of Pharmacology. XLVIII. Nomenclature and structure-function relationships of voltage-gated calcium channels. *Pharmacological Reviews* 57(4), pp. 411–425.

Caviness, V.S., Goto, T., Tarui, T., Takahashi, T., Bhide, P.G. and Nowakowski, R.S. 2003. Cell output, cell cycle duration and neuronal specification: a model of integrated mechanisms of the neocortical proliferative process. *Cerebral Cortex* 13(6), pp. 592–598.

Caviness, V.S., Takahashi, T. and Nowakowski, R.S. 1995. Numbers, time and neocortical neuronogenesis: a general developmental and evolutionary model. *Trends in Neurosciences* 18(9), pp. 379–383.

Cellot, G. and Cherubini, E. 2014. GABAergic signaling as therapeutic target for autism spectrum disorders. *Frontiers in pediatrics* 2, p. 70.

Cestèle, S. and Catterall, W.A. 2000. Molecular mechanisms of neurotoxin action on voltage-gated sodium channels. *Biochimie* 82(9–10), pp. 883–892.

Chakraborty, S., Christoforou, N., Fattahi, A., Herzog, R.W. and Leong, K.W. 2013. A robust strategy for negative selection of Cre-loxP recombination-based excision of transgenes in induced pluripotent stem cells. *Plos One* 8(5), p.

e64342.
Chambers, I., Colby, D., Robertson, M., Nichols, J., Lee, S., Tweedie, S. and Smith, A. 2003. Functional expression cloning of Nanog, a pluripotency sustaining factor in embryonic stem cells. *Cell* 113(5), pp. 643–655.
Chambers, S.M., Fasano, C.A., Papapetrou, E.P., Tomishima, M., Sadelain, M. and Studer, L. 2009. Highly efficient neural conversion of human ES and iPS cells by dual inhibition of SMAD signaling. *Nature Biotechnology* 27(3), pp. 275–280.
Chandy, K.G., Fantino, E., Wittekindt, O., Kalman, K., Tong, L.L., Ho, T.H., Gutman, G.A., Crocq, M.A., Ganguli, R., Nimgaonkar, V., Morris-Rosendahl, D.J. and Gargus, J.J. 1998. Isolation of a novel potassium channel gene hSKCa3 containing a polymorphic CAG repeat: a candidate for schizophrenia and bipolar disorder? *Molecular Psychiatry* 3(1), pp. 32–37.
Chandy, K.G. and Gutman, G.A. 1993. Nomenclature for mammalian potassium channel genes. *Trends in Pharmacological Sciences* 14(12), p. 434.
Cheah, C.S., Yu, F.H., Westenbroek, R.E., Kalume, F.K., Oakley, J.C., Potter, G.B., Rubenstein, J.L. and Catterall, W.A. 2012. Specific deletion of NaV1.1 sodium channels in inhibitory interneurons causes seizures and premature death in a mouse model of Dravet syndrome. *Proceedings of the National Academy of Sciences of the United States of America* 109(36), pp. 14646–14651.
Chen, B., Schaevitz, L.R. and McConnell, S.K. 2005. Fezl regulates the differentiation and axon targeting of layer 5 subcortical projection neurons in cerebral cortex. *Proceedings of the National Academy of Sciences of the United States of America* 102(47), pp. 17184–17189.
Chen, H., Qian, K., Du, Z., Cao, J., Petersen, A., Liu, H., Blackbourn, L.W., Huang, C.-L., Errigo, A., Yin, Y., Lu, J., Ayala, M. and Zhang, S.-C. 2014. Modeling ALS with iPSCs reveals that mutant SOD1 misregulates neurofilament balance in motor neurons. *Cell Stem Cell* 14(6), pp. 796–809.
Chen, J.-G., Rasin, M.-R., Kwan, K.Y. and Sestan, N. 2005. Zfp312 is required for subcortical axonal projections and dendritic morphology of deep-layer pyramidal neurons of the cerebral cortex. *Proceedings of the National Academy of Sciences of the United States of America* 102(49), pp. 17792–17797.
Chen, L.Y., Jiang, M., Zhang, B., Gokce, O. and Südhof, T.C. 2017. Conditional deletion of all neurexins defines diversity of essential synaptic organizer functions for neurexins. *Neuron* 94(3), p. 611–625.e4.
Chen, W.G., Chang, Q., Lin, Y., Meissner, A., West, A.E., Griffith, E.C., Jaenisch, R. and Greenberg, M.E. 2003. Derepression of BDNF transcription involves calcium-dependent phosphorylation of MeCP2. *Science* 302(5646), pp. 885–889.
Chen, X., Leischner, U., Rochefort, N.L., Nelken, I. and Konnerth, A. 2011. Functional mapping of single spines in cortical neurons in vivo. *Nature* 475(7357), pp. 501–505.
Chen, X., Yuan, L.-L., Zhao, C., Birnbaum, S.G., Frick, A., Jung, W.E., Schwarz, T.L., Sweatt, J.D. and Johnston, D. 2006. Deletion of Kv4.2 gene eliminates dendritic A-type K+ current and enhances induction of long-term potentiation in hippocampal CA1 pyramidal neurons. *The Journal of Neuroscience* 26(47), pp. 12143–12151.
Chen, Y.-C., Lin, Y.Q., Banerjee, S., Venken, K., Li, J., Ismat, A., Chen, K., Duraine,

L., Bellen, H.J. and Bhat, M.A. 2012. Drosophila neuroligin 2 is required presynaptically and postsynaptically for proper synaptic differentiation and synaptic transmission. *The Journal of Neuroscience* 32(45), pp. 16018–16030.

Chih, B., Afridi, S.K., Clark, L. and Scheiffele, P. 2004. Disorder-associated mutations lead to functional inactivation of neuroligins. *Human Molecular Genetics* 13(14), pp. 1471–1477.

Chih, B., Engelman, H. and Scheiffele, P. 2005. Control of excitatory and inhibitory synapse formation by neuroligins. *Science* 307(5713), pp. 1324–1328.

Chih, B., Gollan, L. and Scheiffele, P. 2006. Alternative splicing controls selective trans-synaptic interactions of the neuroligin-neurexin complex. *Neuron* 51(2), pp. 171–178.

Ching, M.S.L., Shen, Y., Tan, W.-H., Jeste, S.S., Morrow, E.M., Chen, X., Mukaddes, N.M., Yoo, S.-Y., Hanson, E., Hundley, R., Austin, C., Becker, R.E., Berry, G.T., Driscoll, K., Engle, E.C., Friedman, S., Gusella, J.F., Hisama, F.M., Irons, M.B., Lafiosca, T., LeClair, E., Miller, D.T., Neessen, M., Picker, J.D., Rappaport, L., Rooney, C.M., Sarco, D.P., Stoler, J.M., Walsh, C.A., Wolff, R.R., Zhang, T., Nasir, R.H., Wu, B.-L. and Children's Hospital Boston Genotype Phenotype Study Group 2010. Deletions of NRXN1 (neurexin-1) predispose to a wide spectrum of developmental disorders. *American Journal of Medical Genetics. Part B, Neuropsychiatric Genetics* 153B(4), pp. 937–947.

Choi, Y.-B., Li, H.-L., Kassabov, S.R., Jin, I., Puthanveettil, S.V., Karl, K.A., Lu, Y., Kim, J.-H., Bailey, C.H. and Kandel, E.R. 2011. Neurexin-neuroligin transsynaptic interaction mediates learning-related synaptic remodeling and long-term facilitation in aplysia. *Neuron* 70(3), pp. 468–481.

Christian, S.L., Brune, C.W., Sudi, J., Kumar, R.A., Liu, S., Karamohamed, S., Badner, J.A., Matsui, S., Conroy, J., McQuaid, D., Gergel, J., Hatchwell, E., Gilliam, T.C., Gershon, E.S., Nowak, N.J., Dobyns, W.B. and Cook, E.H. 2008. Novel submicroscopic chromosomal abnormalities detected in autism spectrum disorder. *Biological Psychiatry* 63(12), pp. 1111–1117.

Chubykin, A.A., Atasoy, D., Etherton, M.R., Brose, N., Kavalali, E.T., Gibson, J.R. and Südhof, T.C. 2007. Activity-dependent validation of excitatory versus inhibitory synapses by neuroligin-1 versus neuroligin-2. *Neuron* 54(6), pp. 919–931.

Clark, A.T., Bodnar, M.S., Fox, M., Rodriquez, R.T., Abeyta, M.J., Firpo, M.T. and Pera, R.A.R. 2004. Spontaneous differentiation of germ cells from human embryonic stem cells in vitro. *Human Molecular Genetics* 13(7), pp. 727–739.

Collins, T.J., Berridge, M.J., Lipp, P. and Bootman, M.D. 2002. Mitochondria are morphologically and functionally heterogeneous within cells. *The EMBO Journal* 21(7), pp. 1616–1627.

Comoletti, D., Flynn, R.E., Boucard, A.A. Demeler B., Schirf V., Shi J., Jennings LL., Newlin HR., Sudhof TC and Taylor P. 2006. Gene selection, alternative splicing, and post-translational processing regulate neuroligin selectivity for β-neurexins. *Biochemistry*.45(42).pp.12816-27.

Courchesne, E., Karns, C.M., Davis, H.R., Ziccardi, R., Carper, R.A., Tigue, Z.D., Chisum, H.J., Moses, P., Pierce, K., Lord, C., Lincoln, A.J., Pizzo, S., Schreibman, L., Haas, R.H., Akshoomoff, N.A. and Courchesne, R.Y. 2001. Unusual brain growth patterns in early life in patients with autistic

disorder: an MRI study. *Neurology* 57(2), pp. 245–254.
Courchesne, E., Mouton, P.R., Calhoun, M.E., Semendeferi, K., Ahrens-Barbeau, C., Hallet, M.J., Barnes, C.C. and Pierce, K. 2011. Neuron number and size in prefrontal cortex of children with autism. *The Journal of the American Medical Association* 306(18), pp. 2001–2010.
Courchesne, E.,Redcay E.and Kennedy DP. 2004. The autistic brain: birth through adulthood. *Current opinion in Neurology.*17(4).pp.489-96.
Crick, F. 1970. Central dogma of molecular biology. *Nature* 227(5258), pp. 561–563.
Crick, F.H. 1958. On protein synthesis. *Symposia of the Society for Experimental Biology* 12, pp. 138–163.
Cross-Disorder Group of the Psychiatric Genomics Consortium 2013. Identification of risk loci with shared effects on five major psychiatric disorders: a genome-wide analysis. *The Lancet* 381(9875), pp. 1371–1379.
Curran, S., Ahn, J.W., Grayton, H., Collier, D.A. and Ogilvie, C.M. 2013. NRXN1 deletions identified by array comparative genome hybridisation in a clinical case series - further understanding of the relevance of NRXN1 to neurodevelopmental disorders. *Journal of molecular psychiatry* 1(1), p. 4.
Curtetti, R., Garbossa, D. and Vercelli, A. 2002. Development of dendritic bundles of pyramidal neurons in the rat visual cortex. *Mechanisms of Ageing and Development* 123(5), pp. 473–479.
Dabell, M.P., Rosenfeld, J.A., Bader, P., Escobar, L.F., El-Khechen, D., Vallee, S.E., Dinulos, M.B.P., Curry, C., Fisher, J., Tervo, R., Hannibal, M.C., Siefkas, K., Wyatt, P.R., Hughes, L., Smith, R., Ellingwood, S., Lacassie, Y., Stroud, T., Farrell, S.A., Sanchez-Lara, P.A., Randolph, L.M., Niyazov, D., Stevens, C.A., Schoonveld, C., Skidmore, D., MacKay, S., Miles, J.H., Moodley, M., Huillet, A., Neill, N.J., Ellison, J.W., Ballif, B.C. and Shaffer, L.G. 2013. Investigation of NRXN1 deletions: clinical and molecular characterization. *American Journal of Medical Genetics. Part A* 161A(4), pp. 717–731.
D'Adamo, M.C., Catacuzzeno, L., Di Giovanni, G., Franciolini, F. and Pessia, M. 2013. K(+) channelepsy: progress in the neurobiology of potassium channels and epilepsy. *Frontiers in Cellular Neuroscience* 7, p. 134.
Daly, C. and Ziff, E.B. 1997. Post-transcriptional regulation of synaptic vesicle protein expression and the developmental control of synaptic vesicle formation. *The Journal of Neuroscience* 17(7), pp. 2365–2375.
Damaj, L., Lupien-Meilleur, A., Lortie, A., Riou, É., Ospina, L.H., Gagnon, L., Vanasse, C. and Rossignol, E. 2015. CACNA1A haploinsufficiency causes cognitive impairment, autism and epileptic encephalopathy with mild cerebellar symptoms. *European Journal of Human Genetics* 23(11), pp. 1505–1512.
Davare, M.A. and Hell, J.W. 2003. Increased phosphorylation of the neuronal L-type Ca2+ channel Cav1. 2 during aging. *... of the National Academy of Sciences*.
Davidovitch, M., Hemo, B., Manning-Courtney, P. and Fombonne, E. 2013. Prevalence and incidence of autism spectrum disorder in an Israeli population. *Journal of Autism and Developmental Disorders* 43(4), pp. 785–793.
Davis, A.C., Wims, M., Spotts, G.D., Hann, S.R. and Bradley, A. 1993. A null c-myc mutation causes lethality before 10.5 days of gestation in homozygotes and reduced fertility in heterozygous female mice. *Genes & Development* 7(4),

pp. 671–682.
De Rubeis, S., He, X., Goldberg, A.P., Poultney, C.S., Buxbaum, J.D., et al. 2014. Synaptic, transcriptional and chromatin genes disrupted in autism. *Nature* 515(7526), pp. 209–215.
Dean, C., Scholl, F.G., Choih, J., DeMaria, S., Berger, J., Isacoff, E. and Scheiffele, P. 2003. Neurexin mediates the assembly of presynaptic terminals. *Nature Neuroscience* 6(7), pp. 708–716.
Dehay, C. and Kennedy, H. 2007. Cell-cycle control and cortical development. *Nature Reviews. Neuroscience* 8(6), pp. 438–450.
Deng, P.-Y. and Klyachko, V.A. 2016. Increased Persistent Sodium Current Causes Neuronal Hyperexcitability in the Entorhinal Cortex of Fmr1 Knockout Mice. *Cell reports* 16(12), pp. 3157–3166.
Deng, P.-Y., Rotman, Z., Blundon, J.A., Cho, Y., Cui, J., Cavalli, V., Zakharenko, S.S. and Klyachko, V.A. 2013. FMRP regulates neurotransmitter release and synaptic information transmission by modulating action potential duration via BK channels. *Neuron* 77(4), pp. 696–711.
Deng, P.-Y., Sojka, D. and Klyachko, V.A. 2011. Abnormal presynaptic short-term plasticity and information processing in a mouse model of fragile X syndrome. *The Journal of Neuroscience* 31(30), pp. 10971–10982.
Developmental Disabilities Monitoring Network Surveillance Year 2010 Principal Investigators and Centers for Disease Control and Prevention (CDC) 2014. Prevalence of autism spectrum disorder among children aged 8 years - autism and developmental disabilities monitoring network, 11 sites, United States, 2010. *MMWR. Surveillance summaries : Morbidity and mortality weekly report. Surveillance summaries / CDC* 63(2), pp. 1–21.
Djukic, B., Casper, K.B., Philpot, B.D., Chin, L.-S. and McCarthy, K.D. 2007. Conditional knock-out of Kir4.1 leads to glial membrane depolarization, inhibition of potassium and glutamate uptake, and enhanced short-term synaptic potentiation. *The Journal of Neuroscience* 27(42), pp. 11354–11365.
Dolmetsch, R.E., Pajvani, U., Fife, K., Spotts, J.M. and Greenberg, M.E. 2001. Signaling to the nucleus by an L-type calcium channel-calmodulin complex through the MAP kinase pathway. *Science* 294(5541), pp. 333–339.
Dreyfus-Brisac, C. and Larroche, J.C. 1971. [Discontinuous electroencephalograms in the premature newborn and at term. Electro-anatomo-clinical correlations]. *Revue d'electroencephalographie et de neurophysiologie clinique* 1(1), pp. 95–99.
Duchen, M.R. 1999. Contributions of mitochondria to animal physiology: from homeostatic sensor to calcium signalling and cell death. *The Journal of Physiology* 516 (Pt 1), pp. 1–17.
Durand, C.M., Betancur, C., Boeckers, T.M., Bockmann, J., Chaste, P., Fauchereau, F., Nygren, G., Rastam, M., Gillberg, I.C., Anckarsäter, H., Sponheim, E., Goubran-Botros, H., Delorme, R., Chabane, N., Mouren-Simeoni, M.-C., de Mas, P., Bieth, E., Rogé, B., Héron, D., Burglen, L., Gillberg, C., Leboyer, M. and Bourgeron, T. 2007. Mutations in the gene encoding the synaptic scaffolding protein SHANK3 are associated with autism spectrum disorders. *Nature Genetics* 39(1), pp. 25–27.
Durkin, M.S., Maenner, M.J., Newschaffer, C.J., Lee, L.-C., Cunniff, C.M., Daniels, J.L., Kirby, R.S., Leavitt, L., Miller, L., Zahorodny, W. and Schieve, L.A. 2008. Advanced parental age and the risk of autism spectrum disorder.

American Journal of Epidemiology 168(11), pp. 1268–1276.

Ecker, C., Bookheimer, S.Y. and Murphy, D.G.M. 2015. Neuroimaging in autism spectrum disorder: brain structure and function across the lifespan. *Lancet Neurology* 14(11), pp. 1121–1134.

Ecker, C., Ginestet, C., Feng, Y., Johnston, P., Lombardo, M.V., Lai, M.-C., Suckling, J., Palaniyappan, L., Daly, E., Murphy, C.M., Williams, S.C., Bullmore, E.T., Baron-Cohen, S., Brammer, M., Murphy, D.G.M. and MRC AIMS Consortium 2013. Brain surface anatomy in adults with autism: the relationship between surface area, cortical thickness, and autistic symptoms. *JAMA psychiatry* 70(1), pp. 59–70.

Ecker, C., Shahidiani, A., Feng, Y., Daly, E., Murphy, C., D'Almeida, V., Deoni, S., Williams, S.C., Gillan, N., Gudbrandsen, M., Wichers, R., Andrews, D., Van Hemert, L. and Murphy, D.G.M. 2014. The effect of age, diagnosis, and their interaction on vertex-based measures of cortical thickness and surface area in autism spectrum disorder. *Journal of Neural Transmission* 121(9), pp. 1157–1170.

Enggaard Hoeffding, L.K., Hansen, T., Ingason, A., Doung, L., Thygesen, J.H., Møller, R.S., Tommerup, N., Kirov, G., Rujescu, D., Larsen, L.A. and Werge, T. 2014. Sequence analysis of 17 NRXN1 deletions. *American Journal of Medical Genetics. Part B, Neuropsychiatric Genetics* 165B(1), pp. 52–61.

Englund, C., Fink, A., Lau, C., Pham, D., Daza, R.A.M., Bulfone, A., Kowalczyk, T. and Hevner, R.F. 2005. Pax6, Tbr2, and Tbr1 are expressed sequentially by radial glia, intermediate progenitor cells, and postmitotic neurons in developing neocortex. *The Journal of Neuroscience* 25(1), pp. 247–251.

Epi4K Consortium 2016. De novo mutations in SLC1A2 and CACNA1A are important causes of epileptic encephalopathies. *American Journal of Human Genetics* 99(2), pp. 287–298.

Epi4K Consortium, Epilepsy Phenome/Genome Project, Allen, A.S., Berkovic, S.F., Winawer, M.R., et al. 2013. De novo mutations in epileptic encephalopathies. *Nature* 501(7466), pp. 217–221.

Ermolyuk, Y.S., Alder, F.G., Surges, R., Pavlov, I.Y., Timofeeva, Y., Kullmann, D.M. and Volynski, K.E. 2013. Differential triggering of spontaneous glutamate release by P/Q-, N- and R-type Ca2+ channels. *Nature Neuroscience* 16(12), pp. 1754–1763.

Escayg, A., MacDonald, B.T., Meisler, M.H., Baulac, S., Huberfeld, G., An-Gourfinkel, I., Brice, A., LeGuern, E., Moulard, B., Chaigne, D., Buresi, C. and Malafosse, A. 2000. Mutations of SCN1A, encoding a neuronal sodium channel, in two families with GEFS+2. *Nature Genetics* 24(4), pp. 343–345.

Espuny-Camacho, I., Michelsen, K.A., Gall, D., Linaro, D., Hasche, A., Bonnefont, J., Bali, C., Orduz, D., Bilheu, A., Herpoel, A., Lambert, N., Gaspard, N., Péron, S., Schiffmann, S.N., Giugliano, M., Gaillard, A. and Vanderhaeghen, P. 2013. Pyramidal neurons derived from human pluripotent stem cells integrate efficiently into mouse brain circuits in vivo. *Neuron* 77(3), pp. 440–456.

Estacion, M., O'Brien, J.E., Conravey, A., Hammer, M.F., Waxman, S.G., Dib-Hajj, S.D. and Meisler, M.H. 2014. A novel de novo mutation of SCN8A (Nav1.6) with enhanced channel activation in a child with epileptic encephalopathy. *Neurobiology of Disease* 69, pp. 117–123.

Etherton, M.R., Blaiss, C.A., Powell C.M. and Sudhof TC. 2009. Mouse neurexin-1α deletion causes correlated electrophysiological and behavioral changes consistent with cognitive impairments. *PNAS.*106(42).pp.17998-8003.

Evans, M.J. and Kaufman, M.H. 1981. Establishment in culture of pluripotential cells from mouse embryos. *Nature* 292(5819), pp. 154–156.

Fatemi, S.H. 2008. The hyperglutamatergic hypothesis of autism. *Progress in Neuro-Psychopharmacology & Biological Psychiatry* 32(3), pp. 911, author reply 912-3.

Fatemi, S.H., Folsom, T.D., Kneeland, R.E. and Liesch, S.B. 2011. Metabotropic glutamate receptor 5 upregulation in children with autism is associated with underexpression of both Fragile X mental retardation protein and GABAA receptor beta 3 in adults with autism. *Anatomical Record* 294(10), pp. 1635–1645.

Fatemi, S.H., Folsom, T.D., Reutiman, T.J. and Thuras, P.D. 2009. Expression of GABAB Receptors Is Altered in Brains of Subjects with Autism. *The Cerebellum*.

Fatemi, S.H., Halt, A.R., Realmuto, G., Earle, J., Kist, D.A., Thuras, P. and Merz, A. 2002. Purkinje cell size is reduced in cerebellum of patients with autism. *Cellular and Molecular Neurobiology* 22(2), pp. 171–175.

Feng, B., Jiang, J., Kraus, P., Ng, J.-H., Heng, J.-C.D., Chan, Y.-S., Yaw, L.-P., Zhang, W., Loh, Y.-H., Han, J., Vega, V.B., Cacheux-Rataboul, V., Lim, B., Lufkin, T. and Ng, H.-H. 2009. Reprogramming of fibroblasts into induced pluripotent stem cells with orphan nuclear receptor Esrrb. *Nature Cell Biology* 11(2), pp. 197–203.

Feng, J., Schroer, R., Yan, J., Song, W. and Yang…, C. 2006. High frequency of neurexin 1β signal peptide structural variants in patients with autism. *Neuroscience …*.

Fernández, V., Llinares-Benadero, C. and Borrell, V. 2016. Cerebral cortex expansion and folding: what have we learned? *The EMBO Journal* 35(10), pp. 1021–1044.

Feyder, M., Karlsson, R.-M., Mathur, P., Lyman, M., Bock, R., Momenan, R., Munasinghe, J., Scattoni, M.L., Ihne, J., Camp, M., Graybeal, C., Strathdee, D., Begg, A., Alvarez, V.A., Kirsch, P., Rietschel, M., Cichon, S., Walter, H., Meyer-Lindenberg, A., Grant, S.G.N. and Holmes, A. 2010. Association of mouse Dlg4 (PSD-95) gene deletion and human DLG4 gene variation with phenotypes relevant to autism spectrum disorders and Williams' syndrome. *The American Journal of Psychiatry* 167(12), pp. 1508–1517.

Fietz, S.A. and Huttner, W.B. 2011. Cortical progenitor expansion, self-renewal and neurogenesis-a polarized perspective. *Current Opinion in Neurobiology* 21(1), pp. 23–35.

Florio, M., Borrell, V. and Huttner, W.B. 2017. Human-specific genomic signatures of neocortical expansion. *Current Opinion in Neurobiology* 42, pp. 33–44.

Florio, M. and Huttner, W.B. 2014. Neural progenitors, neurogenesis and the evolution of the neocortex. *Development* 141(11), pp. 2182–2194.

Fong, H., Hohenstein, K.A. and Donovan, P.J. 2008. Regulation of self-renewal and pluripotency by Sox2 in human embryonic stem cells. *Stem Cells* 26(8), pp. 1931–1938.

Frazier, T.W. and Hardan, A.Y. 2009. A meta-analysis of the corpus callosum in autism. *Biological Psychiatry* 66(10), pp. 935–941.

Fuccillo, M.V., Földy, C., Gökce, Ö., Rothwell, P.E., Sun, G.L., Malenka, R.C. and

Südhof, T.C. 2015. Single-Cell mRNA Profiling Reveals Cell-Type-Specific Expression of Neurexin Isoforms. *Neuron* 87(2), pp. 326–340.

Fucile, S. 2004. Ca2+ permeability of nicotinic acetylcholine receptors. *Cell Calcium* 35(1), pp. 1–8.

Fusaki, N., Ban, H., Nishiyama, A., Saeki, K. and Hasegawa, M. 2009. Efficient induction of transgene-free human pluripotent stem cells using a vector based on Sendai virus, an RNA virus that does not integrate into the host genome. *Proceedings of the Japan Academy. Series B, Physical and biological sciences* 85(8), pp. 348–362.

Gai, X., Xie, H.M., Perin, J.C., Takahashi, N., Murphy, K., Wenocur, A.S., D'arcy, M., O'Hara, R.J., Goldmuntz, E., Grice, D.E., Shaikh, T.H., Hakonarson, H., Buxbaum, J.D., Elia, J. and White, P.S. 2012. Rare structural variation of synapse and neurotransmission genes in autism. *Molecular Psychiatry* 17(4), pp. 402–411.

Garber, K.B., Visootsak, J. and Warren, S.T. 2008. Fragile X syndrome. *European Journal of Human Genetics* 16(6), pp. 666–672.

Gauthier, J., Siddiqui, T.J., Huashan, P., Yokomaku, D., Hamdan, F.F., Champagne, N., Lapointe, M., Spiegelman, D., Noreau, A., Lafrenière, R.G., Fathalli, F., Joober, R., Krebs, M.-O., DeLisi, L.E., Mottron, L., Fombonne, E., Michaud, J.L., Drapeau, P., Carbonetto, S., Craig, A.M. and Rouleau, G.A. 2011. Truncating mutations in NRXN2 and NRXN1 in autism spectrum disorders and schizophrenia. *Human Genetics* 130(4), pp. 563–573.

Gauthier, J., Spiegelman, D., Piton, A., Lafrenière, R.G., Laurent, S., St-Onge, J., Lapointe, L., Hamdan, F.F., Cossette, P., Mottron, L., Fombonne, E., Joober, R., Marineau, C., Drapeau, P. and Rouleau, G.A. 2009. Novel de novo SHANK3 mutation in autistic patients. *American Journal of Medical Genetics. Part B, Neuropsychiatric Genetics* 150B(3), pp. 421–424.

Geppert, M., Khvotchev, M., Krasnoperov, V., Goda, Y., Missler, M., Hammer, R.E., Ichtchenko, K., Petrenko, A.G. and Südhof, T.C. 1998. Neurexin I alpha is a major alpha-latrotoxin receptor that cooperates in alpha-latrotoxin action. *The Journal of Biological Chemistry* 273(3), pp. 1705–1710.

Gershon, E.S., Grennan, K., Busnello, J., Badner, J.A., Ovsiew, F., Memon, S., Alliey-Rodriguez, N., Cooper, J., Romanos, B. and Liu, C. 2014. A rare mutation of CACNA1C in a patient with bipolar disorder, and decreased gene expression associated with a bipolar-associated common SNP of CACNA1C in brain. *Molecular Psychiatry* 19(8), pp. 890–894.

Gharani, N., Benayed, R., Mancuso, V., Brzustowicz, L.M. and Millonig, J.H. 2004. Association of the homeobox transcription factor, ENGRAILED 2, 3, with autism spectrum disorder. *Molecular Psychiatry* 9(5), pp. 474–484.

Gillberg, C. 1993. Autism and related behaviours. *Journal of Intellectual Disability Research*.

Gingras, M. Champigny M.F.and Berthod F. 2007. Differentiation of human adult skin-derived neuronal precursors into mature neurons. *Journal of cellular Physiology*.210(2).pp.498-506.

Gleeson, J.G., Allen, K.M., Fox, J.W., Lamperti, E.D., Berkovic, S., Scheffer, I., Cooper, E.C., Dobyns, W.B., Minnerath, S.R., Ross, M.E. and Walsh, C.A. 1998. Doublecortin, a brain-specific gene mutated in human X-linked lissencephaly and double cortex syndrome, encodes a putative signaling protein. *Cell* 92(1), pp. 63–72.

Glessner, J.T., Wang, K., Cai, G., Korvatska, O., Hakonarson, H., et al. 2009. Autism

genome-wide copy number variation reveals ubiquitin and neuronal genes. *Nature* 459(7246), pp. 569–573.

Gnecchi, M. and Melo, L.G. 2009. Bone marrow-derived mesenchymal stem cells: isolation, expansion, characterization, viral transduction, and production of conditioned medium. *Methods in Molecular Biology* 482, pp. 281–294.

Gogolla, N., Leblanc, J.J., Quast, K.B., Südhof, T.C., Fagiolini, M. and Hensch, T.K. 2009. Common circuit defect of excitatory-inhibitory balance in mouse models of autism. *Journal of neurodevelopmental disorders* 1(2), pp. 172–181.

Goldin, A.L., Barchi, R.L., Caldwell, J.H., Hofmann, F., Howe, J.R., Hunter, J.C., Kallen, R.G., Mandel, G., Meisler, M.H., Netter, Y.B., Noda, M., Tamkun, M.M., Waxman, S.G., Wood, J.N. and Catterall, W.A. 2000. Nomenclature of voltage-gated sodium channels. *Neuron* 28(2), pp. 365–368.

Grabundzija, I., Wang, J., Sebe, A., Erdei, Z., Kajdi, R., Devaraj, A., Steinemann, D., Szuhai, K., Stein, U., Cantz, T., Schambach, A., Baum, C., Izsvák, Z., Sarkadi, B. and Ivics, Z. 2013. Sleeping Beauty transposon-based system for cellular reprogramming and targeted gene insertion in induced pluripotent stem cells. *Nucleic Acids Research* 41(3), pp. 1829–1847.

Graef, I.A., Mermelstein, P.G., Stankunas, K., Neilson, J.R., Deisseroth, K., Tsien, R.W. and Crabtree, G.R. 1999. L-type calcium channels and GSK-3 regulate the activity of NF-ATc4 in hippocampal neurons. *Nature* 401(6754), pp. 703–708.

Grayton, H.M., Missler, M., Collier, D.A. and Fernandes, C. 2013. Altered social behaviours in neurexin 1α knockout mice resemble core symptoms in neurodevelopmental disorders. *Plos One* 8(6), p. e67114.

Greenberg, D.S., Houweling, A.R. and Kerr, J.N.D. 2008. Population imaging of ongoing neuronal activity in the visual cortex of awake rats. *Nature Neuroscience* 11(7), pp. 749–751.

Gregor, A., Albrecht, B., Bader, I., Bijlsma, E.K., Ekici, A.B., Engels, H., Hackmann, K., Horn, D., Hoyer, J., Klapecki, J., Kohlhase, J., Maystadt, I., Nagl, S., Prott, E., Tinschert, S., Ullmann, R., Wohlleber, E., Woods, G., Reis, A., Rauch, A. and Zweier, C. 2011. Expanding the clinical spectrum associated with defects in CNTNAP2 and NRXN1. *BMC Medical Genetics* 12, p. 106.

Grynkiewicz, G., Poenie, M. and Tsien, R.Y. 1985. A new generation of Ca2+ indicators with greatly improved fluorescence properties. *The Journal of Biological Chemistry* 260(6), pp. 3440–3450.

Gu, X. and Spitzer, N.C. 1995. Distinct aspects of neuronal differentiation encoded by frequency of spontaneous Ca2+ transients. *Nature* 375(6534), pp. 784–787.

Gubbay, J., Collignon, J., Koopman, P., Capel, B., Economou, A., Münsterberg, A., Vivian, N., Goodfellow, P. and Lovell-Badge, R. 1990. A gene mapping to the sex-determining region of the mouse Y chromosome is a member of a novel family of embryonically expressed genes. *Nature* 346(6281), pp. 245–250.

Hamdan, F.F., Gauthier, J., Araki, Y., Lin, D.-T., Yoshizawa, Y., Higashi, K., Park, A.-R., Spiegelman, D., Dobrzeniecka, S., Piton, A., Tomitori, H., Daoud, H., Massicotte, C., Henrion, E., Diallo, O., S2D Group, Shekarabi, M., Marineau, C., Shevell, M., Maranda, B., Mitchell, G., Nadeau, A., D'Anjou, G., Vanasse, M., Srour, M., Lafrenière, R.G., Drapeau, P., Lacaille, J.C., Kim, E., Lee, J.-R., Igarashi, K., Huganir, R.L., Rouleau, G.A. and Michaud, J.L. 2011. Excess of de novo deleterious mutations in genes

associated with glutamatergic systems in nonsyndromic intellectual disability. *American Journal of Human Genetics* 88(3), pp. 306–316.

Han, S., Tai, C., Westenbroek, R.E., Yu, F.H., Cheah, C.S., Potter, G.B., Rubenstein, J.L., Scheuer, T., de la Iglesia, H.O. and Catterall, W.A. 2012. Autistic-like behaviour in Scn1a+/- mice and rescue by enhanced GABA-mediated neurotransmission. *Nature* 489(7416), pp. 385–390.

Han, W., Kwan, K.Y., Shim, S., Lam, M.M.S., Shin, Y., Xu, X., Zhu, Y., Li, M. and Sestan, N. 2011. TBR1 directly represses Fezf2 to control the laminar origin and development of the corticospinal tract. *Proceedings of the National Academy of Sciences of the United States of America* 108(7), pp. 3041–3046.

Hardingham, G.E., Chawla, S., Cruzalegui, F.H. and Bading, H. 1999. Control of recruitment and transcription-activating function of CBP determines gene regulation by NMDA receptors and L-type calcium channels. *Neuron* 22(4), pp. 789–798.

Harkin, L.A., McMahon, J.M., Iona, X., Dibbens, L., Pelekanos, J.T., Zuberi, S.M., Sadleir, L.G., Andermann, E., Gill, D., Farrell, K., Connolly, M., Stanley, T., Harbord, M., Andermann, F., Wang, J., Batish, S.D., Jones, J.G., Seltzer, W.K., Gardner, A., Infantile Epileptic Encephalopathy Referral Consortium, Sutherland, G., Berkovic, S.F., Mulley, J.C. and Scheffer, I.E. 2007. The spectrum of SCN1A-related infantile epileptic encephalopathies. *Brain: A Journal of Neurology* 130(Pt 3), pp. 843–852.

Hawkins, N.A., Martin, M.S., Frankel, W.N., Kearney, J.A. and Escayg, A. 2011. Neuronal voltage-gated ion channels are genetic modifiers of generalized epilepsy with febrile seizures plus. *Neurobiology of Disease* 41(3), pp. 655–660.

Hazlett, H.C., Poe, M.D., Gerig, G., Styner, M., Chappell, C., Smith, R.G., Vachet, C. and Piven, J. 2011. Early brain overgrowth in autism associated with an increase in cortical surface area before age 2 years. *Archives of General Psychiatry* 68(5), pp. 467–476.

Hemara-Wahanui, A., Berjukow, S., Hope, C.I., Dearden, P.K., Wu, S.-B., Wilson-Wheeler, J., Sharp, D.M., Lundon-Treweek, P., Clover, G.M., Hoda, J.-C., Striessnig, J., Marksteiner, R., Hering, S. and Maw, M.A. 2005. A CACNA1F mutation identified in an X-linked retinal disorder shifts the voltage dependence of Cav1.4 channel activation. *Proceedings of the National Academy of Sciences of the United States of America* 102(21), pp. 7553–7558.

Herbert, M.R. 2010. Contributions of the environment and environmentally vulnerable physiology to autism spectrum disorders. *Current Opinion in Neurology* 23(2), pp. 103–110.

Hevner, R.F., Shi, L., Justice, N., Hsueh, Y., Sheng, M., Smiga, S., Bulfone, A., Goffinet, A.M., Campagnoni, A.T. and Rubenstein, J.L. 2001. Tbr1 regulates differentiation of the preplate and layer 6. *Neuron* 29(2), pp. 353–366.

Heyes, S., Pratt, W.S., Rees, E., Dahimene, S., Ferron, L., Owen, M.J. and Dolphin, A.C. 2015. Genetic disruption of voltage-gated calcium channels in psychiatric and neurological disorders. *Progress in Neurobiology* 134, pp. 36–54.

Hodgkin, A.L. and Huxley, A.F. 1952a. A quantitative description of membrane current and its application to conduction and excitation in nerve. *The*

Journal of Physiology 117(4), pp. 500–544.
Hodgkin, A.L. and Huxley, A.F. 1952b. Currents carried by sodium and potassium ions through the membrane of the giant axon of Loligo. *The Journal of Physiology* 116(4), pp. 449–472.
Holderith, N., Lorincz, A., Katona, G., Rózsa, B., Kulik, A., Watanabe, M. and Nusser, Z. 2012. Release probability of hippocampal glutamatergic terminals scales with the size of the active zone. *Nature Neuroscience* 15(7), pp. 988–997.
Hope, C.I. and Sharp…, D.M. 2005. Clinical manifestations of a unique X-linked retinal disorder in a large New Zealand family with a novel mutation in CACNA1F, the gene responsible for CSNB2. *Clinical & …*.
Horev, G., Ellegood, J., Lerch, J.P., Son, Y.-E.E., Muthuswamy, L., Vogel, H., Krieger, A.M., Buja, A., Henkelman, R.M., Wigler, M. and Mills, A.A. 2011. Dosage-dependent phenotypes in models of 16p11.2 lesions found in autism. *Proceedings of the National Academy of Sciences of the United States of America* 108(41), pp. 17076–17081.
Hu, Wenqin, Tian, C., Li, T., Yang, M., Hou, H. and Shu, Y. 2009. Distinct contributions of Na(v)1.6 and Na(v)1.2 in action potential initiation and backpropagation. *Nature Neuroscience* 12(8), pp. 996–1002.
Hu, W, Tian, C., Li, T., Yang, M., Hou, H. and Shu, Y. 2009. Distinct contributions of Nav1.6 and Nav1.2 in action potential initiation and backpropagation. *Nature neuroscience*.
Huber, K.M., Kayser, M.S. and Bear, M.F. 2000. Role for rapid dendritic protein synthesis in hippocampal mGluR-dependent long-term depression. *Science* 288(5469), pp. 1254–1257.
Hung, A.Y., Futai, K., Sala, C., Valtschanoff, J.G., Ryu, J., Woodworth, M.A., Kidd, F.L., Sung, C.C., Miyakawa, T., Bear, M.F., Weinberg, R.J. and Sheng, M. 2008. Smaller dendritic spines, weaker synaptic transmission, but enhanced spatial learning in mice lacking Shank1. *The Journal of Neuroscience* 28(7), pp. 1697–1708.
Huttenlocher, P.R., de Courten, C., Garey, L.J. and Van der Loos, H. 1982. Synaptogenesis in human visual cortex--evidence for synapse elimination during normal development. *Neuroscience Letters* 33(3), pp. 247–252.
Ichtchenko, K, Hata, Y., Nguyen, T., Ullrich, B., Missler, M., Moomaw, C. and Südhof, T.C. 1995. Neuroligin 1: a splice site-specific ligand for beta-neurexins. *Cell* 81(3), pp. 435–443.
Ichtchenko, Konstantin, Hata, Y., Nguyen, T., Ullrich, B., Missler, M., Moomaw, C. and Südhof, T.C. 1995. Neuroligin 1: A splice site-specific ligand for β-neurexins. *Cell* 81(3), pp. 435–443.
Ichtchenko, K., Nguyen, T. and Südhof, T.C. 1996. Structures, alternative splicing, and neurexin binding of multiple neuroligins. *The Journal of Biological Chemistry* 271(5), pp. 2676–2682.
International Molecular Genetic Study of Autism Consortium (IMGSAC) 2001. Further characterization of the autism susceptibility locus AUTS1 on chromosome 7q. *Human Molecular Genetics* 10(9), pp. 973–982.
International Stem Cell Initiative, Adewumi, O., Aflatoonian, B., Ahrlund-Richter, L., Zhang, W., et al. 2007. Characterization of human embryonic stem cell lines by the International Stem Cell Initiative. *Nature Biotechnology* 25(7), pp. 803–816.
Iossifov, I., Levy, D., Allen, J., Ye, K., Ronemus, M., Lee, Y.-H., Yamrom, B. and

Wigler, M. 2015. Low load for disruptive mutations in autism genes and their biased transmission. *Proceedings of the National Academy of Sciences of the United States of America* 112(41), pp. E5600-7.

Iossifov, I., Ronemus, M., Levy, D., Wang, Z., Hakker, I., Rosenbaum, J., Yamrom, B., Lee, Y.-H., Narzisi, G., Leotta, A., Kendall, J., Grabowska, E., Ma, B., Marks, S., Rodgers, L., Stepansky, A., Troge, J., Andrews, P., Bekritsky, M., Pradhan, K., Ghiban, E., Kramer, M., Parla, J., Demeter, R., Fulton, L.L., Fulton, R.S., Magrini, V.J., Ye, K., Darnell, J.C., Darnell, R.B., Mardis, E.R., Wilson, R.K., Schatz, M.C., McCombie, W.R. and Wigler, M. 2012. De novo gene disruptions in children on the autistic spectrum. *Neuron* 74(2), pp. 285–299.

Isom, L.L., De Jongh, K.S., Patton, D.E., Reber, B.F., Offord, J., Charbonneau, H., Walsh, K., Goldin, A.L. and Catterall, W.A. 1992. Primary structure and functional expression of the beta 1 subunit of the rat brain sodium channel. *Science* 256(5058), pp. 839–842.

Israel, M.A., Yuan, S.H., Bardy, C., Reyna, S.M., Mu, Y., Herrera, C., Hefferan, M.P., Van Gorp, S., Nazor, K.L., Boscolo, F.S., Carson, C.T., Laurent, L.C., Marsala, M., Gage, F.H., Remes, A.M., Koo, E.H. and Goldstein, L.S.B. 2012. Probing sporadic and familial Alzheimer's disease using induced pluripotent stem cells. *Nature* 482(7384), pp. 216–220.

Jamain, S., Betancur, C., Quach, H., Philippe, A., Fellous, M., Giros, B., Gillberg, C., Leboyer, M., Bourgeron, T. and Paris Autism Research International Sibpair (PARIS) Study 2002. Linkage and association of the glutamate receptor 6 gene with autism. *Molecular Psychiatry* 7(3), pp. 302–310.

Jamain, S., Quach, H., Betancur, C., Råstam, M., Colineaux, C., Gillberg, I.C., Soderstrom, H., Giros, B., Leboyer, M., Gillberg, C., Bourgeron, T. and Paris Autism Research International Sibpair Study 2003. Mutations of the X-linked genes encoding neuroligins NLGN3 and NLGN4 are associated with autism. *Nature Genetics* 34(1), pp. 27–29.

James, D., Levine, A.J., Besser, D. and Hemmati-Brivanlou, A. 2005. TGFbeta/activin/nodal signaling is necessary for the maintenance of pluripotency in human embryonic stem cells. *Development* 132(6), pp. 1273–1282.

Jenkins, A.K., Paterson, C., Wang, Y., Hyde, T.M., Kleinman, J.E. and Law, A.J. 2016. Neurexin 1 (NRXN1) splice isoform expression during human neocortical development and aging. *Molecular Psychiatry* 21(5), pp. 701–706.

Jessberger, S., Nakashima, K., Clemenson, G.D., Mejia, E., Mathews, E., Ure, K., Ogawa, S., Sinton, C.M., Gage, F.H. and Hsieh, J. 2007. Epigenetic modulation of seizure-induced neurogenesis and cognitive decline. *The Journal of Neuroscience* 27(22), pp. 5967–5975.

Jiang, Y.-H. and Ehlers, M.D. 2013. Modeling autism by SHANK gene mutations in mice. *Neuron* 78(1), pp. 8–27.

Jin, D., Liu, H.-X., Hirai, H., Torashima, T., Nagai, T., Lopatina, O., Shnayder, N.A., Yamada, K., Noda, M., Seike, T., Fujita, K., Takasawa, S., Yokoyama, S., Koizumi, K., Shiraishi, Y., Tanaka, S., Hashii, M., Yoshihara, T., Higashida, K., Islam, M.S., Yamada, N., Hayashi, K., Noguchi, N., Kato, I., Okamoto, H., Matsushima, A., Salmina, A., Munesue, T., Shimizu, N., Mochida, S., Asano, M. and Higashida, H. 2007. CD38 is critical for social behaviour by regulating oxytocin secretion. *Nature* 446(7131), pp. 41–45.

Jogini, V. and Roux, B. 2007. Dynamics of the Kv1.2 voltage-gated K+ channel in a membrane environment. *Biophysical Journal* 93(9), pp. 3070–3082.

Jones, L., López-Bendito, G., Gruss, P., Stoykova, A. and Molnár, Z. 2002. Pax6 is required for the normal development of the forebrain axonal connections. *Development* 129(21), pp. 5041–5052.

Kamijo, S., Ishii, Y., Horigane, S.-I., Suzuki, K., Ohkura, M., Nakai, J., Fujii, H., Takemoto-Kimura, S. and Bito, H. 2018. A Critical Neurodevelopmental Role for L-Type Voltage-Gated Calcium Channels in Neurite Extension and Radial Migration. *The Journal of Neuroscience* 38(24), pp. 5551–5566.

Kattenstroth, G., Tantalaki, E., Südhof, T.C., Gottmann, K. and Missler, M. 2004. Postsynaptic N-methyl-D-aspartate receptor function requires alpha-neurexins. *Proceedings of the National Academy of Sciences of the United States of America* 101(8), pp. 2607–2612.

Katz, L.C. and Shatz, C.J. 1996. Synaptic activity and the construction of cortical circuits. *Science* 274(5290), pp. 1133–1138.

Kawaguchi, A., Asano, H., Matsushima, K., Wada, T., Yoshida, S. and Ichida, S. 2007. Enhancement of sodium current in NG108-15 cells during neural differentiation is mainly due to an increase in NaV1.7 expression. *Neurochemical Research* 32(9), pp. 1469–1475.

Kearney, J.A., Plummer, N.W., Smith, M.R., Kapur, J., Cummins, T.R., Waxman, S.G., Goldin, A.L. and Meisler, M.H. 2001. A gain-of-function mutation in the sodium channel gene Scn2a results in seizures and behavioral abnormalities. *Neuroscience* 102(2), pp. 307–317.

Kelleher, R.J., Geigenmüller, U., Hovhannisyan, H., Trautman, E., Pinard, R., Rathmell, B., Carpenter, R. and Margulies, D. 2012. High-throughput sequencing of mGluR signaling pathway genes reveals enrichment of rare variants in autism. *Plos One* 7(4), p. e35003.

Kim, D., Kim, C.-H., Moon, J.-I., Chung, Y.-G., Chang, M.-Y., Han, B.-S., Ko, S., Yang, E., Cha, K.Y., Lanza, R. and Kim, K.-S. 2009. Generation of human induced pluripotent stem cells by direct delivery of reprogramming proteins. *Cell Stem Cell* 4(6), pp. 472–476.

Kim, J., Chu, J., Shen, X., Wang, J. and Orkin, S.H. 2008. An extended transcriptional network for pluripotency of embryonic stem cells. *Cell* 132(6), pp. 1049–1061.

Kim, J., Jung, S.-C., Clemens, A.M., Petralia, R.S. and Hoffman, D.A. 2007. Regulation of dendritic excitability by activity-dependent trafficking of the A-type K+ channel subunit Kv4.2 in hippocampal neurons. *Neuron* 54(6), pp. 933–947.

Kim, K.-Y., Hysolli, E. and Park, I.-H. 2011. Neuronal maturation defect in induced pluripotent stem cells from patients with Rett syndrome. *Proceedings of the National Academy of Sciences of the United States of America* 108(34), pp. 14169–14174.

Kim, Y., Rim, Y.A., Yi, H., Park, N., Park, S.-H. and Ju, J.H. 2016. The Generation of Human Induced Pluripotent Stem Cells from Blood Cells: An Efficient Protocol Using Serial Plating of Reprogrammed Cells by Centrifugation. *Stem cells international* 2016, p. 1329459.

Kirov, G., Rees, E., Walters, J.T.R., Escott-Price, V., Georgieva, L., Richards, A.L., Chambert, K.D., Davies, G., Legge, S.E., Moran, J.L., McCarroll, S.A., O'Donovan, M.C. and Owen, M.J. 2014. The penetrance of copy number variations for schizophrenia and developmental delay. *Biological*

Psychiatry 75(5), pp. 378–385.
Kirwan, P., Turner-Bridger, B., Peter, M., Momoh, A., Arambepola, D., Robinson, H.P.C. and Livesey, F.J. 2015. Development and function of human cerebral cortex neural networks from pluripotent stem cells in vitro. *Development* 142(18), pp. 3178–3187.
Kiskinis, E., Sandoe, J., Williams, L.A., Boulting, G.L., Moccia, R., Wainger, B.J., Han, S., Peng, T., Thams, S., Mikkilineni, S., Mellin, C., Merkle, F.T., Davis-Dusenbery, B.N., Ziller, M., Oakley, D., Ichida, J., Di Costanzo, S., Atwater, N., Maeder, M.L., Goodwin, M.J., Nemesh, J., Handsaker, R.E., Paull, D., Noggle, S., McCarroll, S.A., Joung, J.K., Woolf, C.J., Brown, R.H. and Eggan, K. 2014. Pathways disrupted in human ALS motor neurons identified through genetic correction of mutant SOD1. *Cell Stem Cell* 14(6), pp. 781–795.
Ko, J., Zhang, C., Arac, D., Boucard, A.A., Brunger, A.T. and Südhof, T.C. 2009. Neuroligin-1 performs neurexin-dependent and neurexin-independent functions in synapse validation. *The EMBO Journal* 28(20), pp. 3244–3255.
Kogan, M.D., Blumberg, S.J., Schieve, L.A., Boyle, C.A., Perrin, J.M., Ghandour, R.M., Singh, G.K., Strickland, B.B., Trevathan, E. and van Dyck, P.C. 2009. Prevalence of parent-reported diagnosis of autism spectrum disorder among children in the US, 2007. *Pediatrics* 124(5), pp. 1395–1403.
Kondo, T., Asai, M., Tsukita, K., Kutoku, Y., Ohsawa, Y., Sunada, Y., Imamura, K., Egawa, N., Yahata, N., Okita, K., Takahashi, K., Asaka, I., Aoi, T., Watanabe, A., Watanabe, K., Kadoya, C., Nakano, R., Watanabe, D., Maruyama, K., Hori, O., Hibino, S., Choshi, T., Nakahata, T., Hioki, H., Kaneko, T., Naitoh, M., Yoshikawa, K., Yamawaki, S., Suzuki, S., Hata, R., Ueno, S.-I., Seki, T., Kobayashi, K., Toda, T., Murakami, K., Irie, K., Klein, W.L., Mori, H., Asada, T., Takahashi, R., Iwata, N., Yamanaka, S. and Inoue, H. 2013. Modeling Alzheimer's disease with iPSCs reveals stress phenotypes associated with intracellular Aβ and differential drug responsiveness. *Cell Stem Cell* 12(4), pp. 487–496.
Kornack, D.R. and Rakic, P. 1998. Changes in cell-cycle kinetics during the development and evolution of primate neocortex. *Proceedings of the National Academy of Sciences of the United States of America* 95(3), pp. 1242–1246.
Kowalczyk, T., Pontious, A., Englund, C., Daza, R.A.M., Bedogni, F., Hodge, R., Attardo, A., Bell, C., Huttner, W.B. and Hevner, R.F. 2009. Intermediate neuronal progenitors (basal progenitors) produce pyramidal-projection neurons for all layers of cerebral cortex. *Cerebral Cortex* 19(10), pp. 2439–2450.
Krey, J.F. and Dolmetsch, R.E. 2007. Molecular mechanisms of autism: a possible role for Ca2+ signaling. *Current opinion in neurobiology*.
Krey, J.F., Paşca, S.P., Shcheglovitov, A., Yazawa, M., Schwemberger, R., Rasmusson, R. and Dolmetsch, R.E. 2013. Timothy syndrome is associated with activity-dependent dendritic retraction in rodent and human neurons. *Nature Neuroscience* 16(2), pp. 201–209.
Krueger, D.D., Tuffy, L.P., Papadopoulos, T. and Brose, N. 2012. The role of neurexins and neuroligins in the formation, maturation, and function of vertebrate synapses. *Current Opinion in Neurobiology* 22(3), pp. 412–422.
Kwan, K.Y., Lam, M.M.S., Krsnik, Z., Kawasawa, Y.I., Lefebvre, V. and Sestan, N. 2008. SOX5 postmitotically regulates migration, postmigratory

differentiation, and projections of subplate and deep-layer neocortical neurons. *Proceedings of the National Academy of Sciences of the United States of America* 105(41), pp. 16021–16026.

Kwan, K.Y., Sestan, N. and Anton, E.S. 2012. Transcriptional co-regulation of neuronal migration and laminar identity in the neocortex. *Development* 139(9), pp. 1535–1546.

Laarakker, M.C., Reinders, N.R., Bruining, H., Ophoff, R.A. and Kas, M.J.H. 2012. Sex-dependent novelty response in neurexin-1α mutant mice. *Plos One* 7(2), p. e31503.

Lai, T., Jabaudon, D., Molyneaux, B.J., Azim, E., Arlotta, P., Menezes, J.R.L. and Macklis, J.D. 2008. SOX5 controls the sequential generation of distinct corticofugal neuron subtypes. *Neuron* 57(2), pp. 232–247.

Lange, N., Travers, B.G., Bigler, E.D., Prigge, M.B.D., Froehlich, A.L., Nielsen, J.A., Cariello, A.N., Zielinski, B.A., Anderson, J.S., Fletcher, P.T., Alexander, A.A. and Lainhart, J.E. 2015. Longitudinal volumetric brain changes in autism spectrum disorder ages 6-35 years. *Autism research : official journal of the International Society for Autism Research* 8(1), pp. 82–93.

Larsen, J., Carvill, G.L., Gardella, E., Kluger, G., Schmiedel, G., Barisic, N., Depienne, C., Brilstra, E., Mang, Y., Nielsen, J.E.K., Kirkpatrick, M., Goudie, D., Goldman, R., Jähn, J.A., Jepsen, B., Gill, D., Döcker, M., Biskup, S., McMahon, J.M., Koeleman, B., Harris, M., Braun, K., de Kovel, C.G.F., Marini, C., Specchio, N., Djémié, T., Weckhuysen, S., Tommerup, N., Troncoso, M., Troncoso, L., Bevot, A., Wolff, M., Hjalgrim, H., Guerrini, R., Scheffer, I.E., Mefford, H.C., Møller, R.S. and EuroEPINOMICS RES Consortium CRP 2015. The phenotypic spectrum of SCN8A encephalopathy. *Neurology* 84(5), pp. 480–489.

Laumonnier, F., Roger, S., Guérin P., Molinari F., Mrad R., Cahard D., Belhadj A., Halayem M., Persico AM., Elia M., Romano V., Holbert S., Andres C., Chaabouni H., Colleaux L., Constant J., Le Guennec JY and Briault S. 2006. Association of a Functional Deficit of the BK Ca Channel, a Synaptic Regulator of Neuronal Excitability, With Autism and Mental Retardation. *American Journal of Psychiatry.*163(9).pp.1622-9.

Lee, H., Lin, M.A., Kornblum, H.I., Papazian, D.M. and Nelson, S.F. 2014. Exome sequencing identifies de novo gain of function missense mutation in KCND2 in identical twins with autism and seizures that slows potassium channel inactivation. *Human Molecular Genetics* 23(13), pp. 3481–3489.

Lee, H.Y., Ge, W.-P., Huang, W., He, Y., Wang, G.X., Rowson-Baldwin, A., Smith, S.J., Jan, Y.N. and Jan, L.Y. 2011. Bidirectional regulation of dendritic voltage-gated potassium channels by the fragile X mental retardation protein. *Neuron* 72(4), pp. 630–642.

Leek, J.T. and Storey, J.D. 2007. Capturing heterogeneity in gene expression studies by surrogate variable analysis. *PLoS Genetics* 3(9), pp. 1724–1735.

de Lera Ruiz, M. and Kraus, R.L. 2015. Voltage-Gated Sodium Channels: Structure, Function, Pharmacology, and Clinical Indications. *Journal of Medicinal Chemistry* 58(18), pp. 7093–7118.

Leung, Y.M. 2010. Voltage-gated K+ channel modulators as neuroprotective agents. *Life sciences*.

Lewis, J.D., Evans, A.C., Pruett, J.R., Botteron, K., Zwaigenbaum, L., Estes, A., Gerig, G., Collins, L., Kostopoulos, P., McKinstry, R., Dager, S., Paterson, S., Schultz, R.T., Styner, M., Hazlett, H. and Piven, J. 2014. Network

inefficiencies in autism spectrum disorder at 24 months. *Translational psychiatry* 4, p. e388.
Lewis, J.D., Theilmann, R.J., Townsend, J. and Evans, A.C. 2013. Network efficiency in autism spectrum disorder and its relation to brain overgrowth. *Frontiers in Human Neuroscience* 7, p. 845.
Li, B., Tadross, M.R. and Tsien, R.W. 2016. Sequential ionic and conformational signaling by calcium channels drives neuronal gene expression. *Science* 351(6275), pp. 863–867.
Li, B.-M., Liu, X.-R., Yi, Y.-H., Deng, Y.-H., Su, T., Zou, X. and Liao, W.-P. 2011. Autism in Dravet syndrome: prevalence, features, and relationship to the clinical characteristics of epilepsy and mental retardation. *Epilepsy & Behavior* 21(3), pp. 291–295.
Li, J., Ashley, J., Budnik, V. and Bhat, M.A. 2007. Crucial role of Drosophila neurexin in proper active zone apposition to postsynaptic densities, synaptic growth, and synaptic transmission. *Neuron* 55(5), pp. 741–755.
Li, J., You, Y., Yue, W., Jia, M., Yu, H., Lu, T., Wu, Z., Ruan, Y., Wang, L. and Zhang, D. 2015. Genetic evidence for possible involvement of the calcium channel gene CACNA1A in autism pathogenesis in chinese han population. *Plos One* 10(11), p. e0142887.
Liang, P. and Pardee, A.B. 1992. Differential display of eukaryotic messenger RNA by means of the polymerase chain reaction. *Science* 257(5072), pp. 967–971.
Libero, L.E., DeRamus, T.P., Lahti, A.C., Deshpande, G. and Kana, R.K. 2015. Multimodal neuroimaging based classification of autism spectrum disorder using anatomical, neurochemical, and white matter correlates. *Cortex* 66, pp. 46–59.
Lijam, N., Paylor, R., McDonald, M.P., Crawley, J.N., Deng, C.X., Herrup, K., Stevens, K.E., Maccaferri, G., McBain, C.J., Sussman, D.J. and Wynshaw-Boris, A. 1997. Social interaction and sensorimotor gating abnormalities in mice lacking Dvl1. *Cell* 90(5), pp. 895–905.
Lim, S.J., Ho, S.C., Mok, P.L., Tan, K.L., Ong, A.H.K. and Gan, S.C. 2016. Induced pluripotent stem cells from human hair follicle keratinocytes as a potential source for in vitro hair follicle cloning. *PeerJ* 4, p. e2695.
Lin, M., Lachman, H.M. and Zheng, D. 2016. Transcriptomics analysis of iPSC-derived neurons and modeling of neuropsychiatric disorders. *Molecular and Cellular Neurosciences* 73, pp. 32–42.
Lin, M., Pedrosa, E., Shah, A., Hrabovsky, A., Maqbool, S., Zheng, D. and Lachman, H.M. 2011. RNA-Seq of human neurons derived from iPS cells reveals candidate long non-coding RNAs involved in neurogenesis and neuropsychiatric disorders. *Plos One* 6(9), p. e23356.
Lin, T., Chao, C., Saito, S., Mazur, S.J., Murphy, M.E., Appella, E. and Xu, Y. 2005. p53 induces differentiation of mouse embryonic stem cells by suppressing Nanog expression. *Nature Cell Biology* 7(2), pp. 165–171.
Linker, C. and Stern, C.D. 2004. Neural induction requires BMP inhibition only as a late step, and involves signals other than FGF and Wnt antagonists. *Development* 131(22), pp. 5671–5681.
Liu, J., Koscielska, K.A., Cao, Z., Hulsizer, S., Grace, N., Mitchell, G., Nacey, C., Githinji, J., McGee, J., Garcia-Arocena, D., Hagerman, R.J., Nolta, J., Pessah, I.N. and Hagerman, P.J. 2012. Signaling defects in iPSC-derived fragile X premutation neurons. *Human Molecular Genetics* 21(17), pp.

3795–3805.
Lizarraga, S.B., Margossian, S.P., Harris, M.H., Campagna, D.R., Han, A.-P., Blevins, S., Mudbhary, R., Barker, J.E., Walsh, C.A. and Fleming, M.D. 2010. Cdk5rap2 regulates centrosome function and chromosome segregation in neuronal progenitors. *Development* 137(11), pp. 1907–1917.
Lord, C. and Jones, R.M. 2012. Annual research review: re-thinking the classification of autism spectrum disorders. *Journal of Child Psychology and Psychiatry, and Allied Disciplines* 53(5), pp. 490–509.
Lory, P., Monteil, A., Chemin, J., Leuranguer, V. and Bourinet…, E. 2000. Molecular diversity of calcium channel activities by depolarization. *Therapie*.
Lu, A.T.-H., Dai, X., Martinez-Agosto, J.A. and Cantor, R.M. 2012. Support for calcium channel gene defects in autism spectrum disorders. *Molecular autism* 3(1), p. 18.
Luedi, P.P., Dietrich, F.S., Weidman, J.R., Bosko, J.M., Jirtle, R.L. and Hartemink, A.J. 2007. Computational and experimental identification of novel human imprinted genes. *Genome Research* 17(12), pp. 1723–1730.
Lui, J.H., Hansen, D.V. and Kriegstein, A.R. 2011. Development and evolution of the human neocortex. *Cell* 146(1), pp. 18–36.
Luo, R., Sanders, S.J., Tian, Y., Voineagu, I., Huang, N., Chu, S.H., Klei, L., Cai, C., Ou, J., Lowe, J.K., Hurles, M.E., Devlin, B., State, M.W. and Geschwind, D.H. 2012. Genome-wide transcriptome profiling reveals the functional impact of rare de novo and recurrent CNVs in autism spectrum disorders. *American Journal of Human Genetics* 91(1), pp. 38–55.
Luskin, M.B., Zigova, T., Soteres, B.J. and Stewart, R.R. 1997. Neuronal progenitor cells derived from the anterior subventricular zone of the neonatal rat forebrain continue to proliferate in vitro and express a neuronal phenotype. *Molecular and Cellular Neurosciences* 8(5), pp. 351–366.
Ma, D., Salyakina, D., Jaworski, J.M., Konidari, I., Whitehead, P.L., Andersen, A.N., Hoffman, J.D., Slifer, S.H., Hedges, D.J., Cukier, H.N., Griswold, A.J., McCauley, J.L., Beecham, G.W., Wright, H.H., Abramson, R.K., Martin, E.R., Hussman, J.P., Gilbert, J.R., Cuccaro, M.L., Haines, J.L. and Pericak-Vance, M.A. 2009. A genome-wide association study of autism reveals a common novel risk locus at 5p14.1. *Annals of Human Genetics* 73(Pt 3), pp. 263–273.
Mahmood, F., Mozere, M., Zdebik, A.A., Stanescu, H.C., Tobin, J., Beales, P.L., Kleta, R., Bockenhauer, D. and Russell, C. 2013. Generation and validation of a zebrafish model of EAST (epilepsy, ataxia, sensorineural deafness and tubulopathy) syndrome. *Disease Models & Mechanisms* 6(3), pp. 652–660.
Malinow, R. and Malenka, R.C. 2002. AMPA receptor trafficking and synaptic plasticity. *Annual Review of Neuroscience* 25, pp. 103–126.
Mallmann, R.T., Elgueta, C., Sleman, F., Castonguay, J., Wilmes, T., van den Maagdenberg, A. and Klugbauer, N. 2013. Ablation of Ca(V)2.1 voltage-gated Ca^{2+} channels in mouse forebrain generates multiple cognitive impairments. *Plos One* 8(10), p. e78598.
Mao, B.Q., Hamzei-Sichani, F., Aronov, D., Froemke, R.C. and Yuste, R. 2001. Dynamics of spontaneous activity in neocortical slices. *Neuron* 32(5), pp. 883–898.
Mao, Z., Bonni, A., Xia, F., Nadal-Vicens, M. and Greenberg, M.E. 1999. Neuronal activity-dependent cell survival mediated by transcription factor MEF2. *Science* 286(5440), pp. 785–790.

Marchetto, M.C.N., Carromeu, C., Acab, A., Yu, D., Yeo, G.W., Mu, Y., Chen, G., Gage, F.H. and Muotri, A.R. 2010. A model for neural development and treatment of Rett syndrome using human induced pluripotent stem cells. *Cell* 143(4), pp. 527–539.

Mariani, J., Coppola, G., Zhang, P., Abyzov, A., Provini, L., Tomasini, L., Amenduni, M., Szekely, A., Palejev, D., Wilson, M., Gerstein, M., Grigorenko, E.L., Chawarska, K., Pelphrey, K.A., Howe, J.R. and Vaccarino, F.M. 2015. FOXG1-Dependent Dysregulation of GABA/Glutamate Neuron Differentiation in Autism Spectrum Disorders. *Cell* 162(2), pp. 375–390.

Mariani, J., Simonini, M.V., Palejev, D., Tomasini, L., Coppola, G., Szekely, A.M., Horvath, T.L. and Vaccarino, F.M. 2012. Modeling human cortical development in vitro using induced pluripotent stem cells. *Proceedings of the National Academy of Sciences of the United States of America* 109(31), pp. 12770–12775.

Marshall, C.R., Noor, A., Vincent, J.B., Lionel, A.C., Feuk, L., Skaug, J., Shago, M., Moessner, R., Pinto, D., Ren, Y., Thiruvahindrapduram, B., Fiebig, A., Schreiber, S., Friedman, J., Ketelaars, C.E.J., Vos, Y.J., Ficicioglu, C., Kirkpatrick, S., Nicolson, R., Sloman, L., Summers, A., Gibbons, C.A., Teebi, A., Chitayat, D., Weksberg, R., Thompson, A., Vardy, C., Crosbie, V., Luscombe, S., Baatjes, R., Zwaigenbaum, L., Roberts, W., Fernandez, B., Szatmari, P. and Scherer, S.W. 2008. Structural variation of chromosomes in autism spectrum disorder. *American Journal of Human Genetics* 82(2), pp. 477–488.

Martin, M.S., Tang, B., Papale, L.A., Yu, F.H., Catterall, W.A. and Escayg, A. 2007. The voltage-gated sodium channel Scn8a is a genetic modifier of severe myoclonic epilepsy of infancy. *Human Molecular Genetics* 16(23), pp. 2892–2899.

Martynoga, B., Morrison, H., Price, D.J. and Mason, J.O. 2005. Foxg1 is required for specification of ventral telencephalon and region-specific regulation of dorsal telencephalic precursor proliferation and apoptosis. *Developmental Biology* 283(1), pp. 113–127.

Marui, T., Funatogawa, I., Koishi, S., Yamamoto, K., Matsumoto, H., Hashimoto, O., Nanba, E., Nishida, H., Sugiyama, T., Kasai, K., Watanabe, K., Kano, Y., Sasaki, T. and Kato, N. 2009. Association of the neuronal cell adhesion molecule (NRCAM) gene variants with autism. *The International Journal of Neuropsychopharmacology* 12(1), pp. 1–10.

Masui, S., Nakatake, Y., Toyooka, Y., Shimosato, D., Yagi, R., Takahashi, K., Okochi, H., Okuda, A., Matoba, R., Sharov, A.A., Ko, M.S.H. and Niwa, H. 2007. Pluripotency governed by Sox2 via regulation of Oct3/4 expression in mouse embryonic stem cells. *Nature Cell Biology* 9(6), pp. 625–635.

Matsuda, K., Budisantoso, T., Mitakidis, N., Sugaya, Y., Miura, E., Kakegawa, W., Yamasaki, M., Konno, K., Uchigashima, M., Abe, M., Watanabe, I., Kano, M., Watanabe, M., Sakimura, K., Aricescu, A.R. and Yuzaki, M. 2016. Transsynaptic Modulation of Kainate Receptor Functions by C1q-like Proteins. *Neuron* 90(4), pp. 752–767.

McCaffery, P. and Deutsch, C.K. 2005. Macrocephaly and the control of brain growth in autistic disorders. *Progress in Neurobiology* 77(1–2), pp. 38–56.

McCauley, J.L., Li, C., Jiang L., Olson LM., Crockett G., Gainer K., Folstein SE., Haines JL. and Sutcliffe JS. 2005. Genome-wide and Ordered-Subset

linkage analyses provide support for autism loci on 17q and 19p with evidence of phenotypic and interlocus genetic correlates. *BMC Medical genetics.*12;6:1.

McConnell, B.B., Ghaleb, A.M., Nandan, M.O. and Yang, V.W. 2007. The diverse functions of Krüppel-like factors 4 and 5 in epithelial biology and pathobiology. *Bioessays: News and Reviews in Molecular, Cellular and Developmental Biology* 29(6), pp. 549–557.

McEvilly, R.J., de Diaz, M.O., Schonemann, M.D., Hooshmand, F. and Rosenfeld, M.G. 2002. Transcriptional regulation of cortical neuron migration by POU domain factors. *Science* 295(5559), pp. 1528–1532.

McKenna, W.L., Betancourt, J., Larkin, K.A., Abrams, B., Guo, C., Rubenstein, J.L.R. and Chen, B. 2011. Tbr1 and Fezf2 regulate alternate corticofugal neuronal identities during neocortical development. *The Journal of Neuroscience* 31(2), pp. 549–564.

McMahon, J.A., Takada, S., Zimmerman, L.B., Fan, C.M., Harland, R.M. and McMahon, A.P. 1998. Noggin-mediated antagonism of BMP signaling is required for growth and patterning of the neural tube and somite. *Genes & Development* 12(10), pp. 1438–1452.

Meisler, M.H., Kearney, J. Ottman R., and Escayg A. 2001. Identification of epilepsy genes in human and mouse. *Annual review of genetics.*35:567-588.

Menezes, J.R. and Luskin, M.B. 1994. Expression of neuron-specific tubulin defines a novel population in the proliferative layers of the developing telencephalon. *The Journal of Neuroscience* 14(9), pp. 5399–5416.

Menezes, J.R., Smith, C.M., Nelson, K.C. and Luskin, M.B. 1995. The division of neuronal progenitor cells during migration in the neonatal mammalian forebrain. *Molecular and Cellular Neurosciences* 6(6), pp. 496–508.

Mikhailov, A., Choufani, S., Skaug, J. Kolozsvari D.,Marshall C., Scherer SW., Vincent JB. 2008. Chromosomal translocation t (5; 7)(q14; q31) and missense mutations implicate the voltage-gated potassium channel Kv4. 2 gene, KCND2, on 7q31 in in Autism. *Annual Meeting of the autism.*

Mishina, Y. 2003. Function of bone morphogenetic protein signaling during mouse development. *Frontiers in Bioscience* 8, pp. d855-69.

Missler, M., Hammer, R.E. and Südhof, T.C. 1998. Neurexophilin binding to alpha-neurexins. A single LNS domain functions as an independently folding ligand-binding unit. *The Journal of Biological Chemistry* 273(52), pp. 34716–34723.

Missler, M., Südhof, T.C. and Biederer, T. 2012. Synaptic cell adhesion. *Cold Spring Harbor Perspectives in Biology* 4(4), p. a005694.

Missler, M, Zhang, W., Rohlmann, A. and Kattenstroth…, G. 2003. α-Neurexins couple Ca2+ channels to synaptic vesicle exocytosis. *Nature*.

Missler, Markus, Zhang, W., Rohlmann, A., Kattenstroth, G., Hammer, R.E., Gottmann, K. and Südhof, T.C. 2003. Alpha-neurexins couple Ca2+ channels to synaptic vesicle exocytosis. *Nature* 423(6943), pp. 939–948.

Mitsui, K., Tokuzawa, Y., Itoh, H., Segawa, K., Murakami, M., Takahashi, K., Maruyama, M., Maeda, M. and Yamanaka, S. 2003. The homeoprotein Nanog is required for maintenance of pluripotency in mouse epiblast and ES cells. *Cell* 113(5), pp. 631–642.

Moe, M.C., Varghese, M., Danilov, A.I., Westerlund, U., Ramm-Pettersen, J., Brundin, L., Svensson, M., Berg-Johnsen, J. and Langmoen, I.A. 2005. Multipotent progenitor cells from the adult human brain:

neurophysiological differentiation to mature neurons. *Brain: A Journal of Neurology* 128(Pt 9), pp. 2189–2199.

Møller, R.S., Weber, Y.G., Klitten, L.L., Trucks, H., Muhle, H., Kunz, W.S., Mefford, H.C., Franke, A., Kautza, M., Wolf, P., Dennig, D., Schreiber, S., Rückert, I.-M., Wichmann, H.-E., Ernst, J.P., Schurmann, C., Grabe, H.J., Tommerup, N., Stephani, U., Lerche, H., Hjalgrim, H., Helbig, I., Sander, T. and EPICURE Consortium 2013. Exon-disrupting deletions of NRXN1 in idiopathic generalized epilepsy. *Epilepsia* 54(2), pp. 256–264.

Molyneaux, B.J., Arlotta, P., Hirata, T., Hibi, M. and Macklis, J.D. 2005. Fezl is required for the birth and specification of corticospinal motor neurons. *Neuron* 47(6), pp. 817–831.

Moradi, E., Khundrakpam, B., Lewis, J.D., Evans, A.C. and Tohka, J. 2017. Predicting symptom severity in autism spectrum disorder based on cortical thickness measures in agglomerative data. *Neuroimage* 144(Pt A), pp. 128–141.

Morgan, K., Stevens, E.B. Shah B., Cox PJ., Dixon AK., Lee K., Pinnock RD., Hughes J., Richardson PJ., Mizuguchi K., Jackson AP. 2000. β3: an additional auxiliary subunit of the voltage-sensitive sodium channel that modulates channel gating with distinct kinetics. *PNAS*. 97(5).pp.2308-13.

Morrow, E.M., Yoo, S.-Y., Flavell, S.W., Kim, T.-K., Lin, Y., Hill, R.S., Mukaddes, N.M., Balkhy, S., Gascon, G., Hashmi, A., Al-Saad, S., Ware, J., Joseph, R.M., Greenblatt, R., Gleason, D., Ertelt, J.A., Apse, K.A., Bodell, A., Partlow, J.N., Barry, B., Yao, H., Markianos, K., Ferland, R.J., Greenberg, M.E. and Walsh, C.A. 2008. Identifying autism loci and genes by tracing recent shared ancestry. *Science* 321(5886), pp. 218–223.

Mukhopadhyay, M., Shtrom, S., Rodriguez-Esteban, C., Chen, L., Tsukui, T., Gomer, L., Dorward, D.W., Glinka, A., Grinberg, A., Huang, S.P., Niehrs, C., Izpisúa Belmonte, J.C. and Westphal, H. 2001. Dickkopf1 is required for embryonic head induction and limb morphogenesis in the mouse. *Developmental Cell* 1(3), pp. 423–434.

Mullis, K.B. 1994. The polymerase chain reaction (Nobel lecture). *Angewandte Chemie International Edition*.

Mutch, C.A., Poduri, A., Sahin, M., Barry, B., Walsh, C.A. and Barkovich, A.J. 2016. Disorders of microtubule function in neurons: imaging correlates. *American Journal of Neuroradiology* 37(3), pp. 528–535.

Myers, S.M., Johnson, C.P. and American Academy of Pediatrics Council on Children With Disabilities 2007. Management of children with autism spectrum disorders. *Pediatrics* 120(5), pp. 1162–1182.

Nakagawa, M., Koyanagi, M., Tanabe, K., Takahashi, K., Ichisaka, T., Aoi, T., Okita, K., Mochiduki, Y., Takizawa, N. and Yamanaka, S. 2008. Generation of induced pluripotent stem cells without Myc from mouse and human fibroblasts. *Nature Biotechnology* 26(1), pp. 101–106.

Nanou, E. and Catterall, W.A. 2018. Calcium channels, synaptic plasticity, and neuropsychiatric disease. *Neuron* 98(3), pp. 466–481.

Natiq, A., Elalaoui, S.C. Miesch S., Bonnet C., Jonveaux P., Amzazi S and Sefiani A. 2014. A new case of de novo 19p13. 2p13. 12 deletion in a girl with overgrowth and severe developmental delay. *Molecular Cytogenetic*.5,7:40.

Neale, B.M., Kou, Y., Liu, L., Ma'ayan, A., Daly, M.J., et al. 2012. Patterns and rates of exonic de novo mutations in autism spectrum disorders. *Nature* 485(7397), pp. 242–245.

Need, A.C., Ge, D., Weale, M.E., Maia, J., Feng, S., Heinzen, E.L., Shianna, K.V., Yoon, W., Kasperaviciūte, D., Gennarelli, M., Strittmatter, W.J., Bonvicini, C., Rossi, G., Jayathilake, K., Cola, P.A., McEvoy, J.P., Keefe, R.S.E., Fisher, E.M.C., St Jean, P.L., Giegling, I., Hartmann, A.M., Möller, H.-J., Ruppert, A., Fraser, G., Crombie, C., Middleton, L.T., St Clair, D., Roses, A.D., Muglia, P., Francks, C., Rujescu, D., Meltzer, H.Y. and Goldstein, D.B. 2009. A genome-wide investigation of SNPs and CNVs in schizophrenia. *PLoS Genetics* 5(2), p. e1000373.

Neher, E. 1995. The use of fura-2 for estimating Ca buffers and Ca fluxes. *Neuropharmacology* 34(11), pp. 1423–1442.

Neher, E. 1998. Usefulness and limitations of linear approximations to the understanding of Ca++ signals. *Cell Calcium* 24(5–6), pp. 345–357.

Neher, E. and Sakaba, T. 2008. Multiple roles of calcium ions in the regulation of neurotransmitter release. *Neuron* 59(6), pp. 861–872.

Nichols, J., Zevnik, B., Anastassiadis, K., Niwa, H., Klewe-Nebenius, D., Chambers, I., Schöler, H. and Smith, A. 1998. Formation of pluripotent stem cells in the mammalian embryo depends on the POU transcription factor Oct4. *Cell* 95(3), pp. 379–391.

Noctor, S.C., Martínez-Cerdeño, V., Ivic, L. and Kriegstein, A.R. 2004. Cortical neurons arise in symmetric and asymmetric division zones and migrate through specific phases. *Nature Neuroscience* 7(2), pp. 136–144.

Nonaka-Kinoshita, M., Reillo, I., Artegiani, B., Martínez-Martínez, M.Á., Nelson, M., Borrell, V. and Calegari, F. 2013. Regulation of cerebral cortex size and folding by expansion of basal progenitors. *The EMBO Journal* 32(13), pp. 1817–1828.

Nordahl, C.W., Lange, N., Li, D.D., Barnett, L.A., Lee, A., Buonocore, M.H., Simon, T.J., Rogers, S., Ozonoff, S. and Amaral, D.G. 2011. Brain enlargement is associated with regression in preschool-age boys with autism spectrum disorders. *Proceedings of the National Academy of Sciences of the United States of America* 108(50), pp. 20195–20200.

Nusser, Z., Lujan, R., Laube, G., Roberts, J.D., Molnar, E. and Somogyi, P. 1998. Cell type and pathway dependence of synaptic AMPA receptor number and variability in the hippocampus. *Neuron* 21(3), pp. 545–559.

Nwaobi, S.E., Cuddapah, V.A., Patterson, K.C., Randolph, A.C. and Olsen, M.L. 2016. The role of glial-specific Kir4.1 in normal and pathological states of the CNS. *Acta Neuropathologica* 132(1), pp. 1–21.

O'Connell, K.S., McGregor, N.W., Lochner, C., Emsley, R. and Warnich, L. 2018. The genetic architecture of schizophrenia, bipolar disorder, obsessive-compulsive disorder and autism spectrum disorder. *Molecular and Cellular Neurosciences* 88, pp. 300–307.

Ohba, C., Kato, M., Takahashi, S., Lerman-Sagie, T., Lev, D., Terashima, H., Kubota, M., Kawawaki, H., Matsufuji, M., Kojima, Y., Tateno, A., Goldberg-Stern, H., Straussberg, R., Marom, D., Leshinsky-Silver, E., Nakashima, M., Nishiyama, K., Tsurusaki, Y., Miyake, N., Tanaka, F., Matsumoto, N. and Saitsu, H. 2014. Early onset epileptic encephalopathy caused by de novo SCN8A mutations. *Epilepsia* 55(7), pp. 994–1000.

Okamoto, N., Hatsukawa, Y. Shimojima K. and Yamamoto T. 2011. Submicroscopic deletion in 7q31 encompassing CADPS2 and TSPAN12 in a child with autism spectrum disorder and PHPV. *American Journal of medical genetics.*155A(7) pp. 1568-73.

Okita, K., Nakagawa, M., Hyenjong, H., Ichisaka, T. and Yamanaka, S. 2008. Generation of mouse induced pluripotent stem cells without viral vectors. *Science (New York)* 322(5903), pp. 949–953.

O'Roak, B.J., Vives, L., Girirajan, S., Karakoc, E., Krumm, N., Coe, B.P., Levy, R., Ko, A., Lee, C., Smith, J.D., Turner, E.H., Stanaway, I.B., Vernot, B., Malig, M., Baker, C., Reilly, B., Akey, J.M., Borenstein, E., Rieder, M.J., Nickerson, D.A., Bernier, R., Shendure, J. and Eichler, E.E. 2012. Sporadic autism exomes reveal a highly interconnected protein network of de novo mutations. *Nature* 485(7397), pp. 246–250.

Pak, C., Danko, T., Zhang, Y., Aoto, J., Anderson, G., Maxeiner, S., Yi, F., Wernig, M. and Südhof, T.C. 2015. Human Neuropsychiatric Disease Modeling using Conditional Deletion Reveals Synaptic Transmission Defects Caused by Heterozygous Mutations in NRXN1. *Cell Stem Cell* 17(3), pp. 316–328.

Palmieri, L., Papaleo, V., Porcelli, V., Scarcia, P., Gaita, L., Sacco, R., Hager, J., Rousseau, F., Curatolo, P., Manzi, B., Militerni, R., Bravaccio, C., Trillo, S., Schneider, C., Melmed, R., Elia, M., Lenti, C., Saccani, M., Pascucci, T., Puglisi-Allegra, S., Reichelt, K.L. and Persico, A.M. 2010. Altered calcium homeostasis in autism-spectrum disorders: evidence from biochemical and genetic studies of the mitochondrial aspartate/glutamate carrier AGC1. *Molecular Psychiatry* 15(1), pp. 38–52.

Pandolfi, P.P., Roth, M.E., Karis, A., Leonard, M.W., Dzierzak, E., Grosveld, F.G., Engel, J.D. and Lindenbaum, M.H. 1995. Targeted disruption of the GATA3 gene causes severe abnormalities in the nervous system and in fetal liver haematopoiesis. *Nature Genetics* 11(1), pp. 40–44.

Papale, L.A., Beyer, B., Jones, J.M., Sharkey, L.M., Tufik, S., Epstein, M., Letts, V.A., Meisler, M.H., Frankel, W.N. and Escayg, A. 2009. Heterozygous mutations of the voltage-gated sodium channel SCN8A are associated with spike-wave discharges and absence epilepsy in mice. *Human Molecular Genetics* 18(9), pp. 1633–1641.

Papale, L.A., Paul, K.N., Sawyer, N.T., Manns, J.R., Tufik, S. and Escayg, A. 2010. Dysfunction of the Scn8a voltage-gated sodium channel alters sleep architecture, reduces diurnal corticosterone levels, and enhances spatial memory. *The Journal of Biological Chemistry* 285(22), pp. 16553–16561.

Paredes, R.M., Etzler, J.C., Watts, L.T., Zheng, W. and Lechleiter, J.D. 2008. Chemical calcium indicators. *Methods* 46(3), pp. 143–151.

Parellada, M., Penzol, M.J., Pina, L., Moreno, C., González-Vioque, E., Zalsman, G. and Arango, C. 2014. The neurobiology of autism spectrum disorders. *European Psychiatry* 29(1), pp. 11–19.

Park, I.-H., Arora, N., Huo, H., Maherali, N., Ahfeldt, T., Shimamura, A., Lensch, M.W., Cowan, C., Hochedlinger, K. and Daley, G.Q. 2008. Disease-specific induced pluripotent stem cells. *Cell* 134(5), pp. 877–886.

Paşca, S.P., Portmann, T., Voineagu, I., Yazawa, M., Shcheglovitov, A., Paşca, A.M., Cord, B., Palmer, T.D., Chikahisa, S., Nishino, S., Bernstein, J.A., Hallmayer, J., Geschwind, D.H. and Dolmetsch, R.E. 2011. Using iPSC-derived neurons to uncover cellular phenotypes associated with Timothy syndrome. *Nature Medicine* 17(12), pp. 1657–1662.

Patani, R., Compston, A., Puddifoot, C.A., Wyllie, D.J.A., Hardingham, G.E., Allen, N.D. and Chandran, S. 2009. Activin/Nodal inhibition alone accelerates highly efficient neural conversion from human embryonic stem cells and imposes a caudal positional identity. *Plos One* 4(10), p. e7327.

Patel, T.P., Man, K., Firestein, B.L. and Meaney, D.F. 2015. Automated quantification of neuronal networks and single-cell calcium dynamics using calcium imaging. *Journal of Neuroscience Methods* 243, pp. 26–38.

Peça, J., Feliciano, C., Ting, J.T., Wang, W., Wells, M.F., Venkatraman, T.N., Lascola, C.D., Fu, Z. and Feng, G. 2011. Shank3 mutant mice display autistic-like behaviours and striatal dysfunction. *Nature* 472(7344), pp. 437–442.

Peñagarikano, O., Abrahams, B.S., Herman, E.I., Winden, K.D., Gdalyahu, A., Dong, H., Sonnenblick, L.I., Gruver, R., Almajano, J., Bragin, A., Golshani, P., Trachtenberg, J.T., Peles, E. and Geschwind, D.H. 2011. Absence of CNTNAP2 leads to epilepsy, neuronal migration abnormalities, and core autism-related deficits. *Cell* 147(1), pp. 235–246.

Pereira, A. and Furlan, F.A. 2010. Astrocytes and human cognition: modeling information integration and modulation of neuronal activity. *Progress in Neurobiology* 92(3), pp. 405–420.

Persico, A.M., D'Agruma, L., Maiorano, N., Totaro, A., Militerni, R., Bravaccio, C., Wassink, T.H., Schneider, C., Melmed, R., Trillo, S., Montecchi, F., Palermo, M., Pascucci, T., Puglisi-Allegra, S., Reichelt, K.L., Conciatori, M., Marino, R., Quattrocchi, C.C., Baldi, A., Zelante, L., Gasparini, P., Keller, F. and Collaborative Linkage Study of Autism 2001. Reelin gene alleles and haplotypes as a factor predisposing to autistic disorder. *Molecular Psychiatry* 6(2), pp. 150–159.

Pessah, I.N., Seegal, R.F., Lein, P.J., LaSalle, J., Yee, B.K., Van De Water, J. and Berman, R.F. 2008. Immunologic and neurodevelopmental susceptibilities of autism. *Neurotoxicology* 29(3), pp. 532–545.

Pinggera, A., Lieb, A., Benedetti, B., Lampert, M., Monteleone, S., Liedl, K.R., Tuluc, P. and Striessnig, J. 2015. CACNA1D de novo mutations in autism spectrum disorders activate Cav1.3 L-type calcium channels. *Biological Psychiatry* 77(9), pp. 816–822.

Pinggera, A., Mackenroth, L., Rump, A., Schallner, J., Beleggia, F., Wollnik, B. and Striessnig, J. 2017. New gain-of-function mutation shows CACNA1D as recurrently mutated gene in autism spectrum disorders and epilepsy. *Human Molecular Genetics* 26(15), pp. 2923–2932.

Pinggera, A. and Striessnig, J. 2016. Cav1.3 (CACNA1D) L-type Ca2+ channel dysfunction in CNS disorders. *The Journal of physiology*.

Pinto, D., Delaby, E., Merico, D., Barbosa, M., Scherer, S.W., et al. 2014. Convergence of genes and cellular pathways dysregulated in autism spectrum disorders. *American Journal of Human Genetics* 94(5), pp. 677–694.

Pinto, D., Pagnamenta, A.T., Klei, L., Anney, R., Betancur, C., et al. 2010. Functional impact of global rare copy number variation in autism spectrum disorders. *Nature* 466(7304), pp. 368–372.

Poirier, K., Lebrun, N., Broix, L., Tian, G., Saillour, Y., Boscheron, C., Parrini, E., Valence, S., Pierre, B.S., Oger, M., Lacombe, D., Geneviève, D., Fontana, E., Darra, F., Cances, C., Barth, M., Bonneau, D., Bernadina, B.D., N'guyen, S., Gitiaux, C., Parent, P., des Portes, V., Pedespan, J.M., Legrez, V., Castelnau-Ptakine, L., Nitschke, P., Hieu, T., Masson, C., Zelenika, D., Andrieux, A., Francis, F., Guerrini, R., Cowan, N.J., Bahi-Buisson, N. and Chelly, J. 2013. Mutations in TUBG1, DYNC1H1, KIF5C and KIF2A cause malformations of cortical development and microcephaly. *Nature*

Genetics 45(6), pp. 639–647.

Poliak, S., Gollan, L., Martinez, R., Custer, A., Einheber, S., Salzer, J.L., Trimmer, J.S., Shrager, P. and Peles, E. 1999. Caspr2, a new member of the neurexin superfamily, is localized at the juxtaparanodes of myelinated axons and associates with K+ channels. *Neuron* 24(4), pp. 1037–1047.

Poliak, S., Salomon, D., Elhanany, H., Sabanay, H., Kiernan, B., Pevny, L., Stewart, C.L., Xu, X., Chiu, S.-Y., Shrager, P., Furley, A.J.W. and Peles, E. 2003. Juxtaparanodal clustering of Shaker-like K+ channels in myelinated axons depends on Caspr2 and TAG-1. *The Journal of Cell Biology* 162(6), pp. 1149–1160.

Prè, D., Nestor, M.W., Sproul, A.A., Jacob, S., Koppensteiner, P., Chinchalongporn, V., Zimmer, M., Yamamoto, A., Noggle, S.A. and Arancio, O. 2014. A time course analysis of the electrophysiological properties of neurons differentiated from human induced pluripotent stem cells (iPSCs). *Plos One* 9(7), p. e103418.

Purcell, A.E., Jeon, O.H., Zimmerman, A.W., Blue, M.E. and Pevsner, J. 2001. Postmortem brain abnormalities of the glutamate neurotransmitter system in autism. *Neurology* 57(9), pp. 1618–1628.

Purcell, S.M., Moran, J.L., Fromer, M., Ruderfer, D., Solovieff, N., Roussos, P., O'Dushlaine, C., Chambert, K., Bergen, S.E., Kähler, A., Duncan, L., Stahl, E., Genovese, G., Fernández, E., Collins, M.O., Komiyama, N.H., Choudhary, J.S., Magnusson, P.K.E., Banks, E., Shakir, K., Garimella, K., Fennell, T., DePristo, M., Grant, S.G.N., Haggarty, S.J., Gabriel, S., Scolnick, E.M., Lander, E.S., Hultman, C.M., Sullivan, P.F., McCarroll, S.A. and Sklar, P. 2014. A polygenic burden of rare disruptive mutations in schizophrenia. *Nature* 506(7487), pp. 185–190.

Qian, J. and Noebels, J.L. 2001. Presynaptic Ca2+ channels and neurotransmitter release at the terminal of a mouse cortical neuron. *The Journal of Neuroscience* 21(11), pp. 3721–3728.

Qu, Y., Curtis, R., Lawson, D., Gilbride, K. Ge P., DiStefano PS., Silos-Santiago I., Catterall WA., Scheuer T. 2001. Differential modulation of sodium channel gating and persistent sodium currents by the β1, β2, and β3 subunits. *Molecular and Cellular Neuroscience.*18(5).pp.570-80.

Rajakulendran, S., Kaski, D. and Hanna, M.G. 2012. Neuronal P/Q-type calcium channel dysfunction in inherited disorders of the CNS. *Nature Reviews. Neurology* 8(2), pp. 86–96.

Raznahan, A., Lerch, J.P., Lee, N., Greenstein, D., Wallace, G.L., Stockman, M., Clasen, L., Shaw, P.W. and Giedd, J.N. 2011. Patterns of coordinated anatomical change in human cortical development: a longitudinal neuroimaging study of maturational coupling. *Neuron* 72(5), pp. 873–884.

Redies, C., Hertel, N. and Hübner, C.A. 2012. Cadherins and neuropsychiatric disorders. *Brain Research* 1470, pp. 130–144.

Reillo, I., de Juan Romero, C., García-Cabezas, M.Á. and Borrell, V. 2011. A role for intermediate radial glia in the tangential expansion of the mammalian cerebral cortex. *Cerebral Cortex* 21(7), pp. 1674–1694.

Ricciardi, S., Ungaro, F., Hambrock, M., Rademacher, N., Stefanelli, G., Brambilla, D., Sessa, A., Magagnotti, C., Bachi, A., Giarda, E., Verpelli, C., Kilstrup-Nielsen, C., Sala, C., Kalscheuer, V.M. and Broccoli, V. 2012. CDKL5 ensures excitatory synapse stability by reinforcing NGL-1-PSD95 interaction in the postsynaptic compartment and is impaired in patient iPSC-

derived neurons. *Nature Cell Biology* 14(9), pp. 911–923.
Robinton, D.A. and Daley, G.Q. 2012. The promise of induced pluripotent stem cells in research and therapy. *Nature* 481(7381), pp. 295–305.
Rodier, P.M., Ingram, J.L., Tisdale, B. and Croog, V.J. 1997. Linking etiologies in humans and animal models: studies of autism. *Reproductive Toxicology* 11(2–3), pp. 417–422.
Rojas, D.C., Peterson, E., Winterrowd, E., Reite, M.L., Rogers, S.J. and Tregellas, J.R. 2006. Regional gray matter volumetric changes in autism associated with social and repetitive behavior symptoms. *BMC Psychiatry* 6, p. 56.
Ronesi, J.A., Collins, K.A., Hays, S.A., Tsai, N.-P., Guo, W., Birnbaum, S.G., Hu, J.-H., Worley, P.F., Gibson, J.R. and Huber, K.M. 2012. Disrupted Homer scaffolds mediate abnormal mGluR5 function in a mouse model of fragile X syndrome. *Nature Neuroscience* 15(3), pp. 431–40, S1.
Roohi, J., Montagna, C., Tegay, D.H., Palmer, L.E., DeVincent, C., Pomeroy, J.C., Christian, S.L., Nowak, N. and Hatchwell, E. 2009. Disruption of contactin 4 in three subjects with autism spectrum disorder. *Journal of Medical Genetics* 46(3), pp. 176–182.
Rosenberg, S.S. and Spitzer, N.C. 2011. Calcium signaling in neuronal development. *Cold Spring Harbor Perspectives in Biology* 3(10), p. a004259.
Rubenstein, J.L.R. 2010. Three hypotheses for developmental defects that may underlie some forms of autism spectrum disorder. *Current Opinion in Neurology* 23(2), pp. 118–123.
Rubenstein, J.L.R. and Merzenich, M.M. 2003. Model of autism: increased ratio of excitation/inhibition in key neural systems. *Genes, Brain, and Behavior* 2(5), pp. 255–267.
Rujescu, D., Ingason, A., Cichon, S., Pietiläinen, O.P.H., et al., et al. 2009. Disruption of the neurexin 1 gene is associated with schizophrenia. *Human Molecular Genetics* 18(5), pp. 988–996.
Sadakata, T., Washida, M., Iwayama, Y., Shoji, S., Sato, Y., Ohkura, T., Katoh-Semba, R., Nakajima, M., Sekine, Y., Tanaka, M., Nakamura, K., Iwata, Y., Tsuchiya, K.J., Mori, N., Detera-Wadleigh, S.D., Ichikawa, H., Itohara, S., Yoshikawa, T. and Furuichi, T. 2007. Autistic-like phenotypes in Cadps2-knockout mice and aberrant CADPS2 splicing in autistic patients. *The Journal of Clinical Investigation* 117(4), pp. 931–943.
Sanders, S.J. and Ercan, A.G. Multiple recurrent de novo CNVs, including duplications of the 7q11. 23 Williams syndrome region, are strongly associated with autism. *Sencicek*.
Sanders, S.J., Ercan-Sencicek, A.G., Hus, V., Luo, R., State, M.W., et al. 2011. Multiple recurrent de novo CNVs, including duplications of the 7q11.23 Williams syndrome region, are strongly associated with autism. *Neuron* 70(5), pp. 863–885.
Sareen, D., Ebert, A.D., Heins, B.M., McGivern, J.V., Ornelas, L. and Svendsen, C.N. 2012. Inhibition of apoptosis blocks human motor neuron cell death in a stem cell model of spinal muscular atrophy. *Plos One* 7(6), p. e39113.
Sasai, Y., Lu, B., Steinbeisser, H., Geissert, D., Gont, L.K. and De Robertis, E.M. 1994. Xenopus chordin: a novel dorsalizing factor activated by organizer-specific homeobox genes. *Cell* 79(5), pp. 779–790.
Sato, D., Lionel, A.C., Leblond, C.S., Prasad, A., Pinto, D., Walker, S., O'Connor, I., Russell, C., Drmic, I.E., Hamdan, F.F., Michaud, J.L., Endris, V., Roeth, R., Delorme, R., Huguet, G., Leboyer, M., Rastam, M., Gillberg, C.,

Lathrop, M., Stavropoulos, D.J., Anagnostou, E., Weksberg, R., Fombonne, E., Zwaigenbaum, L., Fernandez, B.A., Roberts, W., Rappold, G.A., Marshall, C.R., Bourgeron, T., Szatmari, P. and Scherer, S.W. 2012. SHANK1 Deletions in Males with Autism Spectrum Disorder. *American Journal of Human Genetics* 90(5), pp. 879–887.

Schaaf, C.P., Boone, P.M., Sampath, S., Williams, C., Bader, P.I., Mueller, J.M., Shchelochkov, O.A., Brown, C.W., Crawford, H.P., Phalen, J.A., Tartaglia, N.R., Evans, P., Campbell, W.M., Tsai, A.C.-H., Parsley, L., Grayson, S.W., Scheuerle, A., Luzzi, C.D., Thomas, S.K., Eng, P.A., Kang, S.-H.L., Patel, A., Stankiewicz, P. and Cheung, S.W. 2012. Phenotypic spectrum and genotype-phenotype correlations of NRXN1 exon deletions. *European Journal of Human Genetics* 20(12), pp. 1240–1247.

Schaer, M., Ottet, M.-C., Scariati, E., Dukes, D., Franchini, M., Eliez, S. and Glaser, B. 2013. Decreased frontal gyrification correlates with altered connectivity in children with autism. *Frontiers in Human Neuroscience* 7, p. 750.

Schaller, K.L., Krzemien, D.M., Yarowsky, P.J., Krueger, B.K. and Caldwell, J.H. 1995. A novel, abundant sodium channel expressed in neurons and glia. *The Journal of Neuroscience* 15(5 Pt 1), pp. 3231–3242.

Scheffer, I.E., Zhang, Y.-H., Gecz, J. and Dibbens, L. 2010. Genetics of the epilepsies: genetic twists in the channels and other tales. *Epilepsia* 51 Suppl 1, pp. 33–36.

Scheiffele, P., Fan, J., Choih, J., Fetter, R. and Serafini, T. 2000. Neuroligin expressed in nonneuronal cells triggers presynaptic development in contacting axons. *Cell* 101(6), pp. 657–669.

Schena, M., Shalon, D., Davis, R.W. and Brown, P.O. 1995. Quantitative monitoring of gene expression patterns with a complementary DNA microarray. *Science* 270(5235), pp. 467–470.

Schier, A.F. 2003. Nodal signaling in vertebrate development. *Annual Review of Cell and Developmental Biology* 19, pp. 589–621.

Schmeisser, M.J., Ey, E., Wegener, S., Bockmann, J., Stempel, A.V., Kuebler, A., Janssen, A.-L., Udvardi, P.T., Shiban, E., Spilker, C., Balschun, D., Skryabin, B.V., Dieck, S. tom, Smalla, K.-H., Montag, D., Leblond, C.S., Faure, P., Torquet, N., Le Sourd, A.-M., Toro, R., Grabrucker, A.M., Shoichet, S.A., Schmitz, D., Kreutz, M.R., Bourgeron, T., Gundelfinger, E.D. and Boeckers, T.M. 2012. Autistic-like behaviours and hyperactivity in mice lacking ProSAP1/Shank2. *Nature* 486(7402), pp. 256–260.

Schmidt, H., Brachtendorf, S., Arendt, O., Hallermann, S., Ishiyama, S., Bornschein, G., Gall, D., Schiffmann, S.N., Heckmann, M. and Eilers, J. 2013. Nanodomain coupling at an excitatory cortical synapse. *Current Biology* 23(3), pp. 244–249.

Schmitz, C. and Rezaie, P. 2008. The neuropathology of autism: where do we stand? *Neuropathology and applied neurobiology*.34(1).pp.4-11.

Schmunk, G. and Gargus, J.J. 2013. Channelopathy pathogenesis in autism spectrum disorders. *Frontiers in genetics* 4, p. 222.

Schöler, H.R., Ruppert, S., Suzuki, N., Chowdhury, K. and Gruss, P. 1990. New type of POU domain in germ line-specific protein Oct-4. *Nature* 344(6265), pp. 435–439.

Schreiner, D., Nguyen, T.-M., Russo, G., Heber, S., Patrignani, A., Ahrné, E. and Scheiffele, P. 2014. Targeted combinatorial alternative splicing generates brain region-specific repertoires of neurexins. *Neuron* 84(2), pp. 386–398.

Schumann, C.M., Bloss, C.S., Barnes, C.C., Wideman, G.M., Carper, R.A., Akshoomoff, N., Pierce, K., Hagler, D., Schork, N., Lord, C. and Courchesne, E. 2010. Longitudinal magnetic resonance imaging study of cortical development through early childhood in autism. *The Journal of Neuroscience* 30(12), pp. 4419–4427.

Sebat, J., Lakshmi, B., Malhotra, D., Troge, J., Lese-Martin, C., Walsh, T., Yamrom, B., Yoon, S., Krasnitz, A., Kendall, J., Leotta, A., Pai, D., Zhang, R., Lee, Y.-H., Hicks, J., Spence, S.J., Lee, A.T., Puura, K., Lehtimäki, T., Ledbetter, D., Gregersen, P.K., Bregman, J., Sutcliffe, J.S., Jobanputra, V., Chung, W., Warburton, D., King, M.-C., Skuse, D., Geschwind, D.H., Gilliam, T.C., Ye, K. and Wigler, M. 2007. Strong association of de novo copy number mutations with autism. *Science* 316(5823), pp. 445–449.

Seifert, G. and Steinhäuser, C. 2013. Neuron-astrocyte signaling and epilepsy. *Experimental Neurology* 244, pp. 4–10.

Shah, B.S., Stevens, E.B. Pinnock R.D., Dixon AK., Lee K. 2001. Developmental expression of the novel voltage-gated sodium channel auxiliary subunit β3, in rat CNS. *The Journal of physiology.*534(Pt 3).pp. 763-776.

Shah, N.H. and Aizenman, E. 2014. Voltage-gated potassium channels at the crossroads of neuronal function, ischemic tolerance, and neurodegeneration. *Translational stroke research* 5(1), pp. 38–58.

Shahbazian, M., Young, J., Yuva-Paylor, L., Spencer, C., Antalffy, B., Noebels, J., Armstrong, D., Paylor, R. and Zoghbi, H. 2002. Mice with truncated MeCP2 recapitulate many Rett syndrome features and display hyperacetylation of histone H3. *Neuron* 35(2), pp. 243–254.

Shaw, P., Kabani, N.J., Lerch, J.P., Eckstrand, K., Lenroot, R., Gogtay, N., Greenstein, D., Clasen, L., Evans, A., Rapoport, J.L., Giedd, J.N. and Wise, S.P. 2008. Neurodevelopmental trajectories of the human cerebral cortex. *The Journal of Neuroscience* 28(14), pp. 3586–3594.

Shcheglovitov, A., Shcheglovitova, O., Yazawa, M., Portmann, T., Shu, R., Sebastiano, V., Krawisz, A., Froehlich, W., Bernstein, J.A., Hallmayer, J.F. and Dolmetsch, R.E. 2013. SHANK3 and IGF1 restore synaptic deficits in neurons from 22q13 deletion syndrome patients. *Nature* 503(7475), pp. 267–271.

Sheng, M. and Hoogenraad, C.C. 2007. The postsynaptic architecture of excitatory synapses: a more quantitative view. *Annual Review of Biochemistry* 76, pp. 823–847.

Sheng, M., McFadden, G. and Greenberg, M.E. 1990. Membrane depolarization and calcium induce c-fos transcription via phosphorylation of transcription factor CREB. *Neuron* 4(4), pp. 571–582.

Sheridan, S.D., Theriault, K.M., Reis, S.A., Zhou, F., Madison, J.M., Daheron, L., Loring, J.F. and Haggarty, S.J. 2011. Epigenetic characterization of the FMR1 gene and aberrant neurodevelopment in human induced pluripotent stem cell models of fragile X syndrome. *Plos One* 6(10), p. e26203.

Shi, Y., Kirwan, P. and Livesey, F.J. 2012. Directed differentiation of human pluripotent stem cells to cerebral cortex neurons and neural networks. *Nature Protocols* 7(10), pp. 1836–1846.

Shi, Y., Kirwan, P., Smith, J., Robinson, H.P.C. and Livesey, F.J. 2012. Human cerebral cortex development from pluripotent stem cells to functional excitatory synapses. *Nature Neuroscience* 15(3), pp. 477–86, S1.

Shimada, H., Yoshimura, N. Tsuji A., Kunisada T. 2009. Differentiation of

dopaminergic neurons from human embryonic stem cells: modulation of differentiation by FGF-20. *Journal of bioscience and bioengineering.*107(4).pp.447-54.

Shimomura, O., Johnson, F.H. and Saiga, Y. 1962. Extraction, purification and properties of aequorin, a bioluminescent protein from the luminous hydromedusan, Aequorea. *Journal of Cellular and Comparative Physiology* 59, pp. 223–239.

Shitamukai, A., Konno, D. and Matsuzaki, F. 2011. Oblique radial glial divisions in the developing mouse neocortex induce self-renewing progenitors outside the germinal zone that resemble primate outer subventricular zone progenitors. *The Journal of Neuroscience* 31(10), pp. 3683–3695.

Sicca, F., Ambrosini, E., Marchese, M., Sforna, L., Servettini, I., Valvo, G., Brignone, M.S., Lanciotti, A., Moro, F., Grottesi, A., Catacuzzeno, L., Baldini, S., Hasan, S., D'Adamo, M.C., Franciolini, F., Molinari, P., Santorelli, F.M. and Pessia, M. 2016. Gain-of-function defects of astrocytic Kir4.1 channels in children with autism spectrum disorders and epilepsy. *Scientific reports* 6, p. 34325.

Sicca, F., Imbrici, P., D'adamo, M.C., Moro, F. Bonatti F., Brovedani P., grottesi A., Guerrini R., Masi G., Santorelli FM., Pessia M. 2011. Autism with seizures and intellectual disability: possible causitive role of gain-of-function of The Inwardly Rectifying K+ Channel Kir4. 1. *Neurobiol Dis*.43(1),pp.239-47.

Siddiqui, T.J., Tari, P.K., Connor, S.A., Zhang, P., Dobie, F.A., She, K., Kawabe, H., Wang, Y.T., Brose, N. and Craig, A.M. 2013. An LRRTM4-HSPG complex mediates excitatory synapse development on dentate gyrus granule cells. *Neuron* 79(4), pp. 680–695.

Singh, B., Ogiwara, I., Kaneda, M., Tokonami, N., Mazaki, E., Baba, K., Matsuda, K., Inoue, Y. and Yamakawa, K. 2006. A Kv4.2 truncation mutation in a patient with temporal lobe epilepsy. *Neurobiology of Disease* 24(2), pp. 245–253.

Skafidas, E., Testa, R., Zantomio, D., Chana, G., Everall, I.P. and Pantelis, C. 2014. Predicting the diagnosis of autism spectrum disorder using gene pathway analysis. *Molecular Psychiatry* 19(4), pp. 504–510.

Smeeth, L., Cook, C., Fombonne, P.E., Heavey, L., Rodrigues, L.C., Smith, P.G. and Hall, A.J. 2004. Rate of first recorded diagnosis of autism and other pervasive developmental disorders in United Kingdom general practice, 1988 to 2001. *BMC Medicine* 2, p. 39.

Smith, J.R., Vallier, L., Lupo, G., Alexander, M., Harris, W.A. and Pedersen, R.A. 2008. Inhibition of Activin/Nodal signaling promotes specification of human embryonic stem cells into neuroectoderm. *Developmental Biology* 313(1), pp. 107–117.

Smith, W.C. and Harland, R.M. 1992. Expression cloning of noggin, a new dorsalizing factor localized to the Spemann organizer in Xenopus embryos. *Cell* 70(5), pp. 829–840.

Soghomonian, J.-J., Zhang, K., Reprakash, S. and Blatt, G.J. 2017. Decreased parvalbumin mRNA levels in cerebellar Purkinje cells in autism. *Autism research : official journal of the International Society for Autism Research* 10(11), pp. 1787–1796.

Soldatov, N.M. 2015. CACNB2: an emerging pharmacological target for hypertension, heart failure, arrhythmia and mental disorders. *Current molecular pharmacology* 8(1), pp. 32–42.

Sommer, C.A., Sommer, A.G., Longmire, T.A., Christodoulou, C., Thomas, D.D.,

Gostissa, M., Alt, F.W., Murphy, G.J., Kotton, D.N. and Mostoslavsky, G. 2010. Excision of reprogramming transgenes improves the differentiation potential of iPS cells generated with a single excisable vector. *Stem Cells* 28(1), pp. 64–74.

Song, J.Y., Ichtchenko, K., Südhof, T.C. and Brose, N. 1999. Neuroligin 1 is a postsynaptic cell-adhesion molecule of excitatory synapses. *Proceedings of the National Academy of Sciences of the United States of America* 96(3), pp. 1100–1105.

Song, M., Mohamad, O., Chen, D. and Yu, S.P. 2013. Coordinated development of voltage-gated na(+) and k(+) currents regulates functional maturation of forebrain neurons derived from human induced pluripotent stem cells. *Stem Cells and Development* 22(10), pp. 1551–1563.

Spampanato, J., Escayg, A., Meisler, M.H. and Goldin, A.L. 2001. Functional effects of two voltage-gated sodium channel mutations that cause generalized epilepsy with febrile seizures plus type 2. *The Journal of Neuroscience* 21(19), pp. 7481–7490.

Spigelman, I., Zhang, L. and Carlen, P.L. 1992. Patch-clamp study of postnatal development of CA1 neurons in rat hippocampal slices: membrane excitability and K+ currents. *Journal of Neurophysiology* 68(1), pp. 55–69.

Spitzer, N.C. 1994. Spontaneous Ca2+ spikes and waves in embryonic neurons: signaling systems for differentiation. *Trends in Neurosciences* 17(3), pp. 115–118.

Splawski, I., Timothy, K.W., Decher, N., Kumar, P., Sachse, F.B., Beggs, A.H., Sanguinetti, M.C. and Keating, M.T. 2005. Severe arrhythmia disorder caused by cardiac L-type calcium channel mutations. *Proceedings of the National Academy of Sciences of the United States of America* 102(23), p. 8089–96; discussion 8086.

Splawski, I., Timothy, K.W., Sharpe, L.M. and Decher…, N. 2004. CaV1.2 Calcium Channel Dysfunction Causes a Multisystem Disorder Including Arrhythmia and Autism. *Cell*.

Sridharan, R., Tchieu, J., Mason, M.J., Yachechko, R., Kuoy, E., Horvath, S., Zhou, Q. and Plath, K. 2009. Role of the murine reprogramming factors in the induction of pluripotency. *Cell* 136(2), pp. 364–377.

Stadtfeld, M., Nagaya, M., Utikal, J., Weir, G. and Hochedlinger, K. 2008. Induced pluripotent stem cells generated without viral integration. *Science (New York)* 322(5903), pp. 945–949.

Staerk, J., Dawlaty, M.M., Gao, Q., Maetzel, D., Hanna, J., Sommer, C.A., Mostoslavsky, G. and Jaenisch, R. 2010. Reprogramming of human peripheral blood cells to induced pluripotent stem cells. *Cell Stem Cell* 7(1), pp. 20–24.

Stancik, E.K., Navarro-Quiroga, I., Sellke, R. and Haydar, T.F. 2010. Heterogeneity in ventricular zone neural precursors contributes to neuronal fate diversity in the postnatal neocortex. *The Journal of Neuroscience* 30(20), pp. 7028–7036.

Stanfield, A.C., McIntosh, A.M., Spencer, M.D., Philip, R., Gaur, S. and Lawrie, S.M. 2008. Towards a neuroanatomy of autism: a systematic review and meta-analysis of structural magnetic resonance imaging studies. *European Psychiatry* 23(4), pp. 289–299.

Stanley, E.F. 1993. Single calcium channels and acetylcholine release at a presynaptic nerve terminal. *Neuron* 11(6), pp. 1007–1011.

Stein, E.L.A. and Chetkovich, D.M. 2010. Regulation of stargazin synaptic trafficking by C-terminal PDZ ligand phosphorylation in bidirectional synaptic plasticity. *Journal of Neurochemistry* 113(1), pp. 42–53.

Sterky, F.H., Trotter, J.H., Lee, S.-J., Recktenwald, C.V., Du, X., Zhou, B., Zhou, P., Schwenk, J., Fakler, B. and Südhof, T.C. 2017. Carbonic anhydrase-related protein CA10 is an evolutionarily conserved pan-neurexin ligand. *Proceedings of the National Academy of Sciences of the United States of America* 114(7), pp. E1253–E1262.

Strauss, K.A., Puffenberger, E.G., Huentelman, M.J., Gottlieb, S., Dobrin, S.E., Parod, J.M., Stephan, D.A. and Morton, D.H. 2006. Recessive symptomatic focal epilepsy and mutant contactin-associated protein-like 2. *The New England Journal of Medicine* 354(13), pp. 1370–1377.

Strom, S.P., Stone, J.L., Ten Bosch, J.R., Merriman, B., Cantor, R.M., Geschwind, D.H. and Nelson, S.F. 2010. High-density SNP association study of the 17q21 chromosomal region linked to autism identifies CACNA1G as a novel candidate gene. *Molecular Psychiatry* 15(10), pp. 996–1005.

Südhof, T.C. 2008. Neuroligins and neurexins link synaptic function to cognitive disease. *Nature* 455(7215), pp. 903–911.

Südhof, T.C. 2013. Neurotransmitter release: the last millisecond in the life of a synaptic vesicle. *Neuron* 80(3), pp. 675–690.

Südhof, T.C. 2017. Synaptic neurexin complexes: A molecular code for the logic of neural circuits. *Cell* 171(4), pp. 745–769.

Sugita, S., Ichtchenko, K. and Khvotchev M., Südhof TC 1998. α-Latrotoxin Receptor CIRL/Latrophilin 1 (CL1) defines an unusual Family of Ubiquitous G-protein-linked Receptors. G protein coupling not required for triggering exocytosis. *Journal of Biological chem;* 4273(49):32715-24.

Sugitani, Y., Nakai, S., Minowa, O., Nishi, M., Jishage, K.-I., Kawano, H., Mori, K., Ogawa, M. and Noda, T. 2002. Brn-1 and Brn-2 share crucial roles in the production and positioning of mouse neocortical neurons. *Genes & Development* 16(14), pp. 1760–1765.

Sundararajan, T., Manzardo, A.M. and Butler, M.G. 2018. Functional analysis of schizophrenia genes using GeneAnalytics program and integrated databases. *Gene* 641, pp. 25–34.

Takahashi, K., Okita, K., Nakagawa, M. and Yamanaka, S. 2007. Induction of pluripotent stem cells from fibroblast cultures. *Nature Protocols* 2(12), pp. 3081–3089.

Takahashi, K., Tanabe, K., Ohnuki, M., Narita, M., Ichisaka, T., Tomoda, K. and Yamanaka, S. 2007. Induction of pluripotent stem cells from adult human fibroblasts by defined factors. *Cell* 131(5), pp. 861–872.

Takahashi, K. and Yamanaka, S. 2006. Induction of pluripotent stem cells from mouse embryonic and adult fibroblast cultures by defined factors. *Cell* 126(4), pp. 663–676.

Takahashi, T., Nowakowski, R.S. and Caviness, V.S. 1996. The leaving or Q fraction of the murine cerebral proliferative epithelium: a general model of neocortical neuronogenesis. *The Journal of Neuroscience* 16(19), pp. 6183–6196.

Takumi, Y., Ramírez-León, V., Laake, P., Rinvik, E. and Ottersen, O.P. 1999. Different modes of expression of AMPA and NMDA receptors in hippocampal synapses. *Nature Neuroscience* 2(7), pp. 618–624.

Tanaka, H., Nogi, T., Yasui, N., Iwasaki, K. and Takagi, J. 2011. Structural basis for

variant-specific neuroligin-binding by α-neurexin. *Plos One* 6(4), p. e19411.

Tang, F., Dent, E.W. and Kalil, K. 2003. Spontaneous calcium transients in developing cortical neurons regulate axon outgrowth. *The Journal of Neuroscience* 23(3), pp. 927–936.

Tanguay, P.E. 2011. Autism in DSM-5. *The American Journal of Psychiatry* 168(11), pp. 1142–1144.

Tarabeux, J., Kebir, O., Gauthier, J., Hamdan, F.F., Xiong, L., Piton, A., Spiegelman, D., Henrion, É., Millet, B., S2D team, Fathalli, F., Joober, R., Rapoport, J.L., DeLisi, L.E., Fombonne, É., Mottron, L., Forget-Dubois, N., Boivin, M., Michaud, J.L., Drapeau, P., Lafrenière, R.G., Rouleau, G.A. and Krebs, M.O. 2011. Rare mutations in N-methyl-D-aspartate glutamate receptors in autism spectrum disorders and schizophrenia. *Translational psychiatry* 1, p. e55.

Taverna, E., Götz, M. and Huttner, W.B. 2014. The cell biology of neurogenesis: toward an understanding of the development and evolution of the neocortex. *Annual Review of Cell and Developmental Biology* 30, pp. 465–502.

Tchaconas, A. and Adesman, A. 2013. Autism spectrum disorders: a pediatric overview and update. *Current Opinion in Pediatrics* 25(1), pp. 130–144.

Tempel, B.L., Papazian, D.M., Schwarz, T.L., Jan, Y.N. and Jan, L.Y. 1987. Sequence of a probable potassium channel component encoded at Shaker locus of Drosophila. *Science* 237(4816), pp. 770–775.

Thomson, J.A., Itskovitz-Eldor, J., Shapiro, S.S., Waknitz, M.A., Swiergiel, J.J., Marshall, V.S. and Jones, J.M. 1998. Embryonic stem cell lines derived from human blastocysts. *Science* 282(5391), pp. 1145–1147.

Todarello, G., Feng, N., Kolachana, B.S., Li, C., Vakkalanka, R., Bertolino, A., Weinberger, D.R. and Straub, R.E. 2014. Incomplete penetrance of NRXN1 deletions in families with schizophrenia. *Schizophrenia Research* 155(1–3), pp. 1–7.

Tong, X.-J., López-Soto, E.J., Li, L., Liu, H., Nedelcu, D., Lipscombe, D., Hu, Z. and Kaplan, J.M. 2017. Retrograde Synaptic Inhibition Is Mediated by α-Neurexin Binding to the α2δ Subunits of N-Type Calcium Channels. *Neuron* 95(2), p. 326–340.e5.

Treutlein, B., Gokce, O., Quake, S.R. and Südhof, T.C. 2014. Cartography of neurexin alternative splicing mapped by single-molecule long-read mRNA sequencing. *Proceedings of the National Academy of Sciences of the United States of America* 111(13), pp. E1291-9.

Tropepe, V. and Sive, H.L. 2003. Can zebrafish be used as a model to study the neurodevelopmental causes of autism? *Genes, Brain, and Behavior* 2(5), pp. 268–281.

Trudeau, M.M., Dalton, J.C., Day, J.W., Ranum, L.P.W. and Meisler, M.H. 2006. Heterozygosity for a protein truncation mutation of sodium channel SCN8A in a patient with cerebellar atrophy, ataxia, and mental retardation. *Journal of Medical Genetics* 43(6), pp. 527–530.

Tsetsenis, T., Boucard, A.A., Araç, D., Brunger, A.T. and Südhof, T.C. 2014. Direct visualization of trans-synaptic neurexin-neuroligin interactions during synapse formation. *The Journal of Neuroscience* 34(45), pp. 15083–15096.

Tsien, R.W. 1983. Calcium channels in excitable cell membranes. *Annual Review of Physiology* 45, pp. 341–358.

Tsien, R.Y. 1989. Fluorescent probes of cell signaling. *Annual Review of*

Neuroscience 12, pp. 227–253.

Tsien, R.Y. 1980. New calcium indicators and buffers with high selectivity against magnesium and protons: design, synthesis, and properties of prototype structures. *Biochemistry* 19(11), pp. 2396–2404.

Tsien, R.Y., Pozzan, T. and Rink, T.J. 1982. Calcium homeostasis in intact lymphocytes: cytoplasmic free calcium monitored with a new, intracellularly trapped fluorescent indicator. *The Journal of Cell Biology* 94(2), pp. 325–334.

Tsigelny, I., Shindyalov, I.N., Bourne, P.E., Südhof, T.C. and Taylor, P. 2000. Common EF-hand motifs in cholinesterases and neuroligins suggest a role for Ca2+ binding in cell surface associations. *Protein Science* 9(1), pp. 180–185.

Uemura, T., Lee, S.J., Yasumura, M., Takeuchi, T. and Yoshida…, T. 2010. Trans-Synaptic Interaction of GluRδ2 and Neurexin through Cbln1 Mediates Synapse Formation in the Cerebellum. *Cell*.

Ullrich, B., Ushkaryov, Y.A. and Südhof, T.C. 1995. Cartography of neurexins: more than 1000 isoforms generated by alternative splicing and expressed in distinct subsets of neurons. *Neuron* 14(3), pp. 497–507.

Urbach, A., Bar-Nur, O., Daley, G.Q. and Benvenisty, N. 2010. Differential modeling of fragile X syndrome by human embryonic stem cells and induced pluripotent stem cells. *Cell Stem Cell* 6(5), pp. 407–411.

Ushkaryov, Y.A., Petrenko, A.G., Geppert, M. and Südhof, T.C. 1992. Neurexins: synaptic cell surface proteins related to the alpha-latrotoxin receptor and laminin. *Science (New York)* 257(5066), pp. 50–56.

Vaags, A.K., Lionel, A.C., Sato, D., Goodenberger, M., Stein, Q.P., Curran, S., Ogilvie, C., Ahn, J.W., Drmic, I., Senman, L., Chrysler, C., Thompson, A., Russell, C., Prasad, A., Walker, S., Pinto, D., Marshall, C.R., Stavropoulos, D.J., Zwaigenbaum, L., Fernandez, B.A., Fombonne, E., Bolton, P.F., Collier, D.A., Hodge, J.C., Roberts, W., Szatmari, P. and Scherer, S.W. 2012. Rare deletions at the neurexin 3 locus in autism spectrum disorder. *American Journal of Human Genetics* 90(1), pp. 133–141.

Vaccarino, F.M., Grigorenko, E.L. and Smith K.M., Stevens HE. 2009. Regulation of cerebral cortical size and neuron number by fibroblast growth factors: implications for autism. *Journal of autism and development;* 39(3), pp. 511-520.

Vaher, U., Nõukas, M., Nikopensius, T., Kals, M., Annilo, T., Nelis, M., Ounap, K., Reimand, T., Talvik, I., Ilves, P., Piirsoo, A., Seppet, E., Metspalu, A. and Talvik, T. 2014. De novo SCN8A mutation identified by whole-exome sequencing in a boy with neonatal epileptic encephalopathy, multiple congenital anomalies, and movement disorders. *Journal of Child Neurology* 29(12), pp. NP202-6.

Vallier, L., Alexander, M. and Pedersen, R.A. 2005. Activin/Nodal and FGF pathways cooperate to maintain pluripotency of human embryonic stem cells. *Journal of Cell Science* 118(Pt 19), pp. 4495–4509.

Vallier, L., Reynolds, D. and Pedersen, R.A. 2004. Nodal inhibits differentiation of human embryonic stem cells along the neuroectodermal default pathway. *Developmental Biology* 275(2), pp. 403–421.

Van Esch, H. and Devriendt, K. 2001. Human Genome and Diseases: Review¶ Transcription factor GATA3 and the human HDR syndrome. *Cellular and Molecular Life Sciences CMLS*.58(9), pp 1296-1300.

Van Essen, D.C. 1997. A tension-based theory of morphogenesis and compact wiring in the central nervous system. *Nature* 385(6614), pp. 313–318.
Van Wart, A., Trimmer, J.S. and Matthews, G. 2007. Polarized distribution of ion channels within microdomains of the axon initial segment. *The Journal of Comparative Neurology* 500(2), pp. 339–352.
Varghese, M., Keshav, N., Jacot-Descombes, S., Warda, T., Wicinski, B., Dickstein, D.L., Harony-Nicolas, H., De Rubeis, S., Drapeau, E., Buxbaum, J.D. and Hof, P.R. 2017. Autism spectrum disorder: neuropathology and animal models. *Acta Neuropathologica* 134(4), pp. 537–566.
Varlakhanova, N.V., Cotterman, R.F., deVries, W.N., Morgan, J., Donahue, L.R., Murray, S., Knowles, B.B. and Knoepfler, P.S. 2010. myc maintains embryonic stem cell pluripotency and self-renewal. *Differentiation; Research in Biological Diversity* 80(1), pp. 9–19.
Varoqueaux, F., Jamain, S. and Brose, N. 2004. Neuroligin 2 is exclusively localized to inhibitory synapses. *European Journal of Cell Biology* 83(9), pp. 449–456.
Veeramah, K.R., O'Brien, J.E., Meisler, M.H., Cheng, X., Dib-Hajj, S.D., Waxman, S.G., Talwar, D., Girirajan, S., Eichler, E.E., Restifo, L.L., Erickson, R.P. and Hammer, M.F. 2012. De novo pathogenic SCN8A mutation identified by whole-genome sequencing of a family quartet affected by infantile epileptic encephalopathy and SUDEP. *American Journal of Human Genetics* 90(3), pp. 502–510.
Viñas-Jornet, M., Esteba-Castillo, S., Gabau, E., Ribas-Vidal, N., Baena, N., San, J., Ruiz, A., Coll, M.D., Novell, R. and Guitart, M. 2014. A common cognitive, psychiatric, and dysmorphic phenotype in carriers of NRXN1 deletion. *Molecular genetics & genomic medicine* 2(6), pp. 512–521.
Volkmar, F.R., Lord, C., Bailey, A., Schultz, R.T. and Klin, A. 2004. Autism and pervasive developmental disorders. *Journal of Child Psychology and Psychiatry* 45(1), pp. 135–170.
Vonica, A. and Brivanlou, A.H. 2006. An obligatory caravanserai stop on the silk road to neural induction: inhibition of BMP/GDF signaling. *Seminars in Cell & Developmental Biology* 17(1), pp. 117–132.
Vorstman, J.A.S., Parr, J.R., Moreno-De-Luca, D., Anney, R.J.L., Nurnberger, J.I. and Hallmayer, J.F. 2017. Autism genetics: opportunities and challenges for clinical translation. *Nature Reviews. Genetics* 18(6), pp. 362–376.
Vrijenhoek, T., Buizer-Voskamp, J.E., van der Stelt, I., Strengman, E., Genetic Risk and Outcome in Psychosis (GROUP) Consortium, Sabatti, C., Geurts van Kessel, A., Brunner, H.G., Ophoff, R.A. and Veltman, J.A. 2008. Recurrent CNVs disrupt three candidate genes in schizophrenia patients. *American Journal of Human Genetics* 83(4), pp. 504–510.
Wallace, G.L., Robustelli, B., Dankner, N., Kenworthy, L., Giedd, J.N. and Martin, A. 2013. Increased gyrification, but comparable surface area in adolescents with autism spectrum disorders. *Brain: A Journal of Neurology* 136(Pt 6), pp. 1956–1967.
Walsh, C.A. 1999. Genetic malformations of the human cerebral cortex. *Neuron* 23(1), pp. 19–29.
Walton, M.K., Schaffner, A.E. and Barker, J.L. 1993. Sodium channels, GABAA receptors, and glutamate receptors develop sequentially on embryonic rat spinal cord cells. *The Journal of Neuroscience* 13(5), pp. 2068–2084.
Wang, H. and Doering, L.C. 2012. Induced pluripotent stem cells to model and treat

neurogenetic disorders. *Neural plasticity*.Article ID 346053.
Wang, H., Kunkel, D.D., Martin, T.M., Schwartzkroin, P.A. and Tempel, B.L. 1993. Heteromultimeric K+ channels in terminal and juxtaparanodal regions of neurons. *Nature* 365(6441), pp. 75–79.
Wang, J., Lin, Z.-J., Liu, L., Xu, H.-Q., Shi, Y.-W., Yi, Y.-H., He, N. and Liao, W.-P. 2017. Epilepsy-associated genes. *Seizure* 44, pp. 11–20.
Wang, X. and Dai, J. 2010. Concise review: isoforms of OCT4 contribute to the confusing diversity in stem cell biology. *Stem Cells* 28(5), pp. 885–893.
Wang, X., Tsai, J.-W., LaMonica, B. and Kriegstein, A.R. 2011. A new subtype of progenitor cell in the mouse embryonic neocortex. *Nature Neuroscience* 14(5), pp. 555–561.
Wang, Z., Gerstein, M. and Snyder, M. 2009. RNA-Seq: a revolutionary tool for transcriptomics. *Nature Reviews. Genetics* 10(1), pp. 57–63.
Watt, A.J., van Rossum, M.C., MacLeod, K.M., Nelson, S.B. and Turrigiano, G.G. 2000. Activity coregulates quantal AMPA and NMDA currents at neocortical synapses. *Neuron* 26(3), pp. 659–670.
Weiler, I.J., Irwin, S.A., Klintsova, A.Y., Spencer, C.M., Brazelton, A.D., Miyashiro, K., Comery, T.A., Patel, B., Eberwine, J. and Greenough, W.T. 1997. Fragile X mental retardation protein is translated near synapses in response to neurotransmitter activation. *Proceedings of the National Academy of Sciences of the United States of America* 94(10), pp. 5395–5400.
Weiss, L.A., Escayg, A., Kearney, J.A., Trudeau, M., MacDonald, B.T., Mori, M., Reichert, J., Buxbaum, J.D. and Meisler, M.H. 2003. Sodium channels SCN1A, SCN2A and SCN3A in familial autism. *Molecular Psychiatry* 8(2), pp. 186–194.
Weiss, L.A., Shen, Y., Korn, J.M., Arking, D.E., Miller, D.T., Fossdal, R., Saemundsen, E., Stefansson, H., Ferreira, M.A.R., Green, T., Platt, O.S., Ruderfer, D.M., Walsh, C.A., Altshuler, D., Chakravarti, A., Tanzi, R.E., Stefansson, K., Santangelo, S.L., Gusella, J.F., Sklar, P., Wu, B.-L., Daly, M.J. and Autism Consortium 2008. Association between microdeletion and microduplication at 16p11.2 and autism. *The New England Journal of Medicine* 358(7), pp. 667–675.
Weissman, I.L. 2000. Stem cells: Unites of development, units of regeneration and units of evolution. *cell* 7;100(1):1578-68.
Wen, Y., Alshikho, M.J. and Herbert, M.R. 2016. Pathway network analyses for autism reveal multisystem involvement, major overlaps with other diseases and convergence upon MAPK and calcium signalling 2016. *PloS one*.7;11(4).
Wing, L. 1997. The autistic spectrum. *The Lancet* 350(9093), pp. 1761–1766.
Wiśniowiecka-Kowalnik, B., Nesteruk, M., Peters, S.U., Xia, Z., Cooper, M.L., Savage, S., Amato, R.S., Bader, P., Browning, M.F., Haun, C.L., Duda, A.W., Cheung, S.W. and Stankiewicz, P. 2010. Intragenic rearrangements in NRXN1 in three families with autism spectrum disorder, developmental delay, and speech delay. *American Journal of Medical Genetics. Part B, Neuropsychiatric Genetics* 153B(5), pp. 983–993.
de Wit, J., O'Sullivan, M.L., Savas, J.N., Condomitti, G., Caccese, M.C., Vennekens, K.M., Yates, J.R. and Ghosh, A. 2013. Unbiased discovery of glypican as a receptor for LRRTM4 in regulating excitatory synapse development. *Neuron* 79(4), pp. 696–711.
Won, H., Lee, H.-R., Gee, H.Y., Mah, W., Kim, J.-I., Lee, J., Ha, S., Chung, C., Jung,

E.S., Cho, Y.S., Park, S.-G., Lee, J.-S., Lee, K., Kim, D., Bae, Y.C., Kaang, B.-K., Lee, M.G. and Kim, E. 2012. Autistic-like social behaviour in Shank2-mutant mice improved by restoring NMDA receptor function. *Nature* 486(7402), pp. 261–265.

Won, H., Mah, W. and Kim, E. 2013. Autism spectrum disorder causes, mechanisms, and treatments: focus on neuronal synapses. *Frontiers in Molecular Neuroscience* 6, p. 19.

Wong, J.C., Makinson, C.D., Lamar, T., Cheng, Q., Wingard, J.C., Terwilliger, E.F. and Escayg, A. 2018. Selective targeting of Scn8a prevents seizure development in a mouse model of mesial temporal lobe epilepsy. *Scientific reports* 8(1), p. 126.

Xu, R.-H., Chen, X., Li, D.S., Li, R., Addicks, G.C., Glennon, C., Zwaka, T.P. and Thomson, J.A. 2002. BMP4 initiates human embryonic stem cell differentiation to trophoblast. *Nature Biotechnology* 20(12), pp. 1261–1264.

Yamanaka, S. 2008. Induction of pluripotent stem cells from mouse fibroblasts by four transcription factors. *Cell Proliferation* 41 Suppl 1, pp. 51–56.

Yamanaka, S. 2007. Strategies and new developments in the generation of patient-specific pluripotent stem cells. *Cell Stem Cell* 1(1), pp. 39–49.

Yang, J., Cai, J., Zhang, Y., Wang, X., Li, W., Xu, J., Li, F., Guo, X., Deng, K., Zhong, M., Chen, Y., Lai, L., Pei, D. and Esteban, M.A. 2010. Induced pluripotent stem cells can be used to model the genomic imprinting disorder Prader-Willi syndrome. *The Journal of Biological Chemistry* 285(51), pp. 40303–40311.

Yang, Y.M., Gupta, S.K., Kim, K.J., Powers, B.E., Cerqueira, A., Wainger, B.J., Ngo, H.D., Rosowski, K.A., Schein, P.A., Ackeifi, C.A., Arvanites, A.C., Davidow, L.S., Woolf, C.J. and Rubin, L.L. 2013. A small molecule screen in stem-cell-derived motor neurons identifies a kinase inhibitor as a candidate therapeutic for ALS. *Cell Stem Cell* 12(6), pp. 713–726.

Yellen, G. 2002. The voltage-gated potassium channels and their relatives. *Nature* 419(6902), pp. 35–42.

Ying, Q.L., Nichols, J., Chambers, I. and Smith, A. 2003. BMP induction of Id proteins suppresses differentiation and sustains embryonic stem cell self-renewal in collaboration with STAT3. *Cell* 115(3), pp. 281–292.

Yoo, H.J., Cho, I.H., Park, M., Yang, S.Y. and Kim, S.A. 2012. Family based association of GRIN2A and GRIN2B with Korean autism spectrum disorders. *Neuroscience Letters* 512(2), pp. 89–93.

Yu, F.H. and Catterall, W.A. 2003. Overview of the voltage-gated sodium channel family. *Genome Biology* 4(3), p. 207.

Yu, F.H. and Catterall, W.A. 2004. The VGL-chanome: a protein superfamily specialized for electrical signaling and ionic homeostasis. *Science's STKE: Signal Transduction Knowledge Environment* 2004(253), p. re15.

Yu, J., Vodyanik, M.A., Smuga-Otto, K., Antosiewicz-Bourget, J., Frane, J.L., Tian, S., Nie, J., Jonsdottir, G.A., Ruotti, V., Stewart, R., Slukvin, I.I. and Thomson, J.A. 2007. Induced pluripotent stem cell lines derived from human somatic cells. *Science* 318(5858), pp. 1917–1920.

Yuste, R., Peinado, A. and Katz, L.C. 1992. Neuronal domains in developing neocortex. *Science* 257(5070), pp. 665–669.

Zafra, F., Hengerer, B., Leibrock, J., Thoenen, H. and Lindholm, D. 1990. Activity dependent regulation of BDNF and NGF mRNAs in the rat hippocampus is

mediated by non-NMDA glutamate receptors. *The EMBO Journal* 9(11), pp. 3545–3550.

Zahir, F.R., Baross, A., Delaney, A.D., Eydoux, P., Fernandes, N.D., Pugh, T., Marra, M.A. and Friedman, J.M. 2008. A patient with vertebral, cognitive and behavioural abnormalities and a de novo deletion of NRXN1alpha. *Journal of Medical Genetics* 45(4), pp. 239–243.

Zamponi, G.W. 2016. Targeting voltage-gated calcium channels in neurological and psychiatric diseases. *Nature Reviews. Drug Discovery* 15(1), pp. 19–34.

Zeng, L., Zhang, P., Shi, L., Yamamoto, V., Lu, W. and Wang, K. 2013. Functional impacts of NRXN1 knockdown on neurodevelopment in stem cell models. *Plos One* 8(3), p. e59685.

Zeng, X., Sun, M., Liu, L., Chen, F., Wei, L. and Xie, W. 2007. Neurexin-1 is required for synapse formation and larvae associative learning in Drosophila. *FEBS Letters* 581(13), pp. 2509–2516.

Zhang, C., Atasoy, D., Araç, D., Yang, X. Fucillo, MV. Robinson., AJ. Ko J., Brunger AT., Südhof, TC. M.V. 2010. Neurexins Physically and Functionally Interact with GABAA Receptors. *Neuron* 13;66(3):403-416.

Zhang, N., An, M.C., Montoro, D. and Ellerby, L.M. 2010. Characterization of human Huntington's disease cell model from induced pluripotent stem cells. *PLoS currents*.28;2:RRN1193.

Zhang, P., Andrianakos, R., Yang, Y., Liu, C. and Lu, W. 2010. Kruppel-like factor 4 (Klf4) prevents embryonic stem (ES) cell differentiation by regulating Nanog gene expression. *The Journal of Biological Chemistry* 285(12), pp. 9180–9189.

Zhang, S.C., Wernig, M., Duncan, I.D., Brüstle, O. and Thomson, J.A. 2001. In vitro differentiation of transplantable neural precursors from human embryonic stem cells. *Nature Biotechnology* 19(12), pp. 1129–1133.

Zhang, W., Rohlmann, A., Sargsyan, V., Aramuni, G., Hammer, R.E., Südhof, T.C. and Missler, M. 2005. Extracellular domains of alpha-neurexins participate in regulating synaptic transmission by selectively affecting N- and P/Q-type Ca2+ channels. *The Journal of Neuroscience* 25(17), pp. 4330–4342.

Zhang, Z. and Baldini, A. 2008. In vivo response to high-resolution variation of Tbx1 mRNA dosage. *Human Molecular Genetics* 17(1), pp. 150–157.

Zhou, J., Blundell, J., Ogawa, S., Kwon, C.-H., Zhang, W., Sinton, C., Powell, C.M. and Parada, L.F. 2009. Pharmacological inhibition of mTORC1 suppresses anatomical, cellular, and behavioral abnormalities in neural-specific Pten knock-out mice. *The Journal of Neuroscience* 29(6), pp. 1773–1783.

Zhou, T., Benda, C., Dunzinger, S., Huang, Y., Ho, J.C., Yang, J., Wang, Y., Zhang, Y., Zhuang, Q., Li, Y., Bao, X., Tse, H.-F., Grillari, J., Grillari-Voglauer, R., Pei, D. and Esteban, M.A. 2012. Generation of human induced pluripotent stem cells from urine samples. *Nature Protocols* 7(12), pp. 2080–2089.

Zhou, T., Benda, C., Duzinger, S., Huang, Y., Li, X., Li, Y., Guo, X., Cao, G., Chen, S., Hao, L., Chan, Y.-C., Ng, K.-M., Ho, J.C., Wieser, M., Wu, J., Redl, H., Tse, H.-F., Grillari, J., Grillari-Voglauer, R., Pei, D. and Esteban, M.A. 2011. Generation of induced pluripotent stem cells from urine. *Journal of the American Society of Nephrology* 22(7), pp. 1221–1228.

Zhou, Y. and Zeng, F. 2013. Integration-free methods for generating induced pluripotent stem cells. *Genomics, proteomics & bioinformatics / Beijing Genomics Institute* 11(5), pp. 284–287.

Zhu, X.R., Wulf, A., Schwarz, M., Isbrandt D.,Pongs O. 1999. Characterization of human Kv4. 2 mediating a rapidly-inactivating transient voltage-sensitive K+ current. *Receptors Channels* 6(5):387-400.

Zilbovicius, M., Boddaert, N.,Belin P.,Poline JB., Remy P., Mangin JF., Thivard L., Barthelemy C., Samson Y. 2000. Temporal lobe dysfunction in childhood autism: a PET study. *American Journal of Psychiatry.*157(12):1988-93.

Zucker, R.S. 1999. Calcium- and activity-dependent synaptic plasticity. *Current Opinion in Neurobiology* 9(3), pp. 305–313.